DYNAMIC MODELING AND CONTROL OF SPACECRAFT ROBOTIC SYSTEMS USING DUAL QUATERNIONS

A Dissertation
Presented to
The Academic Faculty

By

Alfredo Valverde Salazar

In Partial Fulfillment
of the Requirements for the Degree
Doctor of Philosophy in the
School of Aerospace

Georgia Institute of Technology

May 2018

DYNAMIC MODELING AND CONTROL OF SPACECRAFT ROBOTIC SYSTEMS USING DUAL QUATERNIONS

Approved by:

Dr. Panagiotis Tsiotras, Advisor
School of Aerospace Engineering
Georgia Institute of Technology

Dr. Marcus J. Holzinger
School of Aerospace Engineering
Georgia Institute of Technology

Dr. Patricio A. Vela
School of Electrical and Computer Engineering
Georgia Institute of Technology

Dr. David S. Bayard
Guidance and Control Analysis Group
Jet Propulsion Laboratory

Dr. Glenn Lightsey
School of Aerospace Engineering
Georgia Institute of Technology

Date Approved: April 6, 2018

Nothing in life is to be feared, it is only to be understood.

Marie Curie

To my mother, who taught me that perfection is not a myth, and to my wife, who stands by my side rain or shine.

ACKNOWLEDGEMENTS

First and foremost, I would like to thank my mother Rosario Salazar and my wife Bailey Valverde, whose unconditional love has no limits, and whose support has never wavered. Taty, Guille, Amis, Rosita, Mari, Laura, Francisco, Tim, Ms. Carol, you are the best family anyone could ever ask for, and each one of you has contributed greatly to me becoming a better person. Thank you for supporting my dreams and enabling me in every possible way.

Professor Panagiotis Tsiotras thank you for being an admirable professional and an even better advisor. Your desire to pursue the highest levels of research has shaped me in ways I could have only wished for when I joined the DCSL. Thank you for providing me, and those who surround you, the opportunity to learn by your side.

I would also like to thank the members of my defense committee for their valuable insight and remarkably keen eye: Dr. Marcus J. Holzinger, Dr. Patricio A. Vela, Dr. Glenn Lightsey and Dr. David S. Bayard. In one way or the other, you all contributed enormously to the work contained in this dissertation, and even that might still be an understatement.

Nuno Filipe and Chiluwata Lungu, as my most impactful non-faculty mentors throughout my journey at Georgia Tech, I would like to thank you for setting the bar so high. Esteban Q., Eduardo B., María José O., Benjamin H., Oliver D., Alex S., Luke N.: thank you for unparalleled levels of friendship. Alex D., thank you for an amazing friendship and for your help with Clifford algebras, most of which I have incorporated in this dissertation. Mehregan D. and Matthew K-S.: thank you for your patience, your persistence, your determination, your hard work, and an uncountable amount of sleepless nights in the lab.

As this space is finite, many people who have played an important role in my life have not been explicitly mentioned, including family, friends, teachers, coaches, mentors, and role models. To each and every person I have come across in my life, contributing to shaping me into the individual I am today: thank you!

TABLE OF CONTENTS

LIST OF TABLES

LIST OF FIGURES

LIST OF SYMBOLS AND ACRONYMS

OPERATORS

$*$	Quaternion multiplication with 4×4 matrix.
$\star$	Dual quaternion multiplication with 8×8 matrix.
$\circ$	Dual quaternion circle product.
$\cdot$	Dot product.
$\times$	Cross product.
$[\![\cdot]\!]_{\text{L}}$	Quaternion left-multiply.
$[\![\cdot]\!]_{\text{R}}$	Quaternion right-multiply.
$\mathbb{[\![} \cdot \mathbb{]\!]}_{\text{L}}$	Dual quaternion left-multiply.
$\mathbb{[\![} \cdot \mathbb{]\!]}_{\text{R}}$	Dual quaternion right-multiply.
$\| \cdot \|_{\infty}$	Infinity norm of time-dependent signal.
$\text{H}(\cdot)$	Matrix swap.
$N(\cdot)$	Negative indices.
$P(\cdot)$	Positive indices.
$r(\cdot)$	Function such that $M^{\text{B}} \star \boldsymbol{a} = r(\boldsymbol{a})\text{v}(M^{\text{B}})$.
$R(\cdot)$	Regressor matrix operator in concurrent learning of single rigid body case.
$\hat{R}(\cdot)$	Regressor matrix operator for single body in concurrent learning of multibody system case.
$\boldsymbol{R}(\cdot)$	Regressor matrix operator in concurrent learning of multibody system case.
$\text{v}(M^B)$	Vectorized dual inertia matrix: $\text{v}(M^B) = [\bar{I}^{\text{B}}_{11}, \bar{I}^{\text{B}}_{12}, \bar{I}^{\text{B}}_{13}, \bar{I}^{\text{B}}_{22}, \bar{I}^{\text{B}}_{23}, \bar{I}^{\text{B}}_{33}, m]^{\text{T}}$.

SUBSCRIPTS

act	Actuation.
ext	External.
r	Real part of dual quaternion.

d	Dual part of dual quaternion, or disturbance, depending on context.
k	At, or corresponding to, timestep $t = t_k$

SUPERSCRIPTS

$^{\mathsf{s}}$	Dual quaternion swap.
*	Quaternion and dual quaternion conjugate.
$^{\mathsf{T}}$	Matrix transpose.
$^{\times}$	Skew matrix operator.

ACCENTS

$\tilde{}$	Reduced wrench.
$\hat{}$	Estimate, or modified, depending on the context.
$\dot{}$	Derivative with respect to time.

SYMBOLS

D	Space of dual numbers.
$C\ell_{p,q,r}$	Clifford algebra of signature $\{p, q, r\}$.
$\boldsymbol{\mathcal{C}}$	Vector that excludes cross terms of the form $\boldsymbol{\omega} \times (M \star (\boldsymbol{\omega})^{\mathsf{s}})$ from $\boldsymbol{\mathcal{B}}_1$ for each body used in concurrent learning.
$\mathbb{H}$	Space of unit quaternions
$\mathbb{H}_d$	Space of dual unit quaternions.
$\mathbb{R}^{m\times n}$	Space of m-by-n matrices of real coefficients.
$\mathrm{SE}(3)$	Special Euclidean group of all rigid-body transformations.
$\mathrm{SO}(3)$	Special orthogonal group of all rotations about the origin of three-dimensional Euclidean space.
0_m	m-by-1 zeros vector.
$0_{m\times n}$	m-by-n zeros matrix.
$\mathbb{I}_n$	n-by-n identity matrix.
$\mathsf{1}$	$(1, \bar{0}) \in \mathbb{H}$.
$\mathsf{0}$	$(0, \bar{0}) \in \mathbb{H}$.

$\mathbf{1}$	$1 + \epsilon 0 \in \mathbb{H}_d$.
$\mathbf{0}$	$0 + \epsilon 0 \in \mathbb{H}_d$.
$\bar{a}^{\mathrm{Z}}_{\mathrm{X/Y}}$	Acceleration vector of point X with respect to frame X, or the origin of frame X, expressed in Z-frame coordinates, [m/s^2].
$a^{\mathrm{Z}}_{\mathrm{X/Y}}$	Acceleration quaternion of point X with respect to frame X, or the origin of frame X, expressed in Z-frame coordinates, [m/s^2].
B	Branch termination matrix.
$B(\bar{x}, \bar{u}, k)$	Control matrix of the linearized system in DDP.
$\mathcal{B}$	Right-hand side vector in decoupled formulation of dynamics.
$\mathcal{B}_1$	Vector that contains known quantities in Newton-Euler equations in decoupled dynamics formulation.
$\mathcal{B}_2$	Vector that contains right-hand side of constraint equations in decoupled dynamics formulation.
$\boldsymbol{\mathcal{B}}$	Right-hand side vector in dual quaternion formulation of dynamics.
$\boldsymbol{\mathcal{B}}_1$	Vector that contains known quantities in Newton-Euler equations for dual quaternion dynamics formulation.
$\boldsymbol{\mathcal{B}}_2$	Vector that contains right-hand side of constraint equations for dual quaternion dynamics formulation.
C	Incidence matrix, or cylindrical joint type, depending on context.
d_i	Degrees of freedom at joint i.
$\delta x(t_k)$	State perturbation with respect to the nominal state $\bar{x}_k$.
$\delta u(t_k)$	Control perturbation with respect to the nominal control $\bar{u}_k$.
E_{23}	3-by-3 identity matrix with third row removed
$\boldsymbol{E}_{\pi(1,2,3,4,5,6,7,8;i)}$	8-by-8 identity matrix with $\pi(1,2,3,4,5,6,7,8;i)$ rows removed.
f^{X}	Force quaternion expressed in X coordinates [N].
$\mathcal{F}$	Storage set for reconstruction of vector F in concurrent learning for single rigid body.
$\boldsymbol{\mathcal{F}}$	Storage set for reconstruction of vector $\boldsymbol{F}$ in concurrent learning for multibody system.

$\boldsymbol{H}^{\mathrm{Z}}_{\mathrm{S}}(O_{\mathrm{X}})$	Dual momentum of body S about point X, or origin of frame X expressed in Z-frame coordinates.
$\bar{I}_{\mathbf{e}_{\mathrm{i}}}$	Inertia about the CoM of body i calculated in $\mathbf{e}_i$-frame coordinates [kg$\cdot$ m^2].
$\bar{I}^{\mathrm{B}}$	Inertia about the CoM of body B calculated in B-frame coordinates [kg$\cdot$ m^2].
$J(x_0, U)$	Objective function for the optimal control problem in DDP algorithm.
$J(x_0, U; i)$	Objective function for the optimal control problem for iteration i in DDP algorithm.
k	Time index.
l	Control feed-forward term in DDP.
L	Control state-feedback gain matrix in DDP.
$\mathcal{L}_f(x_N, N)$	Final cost function.
$\mathcal{L}(\bar{x}_k, \bar{u}_k, k)$	Running cost function.
$m, m_{\mathbf{e}_{\mathrm{i}}}$	Mass, or mass of body i [kg].
$M_{\mathbf{e}_{\mathrm{i}}}$	Dual inertia about the CoM of body i calculated in $\mathbf{e}_i$-frame coordinates [kg, kg$\cdot$ m^2].
N_s	Number of samples to be stored in concurrent learning.
M^{B}	Dual inertia about the CoM of body B calculated in B-frame coordinates [kg, kg$\cdot$ m^2].
P	Prismatic joint type.
P	7-by-7 matrix used in continuous-time concurrent learning
$q_{\mathrm{X/Y}}$	Quaternion describing attitude change from frame Y to frame X.
$\boldsymbol{q}_{\mathrm{X/Y}}$	Dual quaternion describing pose change from frame Y to frame X.
$Q(x(t_k), u(t_k), t_k)$	State-action value function.
Q	7-by-1 vector used in continuous-time concurrent learning
r_i	Reduced wrench dimensionality at joint i.
$\bar{r}^{\mathrm{Z}}_{\mathrm{X/Y}}$	Position vector from point Y to point X, in Z-frame coordinates, [m].

$r^{\mathrm{Z}}_{\mathrm{X/Y}}$	Position quaternion from point Y to point X, in Z-frame coordinates, [m]. $r^{\mathrm{Z}}_{\mathrm{X/Y}} = (0, \bar{r}^{\mathrm{Z}}_{\mathrm{X/Y}})$.
$\boldsymbol{r}^{\mathrm{Z}}_{\mathrm{X/Y}}$	Position dual quaternion from point Y to point X, in Z-frame coordinates, [m]. $\boldsymbol{r}^{\mathrm{Z}}_{\mathrm{X/Y}} = 0 + \epsilon r^{\mathrm{Z}}_{\mathrm{X/Y}}$.
$R(i)$	Penalty matrix for the control effort during iteration i.
R	Revolute joint type.
S	Spherical joint type.
$\boldsymbol{s}$	Plücker coordinates of a line in dual quaternion form.
$\mathcal{S}$	Dynamics and constraints matrix used in left-hand side of decoupled formulation of dynamics.
$\boldsymbol{\mathcal{S}}$	Dynamics and constraints matrix used in left-hand side of dual quaternion formulation of dynamics.
t_k, t	Time [s].
T	Kinetic energy.
$T_{\mathrm{X/Y}}$	Homogeneous transformation matrix describing pose change from frame Y to frame X.
$\mathcal{T}$	Vector of reduced reaction forces and torques in dual quaternion dynamics formulation.
$\boldsymbol{\mathcal{T}}$	Vector of reduced reaction wrenches in dual quaternion dynamics formulation.
U	Set of control inputs, or cartesian joint type, depending on context..
$\bar{v}^{\mathrm{Z}}_{\mathrm{X/Y}}$	Linear velocity vector of point X with respect to point Y, or origin of frame Y, in Z-frame coordinates.
$v^{\mathrm{Z}}_{\mathrm{X/Y}}$	Linear velocity quaternion of point X with respect to point Y, or origin of frame Y, in Z-frame coordinates. $v^{\mathrm{Z}}_{\mathrm{X/Y}} = (0, \bar{v}^{\mathrm{Z}}_{\mathrm{X/Y}})$.
V_i	Mapping matrix between reduced and original reaction wrench at joint i.
$V_{\mathrm{act,i}}$	Mapping matrix between reduced and original actuation wrench at joint i.
$V(x(t_k), (t_k))$	Value function.
$W_{f,x}(i)$	Penalty matrix for state x at the final timestep during iteration i.
$W_{k,x}(i)$	Penalty matrix for state x at timestep k during iteration i.

$\boldsymbol{W}^{\mathfrak{e}_i}_{\mathfrak{e}_i}(O_{\mathfrak{e}_i})$	Body wrench applied at CoM of body i expressed in $\mathfrak{e}_i$ coordinates.
$\boldsymbol{W}^{i}_{\text{ext}}(O_j)$	External wrench applied about point j expressed in i coordinates.
$\boldsymbol{W}^{i}_{\text{act,i}}(O_j)$	Actuation wrench applied at joint i about point j in i coordinates.
$\mathcal{X}$	Storage set for reconstruction of matrix R in concurrent learning.
$\boldsymbol{\mathcal{X}}$	Storage set for reconstruction of matrix $\boldsymbol{R}$ in concurrent learning.
y	Vector of stacked linear and angular velocities.
$\boldsymbol{y}$	Vector of stacked dual velocities.
$\mathcal{Y}$	Unknown vector of linear and angular accelerations, and reduced reaction forces and torques.
$\boldsymbol{\mathcal{Y}}$	Unknown vector of dual accelerations and reduced reaction wrenches.
α	Scalar gain for concurrent-learning term in adaptice estimate of inertia matrix, or iteration-dependent line-search parameter for feedforward control term in DDP control update.
$\beta_{(\cdot,\cdot)}$	Iteration-dependent weighing parameter.
ΔM	Error in the estimate of the dual inertia matrix. $\Delta M = M - \widehat{M}$.
Δt	Time increment [s].
ϵ	Dual unit.
ε	Error-like signal in concurrent learning.
$\Gamma_{\text{J}_\text{i}}$	Generalized coordinate at joint i.
Λ_i	Projection matrix for joint i constraint equation that eliminates generalized speeds of joint.
$\Phi(\bar{x}, \bar{u}, k)$	State transition matrix of the linearized unforced dynamics in DDP.
$\bar{\omega}^{\text{Z}}_{\text{X/Y}}$	Angular velocity vector of frame X relative to frame Y, in Z-frame coordinates.
$\omega^{\text{Z}}_{\text{X/Y}}$	Angular velocity quaternion of frame X relative to frame Y, in Z-frame coordinates. $\omega^{\text{Z}}_{\text{X/Y}} = (0, \bar{\omega}^{\text{Z}}_{\text{X/Y}})$.

$\boldsymbol{\omega}^{\mathrm{Z}}_{\mathrm{X/Y}}$	Dual velocity of frame X relative to frame Y, in Z-frame coordinates.
$\pi(1,\ldots,N_s)$	Permutation of the numbers 1, ..., N_s
$\pi(1,2,3,4,5,6,7,8;i)$	Row selector based on type of joint i.
τ^{X}	Torque quaternion expressed in X coordinates [N.m].
$\boldsymbol{\theta}$	Dual angle.

ACRONYMS

COTS	Commercial off-the-shelf.
CL	Concurrent learning.
CMG	Control Moment Gyroscope.
DARPA	Defense Advanced Research Projects Agency.
DDP	Differential dynamic programming.
DH	Denavit-Hartenberg.
DM/EDM	Disturbance Map, or Enhanced Disturbance Map.
ETS-VII	Engineering Test Satellite No. 7.
EVA	Extra-vehicular activities.
FREND	Front-end Robotics Enabling Near-term Demonstration.
GEO	Geosynchronous Earth Orbit.
GJM	Generalized Jacobian Matrix.
GNC	Guidance, Navigation and Control.
GPS	Global Positioning System.
NASA	National Aeronautics and Space Administration.
NASDA	National Space Development Agency of Japan.
NRL	Naval Research Laboratory.
RSGS	Robotic Servicing of Geosynchronous Satellites.
SOA	Spatial Operator Algebra.
SSPD	Satellite Servicing Projects Division.

SVA	Spatial Vector Algebra.
VSCMG	Variable-Speed Control Moment Gyroscope.

SUMMARY

As of 2014, the space servicing market has a potential revenue of $3-$5B per year due to the ever-present interest to upkeep existing orbiting infrastructure. In space servicing, there is a delicate balance between system complexity and servicer capability. Basic module-exchange servicers decrease the complexity of the servicing spacecraft, but are likely to require a more complex architecture of the serviced satellite (the host) in terms of electrical and mechanical connections.

With increasing dexterity of the servicing satellite, host satellites can remain closer to flight-proven heritage architectures, which is a practice commonly adopted to increase reliability of space missions. This increased dexterity can be provided through the on-orbit exchange of end-effector tools appended to a robotic arm. The dynamic coupling of the arm and the base has been the subject of intense academic scrutiny and its understanding is essential to the implementability and success of robotic servicing missions.

In this work, we propose a framework that implements different phases of a servicing mission in dual quaternion algebra. First, we propose a dual quaternion 6-DOF pose-tracking controller that adaptively estimates the mass properties of a rigid-body spacecraft using the concurrent learning framework. Next, we provide a generalizable case-study of the derivation of the dynamic equations of motion for a spacecraft with a serial robotic manipulator. The derivation uses a Newton-Euler approach. Its results are validated against an analogous derivation that uses a decoupled treatment of the translational and rotational dynamics.

Given the analytical appeal of the formulation of the case-study, the kinematics and the dynamics of the system are generalized to a spacecraft with a rooted-tree topology. In this generalization, five different type of joints are easily incorporated into the formulation which is enabled by the underlying dual quaternion algebra. As an example on how to apply the framework, a two-arm satellite-mounted system is simulated and numerical

performance results are presented.

We conclude with two important applications. The first one is that of performing end-effector control, for both stabilization and tracking maneuvers. The kinematics of the end-effector are succinctly derived in dual quaternion form, which allows for incorporation into a Differential Dynamic Programming framework. The second application is that of estimating the mass properties for the two-arm satellite-mounted robotic arm. For this system with 11 rigid bodies, the task implies estimating 77 different parameters. The proposed modification of the concurrent learning-based approach exploits the structure of the adaptive estimation law to aggressively converge on the true parameters.

CHAPTER 1
INTRODUCTION

1.1 Motivation

Access to space has enabled a wide range of military and commercial activity. From spaced-based experimental laboratories, such as the International Space Station (ISS), to missile-tracking defense networks of satellites, to GPS-enabling satellites that aid our daily commutes, satellites provide valuable services to their operators, the scientific community, and humanity as a whole. Even though launch costs are likely to decrease with the development of reusable first-stage rockets, commercial off-the-shelf (COTS) components, and the miniaturization of components, access to space is, and will remain, expensive for the foreseeable future.

The servicing of orbiting satellites is an essential tool to lower development, equipment and operational costs, as well as to reduce system complexity by means of decreasing required redundancy for a desired lifetime. Satellite servicing encompasses a wide range of uses that aim to extend the satellite lifetime. Common services are visual inspection, scheduled maintenance, refueling, part replacement, repair of worn or broken components, or completion of failed deployment sequences, among others. These services can be split into four broad categories: dexterous servicing, simple servicing, inspection, and orbit reboost [1].

The space servicing market has a potential revenue of $3-$5B per year as of 2014 according to Akin [1]. The Satellite Servicing Capabilities Office (SSCO), now the Satellite Servicing Projects Division (SSPD), at NASA's Goddard Space Flight Center has led the way in conceptualizing and implementing new technologies. The SSPD's mission can be delineated as [2]:

- Advancing the state of robotic servicing technology to enable the routine servicing of satellites that were not designed with servicing in mind
- Positioning the U.S. to be the global leader in in-space repair, maintenance and satellite disposal
- Helping to enable a future U.S. industry for the servicing of satellites

As highlighted by Ellery in [3], the development of a satellite servicing industry would greatly benefit from public funds and participation of state-sponsored entities such as NASA, or ESA, especially in the early stages. Ellery also states that profitability would require that astronauts are not part of the cost equation, making it increasingly important to have autonomous robotic systems that can perform the servicing tasks.

The use of tele-operated or autonomous robotic systems for spacecraft servicing has been a topic of study since the early 70's. The benefits of robotic servicing focus mainly on decreasing risk to astronauts performing extra-vehicular activities (EVA's) or increasing astronaut efficiency [4]. However, emphasis is also given to the lack of humans in the process, decreasing cost, and increasing the frequency of available launch spots. Without the restriction of having astronauts involved, robotic missions can also go beyond Low Earth Orbit (LEO), to regions of higher radiation, or even operate in high-inclination polar orbits.

A commonly overlooked facet of space activity is its long-term sustainability. A study that focused on satellite servicing performed by NASA Goddard [5] emphasizes the importance of a more "refined consciousness" in the use of space since the increasing number of abandoned satellites poses a threat to existing and future missions. As a clear example of this is the existence of more than 150 dead satellites and rocket stages in GEO that did not perform end-of-mission maneuvers towards graveyard orbits.

In space robotics, there is a delicate balance between system complexity and servicer capability. Basic module-exchange servicers decrease the complexity of the servicing

spacecraft [6], but this option is likely to require a more complex architecture of the serviced satellite (the host) in terms of electrical and mechanical connections. With increasing dexterity of the servicing satellite, host satellites can remain closer to flight-proven heritage architectures to increase mission reliability. This increased dexterity can be provided through the on-orbit exchange of the end-effector tool, such as is proposed by Akin with the *Sample Proteus Toolbox* [1]. The price to pay for increased dexterity is a coupling between the dynamics of the robotic arm extending this tool, and the satellite base that holds it. This coupling has been the subject of intense academic scrutiny and its understanding is essential to the success of robotic missions that use an articulated arm.

The Engineering Test Satellite No. 7 (ETS-VII) launched in 1997 by the National Space Development Agency of Japan (NASDA) was the first robotic arm launched into orbit. Among many tests, the appended arm was successfully used for the capture of a target satellite with a teleoperated chaser [7, 8]. In 2007, DARPA's Orbital Express Demonstration System launched with the objective of performing on-orbit satellite refueling, among a host of other autonomous operations involving a 6-DOF manipulator [9, 10].

Current efforts go beyond mere conceptual testing, into the the realm of standardization and profitability. Henshaw in [11] describes the Front-end Robotics Enabling Near-term Demonstration (FREND) program for the demonstration of autonomous rendezvous and docking for the capture and orbit elevation of GEO satellites. The program was sponsored by DARPA and developed by the Naval Research Laboratory (NRL). Roesler in [12] describes the Robotic Servicing of Geosynchronous Satellites (RSGS) program developed by DARPA. The goal of the RSGS initiative is:

> "[t]o create a dexterous robotic operational capability in Geosynchronous Orbit, that can both provide increased resilience for the current U.S. space infrastructure, and be the first concrete step toward a transformed space architecture with revolutionary capabilities."

This statement closely aligns with the National Space Policies [13] published in 2010.

With the RSGS program, DARPA will establish a government-led cohort of companies to develop their own servicing satellite for GEO. After the accomplishment of mission-independent milestones set by DARPA, the participating companies are sent off to profit by servicing existing satellites. In a similar effort, the Restore-L mission aims at developing a suite of tools for on-orbit refueling of a government-owned satellite in polar orbit [14, 13].

Robotic arms are not limited to capturing or minor servicing operations. Their availability in space opens a gamut of possibilities that include in-space assembly of large structures, payload transfer between orbiting satellites, rescue missions of stranded touristic space vehicles, effective momentum transfer of a detumbling spacecraft, debris capture, or unmanned manipulation and disassembly of enemy satellites, just to name a few [15, 16, 17]. These activities mainly consider the interaction with man-made objects. However, one of the largest benefits of robot-wielding satellites will be the capability to capture an asteroid that threatens human life on Earth, and redirect it towards a safe zone. In fact, NASA's Asteroid Redirect Robotic Mission is a variant of this, in which an asteroid is captured and carried into cis-lunar space as a technology demonstration, with a significant contribution to science [18, 19].

The operation of a robotic arm on a spacecraft is not a trivial task. Without appropriate dynamical models of the combined system and effective control algorithms, fuel can be quickly depleted, reaction wheels saturated, power drawn too abruptly, a line-of-sight communication link lost, or the combined system destabilized. Landmark literature initially proposed the use of active attitude control systems [20], which can be useful in cases when strict pointing requirements exist [21]. However, powerful techniques now exist that allow the base to move freely, or in a reaction-less fashion, during the manipulation of the arm, thus avoiding the aforementioned pitfalls of a free-floating robotic manipulator. Current algorithms have to be able to incorporate changes such as when a payload is released or grabbed, or when there is a significant change in the fuel at the base [22]. Another important component of the control problem is the incorporation of constraints beyond simple

inertial pointing, as in the case of relative attitude constraints between spacecraft to avoid plume impingement, line-of-sight constraints to perform visual navigation, or simple obstacle avoidance constraints to avoid collision between satellites.

1.2 Literature Review

In this section we provide an overview of the use of dual quaternions in the field of fixed-base robotics, modeling and control of satellites on 6-DOF (degrees of freedom) motion, and the dynamic modeling of robotic manipulators mounted on a satellite. Particular attention will be paid to the latter to provide appropriate insight into the different strategies and constructs that have been developed since the 70's.

1.2.1 Dual Quaternions in Robotics

Dual quaternions provide a compact numerical representation of position and attitude, equivalently, *pose*. They have been used in robotic forward and inverse kinematics, allowing roboticists to reduce computational time and improve precision for common tasks. It is worth emphasizing that to the best of the author's knowledge, there are no results containing dynamic modeling of robotic arms using dual quaternions. Also, there is no attempt in the literature to model dynamics of a free-floating spacecraft with a robotic arm using dual quaternions. As stated before, the use of dual quaternions except for conventional 6-DOF modeling of rigid body dynamics, has been a mere kinematical tool.

As one of the earlier applications of dual quaternions in robotics, Dooley and McCarthy in [23] developed a framework that uses dual quaternion coordinates for the dynamic modeling and control of cooperating robotic arms on a fixed base. The approach treats dual quaternions as generalized coordinates and the constraints are added to the equations of motion. The authors also provide a version of the Jacobian by expressing the forward kinematics using dual quaternions, and then evaluating its partial derivatives with respect to the joint angles.

Daniilidis in [24] used dual quaternions for one of its most widely used applications: hand-eye calibration. This procedure yields a transformation from an end-effector or mechanical link, to the camera frame of a vision system. In the paper, lines are parametrized in dual quaternion form and appropriate transformations are defined in dual quaternion algebra. The *screw congruence theorem* is proven succinctly using dual quaternions, and due to the similarity between quaternions and dual quaternions, it can be implied that only two motions with non-parallel rotation axes are needed to fully constrain the problem. This insight was not immediate from other pose representations. The hand-eye calibration is then posed as a singular value problem, and the authors show that their results outperform decoupled (rotation and translation) formulations of the problem.

Perez and McCarthy in [25, 26] extensively address the design of fixed-base robotic systems using dual quaternions. Perez states that the dual quaternion representation is particularly useful to eliminate joint variables for kinematic modeling. Their framework allows quantifying the number of equations required to fully constrain the synthesis problem: that of designing a robot that can achieve a discrete set of poses in inertial space. They establish the equations for different serial or parallel constrained configurations, and provide numerical examples on the use of their framework.

In [27], Yavuz uses dual quaternions to avoid the typical singularities that arise in kinematic analysis of robots with an Euler wrist. The paper addresses the inverse kinematics problem with dual quaternions and it provides analytical solutions to two different examples. The chosen robot configurations are RRP and RRR, yielding remarkably simple results after tedious computation that splits up each coordinate of the dual quaternions involved.

Reference [28] by Gan et al. provides a closed form solution to the inverse kinematics of a closed 7-link, 7-R mechanism. The framework allows the authors to cast the problem as a 16th order polynomial in one variable, significantly reducing the computational cost to solve the problem.

In [29], Wang et al. lay out common formalisms of dual quaternions to be used in the area of robotics, in combination with Lie theoretical constructs such as the exponential of the Plücker coordinates of a line, as well as the logarithm of a dual quaternion. The authors make use of the error dual quaternion, and they define a corresponding left-invariant metric using the logarithm operation applied on the error quaternion. The authors prove that there exists a Lie algebra, with a corresponding Lie bracket, defined on the space of vector dual quaternions. Finally, a kinematic control law is proposed, without regards to dynamics. The law is asymptotically stable with respect to the pose of the objects.

In [30], Leclercq et al. provide a framework that allows studying transformations and kinematics associated to points, lines and screw motions encoded as dual quaternions. Their application of dual quaternions to neuroscience aims to model the position and velocity of points as projected onto an eye's retina, and they propose a Jacobian dependent on dual quaternion transformations. Additionally, using dual quaternions and screw theory, the authors perform path planning and control of a 7-DOF robot with a screw-driver. This task requires precise control along a specific direction, and rotation along an axis parallel to that line. Leclercq et al. also provide a generalization for the forward kinematics of an n-link serial robot with a fixed base using the dual quaternion formalism. It is worth emphasizing that [30] makes use of adjoint transformations to extract position coordinates for the points and the lines at every iteration, instead of simply using frame transformations in dual quaternion algebra. This allows to only extract coordinates when a physical interpretation is needed. The authors also use a dual quaternion representation that separates translation and rotations as two different types of dual quaternions. As we will see in this document, we can combine these in a convenient fashion to simplify computations.

In [31], Radavelli et al. use dual quaternions as a tool to transform points, lines, screws and planes. In fact, this work summarizes the right type of conjugation to be used on dual quaternions in order to apply the correct transformation to the aforementioned mathematical constructs. The main contribution in [31] is to provide a straightforward approach to

retrieve a dual quaternion describing the end effector attitude or pose under different circumstances. These are: the combination of vector dual quaternions, the intersection of lines encoded as dual quaternions, or the information provided from combination of a vector, a line and a plane, all encoded in dual quaternion form.

Reference [32] models a 20-DOF humanoid robot using dual quaternions. For this, the authors developed forward kinematics models and different serialization approaches to solve the different tasks. A Jacobian associated to the overall motion of the system using dual quaternion algebra was also developed. The control of the humanoid is hierarchical and the different levels are: balance control, servo-visual control, and manipulation.

In [33], Ulrich and Steger addressed the hand-eye calibration problem for a SCARA robot, where the rotational axes and the translational axes are parallel. The authors extend the result of [24] through the incorporation of additional constraints based on the depth of the calibration object. The authors in [33] also improve the accuracy of the algorithm by proposing a nonlinear optimization approach.

Another common area where dual quaternions have gained popularity is in computer vision, a field essential in many robotic systems. Reference [34] discusses the formulation of a dual quaternion-based SLAM algorithm and shows that for estimation purposes, the dual quaternion formulation possesses a much larger robustness to noise, for both simulated and real sets of data. It is worth highlighting that this paper proposes a multiplicative update to the estimate of the dual quaternion by use of the error dual quaternion. However, this error dual quaternion only makes use of one of the two constraints of a dual quaternion (the unit norm), and does not use the orthogonality of the dual part with respect to the real part of the dual quaternion.

1.2.2 Dynamic Modeling and Control of Rigid Bodies in 6-DOF Motion

The modeling and control of spacecraft in 6-DOF motion is a topic that has been widely studied. This section aims to provide an overview of the role dual quaternions play in

pose stabilization or tracking, and other tasks related to Guidance, Navigation, and Control (GNC).

Quaternions are not the preferred tool to model rigid body dynamics since in general, it is preferable to express the rotational equation of motion in terms of physical quantities such as angular accelerations, angular velocities, and body torques. Udwadia in [35], supported by [36], derived the rotational equations of motion for a rigid body using the Lagrangian formulation. In this case, he used the quaternion components as generalized coordinates, while still ensuring their unit norm is satisfied using an analytical correction term.

In a similar result, Dooley and McCarthy in [37] used dual quaternions as generalized coordinates to describe the 6-DOF dynamics of a single rigid body. Their approach makes use of Kane's equations of motion. The authors in [37] argued that the physical significance of the variables is lost in this formulation. The authors do foresee that by using a different set of coordinates, their constraint multiplier could represent the reaction forces experienced by a body. The authors also praise dual quaternion algebra as useful in simplifying kinematic modeling. They foresee this as an advantage when eventually trying to deal with closed loop kinematic chains.

In [38], Brodsky and Shoham provide an in-depth introduction to the use of dual number theory for the modeling of dynamical quantities and systems, as well as for the treatment of functions of dual variables. They go through a detailed derivation of Lagrange's dual equations of motion using dual numbers, dual vectors, and the dual inertia operator, defined therein. They tie this derivation to Newton-Euler dynamics as the projection onto the generalized axes of the problem. The paper concludes with two major points. One of them is mentioning how their equations of motion could be extended to include the dynamics of a serial manipulator. The second one is an example that includes a fixed-base robotic manipulator with two dual degrees of freedom: each dual angle is composed of an angle and a translation, effectively modeling a revolute and prismatic joint.

The Newton-Euler view of rigid body rotational dynamics using quaternions was first derived in [39, 40]. These equations arise as the rotational component of the 6-DOF equations of motion when cast in dual quaternion form. This derivation makes use of the concept of *vector* quaternions and *vector* dual quaternions. This formulation provided a powerful insight into the analogies that exist between modeling rotational-only or rotational-and-translational dynamics respectively, and even deeper implications in terms of control. The Newton-Euler view of dynamics using quaternions provides no particular advantages when modeling rigid body dynamics. In fact, when using quaternions, vector quantities go from three to four components, and the inertia matrix becomes a four-by-four matrix, instead of the commonly used three-by-three real-valued matrix, thus increasing computational effort. However, this formulation of the equations of motion in dual quaternion form compactly represents the rotational and translational dynamics for rigid bodies. The algebra utilized is familiar to the practitioner by extension of the well-known quaternion algebra, and the variables for the most part represent a physical quantity. This latter characteristic is lost when quaternions or dual quaternions are used as generalized coordinates to derive the dynamics.

Wu et al. in [41] propose an inertial navigation system using dual quaternions. The formulation allows to simplify the number of equations, as well as to use the versatility of quaternions to perform the transformations between the large amount of frames involved in the formulation: Earth, inertial, thrust velocity, and body frames. Additionally, [41] provides an analytical derivation for the error of a dual quaternion formulation as opposed to a screw-based formulation when used for rigid body motion. The authors demonstrated that dual quaternions are better suited to model the translational dynamics, especially if large attitude maneuvers are involved.

In [42], Han et al. provide a kinematic feedback law that uses the logarithm of the dual quaternion, a strategy with roots in the treatement of mechanical systems in Lie group theory. They address the issue of kinematic stabilization, dynamic stabilization and dynamic tracking, and provide controllers for each of the cases without proof. The authors also pro-

vide simple purely kinematic examples in SE(2) to show the usefulness of their control. Their dual quaternion controllers outperform the conventional Lie group theory controller for SE(2).

The modeling and control of 6-DOF rigid body motion has naturally received a lot of attention. Dual quaternions arised as a natural tool to deal with this area of research. In [43], the authors propose a PID controller based on dual quaternions. In [44, 40], Wang et al. make use of dual quaternion algebra to establish finite time controllers for relative navigation. In [45, 46, 47, 48], Filipe et al. proposed a series of control laws that perform pose-tracking. In [49], Seo proposed another tracking controller that makes use of the non-certainty equivalence principle for fast convergence of his adaptive pose-tracking controller. For an overview of pose control methods for spacecraft the interested reader is referred to [50].

Lee and Mesbahi in [51, 52, 53] used dual quaternions to tackle the problem of guidance and control during rendezvous and docking, and powered descent. Their method introduces line-of-sight and glide-slope constraints in dual quaternion form, allowing them to introduce the constraints into their control laws for their MPC framework.

In [54, 55, 56], Wang et al. made use of dual quaternions to establish the control of a distributed network of satellites without a leader. The papers break from other work in the field in the sense that it proposes a singularity-free approach, that is not restricted to attitude synchronization.

One of the main uses of screw-theory and dual quaternions is in the area of motion estimation. In particular, the work of Bayro-Corrochano and Zhang in [57] for estimation using line features in the realm of screw theory is worth emphasizing. In [58, 59], Zu et al. made use of dual quaternions for distributed estimation. Filipe et al. [60] made use of a minimal representation of rigid body motion in the context of dual quaternions, by exploiting dual quaternion constraints. This minimal representation has been further used by Hou et al. in [61] and Yuan et al. [62] to perform relative pose estimation, while

incorporating dynamics and increasing fault tolerance.

It is worth emphasizing that dual quaternions inherit the unwinding phenomenon from quaternion algebra [39]. The unwinding phenomenon describes a large rotation undergone by a rigid body aiming to find the equilibrium point, even though an equivalent physical equilibrium might exist that is closer to the initial attitude. This phenomenon is a physical consequence of the topological structure of $\mathcal{S}^3$, the unit sphere in $\mathbb{R}^4$, and the fact that quaternions are a double covering of SO(3). This structure leads to any given rotation having two corresponding quaternions. In [63], the authors discuss a robust approach to kinematic stabilization that directly deals with this ambiguity. Simpler strategies exist such as those proposed by Han et al. in [42]. In [64] the authors address robust global stabilization at the dynamic level, building upon a control law first proposed in [65].

1.2.3 Dynamic Modeling of Spacecraft-Mounted Robotic Manipulators

The modeling of the dynamics of spacecraft-mounted robotic manipulators is of utmost importance to the successful use of robots in space. The principles of conservation of linear and angular momentum invalidate the simple, kinematically-driven approaches that can be used for fixed-base manipulators. In this section we discuss the main literature dealing with the modeling and control of these systems.

In [66], Hooker aims to derive the equations of motion for a satellite-mounted multibody system with general configuration such that the reaction forces and torques at the joints are not explicit in the formulation. In his derivation, Hooker aims to expose the body axes so that it is convenient to incorporate control laws, internal forces and other disturbance forces into the model that would not be straightforward to introduce using a Lagrangian formulation. Hooker's approach is based on the addition of the independent equations of motion for each of the bodies to cancel the reaction forces, and the cancellation of reaction torques through clever manipulation of the equations of motion. This leads to a system of equations where the unknowns are the angular acceleration of the base, and

the generalized accelerations at the joints.

In [20], Longman et al. developed a model for the operation of a robotic arm mounted on the Space Shuttle when attitude control is enabled. They develop a forward and inverse kinematic model based on an initial determination of where the center of mass of the system is. This allows for identification of where the satellite-body is in inertial space as a function of joint angles, enabling a custom-derived solution of the forward and inverse kinematics problem. The authors then provide an approach to extract the reaction forces and torques applied on the satellite base due to the robotic arm through the extension of results derived using a fixed-base approach.

In [21, 67, 68, 69], Vafa and Dubowsky introduce and apply the concept of the virtual manipulator, which has a virtual ground at the system center of mass. The virtual manipulator is connected through a spherical joint, whose rotations represent the rotations of the base. Rotations, or displacements, about virtual revolute or prismatic joints represent equivalent actual motion about the spacecraft joints. The length of the links of the virtual manipulator are related through a function of the mass of each of the links of the actual spacecraft, and their geometry. The authors suggest that the virtual manipulator be used to simplify the inverse kinematics problem, computation of the system workspace, path planning, and to simplify the analysis, design and control of robotic manipulators in space. For instance, in the case in which the attitude of the base is fixed, the workspace for the virtual manipulator, computed through conventional fixed-based methods, is equivalent to the workspace of the actual manipulator. Furthermore, since the virtual ground is fixed in inertial space, the inverse dynamics problem becomes a simple inverse kinematics problem, as with a fixed-base. Finally, for a desired change in the attitude of the base represented in Euler angles, the authors suggest a method that relies on the cyclic motion of the generalized joint coordinate to achieve it. This allows for general joint trajectories to be performed, with pauses to re-orient the spacecraft base as needed. It is worth emphasizing that this method would introduce unnecessary actuation of the joints, increasing wear of the joint

actuators. However, what the authors do not mention is the fact that this is a first attempt at using the non-holonomic structure of the system to control the base.

Longman [70] studied the generalization of kinematics, inverse kinematics, and robot workspace for the case of a free-floating spacecraft. In this paper, Longman studied the dynamics of the system when the attitude control of the base is disabled, a clear departure from previous work introduced by the same author. Longman also postulated that any attitude can be achieved for the base by actuation of the robotic arm for his specific configuration, and calls the problem of matching initial and final attitudes of the base the "satellite mounted robot inverse dynamics" problem. His approach uses a standard derivation of the derivative of the angular momentum, in combination with a seven-step procedure to achieve this attitude re-orientation of the base. It is also presented that the reachable workspace of the robot arm is a sphere for the free-floating case, and that in a majority of cases, this region is larger than in the case in which the attitude of the base is constant, or inertially fixed.

When it comes to mounting a robotic manipulator on a spacecraft, the development of the equations of motion is not as straightforward, due to the complex interaction between reaction forces that arise at the joints. In [71], a landmark reference in manipulator modeling, Umetani et al. developed the equations of motion for systems with rotational joints and an uncontrolled (not actively controlled) base. Their formulation introduces the concept of *Generalized Jacobian Matrix* (GJM) to solve the inverse kinematics for the generalized velocities that achieve a desired end effector motion. They do this by eliminating base-related kinematics through the use of constraints on the linear and angular momenta of the system. Their approach allows for precise control of the end effector, with minimum or zero fuel usage when the trajectory is in the workspace of the robot. Umetani also highlights the difficulty of studying kinematics of a robotic arm on a free base, stating that since in general pose is history-dependent, it is preferable to work with rates of change of the configuration variables, instead of attempting to model or control their actual values in closed form.

Umetani restricted his application to rotational joints, even though his approach can be extended to prismatic joints as well.

In [22], Masutani et al. inherit the model developed by Umetani and Yoshida which makes use of the GJM. In this paper, they proposed a control law that achieves asymptotic stabilization of the end effector's position and attitude (pose), through feedback constructed geometrically relative to the pose of the target frame. In fact, the GJM is explicitly used in the feedback law and the proof of convergence is done using Lyapunov's direct method. It is worth emphasizing that the authors use LaSalle's invariance principle, thus this proof is not easily extensible to a time-varying desired pose. Additionally, the result is not global, as conditions on the linear and angular parts of the GJM exist, among other constraints. In [72], the same authors analyze a linearized version of the dynamics. In simulation, they show that the performance of the controller when the GJM is substituted by the conventional Jacobian, which is much less computationally intensive, improves with the ratio of masses of the base and the arm.

In [73], Dubowsky et al. dealt with the problem of thruster, or joint actuator saturation as an integral part of path-planning for the manipulators. They argued that for fixed-base manipulators much of the literature focused on minimum-time path planning. However, larger manipulator speeds imply larger disturbances for on-orbit manipulators. Their model consists of a nine-generalized-coordinate system, and they derived the equations of motion using the Lagrangian approach, involving a $9 \times 9 \times 9$ tensor to compute the Coriolis-like term. Their path-planning approach consists of re-casting the equations of motion as a function of a single variable that parametrizes the position and orientation of the end-effector, and determining its dynamics as a function of thruster or actuation inputs. This allows the comutation of the maximum acceleration of this path variable, so that the end effector can physically keep up with the proposed maneuver.

In [74], Dubowsky and Torres make use of the Disturbance Map (DM) proposed in [21], and the Enhanced Disturbance Map (EDM), for path planning purposes. This map can be

computed from knowledge of the configuration-dependent mass matrix of the whole system, and it is given relative to the spacecraft body axes. The authors argue that trajectories parallel to contours of minimum disturbance will minimize fuel usage of the reaction control system. Additionally, they emphasize that fuel usage due to linear disturbances is less than the fuel usage due to attitude disturbances, as well as the fact that a manipulator system is not usually expected to operate under conditions where its attitude or velocity are changing rapidly. The authors then show applications of the proposed method through three different and insightful examples showing that, in fact, making use of the EDM in preparation for a trajectory, or for path planning, can lead to a decrease in fuel consumption.

In [75], Nakamura and Mukerjee introduced the use of holonomicity in the analysis of the equations of motion. These emphasize that, even though the linear and angular momentum conservation equations are a function of the velocities, the linear conservation momentum is simply a function of the center of mass location. This point can in fact be described through the use of generalized coordinates, without the need of generalized velocities, making it a holonomic constraint. In fact, Longman provides an example of this in [20]. In [75], Nakamura and Mukherjee make use of the non-holonomic constraints in order to control the attitude of the satellite using only the motion of the joints. The approach uses the generalized velocities of the joints and Lypanuvov's direct method to avoid neglecting higher order terms, as was done in [21]. Most importantly, the paper introduces a hierarchical construction of the invariant sets other than the desired equilibrium point to aid the convergence of its proposed control law.

Nakamura and Mukherjee delve deeper into formalizing the analysis of the holonomicity of a space robot in [76]. They do this by using the concepts of Lie brackets, and involutivity of the linear space spanned by the vector fields of the system, which they then apply on a given PUMA-type structure mounted on a free-floating base. They then introduce the bi-directional approach, which consists of having a virtual robot with the same dynamics whose initial condition is the desired state. Through design of an appropriate control input

for both systems, if the error dynamics of these robotic arms converge to zero, then the actual control (joint generalized velocities) is just a reflection of the virtual system's control input reflected and shifted in the time domain. The authors do state that while this approach is better than the one in [75], the result is still not global.

In [77], West et al. develop an algorithm to estimate the mass properties of a robotic arm experimentally. They argued that this estimation in general is useful in three broad classes of problems: dynamic modeling, static modeling to counteract for gravitational loads on joints, and static modeling for compensation of gravitational forces for space emulation systems. The authors in [77] show how to derive non-redundant moment equations so that the parameter identification problem can be solved efficiently using a least squares approach. The authors gathered experimental force and moment data for different robot configurations and orientations of the base, which is mounted on a Stewart mechanism through a 6-DOF.

In [78, 79], Papadopoulos and Dubowsky succinctly describe the equations of motion for a robotic arm on a satellite under the assumption of zero initial angular momentum using the *Routhian* and a compact representation of the kinetic energy of the system. The authors proceed to argue that fixed-base and space-based manipulators can *almost* always be controlled using the same control algorithms, given the structural similarities between the model matrices. In [80], Papadopoulos and Dubowsky rewrite the equations of motion of the satellite-mounted robot arm, but this time include actuation of the satellite base, and embed them in a quasi-Lagrangian approach. In [80], the authors' proposed control algorithm becomes a modification of the operational space controller, well-known in fixed-base robot control literature.

Papadopoulos and Dubowsky study dynamic singularities of free-floating robotic arms in [81]. The authors provide the form of a Jacobian that relates the end-effector's linear and angular velocity in inertial space to the joint angular velocities. The singular points of this Jacobian lead to dynamic singularities, namely, singularities that are dependent upon the

mass and inertia properties of the system. The authors also argue that a given end-effector configuration can be achieved with infinite base attitudes, some of which can be singular. For this reason, singularities are called *path dependent*. After introducing the concepts of Path Dependent Workspace (PDW), which includes all points in the reachable workspace that can be reached in a singular configuration, and Path Independent Workspace (PIW), the authors conclude with a planar 5-DOF example and demonstrate their algorithm. In his doctoral work [82], Papadopoulos compiles these results and additionally addresses the topic of failure recovery.

In [4], Xu and Shum developed a dynamical model for a robotic arm mounted on a satellite base in the absence of thruster jets. This implies that the motion of the system obeys linear and angular momentum conservation, a fundamental fact in their derivation. The authors then made use of the GJM to characterize the motion of the end effector as a function of the generalized joint states, as well as those of the base. They used the Lagrangian formulation to derive the dynamics in both the joint space coordinates, and in the inertial coordinates. They also derive a regulator controller that ensures asymptotic convergence to the inertial coordinate, given that the target state is in the non-singular workspace of the robot. Finally, they derived an asymptotically stable tracking controller, which they then simulate successfully.

In [83], Spofford and Akin studied the use of space manipulators for tele-operations. They argue that experimental validation and verification can be performed underwater for robotic systems designed for space, given that drag and buoyancy effects are taken into account. An example of one such operator was the Beam Assembly Teleoperator (BAT) at NASA Marshall Space Flight Center. In this paper, the authors propose a kinematic control law for joint generalized velocities, as a function of desired end effector linear and angular velocities expressed in the inertial frame. They propose the use of pseudo-inverse gradient (PI) control to aid in the minimization of motion-related cost functions, without modifying the desired end effector velocities. Additionally, they introduced reaction compensation

generation, and devise a *blending* method to combine it with PI control. The approach aims to deal with trajectories that would otherwise encounter singular configurations of the robotic arm. The different suggested potential functions used in [83] capture information of the *manipulability* of the end-effector, joint limits, and position of the satellite base.

In [84], Caccavale and Siciliano, making use of the generalized Jacobian, make use of quaternions for attitude representation of the base. They proposed a joint velocity control law that uses the vector part of the quaternion error as feedback, even though this quaternion is computed from the product of rotation matrices. The authors make use of the redundant degrees of freedom to, in a prioritized manner using projections, control the attitude of the spacecraft while maneuvering the manipulator.

In [85], Nanos and Papadopoulos propose a framework that allows keeping the end-effector fixed in space the presence of angular momentum. The authors provide analytic equations of motion, which they use to describe the constant angular momentum of the system, and the fixed linear and angular of the end-effector to incorporate into the formulation as a constraint. In [86], Nanos and Papadopoulos extend their initial results from [85] to include general cartesian or joint-space tracking. The authors also prove several useful properties of the dynamic matrices that appear in the equations of motion for a robotic arm on a spacecraft under non-zero angular momentum conditions, properties then used in the proofs of their controller's stability. The authors argue that the structure is similar to that of a fixed-base robotic manipulator under the influence of a gravitational field.

In [87, 88], Nanos and Papadopoulos address the avoidance of dynamic singularities for free-floating spacecraft. Reference [87] addresses the case of zero-angular momentum and a straight path to be followed by the end-effector, while in [88] the case of non-zero angular momentum and general end-effector path is addressed. The dynamics used are those derived in [81], in combination with facts contained in [85]. The dynamic singularities are defined as the set of configurations that make the generalized Jacobian singular. The authors propose a framework to determine the initial attitude of the base that will allow a

predetermined path to pass through the Path Dependent Workspace, where singularities are possible.

Starting in the 90's, the use of adaptive control methods was incorporated into the study of robotic arms mounted on a satellite. Xu et al. in [89] proposed an adaptive control method that requires the attitude of the base to be actively controlled. In [90] the authors removed this condition, but introduced an outer-loop estimation of the dynamic parameters, allowing them to generate more precise trajectories, without guarantees of stability when the desired reference of the end effector is given in the inertial space.

Walker and Wee in [91] provided the equations of motion and an adaptive control method for a six degree of freedom robotic arm on a satellite base. The method incorporates three reaction wheels and the equations are derived using the Lagrangian formulation. They eliminate the velocity of the satellite base from this formulation, given the constraint of no external forces on the system, without necessarily assuming that the initial momenta of the system are zero. Their proposed adaptive controller can track desired joint angles and desired attitude of the base when the dynamic parameters of the system are uncertain. This, however, cannot ensure that there is tracking of a reference in inertial space.

Yoshida et al. in [92], and Dimitrov in [15] discuss in detail the problem of capturing a tumbling spacecraft. In [92], the authors explain that appropriate planning and allocation of the momentum of the system in the pre-capture phase can enable better controllability in the post-capture phase. The three control strategies are named bias momentum approach for the pre-impact phase, impedance control during impact, and distributed momentum control during post-impact. Their control laws aim at minimizing the transfer of angular momentum from the tumbling body to the satellite base of the chaser. In [15], Dimitrov also expands on the analysis of holonomic and scleronomic constraints (a function of the configuration, but not explicitly of time) present in a robotic system, using an approach reminiscent of Kane's formulation of dynamics. This way, Dimitrov models not only open loop (tree) manipulators, but also closed loop configurations.

Cong et al. [93] also deal with the capture of a tumbling object using two arms in serial configuration, and adaptive control. The author builds on the work of Dimitrov et al., except it is now done adaptively. The mass properties are the object of the adaptation, and the system angular velocity is proven to be asymptotically stable, but there are no assurances about the convergence of the parameters.

Stoneking in [94] provides one of the key results, that will drive the development of the dual quaternion framework for multi-body modeling in this dissertation. Stoneking proposes an approach which exposes the reaction forces of the system, solved for by a matrix inversion that also yields linear and angular accelerations. Stoneking proposes a decoupling of the equations for users not interested in the reaction forces at the joints. Furthermore, he provides a formulation for the case in which the joints are not given by a simple primitive (revolute or prismatic). Bishop et al. in [95] use this method for path planning and control during rapid maneuvering of a robotic arm mounted on a spacecraft. Stoneking in [96] also proposed an approach based on Kane's equations of motion, in which the generalized coordinates appear as part of a minimal representation. In this case, extracting knowledge about the reaction forces and torques at the joints, which are of particular interest during design phases, becomes a more complicated task.

In 2000, Carignan proposed a recursive Newton-Euler algorithm in [97] applied to spacecraft multibody systems. The algorithm is easy to implement and has been well adopted by the engineering community. As an example, work by Dubanchet [17] hinges on this dynamics framework to implement H_∞ control on a linearized version of the plant with the objective of designing a debris collection robotic manipulator in space. Rodriguez, Jain and Kreutz-Delgado in [98, 99, 100] provide a multibody dynamics framework based on Spatial Operator Algebra. Work by Featherstone and Orin [101] and Featherstone [102] provide generalizable and efficient algorithms to model multibody dynamics in the context of Spatial Vector Algebra (SVA). The SVA-based approach reformulates the recursive Newton-Euler algorithm to avoid the decoupling of the rotational and translational dynam-

ics. In Section 9.3 of [102] the author specializes his algorithm to free-floating bases. Another numerical algorithm for dynamics is proposed by Mohan and Sasha in [103], which claims to be even more efficient than the one by Featherstone.

Given that the modeling and control of spacecraft-mounted robotic manipulators started in the early 70's, several references are worth highlighting. In particular, Dubowsky provides a review of related literature up to 1993 in [104]. Ellery [105] provides a wide summary of land-mark papers up to 2004, emphasizing that dynamic analysis algorithms should have the following properties: versatility, adaptability, reliability, computational efficiency, and user friendliness. Moosavian and Papadopoulos [106] summarize common methods and issues that occur in modeling and control of such systems.

Software has also been developed to model general dynamical systems. For example, Moosavian describes SPACEMAPLE in [107], a tool that uses an analytical formulation of the Lagrangian equations of motion. At Tohoku University in Japan, Kazuya Yoshida and his research team developed the SpaceDyn toolbox, which is available online. The toolbox uses a recursive Newton-Euler approach, as proposed in [97]. Other open source toolboxes include SPART [108], developed specifically for spacecraft-mounted manipulators, DART [109], which is aimed for general multibody systems, among others conveniently listed in [110]. Commercial software packages also exist. Among these, SD/FAST [111] is a commonly used software package for spacecraft modeling.

In this large literature for dynamic modeling of spacecraft-mounted robotic manipulators, dual quaternions are mentioned and used, surprisingly perhaps, only a few times. In particular, Dooley and McCarthy [23] proposed using dual quaternions as generalized coordinates, while Brodsky and Shoham [38] proposed a rigorous dual-number based methodology that resulted in a Lagrangian-like framework. Brodsky and Shoham did draw parallelisms with a Newton-Euler-type equation, but these were always projected onto the dual axes of motion for the cases concerning serial manipulators, obscuring any potential insight into the reaction forces and torques at the joints. The lack of previous work us-

ing dual quaternions in a classical Newton-Euler framework to model serial manipulator systems on a spacecraft motivated the work of this dissertation.

1.3 Research Focus and Contributions

The objective of this dissertation will be to provide a unified framework to model the different phases of a capture mission using dual quaternion algebra. We now describe how the content in each of the chapters advances us towards that objective.

Chapter 1: Literature Review - This chapter has focused on providing the motivating force behind why there should be an interest in robotic servicing in space, and in a more pointed manner, setting the ground for the exploration of multibody systems mounted on a spacecraft. The literature review provides the required background for 6-DOF pose control of a rigid body spacecraft and an extensive description of prior work in the field of multibody systems in space, for both dynamics and control. The background material is observed from a point of view that is interested in the use an application of dual quaternions.

Chapter 2: Dual Quaternions - This chapter provides a thorough introduction to dual quaternions. Starting from the Clifford algebra $C\ell^{+}_{0,3,1}$, the properties of general dual quaternions are provided, followed by a development and introduction to dual quaternions for pose representation and encoding of physical quantities, laying the machinery for the use of dual quaternions in a broad range of applications. This is followed by a careful treatment of wrench transformations and the representation of physical quantities, like dual momentum and kinetic energy, followed by a subsequent statement of important equations such as Newton-Euler dynamic equation of motion in dual quaternion algebra. Important proofs that have been left out in the existind dual quaternion literature are provided in this chapter.

Chapter 3: Dual Quaternions in Robotics - This chapter provides insight into

the use of dual quaternion tools in robotic manipulation. In particular, it aims at collecting the most important results from the disperse robotics literature in dual quaternions into one single place. A clear omission in this chapter is any treatment of inverse kinematics, which for fixed-base robots has been extensively treated in dual quaternions, e.g. [26, 25]. Important results from the field of EDL [112] are reimagined for dual quaternion-based robotics. This chapter concludes with basic examples on how to perform forward kinematics of simple robots.

Chapter 4: Adaptive Control with Concurrent Learning - In this chapter the author provides the first major contribution of the dissertation - an adaptive pose-tracking controller for a rigid body spacecraft with strong assurances regarding the convergence of the estimated parameters. The controller is an extension of an existing pose-tracking controller first proposed in [47] and corrected in [50] for a typo. The proposed controller uses concurrent learning in a continuous-time sense, a concept that to the best of the author's knowledge has never been proposed. Subsequently, a discretized concurrent learning version of the controller is provided, which more in line with the work proposed in [113]. Finally, we provide a direct link between rank-type conditions that arise in concurrent learning to guarantee parameter convergence, and the persistency of excitation condition that usually arises in adaptive controllers. It is shown that these are one and the same, and that the concurrent-learning matrix tested for its rank is just one more factor contributing to the positive definiteness in the persistency of excitation test.

Chapter 5: Dynamics of a Spacecraft with One Manipulator - The kinematics and dynamics of a spacecraft with one robotic arm are provided in this chapter. The development of the equations is done in two different approaches. The first one is an extension of the work in [94] to allow the inclusion of revolute joints, as opposed to simpler-to-model spherical joints. The second method used to capture the dynamics

of the model is an original approach based on dual quaternion Newton-Euler dynamics. The methodology is analogous to that provided in [94], but the acceleration-level constraints are formulated differently, and captured in one single, straight-forward relationship. Additionally, the structure used of the resulting system of equations allows for a simple inversion based on the Schur-complement. This approach, compared to [94], avoids complicated model-reduction strategies to avoid computation of undesired reaction forces and torques.

Chapters 6 and 7: Framework Generalization - In these chapters, the generalization of the dynamic system modeling derived in Chapter 5 is provided, as well as an example of a large multibody system with 11 bodies. The generalization allows the use of five different types of joints (revolute, prismatic, spherical, cylindrical, and Cartesian) and is given in the context of dual quaternions. This has particular advantages when it comes to the treatement of joint-dependent quantities which would usually require one type of equation for a rotation-focused joint and another type of equation for a translation-focus joint. The framework, as is clear from the developments through chapters 5 and 6, is not iterative in nature, since it relies on solving a system of equations to determine the dual accelerations of the bodies and the reaction wrenches.

Chapter 8: Control of a Spacecraft-Mounted Manipulator - Next, the use of Differential Dynamic Programming (DDP) is proposed to perform end-effector pose control of a spacecraft-mounted manipulator. The kinematics of the end-effector are derived using dual quaternion algebra, and introduced into the proposed cost functional. The two control tasks performed include a stabilization and tracking. The latter involves a helicoidal motion parameterized using dual-quaternion screw theory. To aid the convergence of the DDP framework, singular configurations of the manipulator are penalized using soft keep-out constraints. Compared to existing

works in the literature of on-orbit robot control, this numerical approach is based on optimal control theory and it allows penalizing the application of forces at the base, which reduces fuel consumption, a valuable expendable in space.

Chapter 9: Estimation for a Spacecraft-Mounted Manipulator - The final major contribution in this dissertation concludes with the formulation of an estimation algorithm that adaptively and aggressively estimates the mass parameters of the different links in a multibody system. The algorithm makes use of the concurrent learning framework again, but close attention is paid to the efficiency and optimization of the implementation. The task at hand is to estimate 77 parameters. When no modification to the adaptive estimation law is performed, this convergence happens slowly. However, when an SVD-based modification to the control is applied, the estimation happens almost instantaneously.

Chapter 10: Conclusions and Future Work - The last chapter provides concluding thoughts, and potentially fruitful research directions in this area.

CHAPTER 2

DUAL QUATERNIONS

This chapter will lay the mathematical foundation on which this dissertation will be based. In particular, we will build up to dual quaternions as our selected tool for robotic modeling. We will highlight how both quaternion and dual quaternion algebras arise in two frameworks with equivalent mathematical structure. The first framework develops quaternions and dual quaternions as a Clifford algebra. The second approach uses Hamilton's proposed quaternion group elements, yielding two different algebras of interest to us, which depend on the chosen field. Furthermore, an overview of how these two algebras fit in the context of pose and kinematic modeling is provided.

2.1 Clifford Algebras

Quaternions and dual quaternions have a formal mathematical definition in the realm of Clifford algebras, and their relation to geometric algebras is explained in depth in [114]. These are unital and associative algebras over a vector space V with a quadratic form $v^2 = Q(v),\ v \in V$. The basis elements are commonly denoted by e_i, where $e_0 = 1$ is the unit, or scalar. The set of basis vectors $\{e_1, \dots e_n\}$ is the *standard* basis for V. Each of these basis elements satisfy $e_i^2 \in \{+1, -1, 0\}$. Clifford algebras are commonly denoted by $C\ell_{p,q,r}(V, Q)$, or $C\ell(p, q, r)$ when the vector space and quadratic form have been previously defined. The elements (p, q, r) are called the signature of the algebra, and they satisfy $n = p + q + r$, where n is the dimension of V. In general, the basis elements

e_i satisfy

$$e_i^2 = \begin{cases} +1 & \text{if} \quad i \in \{1, \ldots, p\}, \\ -1 & \text{if} \quad i \in \{p+1, \ldots, p+q\}, , \\ 0 & \text{if} \quad i \in \{p+q+1, \ldots, n\}. \end{cases} \tag{2.1}$$

The pairwise product of basis vectors satisfies the anti-commutativity property

$$e_i e_j = -e_j e_i \quad \text{if} \quad i \neq j. \tag{2.2}$$

The product of the basis vectors form the different basis elements, or monomials, of the Clifford algebra. For notational simplicity, this product will be displayed as

$$e_{abc\ldots d} \triangleq e_a e_b e_c \ldots e_d, \quad \{a, b, c, \ldots, d\} \subseteq \{1, \ldots, n\}. \tag{2.3}$$

Any product of monomials can be simplified using equations (2.1) and (2.2) so that each e_i appears at most once per element of the Clifford algebra. If in addition,

$$e_{k_1 k_2 \ldots k_p} \triangleq e_{k_1} e_{k_2} \ldots e_{k_p}, \quad k_i \in \{1, \ldots, n\} \tag{2.4}$$

satisfies $0 < k_1 < k_2 < \cdots < k_p$, then we say that $e_{k_1 k_2 \ldots k_p}$ is grade-p, or $e_{k_1 k_2 \ldots k_p} \in \bigwedge^p V$, the $p-$th exterior algebra of V.

This simplification gives rise to a canonical basis for the Clifford algebra described as

$$C\ell(p, q, r) = \bigoplus_{i=0}^{n} \bigwedge {}^i V \tag{2.5}$$

We highlight that the even-graded elements of $C\ell(p, q, r)$ and the unit e_0 form a sub-algebra. That is,

$$C\ell^+(p, q, r) = \bigoplus_{\substack{i=0 \\ i \text{ even}}}^{n} \bigwedge {}^i V \tag{2.6}$$

is closed under multiplication since the basis vectors cancel out in pairs.

We demonstrate how general and relevant Clifford algebras can be with a simple example.

Example 1. Take the Clifford algebra $C\ell(0,1,0)(\mathbb{R}, -v_1^2)$. Then, $V = \mathbb{R}$ and the quadratic form is given by $Q(v) = -v_1^2$ for $v = v_1 e_1 \in V, v_1 \in \mathbb{R}$. The standard basis is $\{e_0, e_1\}$, with $e_0 = 1$ and $e_1^2 = -1$. An element of the Clifford algebra will have the form $z = xe_0 + ye_1 = x + ye_1$, where $x, y \in \mathbb{R}$.. The product of two elements of the algebra can be computed as follows:

$$\begin{aligned}
z_1 z_2 &= (x_1 e_0 + y_1 e_1)(x_2 e_0 + y_2 e_1) \\
&= x_1 e_0 x_2 e_0 + x_1 e_0 y_2 e_1 + y_1 e_1 x_2 e_0 + y_1 e_1 y_2 e_1 \\
&= x_1 x_2 (1)^2 + x_1 y_2 (1) e_1 + y_1 x_2 e_1 (1) + y_1 y_2 e_1^2 \\
&= x_1 x_2 (1)^2 + x_1 y_2 e_1 + y_1 x_2 e_1 + y_1 y_2 (-1) \\
&= (x_1 x_2 - y_1 y_2) + (x_1 y_2 + y_1 x_2) e_1 \\
&= (x_1 x_2 - y_1 y_2) e_0 + (x_1 y_2 + y_1 x_2) e_1
\end{aligned}$$

We see from inspection that elements of this algebra multiply in the same way that complex numbers do. This equivalence is easier to appreciate if we represent the canonical basis element e_1 with j, the letter commonly used to represent the complex unit j. The latter has the well-known property that $j^2 = -1$, much like our element e_1. It is worth highlighting that the underlying field of the vector space is the real numbers.

2.2 Quaternions

We now illustrate the relationship between Clifford algebras and quaternions. Consider the algebra $C\ell_{(0,2,0)}(\mathbb{R}^2, Q(v))$, with standard basis elements (or basis vectors) $\{e_1, e_2\}$ satisfying $e_1^2 = e_2^2 = -1$, and quadratic form $Q(v) = -v_1^2 - v_2^2$ for a given element $v = v_1 e_1 + v_2 e_2$.

The canonical basis for this algebra is given by $\{e_0, e_1, e_2, e_{12}\} = \{1, e_1, e_2, e_{12}\}$. Then, the following relationships hold:

$$e_{12}^2 = e_{12}e_{12} = e_1e_2e_1e_2 = -e_1e_1e_2e_2 = -e_1^2e_2^2 = -(-1)(-1) = -1 \tag{2.7}$$

$$e_1e_2e_{12} = e_1e_2e_1e_2 = -e_1e_1e_2e_2 = -e_1^2e_2^2 = -(-1)(-1) = -1 \tag{2.8}$$

The group of quaternions as defined by Hamilton in 1843 extends the well-known imaginary unit j, which satisfies $j^2 = -1$. This non-abelian group is defined by the presentation $Q_8 \triangleq \{-1, i, j, k : i^2 = j^2 = k^2 = ijk = -1\}$. The algebra constructed from Q_8 over the field of real numbers is the quaternion algebra, $\mathbb{H}$. We define quaternions as $\mathbb{H} \triangleq \{q = q_0 + q_1i + q_2j + q_3k : i^2 = j^2 = k^2 = ijk = -1,\ q_0, q_1, q_2, q_3 \in \mathbb{R}\}$. This defines an associative, non-commutative, division algebra.

Comparing the definitions and relationships between the different elements of $C\ell_{(0,2,0)}$ and $\mathbb{H}$, it is clear that $C\ell_{(0,2,0)} \cong \mathbb{H}$, where the basis elements can be matched as described in Table 2.1.

Table 2.1: Matching of Clifford algebra elements and quaternion algebra elements.

$C\ell_{(0,2,0)}$	$\mathbb{H}$
e_0	1
e_1	i
e_2	j
e_{12}	k

In practice, quaternions are often referred to by their scalar and vectors parts as $q = (q_0, \overline{q})$, where $q_0 \in \mathbb{R}$ and $\overline{q} = [q_1, q_2, q_3]^{\mathrm{T}} \in \mathbb{R}^3$. The properties of quaternion algebra are summarized in Table 2.2. Previous literature has defined quaternion multiplication as the multiplication between a 4×4 matrix and a vector in $\mathbb{R}^4$ [65].

Since any rotation can be described by three parameters, the unit norm constraint is imposed on quaternions for attitude representation. *Unit* quaternions are closed under mul-

Table 2.2: Quaternion Operations

Operation	Definition
Addition	$a + b = (a_0 + b_0, \bar{a} + \bar{b})$
Multiplication by a scalar	$\lambda a = (\lambda a_0, \lambda a)$
Multiplication	$ab = (a_0 b_0 - \bar{a} \cdot \bar{b}, a_0 \bar{b} + b_0 \bar{a} + \bar{a} \times \bar{b})$
Conjugate	$a^* = (a_0, -\bar{a})$
Dot product	$a \cdot b = (a_0 b_0 + \bar{a} \cdot \bar{b}, 0_{3\times 1}) = \frac{1}{2}(a^* b + b^* a)$
Cross product	$a \times b = (0, a_0 \bar{b} + b_0 \bar{a} + \bar{a} \times \bar{b}) = \frac{1}{2}(ab - b^* a^*)$
Norm	$\|a\| = \sqrt{a \cdot a}$
Scalar part	$\mathrm{sc}\big(a\big) = (a_0, 0_{3\times 1})$
Vector part	$\mathrm{vec}\big(a\big) = (0, \bar{a})$

tiplication, but not under addition. A quaternion describing the orientation of frame X with respect to frame Y, $q_{\text{X/Y}}$, satisfies $q^*_{\text{X/Y}} q_{\text{X/Y}} = q_{\text{X/Y}} q^*_{\text{X/Y}} = \mathtt{1}$, where $\mathtt{1} \triangleq (1, \bar{0}_{3\times 1})$. This quaternion can be constructed as $q_{\text{X/Y}} = (\cos(\phi/2), \bar{n}\sin(\theta/2))$, where $\bar{n}$ and θ are the *unit* Euler axis, and Euler angle of the rotation respectively. It is worth emphasizing that $q^*_{\text{Y/X}} = q_{\text{X/Y}}$, and that $q_{\text{X/Y}}$ and $-q_{\text{X/Y}}$ represent the same rotation. Furthermore, given quaternions $q_{\text{Y/X}}$ and $q_{\text{Z/Y}}$, the quaternion describing the rotation from X to Z is given by $q_{\text{Z/X}} = q_{\text{Y/X}} q_{\text{Z/Y}}$. For completeness purposes, we define $\mathtt{0} \triangleq (0, \bar{0}_{3\times 1})$.

Three-dimensional vectors can also be interpreted as special cases of quaternions. Specifically, given $\bar{s}^{\text{X}} \in \mathbb{R}^3$, the coordinates of a vector expressed in frame X, its quaternion representation is given by $s^{\text{X}} = (0, \bar{s}^{\text{X}}) \in \mathbb{H}^v$, where $\mathbb{H}^v$ is the set of *vector* quaternions defined as $\mathbb{H}^v \triangleq \{(q_0, \bar{q}) \in \mathbb{H} : \ q_0 = 0\}$ (see [50] for further information). The change of the reference frame on a vector quaternion is achieved by the adjoint operation, and is given by $s^{\text{Y}} = q^*_{\text{Y/X}} s^{\text{X}} q_{\text{Y/X}}$. Additionally, given $s \in \mathbb{H}^v$, we can define the operation $[\cdot]^\times : \mathbb{H}^v \to \mathbb{R}^{4\times 4}$ as

$$[s]^\times = \begin{bmatrix} 0 & 0_{1\times 3} \\ 0_{3\times 1} & [\bar{s}]^\times \end{bmatrix}, \quad \text{where } [\bar{s}]^\times = \begin{bmatrix} 0 & -s_3 & s_2 \\ s_3 & 0 & -s_1 \\ -s_2 & s_1 & 0 \end{bmatrix}. \tag{2.9}$$

For quaternions $a = (a_0, \overline{a})$ and $b = (b_0, \overline{b}) \in \mathbb{H}$, the left and right quaternion multiplication operators $[\![\cdot]\!]_{\text{L}}, [\![\cdot]\!]_{\text{R}} : \mathbb{H} \to \mathbb{R}^{4\times 4}$ will be defined as

$$[\![a]\!]_{\text{L}} * b \triangleq [\![b]\!]_{\text{R}} * a \triangleq ab, \tag{2.10}$$

where

$$[\![a]\!]_{\text{L}} = \begin{bmatrix} a_0 & -a_1 & -a_2 & -a_3 \\ a_1 & a_0 & -a_3 & a_2 \\ a_2 & a_3 & a_0 & -a_1 \\ a_3 & -a_2 & a_1 & a_0 \end{bmatrix} = \begin{bmatrix} a_0 & -\overline{a}^{\text{T}} \\ \overline{a} & a_0 I_3 + [\overline{a}]^{\times} \end{bmatrix}, \tag{2.11}$$

$$[\![b]\!]_{\text{R}} = \begin{bmatrix} b_0 & -b_1 & -b_2 & -b_3 \\ b_1 & b_0 & b_3 & -b_2 \\ b_2 & -b_3 & b_0 & b_1 \\ b_3 & b_2 & -b_1 & b_0 \end{bmatrix} = \begin{bmatrix} b_0 & -\overline{b}^{\text{T}} \\ \overline{b} & b_0 I_3 - [\overline{b}]^{\times} \end{bmatrix}. \tag{2.12}$$

The three-dimensional attitude kinematics evolve as

$$\dot{q}_{\text{X/Y}} = \tfrac{1}{2} q_{\text{X/Y}} \omega^{\text{X}}_{\text{X/Y}} = \tfrac{1}{2} \omega^{\text{Y}}_{\text{X/Y}} q_{\text{X/Y}}, \tag{2.13}$$

where $\omega^{\text{Z}}_{\text{X/Y}} \triangleq (0, \overline{\omega}^{\text{Z}}_{\text{X/Y}}) \in \mathbb{H}^v$ and $\overline{\omega}^{\text{Z}}_{\text{X/Y}} \in \mathbb{R}^3$ is the angular velocity of frame X with respect to frame Y expressed in Z-frame coordinates.

Let I be the inertial frame of reference, B a frame fixed on the rigid body, and D a desired reference frame. The kinematic equation of motion for the B and D frames relative to the inertial frame is given, respectively, by

$$\dot{q}_{\text{B/I}} = \tfrac{1}{2} q_{\text{B/I}} \omega^{\text{B}}_{\text{B/I}}, \quad \text{and} \quad \dot{q}_{\text{D/I}} = \tfrac{1}{2} q_{\text{D/I}} \omega^{\text{D}}_{\text{D/I}}. \tag{2.14}$$

The attitude error kinematic equation of motion between two non-inertial frames, whose

relative orientation is described by $q_{\text{B/D}}$, can be easily derived to be

$$\dot{q}_{\text{B/D}} = \tfrac{1}{2} q_{\text{B/D}} \omega^{\text{B}}_{\text{B/D}}, \tag{2.15}$$

where $\omega^{\text{B}}_{\text{B/D}} = \omega^{\text{B}}_{\text{B/I}} - \omega^{\text{B}}_{\text{D/I}} = \omega^{\text{B}}_{\text{B/I}} - q^{*}_{\text{B/D}} \omega^{\text{D}}_{\text{D/I}} q_{\text{B/D}}$.

2.3 Dual Quaternions

Let us now consider the Clifford algebra $C\ell^{+}_{(0,3,1)}(\mathbb{R}^4, Q(v))$. Its standard basis (or basis vectors) are $\{e_1, e_2, e_3, e_4\}$ satisfying $e_1^2 = e_2^2 = e_3^2 = -1$ and $e_4^2 = 0$. The quadratic form in this case is degenerate and given by $Q(v) = -v_1^2 - v_2^2 - v_3^2$ for a given element $v = v_1 e_1 + v_2 e_2 + v_3 e_3 + v_4 e_4 \in \mathbb{R}^4$. The canonical basis for this even-graded Clifford algebra is given by $\{e_0, e_{12}, e_{13}, e_{14}, e_{23}, e_{24}, e_{34}, e_{1234}\}$. Using basic properties of Clifford algebra vectors shows that the following relationships hold:

$$e_{12} e_{13} = -e_{21} e_{13} = e_{23} \tag{2.16}$$

$$e_{12}^2 = e_{13}^2 = e_{23}^2 = e_{12} e_{13} e_{23} = -1 \tag{2.17}$$

$$e_{1234} e_{12} = -e_{34},\ e_{1234} e_{13} = e_{24},\ e_{1234} e_{23} = -e_{14} \tag{2.18}$$

$$e_{1234} e_{12} = e_{12} e_{1234},\ e_{1234} e_{13} = e_{13} e_{1234},\ e_{1234} e_{23} = e_{23} e_{1234} \tag{2.19}$$

$$e_{1234} e_{34} = e_{1234} e_{24} = e_{1234} e_{14} = 0 \tag{2.20}$$

$$e_{1234}^2 = -e_{123} e_4^2 e_{123} = 0. \tag{2.21}$$

These properties, closely correspond to the properties of the dual quaternion group. Before we define dual quaternions, we will provide a tip of historical background.

In his paper *Preliminary Sketch of Biquaternions* (1873) [115], Clifford introduces the concept of biquaternion: a mathematical object of the form $s + \omega t$, where $s, t \in \mathbb{H}$, and ω has the especial property that $\omega^2 = 0$. Clifford's intended purpose for biquaternions was to model the division of motors arising in screw theory. Rooney in [116] provides an

extended summary of the content of Clifford's original paper, and a thorough analysis of the importance of biquaternions.

Today, we adopt the name *dual quaternions* for this algebra, instead of Clifford's proposed name of biquaternions. The term biquaternion in modern mathematical language has been reserved to signify three possible entities arising from the complexification of quaternions [117]. In each of the cases, a biquaternion can be described as $q = w + xi + yj + zk$, where i, j and k are the familiar quaternion group elements. The differences arise in the field or ring to which the coefficients belong, such that if

$$w,\ x,\ y,\ z \in \begin{cases} \mathbb{C} & \text{then } q \text{ is an ordinary biquaternion} \\ {}^1\mathbb{C} & \text{then } q \text{ is an ordinary split-biquaternion} \\ \mathbb{D} & \text{then } q \text{ is a dual quaternion.} \end{cases} \tag{2.22}$$

The fields correspond to the complex numbers $\mathbb{C}$ and the split-complex numbers ${}^1\mathbb{C} = \{z | z = x + jy,\ \forall x, y \in \mathbb{R},\ j^2 = +1\}$, while the dual numbers $\mathbb{D} = \{z | z = x + \epsilon y,\ \forall x, y \in \mathbb{R},\ \epsilon \neq 0, \epsilon^2 = 0\}$ define a ring (no inverse exists if $x \neq 0$), where ϵ is known as the dual unit.

With this in mind, we define the dual quaternion group as

$$\begin{aligned} \mathbb{Q}_d := \{-1, i, j, k, \epsilon, \epsilon i, \epsilon j, \epsilon k : \quad & i^2 = j^2 = k^2 = ijk = -1, \\ & \epsilon i = i\epsilon, \epsilon j = j\epsilon, \epsilon k = k\epsilon, \epsilon \neq 0, \epsilon^2 = 0\}. \end{aligned} \tag{2.23}$$

Dual quaternion algebra arises as the algebra of the dual quaternion group $\mathbb{Q}_d$ over the field of real numbers, and is denoted as $\mathbb{H}_d$. When dealing with the modeling of mechanical systems, it is convenient to define this algebra as $\mathbb{H}_d = \{\boldsymbol{q} = q_r + \epsilon q_d : q_r, q_d \in \mathbb{H}\}$, where ϵ is the dual unit. We call q_r the real part, and q_d the dual part of the dual quaternion $\boldsymbol{q}$.

It is now natural to observe the similarities between this dual quaternion algebra, as

originally devised by Clifford in 1873, and $C\ell^{+}(0,3,1)$. Table 2.3 lists the matching of each of the terms. Thus, we say that there exists an the isomorphism $C\ell^{+}(0,3,1) \cong \mathbb{H}_d$.

Table 2.3: Matching of Clifford algebra elements and dual quaternion algebra elements.

$C\ell^{+}_{0,3,1}$	$\mathbb{H}_d$
e_0	1
e_{12}	i
e_{13}	j
e_{23}	k
e_{34}	ϵi
e_{24}	$-\epsilon j$
e_{14}	ϵk
e_{1234}	$-\epsilon$

Filipe et al. [47, 60, 50, 48] have laid out much of the groundwork in terms of the notation and basic properties of dual quaternions. The main properties of dual quaternion algebra are listed in Table 2.4. Filipe et al. [65] also conveniently define a multiplication between matrices and dual quaternions, denoted by the $\star$ operator, that resembles the well-known matrix-vector multiplication by simply representing the dual quaternion coefficients as a vector in $\mathbb{R}^8$. A property that arises from the definition of the circle product for dual quaternions is given by

$$\boldsymbol{a}^{\mathsf{s}} \circ \boldsymbol{b}^{\mathsf{s}} = \boldsymbol{a} \circ \boldsymbol{b} = \boldsymbol{b} \circ \boldsymbol{a}. \tag{2.24}$$

Analogous to the set of vector quaternions $\mathbb{H}^v$, we can define the set of vector dual quaternions as $\mathbb{H}^v_d \triangleq \{\boldsymbol{q} = q_r + \epsilon q_d : \ q_r, q_d \in \mathbb{H}^v\}$. Vector dual quaternions have special properties of interest in the study of kinematics, dynamics and control of rigid bodies. The two main properties are listed below, where $\boldsymbol{a}, \boldsymbol{b} \in \mathbb{H}^v_d$:

$$\boldsymbol{a} \circ (\boldsymbol{b}\boldsymbol{c}) = \boldsymbol{b}^{\mathsf{s}} \circ (\boldsymbol{a}^{\mathsf{s}}\boldsymbol{c}^{*}) = \boldsymbol{c}^{\mathsf{s}} \circ (\boldsymbol{b}^{*}\boldsymbol{a}^{\mathsf{s}}), \tag{2.25}$$

Table 2.4: Dual Quaternion Operations

Operation	Definition
Addition	$\boldsymbol{a}+\boldsymbol{b}=(a_r+b_r)+\epsilon(a_d+b_d)$
Multiplication by a scalar	$\lambda\boldsymbol{a}=(\lambda a_r)+\epsilon(\lambda a_d)$
Multiplication	$\boldsymbol{ab}=(a_r b_r)+\epsilon(a_d b_r+a_r b_d)$
Conjugate	$\boldsymbol{a}^*=(a_r^*)+\epsilon(a_d^*)$
Dot product	$\boldsymbol{a}\cdot\boldsymbol{b}=(a_r\cdot b_r)+\epsilon(a_d\cdot b_r+a_r\cdot b_d)=\frac{1}{2}(\boldsymbol{a}^*\boldsymbol{b}+\boldsymbol{b}^*\boldsymbol{a})$
Cross product	$\boldsymbol{a}\times\boldsymbol{b}=(a_r\times b_r)+\epsilon(a_d\times b_r+a_r\times b_d)=\frac{1}{2}(\boldsymbol{ab}-\boldsymbol{b}^*\boldsymbol{a}^*)$
Circle product	$\boldsymbol{a}\circ\boldsymbol{b}=(a_r\cdot b_r+a_d\cdot b_d)+\epsilon 0$
Swap	$\boldsymbol{a}^{\mathsf{s}}=a_d+\epsilon a_r$
Norm	$\|a\|=\sqrt{a\circ a}$
Vector part	$\mathrm{sc}\big(\boldsymbol{a}\big)=\mathrm{sc}\big(a_r\big)+\epsilon\mathrm{sc}\big(a_d\big)$
Vector part	$\mathrm{vec}\big(\boldsymbol{a}\big)=\mathrm{vec}\big(a_r\big)+\epsilon\mathrm{vec}\big(a_d\big)$

$$\boldsymbol{a}\circ(\boldsymbol{b}\times\boldsymbol{c})=\boldsymbol{b}^{\mathsf{s}}\circ(\boldsymbol{c}\times\boldsymbol{a}^{\mathsf{s}})=\boldsymbol{c}^{\mathsf{s}}\circ(\boldsymbol{a}^{\mathsf{s}}\times\boldsymbol{b}). \tag{2.26}$$

For vector dual quaternions we will define the skew-symmetric operator $[\,\cdot\,]^\times:\mathbb{H}_d^v\to\mathbb{R}^{8\times 8}$,

$$[\boldsymbol{s}]^\times=\begin{bmatrix}[s_r]^\times & 0_{4\times 4}\\ [s_d]^\times & [s_r]^\times\end{bmatrix}. \tag{2.27}$$

For dual quaternions $\boldsymbol{a}=a_r+\epsilon a_d$ and $\boldsymbol{b}=b_r+\epsilon b_d\in\mathbb{H}_d$, the left and right dual quaternion multiplication operators $\llbracket\,\cdot\,\rrbracket_{\mathrm{L}},\llbracket\,\cdot\,\rrbracket_{\mathrm{R}}:\mathbb{H}_d\to\mathbb{R}^{8\times 8}$ are defined as

$$\boldsymbol{ab}\triangleq\llbracket\boldsymbol{a}\rrbracket_{\mathrm{L}}\star\boldsymbol{b}\triangleq\llbracket\boldsymbol{b}\rrbracket_{\mathrm{R}}\star\boldsymbol{a}, \tag{2.28}$$

where

$$\llbracket\boldsymbol{a}\rrbracket_{\mathrm{L}}=\begin{bmatrix}\llbracket a_r\rrbracket_{\mathrm{L}} & 0_{4\times 4}\\ \llbracket a_d\rrbracket_{\mathrm{L}} & \llbracket a_r\rrbracket_{\mathrm{L}}\end{bmatrix}\quad\text{and}\quad\llbracket\boldsymbol{b}\rrbracket_{\mathrm{R}}=\begin{bmatrix}\llbracket b_r\rrbracket_{\mathrm{R}} & 0_{4\times 4}\\ \llbracket b_d\rrbracket_{\mathrm{R}} & \llbracket b_r\rrbracket_{\mathrm{R}}\end{bmatrix}. \tag{2.29}$$

Since rigid body motion has six degrees of freedom, a dual quaternion needs two con-

straints to parameterize it. The dual quaternion describing the relative pose of frame B relative to I is given by $\boldsymbol{q}_{\mathrm{B/I}} = q_{\mathrm{B/I},r} + \epsilon q_{\mathrm{B/I},d} = q_{\mathrm{B/I}} + \epsilon \frac{1}{2} q_{\mathrm{B/I}} r^{\mathrm{B}}_{\mathrm{B/I}}$, where $r^{\mathrm{B}}_{\mathrm{B/I}}$ is the position quaternion describing the location of the origin of frame B relative to that of frame I, expressed in B-frame coordinates. It can be easily observed that $q_{\mathrm{B/I},r} \cdot q_{\mathrm{B/I},r} = \mathtt{1}$ and $q_{\mathrm{B/I},r} \cdot q_{\mathrm{B/I},d} = \mathtt{0}$, where $\mathtt{0} = (0, \bar{0})$, providing the two necessary constraints. Thus, a dual quaternion representing a pose transformation is a *unit* dual quaternion, since it satisfies $\boldsymbol{q} \cdot \boldsymbol{q} = \boldsymbol{q}^* \boldsymbol{q} = \mathbf{1}$, where $\mathbf{1} \triangleq \mathtt{1} + \epsilon \mathtt{0}$. Additionally, we also define $\mathbf{0} \triangleq \mathtt{0} + \epsilon \mathtt{0}$. Analogous to normalization in the space of quaternions, a dual quaternion can be forced to satisfy the unit and orthogonality constraints. For a given unit dual quaternion $\boldsymbol{q} \in \mathbb{H}_d$, a method of enforcing the constraints is given by [50]

$$\begin{aligned} \boldsymbol{q}_r &\coloneqq \frac{\boldsymbol{q}_r}{\|\boldsymbol{q}_r\|}, \\ \boldsymbol{q}_d &\coloneqq \left(I_{4\times 4} - \frac{\boldsymbol{q}_r \boldsymbol{q}_r^{\mathrm{T}}}{\|\boldsymbol{q}_r\|^2} \right) \boldsymbol{q}_d. \end{aligned} \tag{2.30}$$

Similar to the standard quaternion relationships, the frame transformations laid out in Table 2.5 can be easily verified. In [50] it was proven that for a dual unit quaternion $\boldsymbol{q} \in \mathbb{H}_d$,

Table 2.5: Unit Dual Quaternion Operations

Composition of rotations	$\boldsymbol{q}_{\mathrm{Z/X}} = \boldsymbol{q}_{\mathrm{Y/X}} \boldsymbol{q}_{\mathrm{Z/Y}}$
Inverse, Conjugate	$\boldsymbol{q}^*_{\mathrm{Y/X}} = \boldsymbol{q}_{\mathrm{X/Y}}$

$\boldsymbol{q}$ and $-\boldsymbol{q}$ represent the same frame transformation, property inherited from the space of quaternions. Therefore, as is done in practice for quaternions, dual quaternions can be subjected to properization, which is the action of redefining a dual quaternion so that the scalar part of the quaternion is always positive. Formally, we can define the properization of a dual quaternion $\boldsymbol{q} = q_r + \epsilon q_d$ as

$$\boldsymbol{q} \coloneqq -\boldsymbol{q} \qquad \text{if} \quad (q_r)_0 < 0, \tag{2.31}$$

where $(q_r)_0$ is the scalar part of q_r.

The following two results will be used throughout this dissertation. The first result deals with the transformation invariance of the dual quaternion cross product operation.

Lemma 1. *The dual quaternion cross product is invariant to frame transformations. Specifically,*

$$\boldsymbol{a}^{\mathrm{Y}} \times \boldsymbol{b}^{\mathrm{Y}} = (\boldsymbol{q}^{*}_{\mathrm{Y/X}} \boldsymbol{a}^{\mathrm{X}} \boldsymbol{q}_{\mathrm{Y/X}}) \times (\boldsymbol{q}^{*}_{\mathrm{Y/X}} \boldsymbol{b}^{\mathrm{X}} \boldsymbol{q}_{\mathrm{Y/X}}) = \boldsymbol{q}^{*}_{\mathrm{Y/X}} (\boldsymbol{a}^{\mathrm{X}} \times \boldsymbol{b}^{\mathrm{X}}) \boldsymbol{q}_{\mathrm{Y/X}}. \tag{2.32}$$

Proof. From the definition of the dual quaternion cross product given in Table 2.4, we have that

$$\begin{aligned}
\boldsymbol{q}^{*}_{\mathrm{Y/X}} (\boldsymbol{a}^{\mathrm{X}} \times \boldsymbol{b}^{\mathrm{X}}) \boldsymbol{q}_{\mathrm{Y/X}} &= \boldsymbol{q}^{*}_{\mathrm{Y/X}} (\boldsymbol{a}^{\mathrm{X}} \boldsymbol{b}^{\mathrm{X}} - (\boldsymbol{b}^{\mathrm{X}})^{*} (\boldsymbol{a}^{\mathrm{X}})^{*}) \boldsymbol{q}_{\mathrm{Y/X}} \\
&= \boldsymbol{q}^{*}_{\mathrm{Y/X}} \boldsymbol{a}^{\mathrm{X}} \boldsymbol{b}^{\mathrm{X}} \boldsymbol{q}_{\mathrm{Y/X}} - \boldsymbol{q}^{*}_{\mathrm{Y/X}} (\boldsymbol{b}^{\mathrm{X}})^{*} (\boldsymbol{a}^{\mathrm{X}})^{*} \boldsymbol{q}_{\mathrm{Y/X}} \\
&= \boldsymbol{q}^{*}_{\mathrm{Y/X}} \boldsymbol{a}^{\mathrm{X}} \boldsymbol{q}_{\mathrm{Y/X}} \boldsymbol{q}^{*}_{\mathrm{Y/X}} \boldsymbol{b}^{\mathrm{X}} \boldsymbol{q}_{\mathrm{Y/X}} - \boldsymbol{q}^{*}_{\mathrm{Y/X}} (\boldsymbol{b}^{\mathrm{X}})^{*} \boldsymbol{q}_{\mathrm{Y/X}} \boldsymbol{q}^{*}_{\mathrm{Y/X}} (\boldsymbol{a}^{\mathrm{X}})^{*} \boldsymbol{q}_{\mathrm{Y/X}} \\
&= (\boldsymbol{q}^{*}_{\mathrm{Y/X}} \boldsymbol{a}^{\mathrm{X}} \boldsymbol{q}_{\mathrm{Y/X}}) \times (\boldsymbol{q}^{*}_{\mathrm{Y/X}} \boldsymbol{b}^{\mathrm{X}} \boldsymbol{q}_{\mathrm{Y/X}}) \\
&= \boldsymbol{a}^{\mathrm{Y}} \times \boldsymbol{b}^{\mathrm{Y}}.
\end{aligned} \tag{2.33}$$

■

The following lemma recasts the identity operation on a dual quaternion in terms of the left and right dual quaternion multiplication operations. For this result, and the entirety of this dissertation, we will denote the n-by-n identity matrix as $\mathbb{I}_n$.

Lemma 2. *Given unit $\boldsymbol{q} \in \mathbb{H}_d$, the left and right dual quaternion multiplication matrix operators satisfy the following identities:*

$$\begin{aligned}
[\![\boldsymbol{q}]\!]_{\mathrm{L}} [\![\boldsymbol{q}^{*}]\!]_{\mathrm{R}} [\![\boldsymbol{q}^{*}]\!]_{\mathrm{L}} [\![\boldsymbol{q}]\!]_{\mathrm{R}} &= \mathbb{I}_8 \\
[\![\boldsymbol{q}^{*}]\!]_{\mathrm{L}} [\![\boldsymbol{q}]\!]_{\mathrm{R}} [\![\boldsymbol{q}]\!]_{\mathrm{L}} [\![\boldsymbol{q}^{*}]\!]_{\mathrm{R}} &= \mathbb{I}_8.
\end{aligned} \tag{2.34}$$

Proof. To prove the first equality, let us apply the left-hand-side on the generic dual quaternion $\boldsymbol{a} \in \mathbb{H}_d$ and apply the definition of the multiplication matrix operators given in equa-

tion (2.28) as

$$\begin{aligned}
[\![\boldsymbol{q}]\!]_{\mathrm{L}}[\![\boldsymbol{q}^*]\!]_{\mathrm{R}}[\![\boldsymbol{q}^*]\!]_{\mathrm{L}}[\![\boldsymbol{q}]\!]_{\mathrm{R}} \star \boldsymbol{a} &= [\![\boldsymbol{q}]\!]_{\mathrm{L}}[\![\boldsymbol{q}^*]\!]_{\mathrm{R}}[\![\boldsymbol{q}^*]\!]_{\mathrm{L}} \star \boldsymbol{a}\boldsymbol{q} \\
&= [\![\boldsymbol{q}]\!]_{\mathrm{L}}[\![\boldsymbol{q}^*]\!]_{\mathrm{R}} \star (\boldsymbol{q}^*\boldsymbol{a}\boldsymbol{q}) \\
&= [\![\boldsymbol{q}]\!]_{\mathrm{L}} \star (\boldsymbol{q}^*\boldsymbol{a}\boldsymbol{q})\boldsymbol{q}^* \\
&= \boldsymbol{q}(\boldsymbol{q}^*\boldsymbol{a}\boldsymbol{q})\boldsymbol{q}^*,
\end{aligned} \tag{2.35}$$

and since $\boldsymbol{q}\boldsymbol{q}^* = \boldsymbol{q}\boldsymbol{q}^* = \mathbf{1}$, the result follows. The second equality is proven analogously.

■

A useful equation is the generalization of the velocity of a rigid body in dual form, which contains both the linear and angular velocity components. The dual velocity of the Y-frame with respect to the Z-frame, expressed in X-frame coordinates, is defined as

$$\boldsymbol{\omega}^{\mathrm{X}}_{\mathrm{Y/Z}} = \boldsymbol{q}^*_{\mathrm{X/Y}}\boldsymbol{\omega}^{\mathrm{Y}}_{\mathrm{Y/Z}}\boldsymbol{q}_{\mathrm{X/Y}} = \omega^{\mathrm{X}}_{\mathrm{Y/Z}} + \epsilon(v^{\mathrm{X}}_{\mathrm{Y/Z}} + \omega^{\mathrm{X}}_{\mathrm{Y/Z}} \times r^{\mathrm{X}}_{\mathrm{X/Y}}), \tag{2.36}$$

where $\omega^{\mathrm{X}}_{\mathrm{Y/Z}} = (0, \bar{\omega}^{\mathrm{X}}_{\mathrm{Y/Z}})$ and $v^{\mathrm{X}}_{\mathrm{Y/Z}} = (0, \bar{v}^{\mathrm{X}}_{\mathrm{Y/Z}})$, $\bar{\omega}^{\mathrm{X}}_{\mathrm{Y/Z}}$ and $\bar{v}^{\mathrm{X}}_{\mathrm{Y/Z}} \in \mathbb{R}^3$ are respectively the angular and linear velocity of the Y-frame with respect to the Z-frame expressed in X-frame coordinates, and $r^{\mathrm{X}}_{\mathrm{X/Y}} = (0, \bar{r}^{\mathrm{X}}_{\mathrm{X/Y}})$, where $\bar{r}^{\mathrm{X}}_{\mathrm{X/Y}} \in \mathbb{R}^3$ is the position vector from the origin of the Y-frame to the origin of the X-frame expressed in X-frame coordinates. In particular, from equation (2.36) we observe that the dual velocity of a rigid body assigned to frame $\mathfrak{o}_i$ with respect to the inertial frame, expressed in $\mathfrak{o}_i$-frame coordinates is given as $\boldsymbol{\omega}^{\mathfrak{o}_i}_{\mathfrak{o}_i/I} = \omega^{\mathfrak{o}_i}_{\mathfrak{o}_i/I} + \epsilon v^{\mathfrak{o}_i}_{\mathfrak{o}_i/I}$.

In general, the dual quaternion kinematics can be expressed as [65]

$$\dot{\boldsymbol{q}}_{\mathrm{X/Y}} = \tfrac{1}{2}\boldsymbol{q}_{\mathrm{X/Y}}\boldsymbol{\omega}^{\mathrm{X}}_{\mathrm{X/Y}} = \tfrac{1}{2}\boldsymbol{\omega}^{\mathrm{Y}}_{\mathrm{X/Y}}\boldsymbol{q}_{\mathrm{X/Y}}. \tag{2.37}$$

One of the key advantages of dual quaternions is the resemblance, in form, of the *pose* error kinematic equations of motion to the attitude-only error kinematics. The pose error

kinematic equations of motion between non-inertial frames B and D, are given by

$$\dot{\boldsymbol{q}}_{\mathrm{B/D}} = \tfrac{1}{2}\boldsymbol{q}_{\mathrm{B/D}}\boldsymbol{\omega}^{\mathrm{B}}_{\mathrm{B/D}}, \tag{2.38}$$

where $\boldsymbol{\omega}^{\mathrm{B}}_{\mathrm{B/D}} = \boldsymbol{\omega}^{\mathrm{B}}_{\mathrm{B/I}} - \boldsymbol{\omega}^{\mathrm{B}}_{\mathrm{D/I}} = \boldsymbol{\omega}^{\mathrm{B}}_{\mathrm{B/I}} - \boldsymbol{q}^{*}_{\mathrm{B/D}}\boldsymbol{\omega}^{\mathrm{D}}_{\mathrm{D/I}}\boldsymbol{q}_{\mathrm{B/D}}$.

2.3.1 Wrench Notation and Transformations Using Dual Quaternions

In order to take full advantage of the potential of dual quaternions in the context of dynamic modeling of multibody systems, we have to specify how forces and torques are shifted from one frame to another. This will allow us, for example, to easily shift the application of a reaction force at a joint onto the center of mass of a given body, among other applications. A wrench $\boldsymbol{W}^{\mathrm{Z}}(O_p) \in \mathbb{H}^{v}_{d}$ expressed in Z-frame coordinates can be expressed in terms of its components as

$$\boldsymbol{W}^{\mathrm{Z}}(O_p) = f^{\mathrm{Z}} + \epsilon\tau^{\mathrm{Z}}, \tag{2.39}$$

where $f^{\mathrm{Z}} = (0, \bar{f}^{\mathrm{Z}}),\ \tau^{\mathrm{Z}} = (0, \bar{\tau}^{\mathrm{Z}}) \in \mathbb{H}^{v}$ represent force and torque quaternions applied at point O_p as shown in Figure 2.1. Equivalently, we can describe the effect of f^{Z} and τ^{Z} about another point O_q as

$$\boldsymbol{W}^{\mathrm{Z}}(O_q) = f^{\mathrm{Z}} + \epsilon(\tau^{\mathrm{Z}} + r^{\mathrm{Z}}_{\mathrm{p/q}} \times f^{\mathrm{Z}}), \tag{2.40}$$

where the extra torque term is due to the moment arm from point O_q to point O_p, captured by the position vector $r^{\mathrm{Z}}_{\mathrm{p/q}}$. Applying a frame transformation operation on a wrench about point O_{X} expressed in X-frame coordinates, given by $\boldsymbol{W}^{\mathrm{X}}(O_{\mathrm{X}}) = f^{\mathrm{X}} + \epsilon\tau^{\mathrm{X}}$, yields the

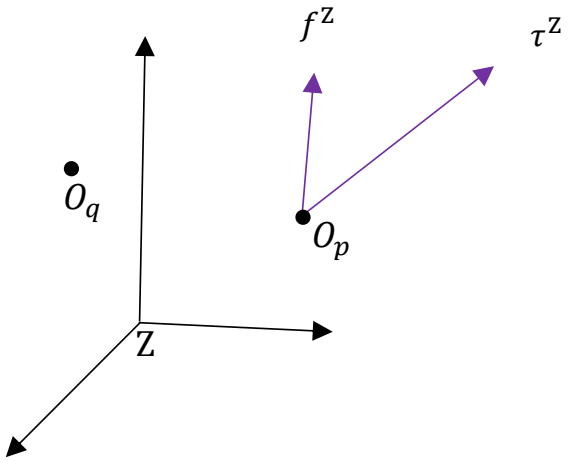

Figure 2.1: Wrench interpretation.

following expression

$$
\begin{aligned}
\boldsymbol{W}^{\mathrm{Y}}(O_{\mathrm{Y}}) &= \boldsymbol{q}^{*}_{\mathrm{Y/X}} \boldsymbol{W}^{\mathrm{X}}(O_{\mathrm{X}}) \boldsymbol{q}_{\mathrm{Y/X}} \\
&= (q_{\mathrm{Y/X}} + \epsilon \tfrac{1}{2} r^{\mathrm{X}}_{\mathrm{Y/X}} q_{\mathrm{Y/X}})^{*} (f^{\mathrm{X}} + \epsilon \tau^{\mathrm{X}})(q_{\mathrm{Y/X}} + \epsilon \tfrac{1}{2} r^{\mathrm{X}}_{\mathrm{Y/X}} q_{\mathrm{Y/X}}) \\
&= (q^{*}_{\mathrm{Y/X}} + \epsilon \tfrac{1}{2} q^{*}_{\mathrm{Y/X}} r^{\mathrm{X}*}_{\mathrm{Y/X}})(f^{\mathrm{X}} + \epsilon \tau^{\mathrm{X}})(q_{\mathrm{Y/X}} + \epsilon \tfrac{1}{2} r^{\mathrm{X}}_{\mathrm{Y/X}} q_{\mathrm{Y/X}}) \\
&= (q^{*}_{\mathrm{Y/X}} - \epsilon \tfrac{1}{2} q^{*}_{\mathrm{Y/X}} r^{\mathrm{X}}_{\mathrm{Y/X}})(f^{\mathrm{X}} + \epsilon \tau^{\mathrm{X}})(q_{\mathrm{Y/X}} + \epsilon \tfrac{1}{2} r^{\mathrm{X}}_{\mathrm{Y/X}} q_{\mathrm{Y/X}}) \\
&= (q^{*}_{\mathrm{Y/X}} - \epsilon \tfrac{1}{2} q^{*}_{\mathrm{Y/X}} r^{\mathrm{X}}_{\mathrm{Y/X}})(f^{\mathrm{X}} q_{\mathrm{Y/X}} + \epsilon(\tau^{\mathrm{X}} q_{\mathrm{Y/X}} + f^{\mathrm{X}} \tfrac{1}{2} r^{\mathrm{X}}_{\mathrm{Y/X}} q_{\mathrm{Y/X}})) \\
&= q^{*}_{\mathrm{Y/X}} f^{\mathrm{X}} q_{\mathrm{Y/X}} - \epsilon(\tfrac{1}{2} q^{*}_{\mathrm{Y/X}} r^{\mathrm{X}}_{\mathrm{Y/X}} f^{\mathrm{X}} q_{\mathrm{Y/X}}) + \epsilon(q^{*}_{\mathrm{Y/X}} \tau^{\mathrm{X}} q_{\mathrm{Y/X}} + q^{*}_{\mathrm{Y/X}} f^{\mathrm{X}} \tfrac{1}{2} r^{\mathrm{X}}_{\mathrm{Y/X}} q_{\mathrm{Y/X}}) \\
&= f^{\mathrm{Y}} + \epsilon(\tau^{\mathrm{Y}} + \tfrac{1}{2} q^{*}_{\mathrm{Y/X}} f^{\mathrm{X}} q_{\mathrm{Y/X}} q^{*}_{\mathrm{Y/X}} r^{\mathrm{X}}_{\mathrm{Y/X}} q_{\mathrm{Y/X}} - \tfrac{1}{2} q^{*}_{\mathrm{Y/X}} r^{\mathrm{X}}_{\mathrm{Y/X}} q_{\mathrm{Y/X}} q^{*}_{\mathrm{Y/X}} f^{\mathrm{X}} q_{\mathrm{Y/X}}) \\
&= f^{\mathrm{Y}} + \epsilon(\tau^{\mathrm{Y}} + \tfrac{1}{2} f^{\mathrm{Y}} r^{\mathrm{Y}}_{\mathrm{Y/X}} - \tfrac{1}{2} r^{\mathrm{Y}}_{\mathrm{Y/X}} f^{\mathrm{Y}}) \\
&= f^{\mathrm{Y}} + \epsilon(\tau^{\mathrm{Y}} + \tfrac{1}{2} f^{\mathrm{Y}} r^{\mathrm{Y}}_{\mathrm{Y/X}} - \tfrac{1}{2} (r^{\mathrm{Y}}_{\mathrm{Y/X}})^{*} (f^{\mathrm{Y}})^{*}),
\end{aligned}
$$

and by the definition of the cross product of two pure quaternion quantities given in Table 2.4, we get that

$$\begin{aligned}\boldsymbol{W}^{\mathrm{Y}}(O_{\mathrm{Y}}) &= \boldsymbol{q}^{*}_{\mathrm{Y/X}}\boldsymbol{W}^{\mathrm{X}}(O_{\mathrm{X}})\boldsymbol{q}_{\mathrm{Y/X}} \\ &= f^{\mathrm{Y}} + \epsilon(\tau^{\mathrm{Y}} + f^{\mathrm{Y}} \times r^{\mathrm{Y}}_{\mathrm{Y/X}}) \\ &= f^{\mathrm{Y}} + \epsilon(\tau^{\mathrm{Y}} + r^{\mathrm{Y}}_{\mathrm{X/Y}} \times f^{\mathrm{Y}}). \end{aligned} \tag{2.41}$$

The transformation described by equation (2.41) implies that, given the dual force (e.g., force and torque) applied on a body at location O_{X}, the equivalent wrench about a different location O_{Y} can be computed by using a simple frame transformation operation, commonly known as the *shifting law*. As expected, the transformation changes the reference frame in which the original (X-frame) force and torque are being expressed, but it also adds a torque term that arises due to the lever of the force f^{X} with respect to the new reference point O_{Y}.

Equivalently, the following transformation of $\boldsymbol{W}^{\mathrm{Y}}(O_{\mathrm{Y}}) = f^{\mathrm{Y}} + \epsilon\tau^{\mathrm{Y}}$ can be easily derived:

$$\begin{aligned}\boldsymbol{W}^{\mathrm{X}}(O_{\mathrm{X}}) &= \boldsymbol{q}_{\mathrm{Y/X}}\boldsymbol{W}^{\mathrm{Y}}(O_{\mathrm{Y}})\boldsymbol{q}^{*}_{\mathrm{Y/X}} \\ &= f^{\mathrm{X}} + \epsilon(\tau^{\mathrm{X}} + r^{\mathrm{X}}_{\mathrm{Y/X}} \times f^{\mathrm{X}}). \end{aligned} \tag{2.42}$$

Finally, when using wrenches, subscripts will be used to denote the source of, or a descriptor for, the wrench. For example, $\boldsymbol{W}^{\mathrm{X}}_{\mathrm{ext}}(O_p)$ denotes that the source of the wrench is "ext", which for our case denotes an external force and torque applied at the end effector of the robotic arm. It is worth emphasizing that the wrench transformation can be used to merely change the orientation of the frame on which the wrench is expressed, or to simply translate the origin, without re-orientating the axes.

The frame transformation relationships we have just derived not only apply to wrenches, but also to twists. Therefore, given the twist $\boldsymbol{s}^{\mathrm{X}} = s^{\mathrm{X}}_r + \epsilon s^{\mathrm{X}}_d$ the adjoint transformation can

be described by

$$\begin{aligned} s^{\mathrm{Y}} &= \boldsymbol{q}^{*}_{\mathrm{Y/X}} \boldsymbol{s}^{\mathrm{X}} \boldsymbol{q}_{\mathrm{Y/X}} \\ &= s^{\mathrm{Y}}_{r} + \epsilon (s^{\mathrm{Y}}_{d} + s^{\mathrm{Y}}_{r} \times r^{\mathrm{Y}}_{\mathrm{Y/X}}) \\ &= s^{\mathrm{Y}}_{r} + \epsilon (s^{\mathrm{Y}}_{d} + r^{\mathrm{Y}}_{\mathrm{X/Y}} \times s^{\mathrm{Y}}_{r}). \end{aligned} \tag{2.43}$$

Equivalently, given $\boldsymbol{s}^{\mathrm{Y}} = s^{\mathrm{Y}}_{r} + \epsilon s^{\mathrm{Y}}_{d}$, the inverse adjoint transformation is described by

$$\begin{aligned} \boldsymbol{s}^{\mathrm{X}} &= \boldsymbol{q}_{\mathrm{Y/X}} \boldsymbol{s}^{\mathrm{Y}} \boldsymbol{q}^{*}_{\mathrm{Y/X}} \\ &= s^{\mathrm{X}}_{r} + \epsilon (s^{\mathrm{X}}_{d} + s^{\mathrm{X}}_{r} \times r^{\mathrm{X}}_{\mathrm{X/Y}}) \\ &= s^{\mathrm{X}}_{r} + \epsilon (s^{\mathrm{X}}_{d} + r^{\mathrm{X}}_{\mathrm{Y/X}} \times s^{\mathrm{X}}_{r}). \end{aligned} \tag{2.44}$$

2.3.2 Dual Inertia Matrix, Dual Momentum and 6-DOF Rigid Body Dynamics

The dual inertia matrix for a rigid body can be defined by [65]

$$M_{\mathfrak{o}_{\mathrm{i}}} \triangleq \begin{bmatrix} 1 & 0_{1\times 3} & 0 & 0_{1\times 3} \\ 0_{3\times 1} & m_{\mathfrak{o}_{\mathrm{i}}} I_{3\times 3} & 0_{3\times 1} & 0_{3\times 3} \\ 0 & 0_{1\times 3} & 1 & 0_{1\times 3} \\ 0_{3\times 1} & 0_{3\times 3} & 0_{3\times 1} & \bar{I}_{\mathfrak{o}_{\mathrm{i}}} \end{bmatrix}, \tag{2.45}$$

where $m_{\mathfrak{o}_{\mathrm{i}}} \in \mathbb{R}$ is the mass of the i-th body, $\bar{I}_{\mathfrak{o}_{\mathrm{i}}} \in \mathbb{R}^{3\times 3}$ is the rigid body mass inertia matrix of the i-th body, and $I_{3\times 3}$ is the 3-by-3 identity matrix.

The dual momentum of body i computed about its center of mass and expressed in frame $\mathfrak{o}_i$ can be defined as

$$\boldsymbol{H}^{\mathfrak{o}_{\mathrm{i}}}_{\mathfrak{o}_{\mathrm{i}}}(O_{\mathfrak{o}_{\mathrm{i}}}) = \boldsymbol{H}^{\mathfrak{o}_{\mathrm{i}}}_{\mathfrak{o}_{\mathrm{i}}/\mathrm{I}} \triangleq M_{\mathfrak{o}_{\mathrm{i}}} \star (\boldsymbol{\omega}^{\mathfrak{o}_{\mathrm{i}}}_{\mathfrak{o}_{\mathrm{i}}/\mathrm{I}})^{\mathsf{s}}, \tag{2.46}$$

where the $\star$ operator can be interpreted as conventional matrix-vector multiplication when the dual quaternion is represented as a vector in $\mathbb{R}^8$, and the superscript s denotes the swap

operation defined in Table 2.4. The kinetic energy for a rigid body can be computed as

$$T = \tfrac{1}{2}(\boldsymbol{\omega}^{\mathfrak{o}_i}_{\mathfrak{o}_i/I})^{\mathsf{s}} \circ (M_{\mathfrak{o}_i} \star (\boldsymbol{\omega}^{\mathfrak{o}_i}_{\mathfrak{o}_i/I})^{\mathsf{s}}). \tag{2.47}$$

We can also define the matrix operator $\mathrm{H}(\cdot) : \mathbb{R}^{8\times 8} \to \mathbb{R}^{8\times 8}$ to eliminate the swap operation in a multiplication. Applied on a matrix multiplying a dual quaternion $\boldsymbol{a} \in \mathbb{H}_d$, we have that

$$\mathrm{H}(M) \star \boldsymbol{a} \triangleq M \star \boldsymbol{a}^{\mathsf{s}}. \tag{2.48}$$

In block form, this operator acts on $M \in \mathbb{R}^{8\times 8}$, composed of blocks $M_1, M_2 \in \mathbb{R}^{8\times 4}$, as follows

$$\mathrm{H}(M) = \mathrm{H}([M_1, M_2]) = [M_2, M_1], \tag{2.49}$$

and, in particular, it acts on the dual inertia matrix $M_{\mathfrak{o}_i}$ as

$$\mathrm{H}\left(M_{\mathfrak{o}_i}\right) = \begin{bmatrix} 0 & 0_{1\times 3} & 1 & 0_{1\times 3} \\ 0_{3\times 1} & 0_{3\times 3} & 0_{3\times 1} & m_{\mathfrak{o}_i} I_{3\times 3} \\ 1 & 0_{1\times 3} & 0 & 0_{1\times 3} \\ 0_{3\times 1} & \bar{I}_{\mathfrak{o}_i} & 0_{3\times 1} & 0_{3\times 3} \end{bmatrix}. \tag{2.50}$$

Therefore, we can also write the dual momentum as

$$\boldsymbol{H}^{\mathfrak{o}_i}_{\mathfrak{o}_i/I} = \mathrm{H}\left(M_{\mathfrak{o}_i}\right) \star \boldsymbol{\omega}^{\mathfrak{o}_i}_{\mathfrak{o}_i/I}. \tag{2.51}$$

The following lemma deals with the invertibility of $\mathrm{H}\left(M_{\mathfrak{o}_i}\right)$.

Lemma 3. *The inverse of* $\mathrm{H}\left(M_{\mathfrak{e}_i}\right)$, $\mathrm{H}\left(M_{\mathfrak{e}_i}\right)^{-1}$, *exists and is given by*

$$\mathrm{H}\left(M_{\mathfrak{e}_i}\right)^{-1} = \begin{bmatrix} 0 & 0_{1\times 3} & 1 & 0_{1\times 3} \\ 0_{3\times 1} & 0_{3\times 3} & 0_{3\times 1} & \bar{I}_{\mathfrak{e}_i}^{-1} \\ 1 & 0_{1\times 3} & 0 & 0_{1\times 3} \\ 0_{3\times 1} & \frac{1}{m_{\mathfrak{e}_i}} I_{3\times 3} & 0_{3\times 1} & 0_{3\times 3} \end{bmatrix}. \tag{2.52}$$

Proof. Through evaluation, $\mathrm{H}\left(M_{\mathfrak{e}_i}\right)^{-1}\mathrm{H}\left(M_{\mathfrak{e}_i}\right) = \mathrm{H}\left(M_{\mathfrak{e}_i}\right)\mathrm{H}\left(M_{\mathfrak{e}_i}\right)^{-1} = I_{8\times 8}$. ■

For a multibody system S, with B rigid bodies whose centers of mass are located at $\mathfrak{e}_i$, equation (2.46) can be generalized to

$$\boldsymbol{H}^{\mathrm{I}}_{S}(O_{\mathrm{I}}) = \sum_{i=1}^{\mathrm{B}} \boldsymbol{q}_{\mathfrak{e}_i/\mathrm{I}} \boldsymbol{H}^{\mathfrak{e}_i}_{\mathfrak{e}_i}(O_{\mathfrak{e}_i}) \boldsymbol{q}^{*}_{\mathfrak{e}_i/\mathrm{I}} = \sum_{i=1}^{\mathrm{B}} \boldsymbol{q}_{\mathfrak{e}_i/\mathrm{I}} (M_{\mathfrak{e}_i} \star (\boldsymbol{\omega}^{\mathfrak{e}_i}_{\mathfrak{e}_i/\mathrm{I}})^{\mathsf{s}}) \boldsymbol{q}^{*}_{\mathfrak{e}_i/\mathrm{I}}, \tag{2.53}$$

yielding the dual momentum of the system computed about the origin of the inertial frame and expressed in I-frame coordinates. The kinetic energy of equation (2.47) can be generalized as

$$T = \tfrac{1}{2} \sum_{i=1}^{\mathrm{B}} (\boldsymbol{\omega}^{\mathfrak{e}_i}_{\mathfrak{e}_i/\mathrm{I}})^{\mathsf{s}} \circ (M_{\mathfrak{e}_i} \star (\boldsymbol{\omega}^{\mathfrak{e}_i}_{\mathfrak{e}_i/\mathrm{I}})^{\mathsf{s}}). \tag{2.54}$$

From equation (2.46), we can compute the 6-DOF dynamic equations of motion of body i as

$$\dot{\boldsymbol{H}}^{\mathfrak{e}_i}_{\mathfrak{e}_i/\mathrm{I}} + \boldsymbol{\omega}^{\mathfrak{e}_i}_{\mathfrak{e}_i/\mathrm{I}} \times \boldsymbol{H}^{\mathfrak{e}_i}_{\mathfrak{e}_i/\mathrm{I}} = \boldsymbol{W}^{\mathfrak{e}_i}_{\mathrm{i}}(O_{\mathfrak{e}_i}), \tag{2.55}$$

or equivalently,

$$M_{\mathfrak{e}_i} \star (\dot{\boldsymbol{\omega}}^{\mathfrak{e}_i}_{\mathfrak{e}_i/\mathrm{I}})^{\mathsf{s}} + \boldsymbol{\omega}^{\mathfrak{e}_i}_{\mathfrak{e}_i/\mathrm{I}} \times \left(M_{\mathfrak{e}_i} \star (\boldsymbol{\omega}^{\mathfrak{e}_i}_{\mathfrak{e}_i/\mathrm{I}})^{\mathsf{s}}\right) = \boldsymbol{W}^{\mathfrak{e}_i}_{\mathrm{i}}(O_{\mathfrak{e}_i}), \tag{2.56}$$

where $\boldsymbol{W}^{\mathfrak{e}_i}_{\mathrm{i}}(O_{\mathfrak{e}_i}) = f^{\mathfrak{e}_i} + \epsilon\tau^{\mathfrak{e}_i}$ is the net wrench applied on body i about its center of mass.

For cases in which there is no ambiguity about the rigid body in question, we will denote the frame at the center of mass by B as opposed to $\mathfrak{e}_i$; we will denote the inertia matrix by M^{B} instead of $M_{\mathfrak{e}_i}$; and the net wrench about the center of mass will be identified

simply as $\boldsymbol{f}$, instead of $\boldsymbol{W}_{\mathrm{i}}^{\mathfrak{s}_{\mathrm{i}}}(O_{\mathfrak{s}_{\mathrm{i}}})$. This nomenclature follows the conventions adopted by the existing literature on the subject of 6-DOF pose control. Using this notation, the 6-DOF dynamics for a rigid body are given as

$$M^{\mathrm{B}} \star (\dot{\boldsymbol{\omega}}^{\mathrm{B}}_{\mathrm{B/I}})^{\mathsf{s}} + \boldsymbol{\omega}^{\mathrm{B}}_{\mathrm{B/I}} \times \left(M^{\mathrm{B}} \star (\boldsymbol{\omega}^{\mathrm{B}}_{\mathrm{B/I}})^{\mathsf{s}}\right) = \boldsymbol{f}^{\mathrm{B}}. \tag{2.57}$$

In [65], the authors also provide the *pose* error dynamics in a manner that closely resembles the attitude(-only) error dynamic equations of motion. The pose error dynamics can be derived by substituting the expression $\boldsymbol{\omega}^{\mathrm{B}}_{\mathrm{B/I}} = \boldsymbol{\omega}^{\mathrm{B}}_{\mathrm{B/D}} + \boldsymbol{\omega}^{\mathrm{B}}_{\mathrm{D/I}} = \boldsymbol{\omega}^{\mathrm{B}}_{\mathrm{B/D}} + \boldsymbol{q}^{*}_{\mathrm{B/D}} \boldsymbol{\omega}^{\mathrm{D}}_{\mathrm{D/I}} \boldsymbol{q}_{\mathrm{B/D}}$ into equation (2.57) to yield

$$\begin{aligned} M^{\mathrm{B}} \star (\dot{\boldsymbol{\omega}}^{\mathrm{B}}_{\mathrm{B/D}})^{\mathsf{s}} = \boldsymbol{f}^{\mathrm{B}} - (\boldsymbol{\omega}^{\mathrm{B}}_{\mathrm{B/D}} + \boldsymbol{\omega}^{\mathrm{B}}_{\mathrm{D/I}}) \times \left(M^{\mathrm{B}} \star ((\boldsymbol{\omega}^{\mathrm{B}}_{\mathrm{B/D}})^{\mathsf{s}} + (\boldsymbol{\omega}^{\mathrm{B}}_{\mathrm{D/I}})^{\mathsf{s}})\right) \\ - M^{\mathrm{B}} \star (\boldsymbol{q}^{*}_{\mathrm{B/D}} \dot{\boldsymbol{\omega}}^{\mathrm{D}}_{\mathrm{D/I}} \boldsymbol{q}_{\mathrm{B/D}})^{\mathsf{s}} - M^{\mathrm{B}} \star (\boldsymbol{\omega}^{\mathrm{B}}_{\mathrm{D/I}} \times \boldsymbol{\omega}^{\mathrm{B}}_{\mathrm{B/D}})^{\mathsf{s}}. \end{aligned} \tag{2.58}$$

Equation (2.58) describes the time-evolution of the dual velocity of a frame fixed to a rigid body B relative to a desired reference frame D, both of which are evolving with respect to a third frame I.

Lemma 4. *The real part of equation* (2.58) *encodes the translational dynamic equation of motion as*

$$\begin{aligned} m\dot{v}^{\mathrm{B}}_{\mathrm{B/D}} = f^{\mathrm{B}} - m(\dot{v}^{\mathrm{B}}_{\mathrm{D/I}} + \dot{\omega}^{\mathrm{B}}_{\mathrm{D/I}} \times r^{\mathrm{B}}_{\mathrm{B/D}}) - m\omega^{\mathrm{B}}_{\mathrm{B/D}} \times v^{\mathrm{B}}_{\mathrm{B/D}} \\ - 2m\omega^{\mathrm{B}}_{\mathrm{D/I}} \times v^{\mathrm{B}}_{\mathrm{B/D}} - m\omega^{\mathrm{B}}_{\mathrm{D/I}} \times v^{\mathrm{B}}_{\mathrm{D/I}} - m\omega^{\mathrm{B}}_{\mathrm{D/I}} \times (\omega^{\mathrm{B}}_{\mathrm{D/I}} \times r^{\mathrm{B}}_{\mathrm{B/D}}) \end{aligned} \tag{2.59}$$

while the dual part encodes the rotational dynamic equation of motion as

$$\begin{aligned} \bar{I}^{\mathrm{B}} * \dot{\omega}^{\mathrm{B}}_{\mathrm{B/D}} = \tau^{\mathrm{B}} - ((\omega^{\mathrm{B}}_{\mathrm{B/D}} + \omega^{\mathrm{B}}_{\mathrm{D/I}}) \times (\bar{I}^{\mathrm{B}} * \omega^{\mathrm{B}}_{\mathrm{B/D}} + \bar{I}^{\mathrm{B}} * \omega^{\mathrm{B}}_{\mathrm{D/I}})) \\ - \bar{I}^{\mathrm{B}} * \dot{\omega}^{\mathrm{B}}_{\mathrm{D/I}} - \bar{I}^{\mathrm{B}} * \omega^{\mathrm{B}}_{\mathrm{D/I}} \times \omega^{\mathrm{B}}_{\mathrm{B/D}}. \end{aligned} \tag{2.60}$$

Proof. From equation (2.36) we know that $\boldsymbol{\omega}^{\mathrm{B}}_{\mathrm{D/I}} = \omega^{\mathrm{B}}_{\mathrm{D/I}} + \epsilon(v^{\mathrm{B}}_{\mathrm{D/I}} + \omega^{\mathrm{B}}_{\mathrm{D/I}} \times r^{\mathrm{B}}_{\mathrm{B/D}})$. Therefore,

$\boldsymbol{\omega}^{\mathrm{B}}_{\mathrm{D/I}} \times \boldsymbol{\omega}^{\mathrm{B}}_{\mathrm{B/D}} = (\omega^{\mathrm{B}}_{\mathrm{D/I}} + \epsilon(v^{\mathrm{B}}_{\mathrm{D/I}} + \omega^{\mathrm{B}}_{\mathrm{D/I}} \times r^{\mathrm{B}}_{\mathrm{B/D}})) \times (\omega^{\mathrm{B}}_{\mathrm{B/D}} + \epsilon v^{\mathrm{B}}_{\mathrm{B/D}}) = \omega^{\mathrm{B}}_{\mathrm{D/I}} \times \omega^{\mathrm{B}}_{\mathrm{B/D}} + \epsilon(\omega^{\mathrm{B}}_{\mathrm{D/I}} \times v^{\mathrm{B}}_{\mathrm{B/D}} + (v^{\mathrm{B}}_{\mathrm{D/I}} + \omega^{\mathrm{B}}_{\mathrm{D/I}} \times r^{\mathrm{B}}_{\mathrm{B/D}}) \times \omega^{\mathrm{B}}_{\mathrm{B/D}}) = \omega^{\mathrm{B}}_{\mathrm{D/I}} \times \omega^{\mathrm{B}}_{\mathrm{B/D}} + \epsilon(\omega^{\mathrm{B}}_{\mathrm{D/I}} \times v^{\mathrm{B}}_{\mathrm{B/D}} + v^{\mathrm{B}}_{\mathrm{D/I}} \times \omega^{\mathrm{B}}_{\mathrm{B/D}} + (\omega^{\mathrm{B}}_{\mathrm{D/I}} \times r^{\mathrm{B}}_{\mathrm{B/D}}) \times \omega^{\mathrm{B}}_{\mathrm{B/D}})$. Additionally, using equation (2.43) and $\dot{\boldsymbol{\omega}}^{\mathrm{D}}_{\mathrm{D/I}} = \dot{\omega}^{\mathrm{D}}_{\mathrm{D/I}} + \epsilon \dot{v}^{\mathrm{D}}_{\mathrm{D/I}}$, we have that $\boldsymbol{q}^{*}_{\mathrm{B/D}} \dot{\boldsymbol{\omega}}^{\mathrm{D}}_{\mathrm{D/I}} \boldsymbol{q}_{\mathrm{B/D}} = \dot{\omega}^{\mathrm{B}}_{\mathrm{D/I}} + \epsilon(\dot{v}^{\mathrm{B}}_{\mathrm{D/I}} + \dot{\omega}^{\mathrm{B}}_{\mathrm{D/I}} \times r^{\mathrm{B}}_{\mathrm{B/D}})$. Since $\boldsymbol{\omega}^{\mathrm{B}}_{\mathrm{B/D}} + \boldsymbol{\omega}^{\mathrm{B}}_{\mathrm{D/I}} = \omega^{\mathrm{B}}_{\mathrm{B/D}} + \omega^{\mathrm{B}}_{\mathrm{D/I}} + \epsilon(v^{\mathrm{B}}_{\mathrm{B/D}} + v^{\mathrm{B}}_{\mathrm{D/I}} + \omega^{\mathrm{B}}_{\mathrm{D/I}} \times r^{\mathrm{B}}_{\mathrm{B/D}})$, we have that $(\boldsymbol{\omega}^{\mathrm{B}}_{\mathrm{B/D}} + \boldsymbol{\omega}^{\mathrm{B}}_{\mathrm{D/I}}) \times \left(M^{\mathrm{B}} \star ((\boldsymbol{\omega}^{\mathrm{B}}_{\mathrm{B/D}})^{\mathsf{s}} + (\boldsymbol{\omega}^{\mathrm{B}}_{\mathrm{D/I}})^{\mathsf{s}})\right) = (\omega^{\mathrm{B}}_{\mathrm{B/D}} + \omega^{\mathrm{B}}_{\mathrm{D/I}}) \times m(v^{\mathrm{B}}_{\mathrm{B/D}} + v^{\mathrm{B}}_{\mathrm{D/I}} + \omega^{\mathrm{B}}_{\mathrm{D/I}} \times r^{\mathrm{B}}_{\mathrm{B/D}}) + \epsilon((\omega^{\mathrm{B}}_{\mathrm{B/D}} + \omega^{\mathrm{B}}_{\mathrm{D/I}}) \times (\bar{I}^{\mathrm{B}} * \omega^{\mathrm{B}}_{\mathrm{B/D}} + \bar{I}^{\mathrm{B}} * \omega^{\mathrm{B}}_{\mathrm{D/I}}))$. Plugging each of these expressions into equation (2.58) yields the dual quaternion expression $m\dot{v}^{\mathrm{B}}_{\mathrm{B/D}} + \epsilon \bar{I}^{\mathrm{B}} * \dot{\omega}^{\mathrm{B}}_{\mathrm{B/D}} = f^{\mathrm{B}} + \epsilon \tau^{\mathrm{B}} - (\omega^{\mathrm{B}}_{\mathrm{B/D}} + \omega^{\mathrm{B}}_{\mathrm{D/I}}) \times m(v^{\mathrm{B}}_{\mathrm{B/D}} + v^{\mathrm{B}}_{\mathrm{D/I}} + \omega^{\mathrm{B}}_{\mathrm{D/I}} \times r^{\mathrm{B}}_{\mathrm{B/D}}) - \epsilon((\omega^{\mathrm{B}}_{\mathrm{B/D}} + \omega^{\mathrm{B}}_{\mathrm{D/I}}) \times (\bar{I}^{\mathrm{B}} * \omega^{\mathrm{B}}_{\mathrm{B/D}} + \bar{I}^{\mathrm{B}} * \omega^{\mathrm{B}}_{\mathrm{D/I}})) - m(\dot{v}^{\mathrm{B}}_{\mathrm{D/I}} + \dot{\omega}^{\mathrm{B}}_{\mathrm{D/I}} \times r^{\mathrm{B}}_{\mathrm{B/D}}) - \epsilon \bar{I}^{\mathrm{B}} * \dot{\omega}^{\mathrm{B}}_{\mathrm{D/I}} - m(\omega^{\mathrm{B}}_{\mathrm{D/I}} \times v^{\mathrm{B}}_{\mathrm{B/D}} + v^{\mathrm{B}}_{\mathrm{D/I}} \times \omega^{\mathrm{B}}_{\mathrm{B/D}} + (\omega^{\mathrm{B}}_{\mathrm{D/I}} \times r^{\mathrm{B}}_{\mathrm{B/D}}) \times \omega^{\mathrm{B}}_{\mathrm{B/D}}) - \epsilon \bar{I}^{\mathrm{B}} * \omega^{\mathrm{B}}_{\mathrm{D/I}} \times \omega^{\mathrm{B}}_{\mathrm{B/D}}$. Collecting real and dual terms yields $m\dot{v}^{\mathrm{B}}_{\mathrm{B/D}} + \epsilon \bar{I}^{\mathrm{B}} * \dot{\omega}^{\mathrm{B}}_{\mathrm{B/D}} = f^{\mathrm{B}} - (\omega^{\mathrm{B}}_{\mathrm{B/D}} + \omega^{\mathrm{B}}_{\mathrm{D/I}}) \times m(v^{\mathrm{B}}_{\mathrm{B/D}} + v^{\mathrm{B}}_{\mathrm{D/I}} + \omega^{\mathrm{B}}_{\mathrm{D/I}} \times r^{\mathrm{B}}_{\mathrm{B/D}}) - m(\dot{v}^{\mathrm{B}}_{\mathrm{D/I}} + \dot{\omega}^{\mathrm{B}}_{\mathrm{D/I}} \times r^{\mathrm{B}}_{\mathrm{B/D}}) - m(\omega^{\mathrm{B}}_{\mathrm{D/I}} \times v^{\mathrm{B}}_{\mathrm{B/D}} + v^{\mathrm{B}}_{\mathrm{D/I}} \times \omega^{\mathrm{B}}_{\mathrm{B/D}} + (\omega^{\mathrm{B}}_{\mathrm{D/I}} \times r^{\mathrm{B}}_{\mathrm{B/D}}) \times \omega^{\mathrm{B}}_{\mathrm{B/D}}) + \epsilon(\tau^{\mathrm{B}} - ((\omega^{\mathrm{B}}_{\mathrm{B/D}} + \omega^{\mathrm{B}}_{\mathrm{D/I}}) \times (\bar{I}^{\mathrm{B}} * \omega^{\mathrm{B}}_{\mathrm{B/D}} + \bar{I}^{\mathrm{B}} * \omega^{\mathrm{B}}_{\mathrm{D/I}})) - \bar{I}^{\mathrm{B}} * \dot{\omega}^{\mathrm{B}}_{\mathrm{D/I}} - \bar{I}^{\mathrm{B}} * \omega^{\mathrm{B}}_{\mathrm{D/I}} \times \omega^{\mathrm{B}}_{\mathrm{B/D}})$. The extraction of the real and dual parts yields the desired result upon simplification. ■

We now provide a typical decomposition of $\boldsymbol{f}^{\mathrm{B}}$, the total external dual force acting on an Earth-orbiting spacecraft. Without loss of generality, $\boldsymbol{f}^{\mathrm{B}}$ can be described as follows [50]:

$$\boldsymbol{f}^{\mathrm{B}} = \boldsymbol{f}^{\mathrm{B}}_{g} + \boldsymbol{f}^{\mathrm{B}}_{\nabla g} + \boldsymbol{f}^{\mathrm{B}}_{J_2} + \boldsymbol{f}^{\mathrm{B}}_{d} + \boldsymbol{f}^{\mathrm{B}}_{c}, \tag{2.61}$$

where $\boldsymbol{f}^{\mathrm{B}}_{g}$ is the dual gravitational force, $\boldsymbol{f}^{\mathrm{B}}_{\nabla g}$ is the dual gravity gradient force, $\boldsymbol{f}^{\mathrm{B}}_{J_2}$ is the dual perturbing force due to Earth's oblateness, $\boldsymbol{f}^{\mathrm{B}}_{d}$ is a dual disturbance force, and $\boldsymbol{f}^{\mathrm{B}}_{c}$ is the dual control force. In application, the dual control force is calculated as $\boldsymbol{f}^{\mathrm{B}}_{c} = \boldsymbol{f}^{\mathrm{B}} - \boldsymbol{f}^{\mathrm{B}}_{g} - \boldsymbol{f}^{\mathrm{B}}_{\nabla g} - \boldsymbol{f}^{\mathrm{B}}_{J_2} - \boldsymbol{f}^{\mathrm{B}}_{d}$, where $\boldsymbol{f}^{\mathrm{B}}$ is usually the variable designed in pose controllers. For the sake of completeness, we provide common expressions for the gravitational terms and the J_2 term.

The dual gravitational force can be described as $\boldsymbol{f}^{\mathrm{B}}_{g} = m\boldsymbol{a}^{\mathrm{B}}_{g}, \boldsymbol{a}^{\mathrm{B}}_{g} = a^{\mathrm{B}}_{g} + \epsilon 0, a^{\mathrm{B}}_{g} = (0, \bar{a}^{\mathrm{B}}_{g})$,

where $\bar{a}_g^{\mathrm{B}} \in \mathbb{R}^3$ is the gravitational acceleration given by

$$\bar{a}_g^{\mathrm{B}} = -\mu \frac{\bar{r}_{\mathrm{B/I}}^{\mathrm{B}}}{\|\bar{r}_{\mathrm{B/I}}^{\mathrm{B}}\|^3}, \tag{2.62}$$

$\mu = 398600.4418$ km^3/s^2 is Earth's gravitational parameter.

The dual gravity gradient force can be described as $\boldsymbol{f}_{\nabla g}^{\mathrm{B}} = 0 + \epsilon \tau_{\nabla g}^{\mathrm{B}}$, $\tau_{\nabla g}^{\mathrm{B}} = (0, \bar{\tau}_{\nabla g}^{\mathrm{B}})$, where $\bar{\tau}_{\nabla g}^{\mathrm{B}} \in \mathbb{R}^3$ is the gravity gradient torque, which can be written as

$$\bar{\tau}_{\nabla g}^{\mathrm{B}} = 3\mu \frac{\bar{r}_{\mathrm{B/I}}^{\mathrm{B}} \times (\bar{I}^{\mathrm{B}} \bar{r}_{\mathrm{B/I}}^{\mathrm{B}})}{\|\bar{r}_{\mathrm{B/I}}^{\mathrm{B}}\|^5}. \tag{2.63}$$

The dual perturbing force due to Earth's oblateness can be described as $\boldsymbol{f}_{J_2}^{\mathrm{B}} = m\boldsymbol{a}_{J_2}^{\mathrm{B}}$, $\boldsymbol{a}_{J_2}^{\mathrm{B}} = a_{J_2}^{\mathrm{B}} + \epsilon 0$, $a_{J_2}^{\mathrm{B}} = (0, \bar{a}_{J_2}^{\mathrm{B}})$, where $\bar{a}_{J_2}^{\mathrm{B}} \in \mathbb{R}^3$ is the perturbing acceleration due to J_2. This acceleration can be computed in inertial frame coordinates as

$$\bar{a}_{J_2}^{\mathrm{I}} = -\frac{3}{2} \frac{\mu J_2 R_e^2}{\|\bar{r}_{\mathrm{B/I}}^{\mathrm{I}}\|^4} \begin{bmatrix} \left(1 - 5\left(\frac{z_{\mathrm{B/I}}^{\mathrm{I}}}{\|\bar{r}_{\mathrm{B/I}}^{\mathrm{I}}\|}\right)^2\right) \frac{x_{\mathrm{B/I}}^{\mathrm{I}}}{\|\bar{r}_{\mathrm{B/I}}^{\mathrm{I}}\|} \\ \left(1 - 5\left(\frac{z_{\mathrm{B/I}}^{\mathrm{I}}}{\|\bar{r}_{\mathrm{B/I}}^{\mathrm{I}}\|}\right)^2\right) \frac{y_{\mathrm{B/I}}^{\mathrm{I}}}{\|\bar{r}_{\mathrm{B/I}}^{\mathrm{I}}\|} \\ \left(3 - 5\left(\frac{z_{\mathrm{B/I}}^{\mathrm{I}}}{\|\bar{r}_{\mathrm{B/I}}^{\mathrm{I}}\|}\right)^2\right) \frac{z_{\mathrm{B/I}}^{\mathrm{I}}}{\|\bar{r}_{\mathrm{B/I}}^{\mathrm{I}}\|} \end{bmatrix}, \tag{2.64}$$

where $J_2 = 0.0010826267$ and $R_e = 6378.137\ km$ is Earth's mean equatorial radius.

In [50], expressions for the gravitational dual force, the gravity gradient dual force, and perturbations due to J_2 are provided in terms of the dual inertia matrix as:

$$\boldsymbol{f}_g^{\mathrm{B}} = M^{\mathrm{B}} \star \boldsymbol{a}_g^{\mathrm{B}}, \tag{2.65}$$

$$\boldsymbol{f}_{J_2}^{\mathrm{B}} = M^{\mathrm{B}} \star \boldsymbol{a}_{J_2}^{\mathrm{B}}, \tag{2.66}$$

We propose re-defining the gravity gradient dual force as

$$\text{New} : \quad \boldsymbol{f}_{\nabla g}^{\mathrm{B}} = \frac{3\mu(\boldsymbol{r}_{\mathrm{B/I}}^{\mathrm{B}})^{\mathsf{S}}}{\|\boldsymbol{r}_{\mathrm{B/I}}^{\mathrm{B}}\|^5} \times (M^{\mathrm{B}} \star \boldsymbol{r}_{\mathrm{B/I}}^{\mathrm{B}}), \quad \boldsymbol{r}_{\mathrm{B/I}}^{\mathrm{B}} \triangleq 0 + \epsilon r_{\mathrm{B/I}}^{\mathrm{B}} \tag{2.67}$$

as opposed to

$$\text{Old [50]:} \quad \boldsymbol{f}^{\text{B}}_{\nabla g} = \frac{3\mu \boldsymbol{r}^{\text{B}}_{\text{В/Л}}}{\|\boldsymbol{r}^{\text{B}}_{\text{В/Л}}\|^5} \times (M^{\text{B}} \star (\boldsymbol{r}^{\text{B}}_{\text{В/Л}})^{\text{s}}), \quad \boldsymbol{r}^{\text{B}}_{\text{В/Л}} \triangleq r^{\text{B}}_{\text{В/Л}} + \epsilon 0, \tag{2.68}$$

since the former uses the appropriate native representation of a position vector expressed in dual quaternion algebra [31].

CHAPTER 3

DUAL QUATERNIONS IN ROBOTICS

3.1 Dual Quaternion Notation

The forward kinematics of a robot can be easily laid out in dual quaternion form. In general, a dual quaternion is given as

$$\boldsymbol{q}_{\mathrm{B/A}} = q_{\mathrm{B/A}} + \epsilon\tfrac{1}{2} q_{\mathrm{B/A}} r^{\mathrm{B}}_{\mathrm{B/A}}, \tag{3.1}$$

$$\boldsymbol{q}_{\mathrm{B/A}} = q_{\mathrm{B/A}} + \epsilon\tfrac{1}{2} r^{\mathrm{A}}_{\mathrm{B/A}} q_{\mathrm{B/A}}, \tag{3.2}$$

where $q_{\mathrm{B/A}}$ is the quaternion that represents the attitude change in going from reference frame A, to reference frame B. The position vectors $r^{\mathrm{B}}_{\mathrm{B/A}}$ and $r^{\mathrm{A}}_{\mathrm{B/A}}$ represent the position vector from the origin of frame A to the origin of frame B expressed in frame B, and frame A coordinates respectively. Notice that equations (3.1) and (3.2) can be equivalently expressed as follows:

$$\text{Rotation First:} \quad \boldsymbol{q}_{\mathrm{B/A}} = (q_{\mathrm{B/A}} + \epsilon 0)(1 + \epsilon\tfrac{1}{2} r^{\mathrm{B}}_{\mathrm{B/A}}), \tag{3.3}$$

$$\text{Translation First:} \quad \boldsymbol{q}_{\mathrm{B/A}} = (1 + \epsilon\tfrac{1}{2} r^{\mathrm{A}}_{\mathrm{B/A}})(q_{\mathrm{B/A}} + \epsilon 0), \tag{3.4}$$

leading to an intuitive decomposition of the underlying operations. In the forward kinematics, equation (3.3) implies that the frame rotation is carried out first, and then a translation is carried out relative to the new frame. Equation (3.4) denotes a translation in the base frame, followed by an attitude change of the resulting frame. Throughout this disseration we will use the *translation first* approach.

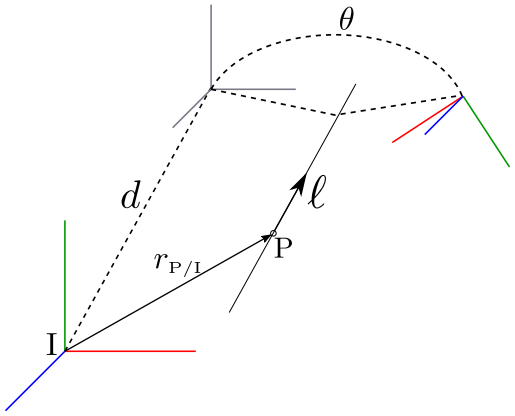

Figure 3.1: Screw motion parametrized by $\boldsymbol{\theta}$ and $\boldsymbol{s}$.

3.2 Product of Exponentials Formula in Dual-Quaternion Form

The product of exponentials formula has been long used to study the forward kinematics of robots. Reference [118] has a thorough introduction to the topic, with examples and uses. In this section we lay out the main results that cast the product of exponentials (POE) formula in dual quaternion form. In particular, [119] has made use of the dual quaternion formalism to perform geometric control on a fixed-base robotic arm, where the forward kinematics of the robot are expressed using the POE formula.

As commonly used in robotics, the exponential operation takes an element of the Lie algebra for a given Lie group, and renders a group element. For the dual quaternion case, let the set of parameters $(\boldsymbol{\theta}, \boldsymbol{s}) \in \mathrm{D} \times \mathbb{H}_d^v$ parametrize a screw motion as shown in Figure 3.1. In particular, $\boldsymbol{\theta}$ and $\boldsymbol{s}$ are given by

$$\boldsymbol{\theta} = \theta + \epsilon d, \qquad \boldsymbol{\theta} \in \mathrm{D}, \qquad \theta, d \in \mathbb{R}, \tag{3.5}$$

$$\boldsymbol{s} = \ell + \epsilon m, \qquad \boldsymbol{s} \in \mathbb{H}_d^v, \qquad \ell, m \in \mathbb{H}^v, \tag{3.6}$$

where θ is the angle of the screw motion, d is the translation along the screw axis, ℓ is the unit screw axis of the joint, and m is the moment vector of the screw axis of direction ℓ

with respect to the origin of the local inertial frame. This implies that

$$m = r^{\mathrm{I}}_{\mathrm{P/I}} \times \ell, \tag{3.7}$$

where the point P lies on the screw axis. In robotic systems, the exponential mapping is commonly used to evaluate the forward kinematics of fixed-base robotic systems. We summarize the dual quaternion exponential mapping in the following lemma.

Lemma 5. *The exponential operation,* $\exp : \mathrm{D} \times \mathbb{H}_d^v \to \mathbb{H}_d$ *for a given pair* $(\boldsymbol{\theta}, \boldsymbol{s}) \in \mathrm{D} \times \mathbb{H}_d^v$ *defined as in equations* (3.5) *and* (3.6) *is given as ([119, 120])*

$$\boldsymbol{q} = \exp\left(\tfrac{1}{2}\boldsymbol{\theta}\boldsymbol{s}\right), \quad \boldsymbol{q} \in \mathbb{H}_d \tag{3.8}$$

$$= \cos\left(\tfrac{1}{2}\boldsymbol{\theta}\right) + \boldsymbol{s}\sin\left(\tfrac{1}{2}\boldsymbol{\theta}\right) \tag{3.9}$$

$$= \left(\cos\left(\tfrac{1}{2}\theta\right),\ \ell\sin\left(\tfrac{1}{2}\theta\right)\right) + \epsilon\left(-\tfrac{1}{2}d\sin\left(\tfrac{1}{2}\theta\right),\ \tfrac{1}{2}d\ell\cos\left(\tfrac{1}{2}\theta\right) + m\sin\left(\tfrac{1}{2}\theta\right)\right). \tag{3.10}$$

Proof. Since $\boldsymbol{\theta} = \theta + \epsilon d \in \mathrm{D}$, we have that

$$\cos\left(\tfrac{1}{2}\boldsymbol{\theta}\right) = \cos\left(\tfrac{1}{2}\theta\right) + \epsilon\frac{d}{2}\left(-\sin(\tfrac{1}{2}\theta)\right) \tag{3.11}$$

$$\sin\left(\tfrac{1}{2}\boldsymbol{\theta}\right) = \sin\left(\tfrac{1}{2}\theta\right) + \epsilon\frac{d}{2}\cos\left(\tfrac{1}{2}\theta\right). \tag{3.12}$$

It follows that

$$\boldsymbol{q} = \cos\left(\tfrac{1}{2}\boldsymbol{\theta}\right) + \boldsymbol{s}\sin\left(\tfrac{1}{2}\boldsymbol{\theta}\right) \tag{3.13}$$

$$= \cos\left(\tfrac{1}{2}\theta\right) - \epsilon\frac{d}{2}\sin\left(\tfrac{1}{2}\theta\right) + (\ell + \epsilon m)\left(\sin\left(\tfrac{1}{2}\theta\right) + \epsilon\frac{d}{2}\cos\left(\tfrac{1}{2}\theta\right)\right), \tag{3.14}$$

which yields the desired result upon expansion. ■

Remark 1. By comparing equation (3.2) and equation (3.10), it can be deduced that the effect of a joint motion can be characterized by an equivalent rotation and a translation. In

particular, by equating the real parts of the dual quaternions, we have that

$$q_{\text{B/A}} = \left(\cos\left(\tfrac{1}{2}\theta\right),\ \ell\sin\left(\tfrac{1}{2}\theta\right)\right), \tag{3.15}$$

and from the dual parts

$$\tfrac{1}{2}r^{\text{A}}_{\text{B/A}}q_{\text{B/A}} = \left(-\tfrac{1}{2}d\sin\left(\tfrac{1}{2}\theta\right),\ \tfrac{1}{2}d\ell\cos\left(\tfrac{1}{2}\theta\right) + m\sin\left(\tfrac{1}{2}\theta\right)\right). \tag{3.16}$$

Equivalently, $r^{\text{A}}_{\text{B/A}}$ can be described as

$$r^{\text{A}}_{\text{B/A}} = (0, d\ell + m\sin(\theta) + (\cos(\theta) - 1)m \times \ell). \tag{3.17}$$

The inverse to the exponential mapping is the logarithmic mapping, $\ln : \mathbb{H}_d \rightarrow \mathbb{H}_d$, which is defined as

$$\ln \boldsymbol{q} = \tfrac{1}{2}\boldsymbol{\theta}\boldsymbol{s} = \tfrac{1}{2}\theta\ell + \epsilon\tfrac{1}{2}(\theta m + d\ell). \tag{3.18}$$

Appendix A.6. of [119] explains how to retrieve $\{\theta, d, \ell, m\}$ given a dual quaternion, $\boldsymbol{q}$.

Now, given the dual quaternion from the inertial (base) frame to the end effector, at the robots's home configuration, $\boldsymbol{q}_{\text{e,0/I}}$, and parameter $\boldsymbol{s}_i$ for each of the n joints of a robot at its home configuration, the product of exponentials formula yields

$$\boldsymbol{q}_{\text{e/I}} = \exp\left(\tfrac{1}{2}\boldsymbol{\theta}_1\boldsymbol{s}_1\right)\ldots\exp\left(\tfrac{1}{2}\boldsymbol{\theta}_n\boldsymbol{s}_n\right)\boldsymbol{q}_{\text{e,0/I}}, \tag{3.19}$$

where joint 1 is closest to the base and joint n is closest to the end-effector. The exponential formula is effectively changing the spatial frame, as opposed to the body frame of the end-effector. Besides from the algebraic appeal of using an exponential function to compute forward kinematics, the POE formula is straightforward to compute for a given configuration once the type of joint is known and the geometric properties of the robot are selected.

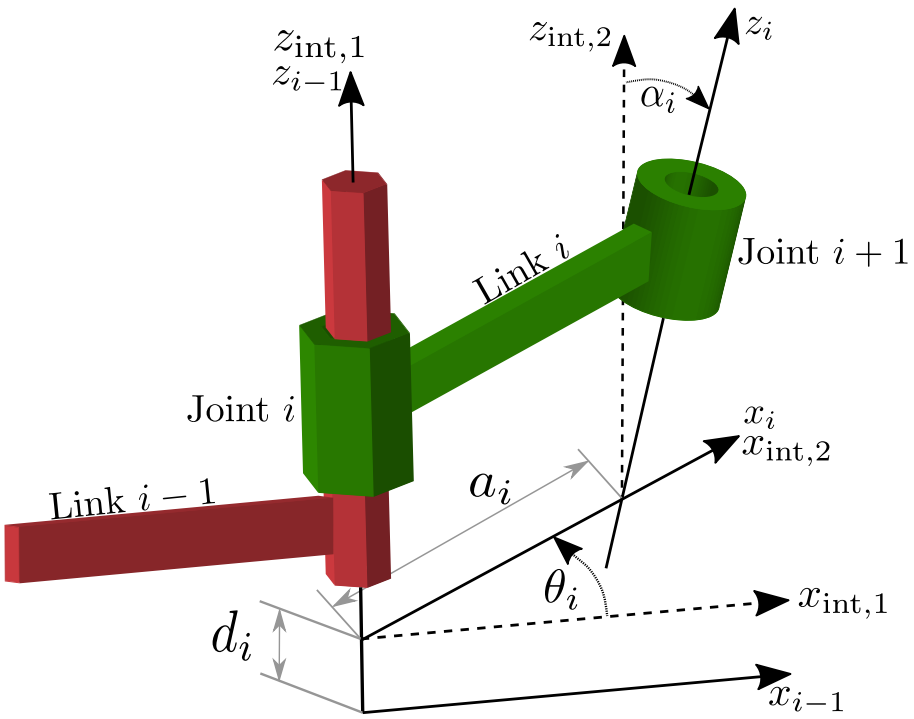

Figure 3.2: Denavit-Hartenberg parameters.

3.3 Denavit-Hartenberg Parameters in Dual Quaternion Form

The Denavit-Hartenberg parameters, commonly referred to as DH parameters, are four geometric quantities that allow identifying the relative pose of a joint with respect to another in a systematic manner. We will denote a set of DH parameters as $\{d_i, \theta_i, a_i, \alpha_i\}$ for joint i. The parameters d_i and θ_i are commonly referred as *joint* parameters, while a_i and α_i are known as the *link* parameters. A complete description of the DH parameters for R and P joint types, and several examples of their use are provided in [121]. In [121] a thorough description of the orientation of the frames is also provided, to which the reader is referred. In [28], Gan et al. have used dual quaternions in combination with the DH parameter convention to capture the pose transformation between joints. For completeness purposes, we provide these equations herein making use of Figure 3.2.

In words, the transformation from the reference frame assigned to the proximal joint[1]

[1]For a given link, its *proximal joint* is closer to the base of the robot.

of a given link i, to the reference frame assigned to its distal joint[2], is described in terms of the DH parameters as:

1. From the origin O_{i-1}, displace along the Z_{i-1} (joint) axis by an amount d_i. Define this intermediate frame as $\{\text{int}, 1\}$.

2. Rotate about the Z_{i-1} axis by θ_i until axis X_{i-1} is superimposed to X_i

3. Translate along X_i by a distance of a_i. Define this intermediate frame as $\{\text{int}, 2\}$.

4. Rotate about the X_i axis by α_i

Mathematically, we can write this as the composition of four elementary dual quaternion operations, and summarized further into two composite dual quaternions as

$$\boldsymbol{q}_{\text{i/i-1}} = (1 + \epsilon r^{\text{int,1}}_{\text{int,1/i-1}})(q_{\text{int,2/int,1}} + \epsilon 0)(1 + \epsilon r^{\text{int,2}}_{\text{int,2/int,1}})(q_{\text{i/int,2}} + \epsilon 0) \tag{3.20}$$

$$= (q_{\text{int,2/int,1}} + \epsilon r^{\text{int,1}}_{\text{int,1/i-1}} q_{\text{int,2/int,1}})(q_{\text{i/int,2}} + \epsilon r^{\text{int,2}}_{\text{int,2/int,1}} q_{\text{i/int,2}}) \tag{3.21}$$

where

$$r^{\text{int,1}}_{\text{int,1/i-1}} = (0, [0, 0, d_i]^{\text{T}}) \tag{3.22}$$

$$q_{\text{int,2/int,1}} = (\cos\theta_i/2, [0, 0, \sin\theta_i/2]^{\text{T}}) \tag{3.23}$$

$$r^{\text{int,2}}_{\text{int,2/int,1}} = (0, [a_i, 0, 0]^{\text{T}}) \tag{3.24}$$

$$q_{\text{i/int,2}} = (\cos\alpha_i/2, [\sin\alpha_i/2, 0, 0]^{\text{T}}) \tag{3.25}$$

Notice that while this is compact and readable up to multiplication of the dual quaternions, the same cannot be said about the end result compared to its homogeneous transformation matrix (HTM) counterpart. In fact, if we express $\boldsymbol{q}_{\text{i/i-1}}$ component-wise, and cast it as a vector in $\mathbb{R}^8$ which is the typical representation of dual quaternions for numerical purposes,

[2]For a given link, its *distal joint* is closer to the end effector.

and compute the equivalent HTM, we get the following:

$$\boldsymbol{q}_{\text{i/i-1}} = \begin{bmatrix} \cos(\alpha/2)\cos(\theta/2) \\ \sin(\alpha/2)\cos(\theta/2) \\ \sin(\alpha/2)\sin(\theta/2) \\ \cos(\alpha/2)\sin(\theta/2) \\ -\frac{1}{2}a_i\sin(\alpha_i/2)\cos(\theta_i/2) - \frac{1}{2}d_i\cos(\alpha_i/2)\sin(\theta_i/2) \\ \frac{1}{2}a_i\cos(\alpha_i/2)\cos(\theta_i/2) - \frac{1}{2}d_i\sin(\alpha_i/2)\sin(\theta_i/2) \\ \frac{1}{2}a_i\cos(\alpha_i/2)\sin(\theta_i/2) + \frac{1}{2}d_i\sin(\alpha_i/2)\cos(\theta_i/2) \\ \frac{1}{2}d_i\cos(\alpha_i/2)\cos(\theta_i/2) - \frac{1}{2}a_i\sin(\alpha_i/2)\sin(\theta_i/2) \end{bmatrix} \tag{3.26}$$

$$T_{\text{i/i-1}} = \left[\begin{array}{ccc|c} \cos(\theta_i) & \sin(\theta_i) & 0 & -a_i \\ -\cos(\alpha_i)\sin(\theta_i) & \cos(\alpha_i)\cos(\theta_i) & \sin(\alpha_i) & -d_i\sin(\alpha_i) \\ \sin(\alpha_i)\sin(\theta_i) & -\sin(\alpha_i)\cos(\theta_i) & \cos(\alpha_i) & -d_i\cos(\alpha_i) \\ \hline 0 & 0 & 0 & 1 \end{array}\right]. \tag{3.27}$$

While the HTM is more readable and faster to code, it uses 16 doubles and a multi-dimensional array to store the information and operate in the underlying algebra. Here, it is worth emphasizing that the more commonly used backward HTM used with the DH convention is

$$T_{\text{i-1/i}} = \left[\begin{array}{ccc|c} \cos\theta_i & -\sin\theta_i\cos\alpha_i & \sin\theta_i\sin\alpha_i & a_i\cos\theta_i \\ \sin\theta_i & \cos\theta_i\cos\alpha_i & -\cos\theta_i\sin\alpha_i & a_i\sin\theta_i \\ 0 & \sin\alpha_i & \cos\alpha_i & d_i \\ \hline 0 & 0 & 0 & 1 \end{array}\right]. \tag{3.28}$$

Remark 2. Since the transformations associated to θ_i and d_i are about z_{i-1} and the operations associated to α_i and a_i happen about x_i, both stages of the DH transformation

can be interpreted in the context of screw theory. Hence, the operation described by equation (3.20) can be equivalently expressed as the composition of exponential operations given by

$$q_{i/i\text{-}1} = \exp(\tfrac{1}{2}\boldsymbol{\theta}_1 \boldsymbol{s}_1)\exp(\tfrac{1}{2}\boldsymbol{\theta}_2 \boldsymbol{s}_2) \tag{3.29}$$

where $\boldsymbol{\theta}_1 = \theta_i + \epsilon d_i$ and $\boldsymbol{s}_1 = (0, [0,0,1]^{\mathrm{T}}) + \epsilon 0$ and $\boldsymbol{\theta}_2 = \alpha_i + \epsilon a_i$ and $\boldsymbol{s}_2 = (0, [1,0,0]^{\mathrm{T}}) + \epsilon 0$.

3.4 Convex Constraints Using Dual Quaternions

In [112], the authors use dual quaternions as a pose parametrization representation to model convex state constraints for a powered landing scenario. In this section, we repurpose the constraints for a space robotic servicing mission. The dual quaternion-based constraints will be provided without proof of convexity, since this is done in [112]. However, some properties of quaternions and some definitions are in order for a proper description of the results.

Lemma 6. *Given the quaternion $q \in \mathbb{H}$ and quaternions $r = (0, \bar{r}) \in \mathbb{H}^v$ and $y = (0, \bar{y}) \in \mathbb{H}^v$, the following equalities hold:*

$$(rq) \cdot (yq) = r \cdot y = (qr) \cdot (qy) \tag{3.30}$$

Proof. Using the definition of the quaternion dot product given in Table 2.2, the expression

on the left becomes

$$\begin{aligned}
(rq)\cdot(yq) &= \tfrac{1}{2}\left[(rq)^* yq + (yq)^* rq\right] \\
&= \tfrac{1}{2}\left[q^* r^* yq + q^* y^* rq\right] \\
&= \tfrac{1}{2} q^* \left[r^* y + y^* r\right] q \\
&= q^*(r\cdot y)q, \;\; \text{and since } r\cdot y = (\bar{r}\cdot\bar{y}, 0_{3\times 1}) = (\bar{r}\cdot\bar{y})\mathtt{1} \\
&= (\bar{r}\cdot\bar{y}) q^* q \\
&= (\bar{r}\cdot\bar{y})\mathtt{1} \\
&= r\cdot y.
\end{aligned} \tag{3.31}$$

The second equality can be proven in the same manner. ■

For the following facts, let us define

$$E_u \triangleq \begin{bmatrix} \mathbb{I}_4 & 0_{4\times 4} \\ 0_{4\times 4} & 0_{4\times 4} \end{bmatrix} \tag{3.32}$$

and

$$E_d \triangleq \begin{bmatrix} 0_{4\times 4} & 0_{4\times 4} \\ 0_{4\times 4} & \mathbb{I}_4 \end{bmatrix}. \tag{3.33}$$

Lemma 7. *Consider the dual quaternion* $\boldsymbol{q}_{\text{B/A}} = q_{\text{B/A}} + \epsilon\frac{1}{2} q_{\text{B/A}} r^{\text{B}}_{\text{B/A}}$. *Then,* $\boldsymbol{q}_{\text{B/A}} \circ \boldsymbol{q}_{\text{B/A}} = (1 + \frac{1}{4}\|r^{\text{B}}_{\text{B/A}}\|^2, 0_{3\times 1}) + \epsilon\mathtt{0}$

Proof. By definition, $\boldsymbol{q}_{\text{B/A}} \circ \boldsymbol{q}_{\text{B/A}} = (q_{\text{B/A}} + \epsilon\frac{1}{2} q_{\text{B/A}} r^{\text{B}}_{\text{B/A}}) \circ (q_{\text{B/A}} + \epsilon\frac{1}{2} q_{\text{B/A}} r^{\text{B}}_{\text{B/A}}) = q_{\text{B/A}} \cdot q_{\text{B/A}} + (\frac{1}{2} q_{\text{B/A}} r^{\text{B}}_{\text{B/A}}) \cdot (\frac{1}{2} q_{\text{B/A}} r^{\text{B}}_{\text{B/A}}) + \epsilon\mathtt{0}$. By the unit norm constraint of the unit quaternions and applying Lemma 6 on the second summand, $\boldsymbol{q}_{\text{B/A}} \circ \boldsymbol{q}_{\text{B/A}} = (1 + \frac{1}{4} r^{\text{B}}_{\text{B/A}} \cdot r^{\text{B}}_{\text{B/A}}, 0_{3\times 1}) + \epsilon\mathtt{0}$, from which the result follows. ■

Lemma 8. *Consider the dual quaternion* $\boldsymbol{q}_{\text{B/A}} = q_{\text{B/A}} + \epsilon\frac{1}{2} q_{\text{B/A}} r^{\text{B}}_{\text{B/A}}$. *Then,* $\boldsymbol{q}_{\text{B/A}} \circ (E_u \star \boldsymbol{q}_{\text{B/A}}) = \mathbf{1}$.

Proof. Using the definition of E_u, we have $\boldsymbol{q}_{\text{B/A}} \circ (E_u \star \boldsymbol{q}_{\text{B/A}}) = \boldsymbol{q}_{\text{B/A}} \circ (q_{\text{B/A}} + \epsilon 0) = q_{\text{B/A}} \cdot q_{\text{B/A}} + \epsilon 0$. The result follows from the unit constraint of a unit quaternion. ■

Lemma 9. *Consider the dual quaternion* $\boldsymbol{q}_{\text{B/A}} = q_{\text{B/A}} + \epsilon \frac{1}{2} q_{\text{B/A}} r^{\text{B}}_{\text{B/A}}$. *Then,* $\boldsymbol{q}_{\text{B/A}} \circ (E_d \star \boldsymbol{q}_{\text{B/A}}) = \frac{1}{4} \| r^{\text{B}}_{\text{B/A}} \|^2 + \epsilon 0$.

Proof. Using the definition of E_d, we have $\boldsymbol{q}_{\text{B/A}} \circ (E_d \star \boldsymbol{q}_{\text{B/A}}) = \boldsymbol{q}_{\text{B/A}} \circ (0 + \epsilon \frac{1}{2} q_{\text{B/A}} r^{\text{B}}_{\text{B/A}}) = (\frac{1}{2} q_{\text{B/A}} r^{\text{B}}_{\text{B/A}}) \cdot (\frac{1}{2} q_{\text{B/A}} r^{\text{B}}_{\text{B/A}}) + \epsilon 0$. The result follows from application of Lemma 6. ■

Lemma 10. *Consider* $\| r^{\text{B}}_{\text{B/A}} \| \leq \delta$. *Then,* $\boldsymbol{q}_{\text{B/A}} \circ \boldsymbol{q}_{\text{B/A}} \leq 1 + \frac{1}{4} \delta^2$.

Proof. From Lemma 7, it follows that $\boldsymbol{q}_{\text{B/A}} \circ \boldsymbol{q}_{\text{B/A}} = 1 + \frac{1}{4} \| r^{\text{B}}_{\text{B/A}} \|^2 \leq 1 + \frac{1}{4} \delta^2$. ■

Corollary 1. *Given the bound* $\| r^{\text{B}}_{\text{B/A}} \| \leq \delta$, *it follows that* $\boldsymbol{q}_{\text{B/A}} \circ \boldsymbol{q}_{\text{B/A}} \in \left[1, 1 + \frac{1}{4} \delta^2\right]$, *which is a closed and bounded set.*

It is worth emphasizing that in Lemma 10 and Lemma 7 the bijective mapping between the circle product and the real-line is implied. In other words, since the circle product between two dual quaternions $\boldsymbol{a} \circ \boldsymbol{b} = s\mathbf{1}$ for some $s \in \mathbb{R}$, it will be commonly interpreted as $\boldsymbol{a} \circ \boldsymbol{b} = s$ for simplicity of exposition.

We are now ready to introduce three types of constraints in terms of dual quaternions:

1) Line-of-sight constraints.

2) Approach slope angle constraints, of which upper-and-lower bound constraints is a re-interpretation of the geometry.

3) Body attitude constraint with respect to an inertial direction.

For this, we will use notation consistent with [112]. Additionally, we require two auxiliary frames. We will define G as fixed on a gripper, and A as fixed on an asteroid, or an object of interest to be captured.

Proposition 1. *Consider the domain* $\mathcal{D} = \{\boldsymbol{q}_{\text{G/A}} \in \mathbb{H}_d : \boldsymbol{q}_{\text{G/A}} \circ \boldsymbol{q}_{\text{G/A}} \leq 1 + \frac{1}{4}\delta^2\}$. *The line of sight constraint depicted in Figure 3.3 can be encoded as*

$$r^{\text{G}}_{\text{A/G}} \cdot \hat{y}^{\text{G}} \geq \|r^{\text{G}}_{\text{A/G}}\| \cos\theta, \tag{3.34}$$

and it requires that the angle between $r^{\text{G}}_{\text{A/G}}$ *and* $\hat{y}^{\text{G}}$ *remains less than* θ. *Using dual quaternions, this constraint can be equivalently expressed as*

$$-\boldsymbol{q}_{\text{G/A}} \circ (M_H \star \boldsymbol{q}_{\text{G/A}}) + 2\|E_d \boldsymbol{q}_{\text{G/A}}\| \cos\theta \leq 0, \tag{3.35}$$

where

$$M_H = \begin{bmatrix} 0_{4\times 4} & [\![\hat{y}^{\text{G}}]\!]^{\text{T}}_{\text{R}} \\ [\![\hat{y}^{\text{G}}]\!]_{\text{R}} & 0_{4\times 4} \end{bmatrix}, \tag{3.36}$$

and it is convex over $\mathcal{D}$.

Proposition 2. *Consider the domain* $\mathcal{D} = \{\boldsymbol{q}_{\text{G/A}} \in \mathbb{H}_d : \boldsymbol{q}_{\text{G/A}} \circ \boldsymbol{q}_{\text{G/A}} \leq 1 + \frac{1}{4}\delta^2\}$. *The approach slope constraint depicted in Figure 3.4, and the upper-and-lower bounded approach constraint depicted in Figure 3.5, can be encoded as*

$$r^{\text{A}}_{\text{G/A}} \cdot \hat{z}^{\text{A}} \geq \|r^{\text{A}}_{\text{G/A}}\| \cos\phi, \tag{3.37}$$

and it requires that the angle between $r^{\text{A}}_{\text{G/A}}$ *and* $\hat{z}^{\text{A}}$ *remains less than* ϕ. *Using dual quaternions, this constraint can be equivalently expressed as*

$$-\boldsymbol{q}_{\text{G/A}} \circ (M_G \star \boldsymbol{q}_{\text{G/A}}) + 2\|E_d \boldsymbol{q}_{\text{G/A}}\| \cos\phi \leq 0, \tag{3.38}$$

where

$$M_G = \begin{bmatrix} 0_{4\times 4} & [\![\hat{z}^{\text{A}}]\!]^{\text{T}}_{\text{L}} \\ [\![\hat{z}^{\text{A}}]\!]_{\text{L}} & 0_{4\times 4} \end{bmatrix}, \tag{3.39}$$

and it is convex over $\mathcal{D}$.

Proposition 3. *Consider the domain $\mathcal{D} = \{\boldsymbol{q}_{\text{В/И}} \in \mathbb{H}_d : \boldsymbol{q}_{\text{В/И}} \circ \boldsymbol{q}_{\text{В/И}} \leq 1 + \frac{1}{4}\delta^2\}$. The attitude constraint depicted in Figure 3.6 can be encoded as*

$$\hat{n}^{\text{I}} \cdot (q_{\text{В/И}} \hat{n}^{\text{B}} q^{*}_{\text{В/И}}) \geq \cos\psi, \tag{3.40}$$

and it requires that the angle between the inertially fixed vector $\hat{n}^{\text{I}}$ and the body fixed vector $\hat{n}^{\text{B}}$ remains less than ψ. Using dual quaternions, this constraint can be equivalently expressed as

$$\boldsymbol{q}_{\text{В/И}} \circ (M_A \star \boldsymbol{q}_{\text{В/И}}) + \cos\psi \leq 0, \tag{3.41}$$

where

$$M_A = \begin{bmatrix} [\![\hat{z}^{\text{I}}]\!]_{\text{L}} [\![\hat{z}^{\text{B}}]\!]_{\text{R}} & 0_{4\times4} \\ 0_{4\times4} & 0_{4\times4} \end{bmatrix}, \tag{3.42}$$

and it is convex over $\mathcal{D}$.

3.5 Example: Forward Kinematics with an Inertially Fixed Base

The serial RR configuration in Figure 3.7 will be used as an example on how to use dual quaternions for forward kinematics. Notice that the pose of the end effector with respect to the inertial frame is given by

$$\boldsymbol{q}_{\text{e/И}} = \boldsymbol{q}_{\text{1/И}} \boldsymbol{q}_{\text{2/1}} \boldsymbol{q}_{\text{e/2}} \tag{3.43}$$

For the sake of exposition, these are given by

$$\boldsymbol{q}_{\text{1/И}} = (1 + \epsilon\tfrac{1}{2} r^{\text{I}}_{\text{1/И}})(q_{\text{1/И}} + \epsilon 0) \tag{3.44}$$

$$\boldsymbol{q}_{\text{2/1}} = (1 + \epsilon\tfrac{1}{2} r^{\text{1}}_{\text{2/1}})(q_{\text{2/1}} + \epsilon 0) \tag{3.45}$$

$$\boldsymbol{q}_{\text{e/2}} = (1 + \epsilon\tfrac{1}{2} r^{\text{2}}_{\text{e/2}})(q_{\text{e/2}} + \epsilon 0), \tag{3.46}$$

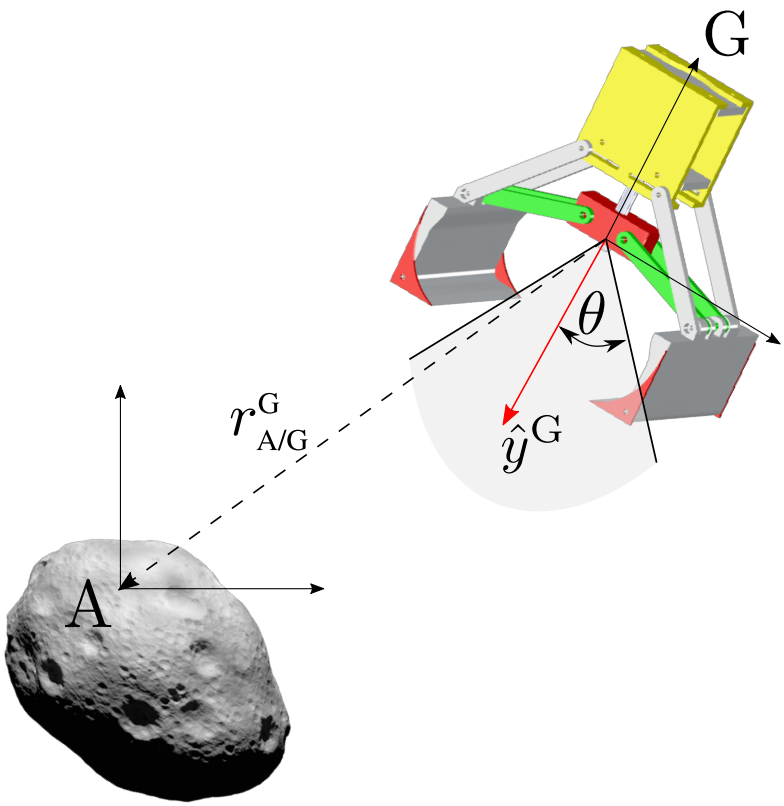

Figure 3.3: Line-of-sight constraint during grappling.

where the *translation-first* approach has been used. Each of these quantities can be easily determined from the geometry of the problem. The position quaternions are given by $r^{Y}_{X/Y} = (0, \bar{r}^{Y}_{X/Y})$, and

$$\bar{r}^{I}_{1/I} = [0, 0, 0]^{T} \tag{3.47}$$

$$\bar{r}^{1}_{2/1} = [l_1, 0, 0]^{T} \tag{3.48}$$

$$\bar{r}^{2}_{e/2} = [l_2, 0, 0]^{T} \tag{3.49}$$

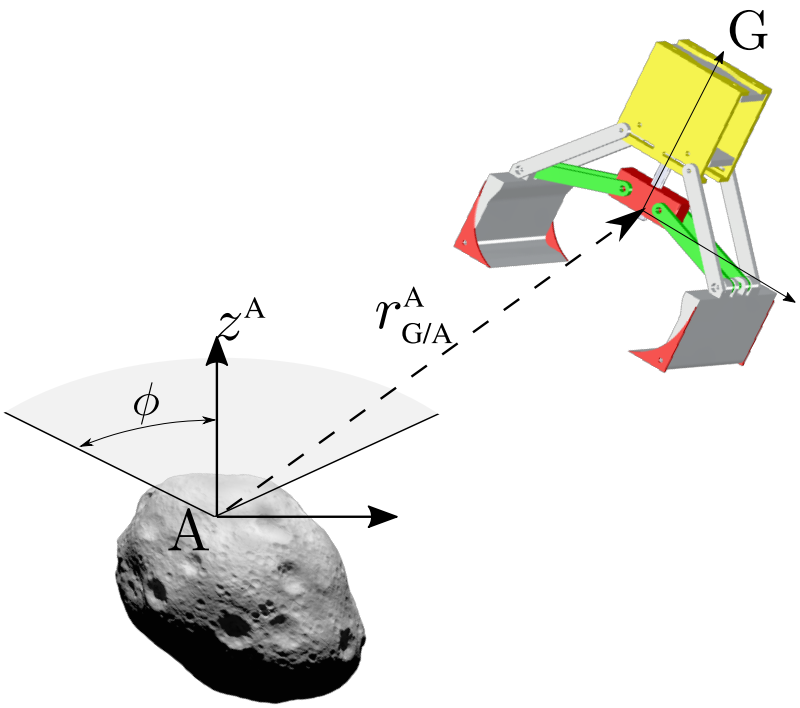

Figure 3.4: Approach slope constraint.

while the quaternions are given by

$$q_{1/I} = (\cos \alpha_1/2, [0, 0, \sin \alpha_1/2]^{T}) \tag{3.50}$$

$$q_{1/I} = (\cos \alpha_2/2, [0, 0, \sin \alpha_2/2]^{T}) \tag{3.51}$$

$$q_{e/2} = 1. \tag{3.52}$$

The time derivative of the dual quaternion yields information about the angular and linear velocity of the end-effector. In particular, we have that for a dual quaternion:

$$\dot{\boldsymbol{q}}_{X/Y} = \tfrac{1}{2}\boldsymbol{q}_{X/Y}\boldsymbol{\omega}^{X}_{X/Y} \tag{3.53}$$

$$\dot{\boldsymbol{q}}_{X/Y} = \tfrac{1}{2}\boldsymbol{\omega}^{Y}_{X/Y}\boldsymbol{q}_{X/Y} \tag{3.54}$$

where equation (3.53) is associated with a body-frame time derivative, while equation (3.54) is associated with a spatial-frame time derivative.

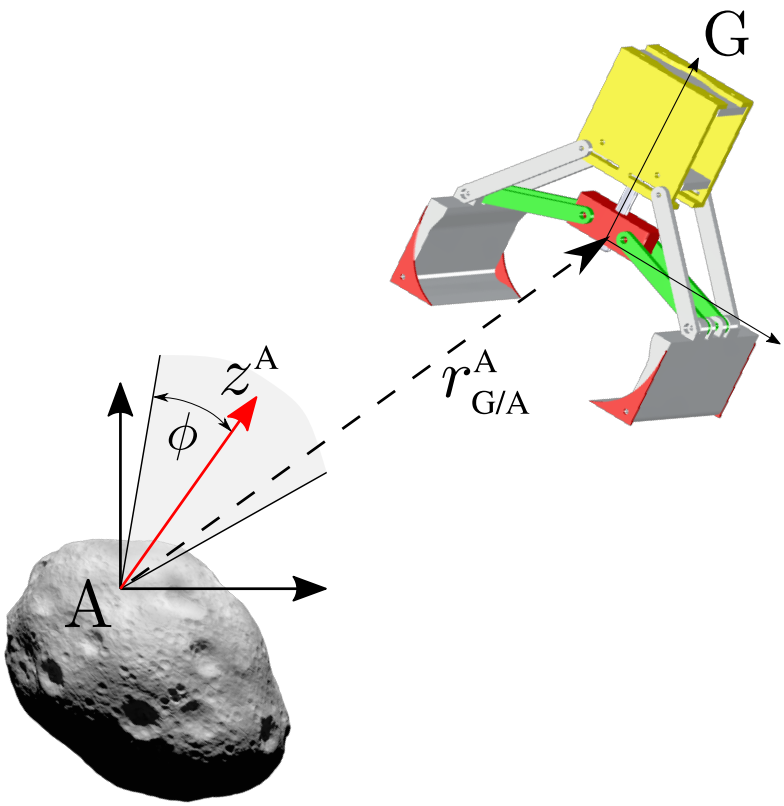

Figure 3.5: Upper-and-lower bounds constraint.

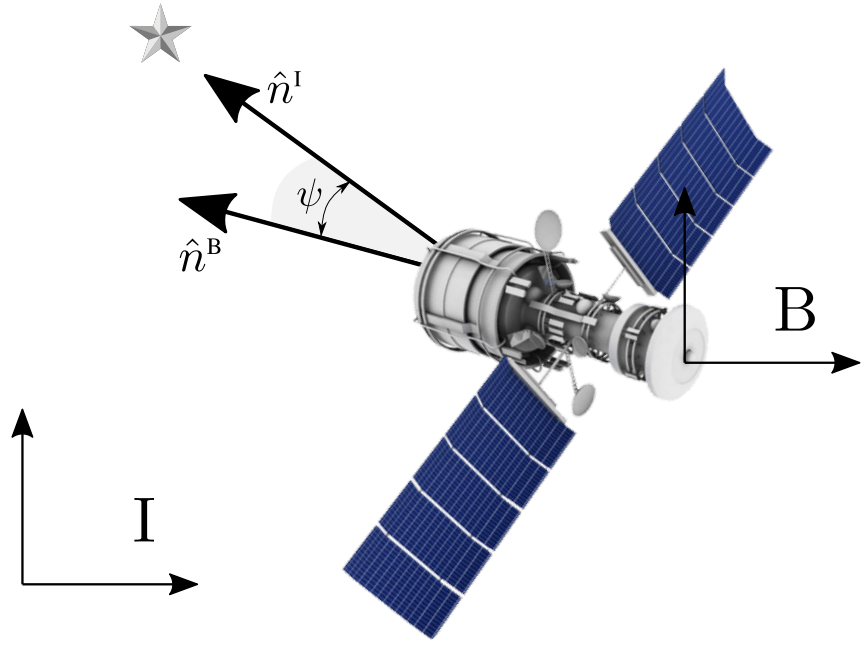

Figure 3.6: General attitude constraint with respect to inertial directions.

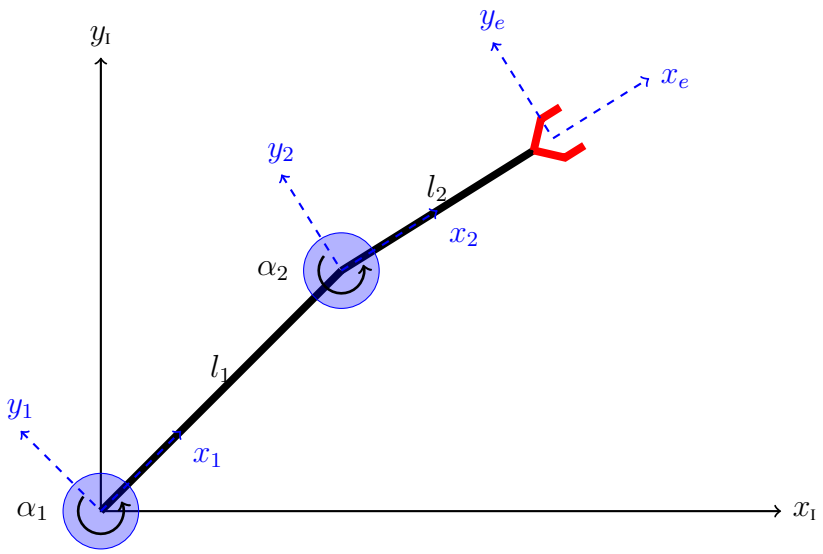

Figure 3.7: Robot arm configuration.

With these definitions in mind, we compute the time-rate of change of the pose of the end-effector as

$$\dot{\boldsymbol{q}}_{e/I} = \dot{\boldsymbol{q}}_{1/I}\boldsymbol{q}_{2/1}\boldsymbol{q}_{e/2} + \boldsymbol{q}_{1/I}\dot{\boldsymbol{q}}_{2/1}\boldsymbol{q}_{e/2} + \boldsymbol{q}_{1/I}\boldsymbol{q}_{2/1}\dot{\boldsymbol{q}}_{e/2} \tag{3.55}$$

$$= \tfrac{1}{2}\boldsymbol{q}_{1/I}\boldsymbol{\omega}^{1}_{1/I}\boldsymbol{q}_{2/1}\boldsymbol{q}_{e/2} + \boldsymbol{q}_{1/I}\tfrac{1}{2}\boldsymbol{q}_{2/1}\boldsymbol{\omega}^{2}_{2/1}\boldsymbol{q}_{e/2} + \boldsymbol{q}_{1/I}\boldsymbol{q}_{2/1}\tfrac{1}{2}\boldsymbol{q}_{e/2}\boldsymbol{\omega}^{e}_{e/2}. \tag{3.56}$$

Then, using equation (3.53), we get that the dual velocity of the end effector with respect

to the inertial frame is given by

$$
\begin{aligned}
\boldsymbol{\omega}^{\mathrm{e}}_{\mathrm{e/I}} &= 2\boldsymbol{q}^{*}_{\mathrm{e/I}}\dot{\boldsymbol{q}}_{\mathrm{e/I}} \\
&= \boldsymbol{q}^{*}_{\mathrm{e/I}}\boldsymbol{q}_{1/\mathrm{I}}\boldsymbol{\omega}^{1}_{1/\mathrm{I}}\boldsymbol{q}_{2/1}\boldsymbol{q}_{\mathrm{e/2}}+\boldsymbol{q}^{*}_{\mathrm{e/I}}\boldsymbol{q}_{1/\mathrm{I}}\boldsymbol{q}_{2/1}\boldsymbol{\omega}^{2}_{2/1}\boldsymbol{q}_{\mathrm{e/2}}+\boldsymbol{q}^{*}_{\mathrm{e/I}}\boldsymbol{q}_{1/\mathrm{I}}\boldsymbol{q}_{2/1}\boldsymbol{q}_{\mathrm{e/2}}\overbrace{\boldsymbol{\omega}^{\mathrm{e}}_{\mathrm{e/2}}}^{=\mathbf{0}} \\
&= \boldsymbol{q}^{*}_{\mathrm{e/2}}\boldsymbol{q}^{*}_{2/1}\boldsymbol{q}^{*}_{1/\mathrm{I}}\boldsymbol{q}_{1/\mathrm{I}}\boldsymbol{\omega}^{1}_{1/\mathrm{I}}\boldsymbol{q}_{2/1}\boldsymbol{q}_{\mathrm{e/2}}+\boldsymbol{q}^{*}_{\mathrm{e/2}}\boldsymbol{q}^{*}_{2/1}\boldsymbol{q}^{*}_{1/\mathrm{I}}\boldsymbol{q}_{1/\mathrm{I}}\boldsymbol{q}_{2/1}\boldsymbol{\omega}^{2}_{2/1}\boldsymbol{q}_{\mathrm{e/2}} \\
&= \boldsymbol{q}^{*}_{\mathrm{e/2}}\boldsymbol{q}^{*}_{2/1}\boldsymbol{\omega}^{1}_{1/\mathrm{I}}\boldsymbol{q}_{2/1}\boldsymbol{q}_{\mathrm{e/2}}+\boldsymbol{q}^{*}_{\mathrm{e/2}}\boldsymbol{\omega}^{2}_{2/1}\boldsymbol{q}_{\mathrm{e/2}} \\
&= \mathrm{Ad}_{\boldsymbol{q}^{*}_{\mathrm{e/2}}\boldsymbol{q}^{*}_{2/1}}\boldsymbol{\omega}^{1}_{1/\mathrm{I}}+\mathrm{Ad}_{\mathrm{q}^{*}_{\mathrm{e/2}}}\boldsymbol{\omega}^{2}_{2/1} \\
&= \mathrm{Ad}_{(\boldsymbol{q}_{2/1}\boldsymbol{q}_{\mathrm{e/2}})^{*}}\boldsymbol{\omega}^{1}_{1/\mathrm{I}}+\mathrm{Ad}_{(\mathrm{q_{e/2}})^{*}}\boldsymbol{\omega}^{2}_{2/1} \\
&= \left[\mathrm{Ad}_{(\boldsymbol{q}_{2/1}\boldsymbol{q}_{\mathrm{e/2}})^{*}}\boldsymbol{\xi}^{1}_{1/\mathrm{I}}, \quad \mathrm{Ad}_{(\mathrm{q_{e/2}})^{*}}\boldsymbol{\xi}^{2}_{2/1}\right]\dot{\bar{\alpha}} \qquad (3.57) \\
&= J^{\mathrm{B}}(\boldsymbol{q},\boldsymbol{\xi})\dot{\bar{\alpha}} \qquad (3.58)
\end{aligned}
$$

where $J^{\mathrm{B}}(\boldsymbol{q},\boldsymbol{\xi})$ is the Jacobian expressed in the body frame, the group adjoint operation for dual quaternions is defined as

$$\mathrm{Ad}_{\boldsymbol{q}}\boldsymbol{h} = \boldsymbol{q}\boldsymbol{h}\boldsymbol{q}^{-1} = \boldsymbol{q}\boldsymbol{h}\boldsymbol{q}^{*}, \qquad (3.59)$$

and

$$\bar{\alpha} = \begin{bmatrix}\alpha_1 \\ \\ \alpha_2\end{bmatrix} \quad \text{and} \quad \dot{\bar{\alpha}} = \begin{bmatrix}\dot{\alpha}_1 \\ \\ \dot{\alpha}_2\end{bmatrix}. \qquad (3.60)$$

The elements $\boldsymbol{\xi}_i$ are the screws for each of the joints. In general, the screws for revolute and prismatic joints are listed in Table 3.1, and these are independent of the current robot configuration.

Table 3.1: Screw ($\boldsymbol{\xi}_i$) for revolute and prismatic joints.

	Revolute Joint	Prismatic Joint
X-axis	$(0,[1,0,0]^{\mathrm{T}})+\epsilon 0$	$0+\epsilon(0,[1,0,0]^{\mathrm{T}})$
Y-axis	$(0,[0,1,0]^{\mathrm{T}})+\epsilon 0$	$0+\epsilon(0,[0,1,0]^{\mathrm{T}})$
Z-axis	$(0,[0,0,1]^{\mathrm{T}})+\epsilon 0$	$0+\epsilon(0,[0,0,1]^{\mathrm{T}})$

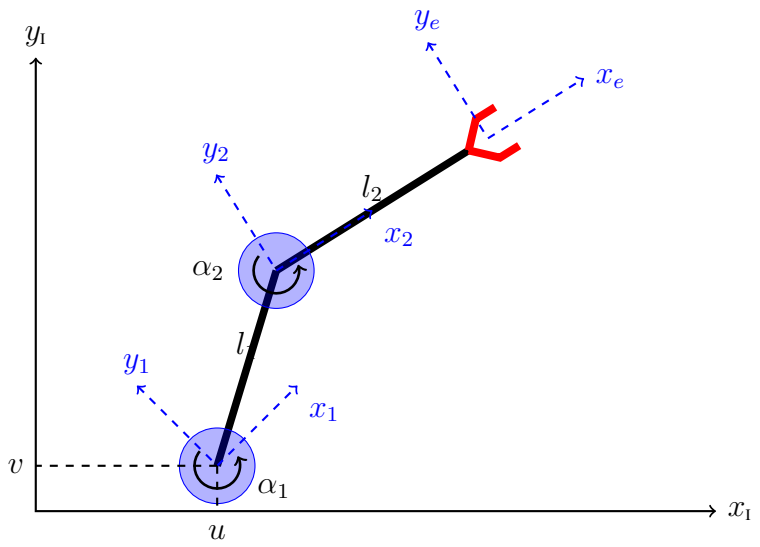

Figure 3.8: Robot arm configuration.

3.6 Example: Forward Kinematics of a Floating Double Pendulum with End-Effector

Given the floating double pendulum shown in Figure 3.8, we want to model its kinematics. The difference with respect to the one shown in Figure 3.7 is that the first revolute joint is free to translate in space.

The kinematic equations of motion can thus be derived as follows using a geometric description of the forward kinematics

$$\boldsymbol{q}_{e/I} = \boldsymbol{q}_{1/I}\boldsymbol{q}_{2/1}\boldsymbol{q}_{e/2}, \tag{3.61}$$

where $\boldsymbol{q}_{1/I}$, $\boldsymbol{q}_{2/1}$, $\boldsymbol{q}_{e/2}$ are given by Equations (3.44) to (3.46). However, $\bar{r}^{I}_{1/I} = [u, v, 0]^{T}$ determines the translation of the first revolute joint in 2D. It is clear that

$$\frac{\mathrm{d}}{\mathrm{d}t}\bar{r}^{I}_{1/I} = \dot{\bar{r}}^{I}_{1/I} = \bar{v}^{I}_{1/I} = [\dot{u}, \dot{v}, 0]^{T} \tag{3.62}$$

In this case, the time evolution of $\boldsymbol{q}_{1/\mathrm{I}}$ is given by

$$\dot{\boldsymbol{q}}_{1/\mathrm{I}} = \tfrac{1}{2}\boldsymbol{\omega}^{\mathrm{I}}_{1/\mathrm{I}}\boldsymbol{q}_{1/\mathrm{I}} \tag{3.63}$$

as before, but we redefine the dual velocity as dictated by the definition in equation (2.36) as

$$\boldsymbol{\omega}^{\mathrm{I}}_{1/\mathrm{I}} = \omega^{\mathrm{I}}_{1/\mathrm{I}} + \epsilon(v^{\mathrm{I}}_{1/\mathrm{I}} - \omega^{\mathrm{I}}_{1/\mathrm{I}} \times r^{\mathrm{I}}_{1/\mathrm{I}}). \tag{3.64}$$

The relationship derived earlier

$$\boldsymbol{\omega}^{\mathrm{e}}_{e/\mathrm{I}} = \mathrm{Ad}_{\boldsymbol{q}^*_{e/2}\boldsymbol{q}^*_{2/1}}\boldsymbol{\omega}^{1}_{1/\mathrm{I}} + \mathrm{Ad}_{\mathrm{q}^*_{e/2}}\boldsymbol{\omega}^{2}_{2/1}$$

still holds. However, $\boldsymbol{\omega}^{1}_{1/\mathrm{I}}$ must be computed from our knowledge of $\boldsymbol{\omega}^{\mathrm{I}}_{1/\mathrm{I}}$. While in quaternion and vector notation this might be troublesome, the expression using dual quaternions is simple and given by

$$\begin{aligned} \boldsymbol{\omega}^{1}_{1/\mathrm{I}} &= \boldsymbol{q}^*_{1/\mathrm{I}}\boldsymbol{\omega}^{\mathrm{I}}_{1/\mathrm{I}}\boldsymbol{q}_{1/\mathrm{I}} \\ &= \mathrm{Ad}_{\boldsymbol{q}_{1/\mathrm{I}}}\boldsymbol{\omega}^{\mathrm{I}}_{1/\mathrm{I}}. \end{aligned} \tag{3.65}$$

In general, a change of reference frame for a dual vector quantity (in particular, twists[3]) can be performed as follows

$$\boldsymbol{s}^{\mathrm{Y}} = \boldsymbol{q}^*_{\mathrm{Y/X}}\boldsymbol{s}^{\mathrm{X}}\boldsymbol{q}_{\mathrm{Y/X}} \tag{3.66}$$

$$= \mathrm{Ad}_{\boldsymbol{q}^*_{\mathrm{Y/X}}}\boldsymbol{s}^{\mathrm{X}}. \tag{3.67}$$

In this chapter we provide a broad overview of different applications that dual quaternions have in the literature. These included basic fixed-base robotics concepts such as forward kinematics, but also included preliminary results on the use of dual quaternions

[3]The effect of the frame change operation on a wrench will change the point of application of the wrench. This transformation is explored in detail in Section 2.3.1.

for constraint and kinematic modeling of systems mounted on a satellite base. The results provided in this chapter merely represent a toolbox to be used in solving more complex engineering problems.

CHAPTER 4

POSE TRACKING AND DUAL INERTIA ESTIMATION USING CONCURRENT LEARNING WITH DUAL QUATERNIONS

In the past, much of spacecraft control literature has focused on performing attitude reference tracking through the use of a wide range of techniques and attitude parameterizations [122, 123, 124, 125, 126]. With the advent of space missions (both commercial and military), spacecraft proximity operations have become increasingly common, and they remain among the most critical phases for space-related activities. Ranging from on-orbit servicing, asteroid sample return, or just rendezvous and docking, these maneuvers pose a challenging technological problem that requires addressing the natural coupling between the spacecraft's attitude and its relative position.

Originally, the modeling of rigid body motion to address proximity operations was decoupled into the corresponding attitude and position (pose) subproblems [127, 128]. This tends to be the simpler approach, as it makes use of conventional techniques. The cost is usually efficiency and accuracy. New techniques treat attitude and position on the same footing and thus increase numerical efficiency and accuracy. The benefits have been especially dominant in the field of estimation, where combined representations of pose have led to significant improvements in the estimation of position [57, 129, 130, 131].

Within the area of kinematic and dynamic modeling, *fixed-base* robotics literature has flourished, making extensive use of Lie-algebraic techniques, or Spatial Vector Algebra, formalized by Featherstone et al. [101, 102]. However, modeling of a *freely-rotating* body and its dynamics under the same framework requires in-depth knowledge of the corresponding algebra and the associated geometric mechanics formalisms for appropriate use and implementation (see [132] as an example of a Lie-algebraic-based approach). This added complexity makes quaternions and, in particular, dual quaternions an appealing al-

ternative to work with for most practitioners.

A large amount of literature exists that addresses the problem of the estimation of the inertia matrix of a spacecraft in orbit. It has been recurrently addressed and different solution approaches exist. The contribution in [133] uses asymptotic results in statistics for estimation. In particular, [133] provides assurances as the number of samples tends to infinity using least-correlation methods, without the assumption that the angular acceleration is known. References [134, 135, 136] also provide least-squares solutions, posing the estimation as an optimization problem with convexity properties that aid in providing a fast convergence to a solution. Though theoretically sound, these approaches can be computationally costly, in many cases requiring matrix inversions or decompositions, or make use of optimization software that may not be flight-rated. In fact, an on-line update of the inertia matrix using these methods could introduce undesired discontinuities to the actuators, making them undesirable for actual on-board implementation, or in a worst-case scenario, destabilize the overall system if the convergence criteria for the estimation of the parameters are not met. Thus, other methods that can account for the closed-loop behavior of the system, and in fact provide guarantees in terms of the boundedness of all control signals, are required.

The field of adaptive control provides the right tools to address the aforementioned concerns about incorporating a varying estimate of the mass properties of the system into a control framework. In the field of adaptive control a common requirement to achieve the estimation task is that of persistency of excitation. This requirement arises in the study of systems with structured uncertainties, as is the case with the estimation of the mass properties of a rigid body, and it represents a rather stringent requirement [137, 46, 49, 138]. The necessary rank conditions on the integral with respect to time of certain regressor matrices can be ensured by actuating the different axes of the spacecraft, as is done in [46]. However, this may lead to unnecessary maneuvering, thus wasting fuel and power.

The main objective of this chapter is to provide an adaptive controller capable of track-

ing time-varying reference maneuvers for 6-DOF motion. This controller will be augmented with a concurrent learning-based adaptation of the dual inertia matrix, providing stronger parameter convergence assurances than those provided by the well-known persistency of excitation requirement. Concurrent learning was initially proposed by Chowdhary et al. [139, 140], and it claims to bypass the requirement of persistency of excitation, instead requiring that the rank of a matrix built from a finite set of input-output data be the same as the dimensionality of the uncertainty. Additionally, it avoids matrix inversion, which for ill-conditioned estimation problems can lead to numerical complications, while still being seamlessly integrated into an existing 6-DOF pose tracking controller.

In this chapter we will provide the necessary background for concurrent learning and proceed to formalize the use of the framework in the continuous-time setting, which to the best of the author's knowledge, has not been done. This continuous-time formalism is embedded into an adaptive pose-tracking controller for a rigid body in the context of dual quaternions. The more practical implementation of the proposed controller, which is based on discrete sampling, is then formulated. We conclude by showing that persistency of excitation and the rank condition required in concurrent learning are one and the same, with the important distinction that incorporating the concurrent learning framework during the estimation will always aid in achieving the positive definite condition required in persistency of excitation. Results for both proposed controllers are then compared to a baseline controller that possesses no concurrent learning-based estimation.

4.1 Concurrent Learning

Concurrent learning is a recently proposed approach that makes use of the current measured state of the system, and possibly previous recorded data, to modify the adaptation of the unknown parameters in an adaptive control setting. Section 3 of [140] lays out the fundamental results for the theory. An overview of how the concept feeds into Lyapunov stability theory is provided here for the reader's convenience, in the context of the estimation of the

mass properties for a spacecraft.

The first step is to recast the dynamics from equation (2.58) in a way amenable to the concurrent learning framework. Specifically, we want the unknown parameters to appear linearly with respect to the regressors, as is the case in most adaptive control approaches. In our case, we will define $\mathrm{v}(M^{\mathrm{B}}) = [I_{11}\ I_{12}\ I_{13}\ I_{22}\ I_{23}\ I_{33}\ m]^{\mathrm{T}}$, a vectorized version of the dual inertia matrix M^{B}, and the error in the estimation of the dual inertia matrix as

$$\Delta M^{\mathrm{B}} = \widehat{M^{\mathrm{B}}} - M^{\mathrm{B}}, \tag{4.1}$$

as they were originally defined in [46]. This allows us to define the auxiliary function $r : \mathbb{H}_d^v \to \mathbb{R}^{8\times 7}$ that satisfies

$$M^{\mathrm{B}} \star \boldsymbol{a} \triangleq r(\boldsymbol{a})\mathrm{v}(M^{\mathrm{B}}) = \begin{bmatrix} 0 & 0 & 0 & 0 & 0 & 0 & 0 \\ 0 & 0 & 0 & 0 & 0 & 0 & a_2 \\ 0 & 0 & 0 & 0 & 0 & 0 & a_3 \\ 0 & 0 & 0 & 0 & 0 & 0 & a_4 \\ 0 & 0 & 0 & 0 & 0 & 0 & 0 \\ a_6 & a_7 & a_8 & 0 & 0 & 0 & 0 \\ 0 & a_6 & 0 & a_7 & a_8 & 0 & 0 \\ 0 & 0 & a_6 & 0 & a_7 & a_8 & 0 \end{bmatrix} \mathrm{v}(M^{\mathrm{B}}). \tag{4.2}$$

Using this expression to manipulate equation (2.58) yields the following affine representa-

tion with respect to $\mathrm{v}(M^{\mathrm{B}})$

$$
\begin{aligned}
\boldsymbol{f}^{\mathrm{B}} &= r((\dot{\boldsymbol{\omega}}^{\mathrm{B}}_{\mathrm{B/D}})^{\mathsf{s}})\mathrm{v}(M^{\mathrm{B}}) + [(\boldsymbol{\omega}^{\mathrm{B}}_{\mathrm{B/D}} + \boldsymbol{\omega}^{\mathrm{B}}_{\mathrm{D/I}})]^{\times} r((\boldsymbol{\omega}^{\mathrm{B}}_{\mathrm{B/D}})^{\mathsf{s}} + (\boldsymbol{\omega}^{\mathrm{B}}_{\mathrm{D/I}})^{\mathsf{s}})\mathrm{v}(M^{\mathrm{B}}) \\
&\quad + r((\boldsymbol{q}^{*}_{\mathrm{B/D}} \dot{\boldsymbol{\omega}}^{\mathrm{D}}_{\mathrm{D/I}} \boldsymbol{q}_{\mathrm{B/D}})^{\mathsf{s}})\mathrm{v}(M^{\mathrm{B}}) + r((\boldsymbol{\omega}^{\mathrm{B}}_{\mathrm{D/I}} \times \boldsymbol{\omega}^{\mathrm{B}}_{\mathrm{B/D}})^{\mathsf{s}})\mathrm{v}(M^{\mathrm{B}}) \\
&= \Big[r((\dot{\boldsymbol{\omega}}^{\mathrm{B}}_{\mathrm{B/D}} + \boldsymbol{q}^{*}_{\mathrm{B/D}} \dot{\boldsymbol{\omega}}^{\mathrm{D}}_{\mathrm{D/I}} \boldsymbol{q}_{\mathrm{B/D}} + \boldsymbol{\omega}^{\mathrm{B}}_{\mathrm{D/I}} \times \boldsymbol{\omega}^{\mathrm{B}}_{\mathrm{B/D}})^{\mathsf{s}}) + [(\boldsymbol{\omega}^{\mathrm{B}}_{\mathrm{B/D}} + \boldsymbol{\omega}^{\mathrm{B}}_{\mathrm{D/I}})]^{\times} r((\boldsymbol{\omega}^{\mathrm{B}}_{\mathrm{B/D}} + \boldsymbol{\omega}^{\mathrm{B}}_{\mathrm{D/I}})^{\mathsf{s}}) \Big] \mathrm{v}(M^{\mathrm{B}}) \\
&\triangleq \underbrace{R(\dot{\boldsymbol{\omega}}^{\mathrm{B}}_{\mathrm{B/D}}, \boldsymbol{\omega}^{\mathrm{B}}_{\mathrm{B/D}}, \dot{\boldsymbol{\omega}}^{\mathrm{D}}_{\mathrm{D/I}}, \boldsymbol{\omega}^{\mathrm{D}}_{\mathrm{D/I}}, \boldsymbol{q}_{\mathrm{B/D}})}_{\text{regressor matrix}} \mathrm{v}(M^{\mathrm{B}}) = R\mathrm{v}(M^{\mathrm{B}}),
\end{aligned} \tag{4.3}
$$

where $R : \mathbb{H}^{v}_{d} \times \mathbb{H}^{v}_{d} \times \mathbb{H}^{v}_{d} \times \mathbb{H}^{v}_{d} \times \mathbb{H}^{u}_{d} \to \mathbb{R}^{8\times 7}$. Dropping the arguments of R for convenience and defining the variable ε as

$$
\varepsilon \triangleq R\mathrm{v}(\widehat{M^{\mathrm{B}}}) - \boldsymbol{f}^{\mathrm{B}}, \tag{4.4}
$$

and using equation (4.3), the above equation can be re-interpreted as

$$
\begin{aligned}
\varepsilon &\triangleq R\mathrm{v}(\widehat{M^{\mathrm{B}}}) - \boldsymbol{f}^{\mathrm{B}} \\
&= R\mathrm{v}(\widehat{M^{\mathrm{B}}}) - R\mathrm{v}(M^{\mathrm{B}}) \\
&= R\left(\mathrm{v}(\widehat{M^{\mathrm{B}}}) - \mathrm{v}(M^{\mathrm{B}})\right) \\
&= R\mathrm{v}(\Delta M^{\mathrm{B}}),
\end{aligned} \tag{4.5}
$$

effectively making ε a signal that quantifies the error in the dual inertia matrix for a given estimate $\mathrm{v}(\widehat{M^{\mathrm{B}}})$. This quantification of the error in the inertia matrix is, in fact, the key step in concurrent learning, since it will allow us to introduce information about the dynamical state of the system at every timestep. Additionally, since the dynamics of the system are captured in a dual quaternion form, we must only include one dynamical equation of motion to capture both rotational and translational information. At this point, it is also worth emphasizing that in generating the variable ε there is no need for the true inertia matrix parameters; only knowledge of the regressor matrix R, the *estimated* dual inertia, and the

applied dual force are needed, as in equation (4.4).

4.2 Adaptive Control with Continuous Concurrent Learning

In this section we provide an adaptive pose-tracking controller that uses a new continuous formulation of the concurrent learning algorithm to provide strong assurances on the convergence of the mass and the inertia matrix of the spacecraft. The result is an extension of the controller first described in [46], with the corrections incorporated in [50]. The proof closely mimics the proof provided therein with two modifications. The main modification is the incorporation of a new concurrent learning-based term which leads to improved performance in the estimation of the mass properties, while still providing a controller that can achieve the tracking objective. Second, a more logical sequence of steps for the use of Barbalat's Lemma is provided, compared to the approach followed in [50].

For the proof of the adaptive controller result, we will make use of the following lemma.

Lemma 11. *The equality* $\boldsymbol{q}^*_{\text{B/D}}(\boldsymbol{q}^{\mathsf{s}}_{\text{B/D}} - \mathbf{1}^{\mathsf{s}}) = \mathbf{0}$ *implies* $\boldsymbol{q}_{\text{B/D}} = \mathbf{1}$ *(i.e.,* $q_{\text{B/D}} = 1$ *and* $r^{\text{B}}_{\text{B/D}} = 0$*).*

Proof. From the definition of a unit dual quaternion $\boldsymbol{q}_{\text{B/D}}$, the swap operator, and the unit dual quaternion we obtain

$$\begin{aligned}\mathbf{0} = \boldsymbol{q}^*_{\text{B/D}}(\boldsymbol{q}^{\mathsf{s}}_{\text{B/D}} - \mathbf{1}^{\mathsf{s}}) &= (q^*_{\text{B/D}} + \epsilon\tfrac{1}{2}(r^{\text{B}}_{\text{B/D}})^* q^*_{\text{B/D}})(\tfrac{1}{2} q_{\text{B/D}} r^{\text{B}}_{\text{B/D}} + \epsilon(q_{\text{B/D}} - 1)) \\ &= \tfrac{1}{2} q^*_{\text{B/D}} q_{\text{B/D}} r^{\text{B}}_{\text{B/D}} + \epsilon(\tfrac{1}{4}(r^{\text{B}}_{\text{B/D}})^* q^*_{\text{B/D}} q_{\text{B/D}} r^{\text{B}}_{\text{B/D}} + q^*_{\text{B/D}}(q_{\text{B/D}} - 1)) \\ &= \tfrac{1}{2} r^{\text{B}}_{\text{B/D}} + \epsilon(\tfrac{1}{4}(r^{\text{B}}_{\text{B/D}})^* r^{\text{B}}_{\text{B/D}} + 1 - q^*_{\text{B/D}}),\end{aligned} \tag{4.6}$$

where the real part must be 0, meaning that $r^{\text{B}}_{\text{B/D}} = 0$. In an analogous way, the dual part must satisfy $0 = \frac{1}{4}(r^{\text{B}}_{\text{B/D}})^* r^{\text{B}}_{\text{B/D}} + 1 - q^*_{\text{B/D}} = 1 - q^*_{\text{B/D}}$. From this relationship, we conclude that $1 = q_{\text{B/D}}$. ■

Remark 3. The dual quaternion $-\mathbf{1}$ does not satisfy the condition $\boldsymbol{q}^*_{\text{B/D}}(\boldsymbol{q}^{\mathsf{s}}_{\text{B/D}} - \mathbf{1}^{\mathsf{s}}) = \mathbf{0}$. In fact, evaluating $\boldsymbol{q}_{\text{B/D}} = -\mathbf{1}$ in the expression $\boldsymbol{q}^*_{\text{B/D}}(\boldsymbol{q}^{\mathsf{s}}_{\text{B/D}} - \mathbf{1}^{\mathsf{s}})$ yields $(-\mathbf{1})^*((-\mathbf{1})^{\mathsf{s}} - \mathbf{1}^{\mathsf{s}}) = 0 + \epsilon(2, 0_{3\times 1})$.

Lemma 12. *As shown in [50], the equality* $\mathrm{vec}\big(\boldsymbol{q}^{*}_{\mathrm{B/D}}(\boldsymbol{q}^{\mathrm{S}}_{\mathrm{B/D}} - \mathbf{1}^{\mathrm{S}})\big) = \mathbf{0}$ *implies* $\boldsymbol{q}_{\mathrm{B/D}} = \pm\mathbf{1}$.

Proof. From the proof of Lemma 11,

$$\mathbf{0} = \tfrac{1}{2} r^{\mathrm{B}}_{\mathrm{B/D}} + \epsilon(\tfrac{1}{4}(r^{\mathrm{B}}_{\mathrm{B/D}})^{*} r^{\mathrm{B}}_{\mathrm{B/D}} + 1 - q^{*}_{\mathrm{B/D}}). \tag{4.7}$$

Applying the $\mathrm{vec}\big(\ \cdot\ \big)$ operator on both sides, we obtain

$$\begin{aligned}
\mathbf{0} &= \mathrm{vec}\big(\tfrac{1}{2} r^{\mathrm{B}}_{\mathrm{B/D}} + \epsilon(\tfrac{1}{4}(r^{\mathrm{B}}_{\mathrm{B/D}})^{*} r^{\mathrm{B}}_{\mathrm{B/D}} + 1 - q^{*}_{\mathrm{B/D}})\big) \\
&= \mathrm{vec}\big(\tfrac{1}{2} r^{\mathrm{B}}_{\mathrm{B/D}}\big) + \epsilon \mathrm{vec}\big((\tfrac{1}{4}(r^{\mathrm{B}}_{\mathrm{B/D}})^{*} r^{\mathrm{B}}_{\mathrm{B/D}} + 1 - q^{*}_{\mathrm{B/D}})\big) \\
&= \tfrac{1}{2} r^{\mathrm{B}}_{\mathrm{B/D}} - \epsilon \mathrm{vec}\big(q^{*}_{\mathrm{B/D}}\big) \\
&= \tfrac{1}{2} r^{\mathrm{B}}_{\mathrm{B/D}} + \epsilon \mathrm{vec}\big(q_{\mathrm{B/D}}\big).
\end{aligned} \tag{4.8}$$

Therefore, $r^{\mathrm{B}}_{\mathrm{B/D}} = 0$ and $\overline{q_{\mathrm{B/D}}} = 0_{3\times 1}$, which implies that $q_{\mathrm{B/D}} = \pm 1$, and thus, $\boldsymbol{q}_{\mathrm{B/D}} = \pm\mathbf{1}$.

■

The next theorem presents the main result of this chapter, and shows that it ensures *almost* global asymptotic stability of the linear and angular motion relative to the desired reference, which is the strongest kind of stability that can be proven for this problem for the given parametrization.

Theorem 1. *Consider the relative kinematic and dynamic equations given by equation* (2.38) *and equation* (2.58) *respectively. Let the dual control force be defined by the feedback control law*

$$\begin{aligned}
\boldsymbol{f}^{\mathrm{B}}_{c} = &-\mathrm{vec}\big(\boldsymbol{q}^{*}_{\mathrm{B/D}}(\boldsymbol{q}^{\mathrm{S}}_{\mathrm{B/D}} - \mathbf{1}^{\mathrm{S}})\big) - K_d \star \boldsymbol{s}^{\mathrm{S}} + \boldsymbol{\omega}^{\mathrm{B}}_{\mathrm{B/I}} \times (\widehat{M^{\mathrm{B}}} \star (\boldsymbol{\omega}^{\mathrm{B}}_{\mathrm{B/I}})^{\mathrm{S}}) + \widehat{M^{\mathrm{B}}} \star (\boldsymbol{q}^{*}_{\mathrm{B/D}} \dot{\boldsymbol{\omega}}^{\mathrm{D}}_{\mathrm{D/I}} \boldsymbol{q}_{\mathrm{B/D}})^{\mathrm{S}} \\
&+ \widehat{M^{\mathrm{B}}} \star (\boldsymbol{\omega}^{\mathrm{B}}_{\mathrm{D/I}} \times \boldsymbol{\omega}^{\mathrm{B}}_{\mathrm{B/D}})^{\mathrm{S}} - \widehat{M^{\mathrm{B}}} \star (K_p \star \frac{\mathrm{d}}{\mathrm{d}t}(\boldsymbol{q}^{*}_{\mathrm{B/D}}(\boldsymbol{q}^{\mathrm{S}}_{\mathrm{B/D}} - \mathbf{1}^{\mathrm{S}})))^{\mathrm{S}},
\end{aligned} \tag{4.9}$$

where

$$\boldsymbol{s} = \boldsymbol{\omega}^{\mathrm{B}}_{\mathrm{B/D}} + (K_p \star (\boldsymbol{q}^{*}_{\mathrm{B/D}}(\boldsymbol{q}^{\mathrm{S}}_{\mathrm{B/D}} - \mathbf{1}^{\mathrm{S}})))^{\mathrm{S}}, \tag{4.10}$$

$$K_p = \begin{bmatrix} K_r & 0_{4\times4} \\ 0_{4\times4} & K_q \end{bmatrix},\ K_r = \begin{bmatrix} 0 & 0_{1\times3} \\ 0_{3\times1} & \bar{K}_r \end{bmatrix},\ K_q = \begin{bmatrix} 0 & 0_{1\times3} \\ 0_{3\times1} & \bar{K}_q \end{bmatrix}, \tag{4.11}$$

$$K_d = \begin{bmatrix} K_v & 0_{4\times4} \\ 0_{4\times4} & K_\omega \end{bmatrix},\ K_v = \begin{bmatrix} 0 & 0_{1\times3} \\ 0_{3\times1} & \bar{K}_v \end{bmatrix},\ K_\omega = \begin{bmatrix} 0 & 0_{1\times3} \\ 0_{3\times1} & \bar{K}_\omega \end{bmatrix}, \tag{4.12}$$

and $\bar{K}_r, \bar{K}_q, \bar{K}_v, \bar{K}_\omega \in \mathbb{R}^{3\times3}$ *are positive definite matrices,* $\widehat{M^{\mathrm{B}}}$ *is an estimate of* M^{B} *updated according to*

$$\begin{aligned}\frac{\mathrm{d}}{\mathrm{d}t}\mathrm{v}(\widehat{M^{\mathrm{B}}}) = -\alpha K_i\left(\mathsf{P}\mathrm{v}(\widehat{M^{\mathrm{B}}}) - \mathsf{Q}\right) + K_i\Big[-\mathrm{h}((\boldsymbol{s}\times\boldsymbol{\omega}^{\mathrm{B}}_{\mathrm{B/I}})^{\mathsf{s}}, (\boldsymbol{\omega}^{\mathrm{B}}_{\mathrm{B/I}})^{\mathsf{s}}) \\ -\mathrm{h}(\boldsymbol{s}^{\mathsf{s}}, (\boldsymbol{q}^{*}_{\mathrm{B/D}}\dot{\boldsymbol{\omega}}^{\mathrm{D}}_{\mathrm{D/I}}\boldsymbol{q}_{\mathrm{B/D}})^{\mathsf{s}} + (\boldsymbol{\omega}^{\mathrm{B}}_{\mathrm{D/I}}\times\boldsymbol{\omega}^{\mathrm{B}}_{\mathrm{B/D}})^{\mathsf{s}} - K_p\star\frac{\mathrm{d}(\boldsymbol{q}^{*}_{\mathrm{B/D}}(\boldsymbol{q}^{\mathsf{s}}_{\mathrm{B/D}} - \mathbf{1}^{\mathsf{s}}))}{\mathrm{d}t})\Big],\end{aligned} \tag{4.13}$$

where $\alpha > 0$, $K_i \in \mathbb{R}^{7\times7}$ *is a positive definite matrix, the function* $\mathrm{h} : \mathbb{H}^v_d \times \mathbb{H}^v_d \to \mathbb{R}^7$ *is defined as* $\boldsymbol{a}\circ(M^B \star \boldsymbol{b}) = \mathrm{h}(\boldsymbol{a},\boldsymbol{b})^{\mathsf{T}}\mathrm{v}(M^B) = \mathrm{v}(M^B)^{\mathsf{T}}\mathrm{h}(\boldsymbol{a},\boldsymbol{b})$ *or, equivalently,* $\mathrm{h}(\boldsymbol{a},\boldsymbol{b}) = [a_6b_6,\ a_7b_6{+}a_6b_7,\ a_8b_6{+}a_6b_8,\ a_7b_7,\ a_8b_7{+}a_7b_8,\ a_8b_8,\ a_2b_2{+}a_3b_3{+}a_4b_4]^{\mathsf{T}}$*, and* $\mathsf{P}\in\mathbb{R}^{7\times7}$ *and* $\mathsf{Q}\in\mathbb{R}^7$ *evolve as*

$$\mathsf{P}(t) = \int_{t-\tau}^{t} R^{\mathsf{T}}R\,\mathrm{d}t, \qquad \mathsf{P}(t-\tau) = 0_{7\times7} \text{ and } \tau > 0, \tag{4.14}$$

and

$$\mathsf{Q}(t) = \int_{t-\tau}^{t} R^{\mathsf{T}}\boldsymbol{f}^{\mathrm{B}}\,\mathrm{d}t, \qquad \mathsf{Q}(t-\tau) = 0_{7\times1} \text{ and } \tau > 0, \tag{4.15}$$

where R *and* $\boldsymbol{f}^{\mathrm{B}}$ *are defined as in equation* (4.3)*. Assume that* $\boldsymbol{q}_{\mathrm{D/I}}, \boldsymbol{\omega}^{\mathrm{D}}_{\mathrm{D/I}}, \dot{\boldsymbol{\omega}}^{\mathrm{D}}_{\mathrm{D/I}} \in \mathcal{L}_\infty$*. Then, for all initial conditions,* $\lim_{t\to\infty}\boldsymbol{q}_{\mathrm{B/D}} = \pm\mathbf{1}$ *(i.e.,* $\lim_{t\to\infty} q_{\mathrm{B/D}} = \pm1$ *and* $\lim_{t\to\infty} r^{\mathrm{B}}_{\mathrm{B/D}} = 0$*), and* $\lim_{t\to\infty}\boldsymbol{\omega}^{\mathrm{B}}_{\mathrm{B/D}} = \mathbf{0}$ *(i.e.,* $\lim_{t\to\infty}\omega^{\mathrm{B}}_{\mathrm{B/D}} = 0$ *and* $\lim_{t\to\infty} v^{\mathrm{B}}_{\mathrm{B/D}} = 0$*).*

If, in addition,

$$\operatorname{rank}\mathsf{P} = 7, \tag{4.16}$$

then $\lim_{t\to\infty}\mathrm{v}(\widehat{M^{\mathrm{B}}}) = \mathrm{v}(M^{\mathrm{B}})$.

Proof. Note that $\boldsymbol{q}_{\text{B/D}} = \pm\mathbf{1}$, $\boldsymbol{s} = \mathbf{0}$, and $\mathrm{v}(\Delta M^{\text{B}}) = 0_{7\times 1}$ are the equilibrium conditions of the closed-loop system with dynamics given by equation (2.58), kinematics described by equation (2.38), feedback control law given by equation (4.9), and a dual inertia matrix update as in equation (4.13), with P and Q evolving as described by equations (4.14) and (4.15). Consider now the following candidate Lyapunov function for the equilibrium point $(\boldsymbol{q}_{\text{B/D}}, \boldsymbol{s}, \mathrm{v}(\Delta M^{\text{B}})) = (+\mathbf{1}, \mathbf{0}, 0_{7\times 1})$:

$$V(\boldsymbol{q}_{\text{B/D}}, \boldsymbol{s}, \mathrm{v}(\Delta M^{\text{B}})) = (\boldsymbol{q}_{\text{B/D}} - \mathbf{1}) \circ (\boldsymbol{q}_{\text{B/D}} - \mathbf{1}) + \tfrac{1}{2}\boldsymbol{s}^{\mathsf{S}} \circ (M^{\text{B}} \star \boldsymbol{s}^{\mathsf{S}}) + \tfrac{1}{2}\mathrm{v}(\Delta M^{\text{B}})^{\intercal} K_i^{-1} \mathrm{v}(\Delta M^{\text{B}}). \quad (4.17)$$

Note that V is a valid candidate Lyapunov function since

$$V(\boldsymbol{q}_{\text{B/D}} = \mathbf{1}, \boldsymbol{s} = \mathbf{0}, \mathrm{v}(\Delta M^{\text{B}}) = 0_{7\times 1}) = 0$$

and

$$V(\boldsymbol{q}_{\text{B/D}}, \boldsymbol{s}, \mathrm{v}(\Delta M^{\text{B}})) > 0, \ \forall (\boldsymbol{q}_{\text{B/D}}, \boldsymbol{s}, \mathrm{v}(\Delta M^{\text{B}})) \ \in \mathbb{H}_d^u \times \mathbb{H}_d^v \times \mathbb{R}^7 \backslash \{\mathbf{1}, \mathbf{0}, 0_{7\times 1}\}.$$

The time derivative of V is equal to

$$\dot{V} = 2(\boldsymbol{q}_{\text{B/D}} - \mathbf{1}) \circ \dot{\boldsymbol{q}}_{\text{B/D}} + \boldsymbol{s}^{\mathsf{S}} \circ (M^{\text{B}} \star \dot{\boldsymbol{s}}^{\mathsf{S}}) + \mathrm{v}(\Delta M^{\text{B}})^{\intercal} K_i^{-1} \frac{\mathrm{dv}(\Delta M^{\text{B}})}{\mathrm{d}t}.$$

From equation (2.38) and equation (4.26) we can write $\dot{\boldsymbol{q}}_{\text{B/D}} = \frac{1}{2}\boldsymbol{q}_{\text{B/D}}\boldsymbol{s} - \frac{1}{2}\boldsymbol{q}_{\text{B/D}}(K_p \star (\boldsymbol{q}^*_{\text{B/D}}(\boldsymbol{q}^{\mathsf{S}}_{\text{B/D}} - \mathbf{1}^{\mathsf{S}})))^{\mathsf{S}}$, which can then be plugged into $\dot{V}$, together with the time derivative of equation (4.10), to yield

$$\dot{V} = (\boldsymbol{q}_{\text{B/D}} - \mathbf{1}) \circ (\boldsymbol{q}_{\text{B/D}}\boldsymbol{s} - \boldsymbol{q}_{\text{B/D}}(K_p \star (\boldsymbol{q}^*_{\text{B/D}}(\boldsymbol{q}^{\mathsf{S}}_{\text{B/D}} - \mathbf{1}^{\mathsf{S}})))^{\mathsf{S}}) + \mathrm{v}(\Delta M^{\text{B}})^{\intercal} K_i^{-1} \frac{\mathrm{d}}{\mathrm{d}t}\mathrm{v}(\Delta M^{\text{B}}) + \boldsymbol{s}^{\mathsf{S}} \circ (M^{\text{B}} \star (\dot{\boldsymbol{\omega}}^{\text{B}}_{\text{B/D}})^{\mathsf{S}}) + \boldsymbol{s}^{\mathsf{S}} \circ (M^{\text{B}} \star (K_p \star \frac{\mathrm{d}(\boldsymbol{q}^*_{\text{B/D}}(\boldsymbol{q}^{\mathsf{S}}_{\text{B/D}} - \mathbf{1}^{\mathsf{S}}))}{\mathrm{d}t})).$$

Applying equation (2.25) to the first term, evaluating the dynamics from equation (2.58), and using the identity $\boldsymbol{\omega}^{\mathrm{B}}_{\mathrm{B/D}} + \boldsymbol{\omega}^{\mathrm{B}}_{\mathrm{D/I}} = \boldsymbol{\omega}^{\mathrm{B}}_{\mathrm{B/I}}$ yields

$$\begin{aligned}\dot{V} =& -(K_p \star (\boldsymbol{q}^{*}_{\mathrm{B/D}}(\boldsymbol{q}^{\mathsf{S}}_{\mathrm{B/D}} - \mathbf{1}^{\mathsf{S}}))) \circ (\boldsymbol{q}^{*}_{\mathrm{B/D}}(\boldsymbol{q}^{\mathsf{S}}_{\mathrm{B/D}} - \mathbf{1}^{\mathsf{S}})) + \boldsymbol{s}^{\mathsf{S}} \circ (\boldsymbol{f}^{\mathrm{B}} - \boldsymbol{\omega}^{\mathrm{B}}_{\mathrm{B/I}} \times \left(M^{\mathrm{B}} \star (\boldsymbol{\omega}^{\mathrm{B}}_{\mathrm{B/I}})^{\mathsf{S}}\right) \\ & - M^{\mathrm{B}} \star (\boldsymbol{q}^{*}_{\mathrm{B/D}} \dot{\boldsymbol{\omega}}^{\mathrm{D}}_{\mathrm{D/I}} \boldsymbol{q}_{\mathrm{B/D}})^{\mathsf{S}} - M^{\mathrm{B}} \star (\boldsymbol{\omega}^{\mathrm{B}}_{\mathrm{D/I}} \times \boldsymbol{\omega}^{\mathrm{B}}_{\mathrm{B/D}})^{\mathsf{S}}) + \boldsymbol{s}^{\mathsf{S}} \circ (M^{\mathrm{B}} \star (K_p \star \frac{\mathrm{d}(\boldsymbol{q}^{*}_{\mathrm{B/D}}(\boldsymbol{q}^{\mathsf{S}}_{\mathrm{B/D}} - \mathbf{1}^{\mathsf{S}}))}{\mathrm{d}t})) \\ & + \mathrm{v}(\Delta M^{\mathrm{B}})^{\intercal} K_i^{-1} \frac{\mathrm{d}}{\mathrm{d}t} \mathrm{v}(\Delta M^{\mathrm{B}}) + \boldsymbol{s}^{\mathsf{S}} \circ (\boldsymbol{q}^{*}_{\mathrm{B/D}}(\boldsymbol{q}^{\mathsf{S}}_{\mathrm{B/D}} - \mathbf{1}^{\mathsf{S}})).\end{aligned}$$

Introducing the feedback control law given by equation (4.25) and using equations (2.24) and (2.26) yields

$$\begin{aligned}\dot{V} =& -(\boldsymbol{q}^{*}_{\mathrm{B/D}}(\boldsymbol{q}^{\mathsf{S}}_{\mathrm{B/D}} - \mathbf{1}^{\mathsf{S}})) \circ (K_p \star (\boldsymbol{q}^{*}_{\mathrm{B/D}}(\boldsymbol{q}^{\mathsf{S}}_{\mathrm{B/D}} - \mathbf{1}^{\mathsf{S}}))) + \boldsymbol{s}^{\mathsf{S}} \circ (\boldsymbol{\omega}^{\mathrm{B}}_{\mathrm{B/I}} \times \left(\Delta M^{\mathrm{B}} \star (\boldsymbol{\omega}^{\mathrm{B}}_{\mathrm{B/I}})^{\mathsf{S}}\right) \\ & + \Delta M^{\mathrm{B}} \star (\boldsymbol{q}^{*}_{\mathrm{B/D}} \dot{\boldsymbol{\omega}}^{\mathrm{D}}_{\mathrm{D/I}} \boldsymbol{q}_{\mathrm{B/D}})^{\mathsf{S}} + \Delta M^{\mathrm{B}} \star (\boldsymbol{\omega}^{\mathrm{B}}_{\mathrm{D/I}} \times \boldsymbol{\omega}^{\mathrm{B}}_{\mathrm{B/D}})^{\mathsf{S}} - \Delta M^{\mathrm{B}} \star (K_p \star \frac{\mathrm{d}(\boldsymbol{q}^{*}_{\mathrm{B/D}}(\boldsymbol{q}^{\mathsf{S}}_{\mathrm{B/D}} - \mathbf{1}^{\mathsf{S}}))}{\mathrm{d}t})) \\ & - \boldsymbol{s}^{\mathsf{S}} \circ (K_d \star \boldsymbol{s}^{\mathsf{S}}) + \mathrm{v}(\Delta M^{\mathrm{B}})^{\intercal} K_i^{-1} \frac{\mathrm{d}}{\mathrm{d}t} \mathrm{v}(\Delta M^{\mathrm{B}})\end{aligned}$$

or

$$\begin{aligned}\dot{V} =& -(\boldsymbol{q}^{*}_{\mathrm{B/D}}(\boldsymbol{q}^{\mathsf{S}}_{\mathrm{B/D}} - \mathbf{1}^{\mathsf{S}})) \circ (K_p \star (\boldsymbol{q}^{*}_{\mathrm{B/D}}(\boldsymbol{q}^{\mathsf{S}}_{\mathrm{B/D}} - \mathbf{1}^{\mathsf{S}}))) + (\boldsymbol{s} \times \boldsymbol{\omega}^{\mathrm{B}}_{\mathrm{B/I}})^{\mathsf{S}} \circ (\Delta M^{\mathrm{B}} \star (\boldsymbol{\omega}^{\mathrm{B}}_{\mathrm{B/I}})^{\mathsf{S}}) \\ & + \boldsymbol{s}^{\mathsf{S}} \circ (\Delta M^{\mathrm{B}} \star (\boldsymbol{q}^{*}_{\mathrm{B/D}} \dot{\boldsymbol{\omega}}^{\mathrm{D}}_{\mathrm{D/I}} \boldsymbol{q}_{\mathrm{B/D}})^{\mathsf{S}} + \Delta M^{\mathrm{B}} \star (\boldsymbol{\omega}^{\mathrm{B}}_{\mathrm{D/I}} \times \boldsymbol{\omega}^{\mathrm{B}}_{\mathrm{B/D}})^{\mathsf{S}} - \Delta M^{\mathrm{B}} \star (K_p \star \frac{\mathrm{d}(\boldsymbol{q}^{*}_{\mathrm{B/D}}(\boldsymbol{q}^{\mathsf{S}}_{\mathrm{B/D}} - \mathbf{1}^{\mathsf{S}}))}{\mathrm{d}t})) \\ & - \boldsymbol{s}^{\mathsf{S}} \circ (K_d \star \boldsymbol{s}^{\mathsf{S}}) + \mathrm{v}(\Delta M^{\mathrm{B}})^{\intercal} K_i^{-1} \frac{\mathrm{d}}{\mathrm{d}t} \mathrm{v}(\Delta M^{\mathrm{B}}).\end{aligned}$$

From equation (4.14), we know that

$$\mathsf{P}(t) = \int_{t-\tau}^{t} R^{\mathrm{T}} R \, \mathrm{d}t \geq 0. \tag{4.18}$$

Using equations (4.14) and (4.15), we have

$$\mathsf{P}(t)\mathrm{v}(\widehat{M^{\mathrm{B}}}) - \mathsf{Q}(t) = \int_{t-\tau}^{t} R^{\mathrm{T}} R \, \mathrm{d}t \mathrm{v}(\widehat{M^{\mathrm{B}}}) - \int_{t-\tau}^{t} R^{\mathrm{T}} \boldsymbol{f}^{\mathrm{B}} \, \mathrm{d}t. \tag{4.19}$$

Using equation (4.3), we then obtain

$$\begin{aligned}
\mathsf{P}(t)\mathrm{v}(\widehat{M}^{\mathrm{B}}) - \mathsf{Q}(t) &= \int_{t-\tau}^{t} R^{\mathrm{T}} R \,\mathrm{d}t \; \mathrm{v}(\widehat{M}^{\mathrm{B}}) - \int_{t-\tau}^{t} R^{\mathrm{T}} R \mathrm{v}(M^{\mathrm{B}}) \,\mathrm{d}t \\
&= \int_{t-\tau}^{t} R^{\mathrm{T}} R \,\mathrm{d}t \; \mathrm{v}(\widehat{M}^{\mathrm{B}}) - \int_{t-\tau}^{t} R^{\mathrm{T}} R \,\mathrm{d}t \; \mathrm{v}(M^{\mathrm{B}}) \\
&= \int_{t-\tau}^{t} R^{\mathrm{T}} R \,\mathrm{d}t \; \Big(\mathrm{v}(\widehat{M}^{\mathrm{B}}) - \mathrm{v}(M^{\mathrm{B}}) \Big) \\
&= \int_{t-\tau}^{t} R^{\mathrm{T}} R \,\mathrm{d}t \; \mathrm{v}(\Delta M^{\mathrm{B}}) \\
&= \mathsf{P}(t)\mathrm{v}(\Delta M^{\mathrm{B}}),
\end{aligned} \tag{4.20}$$

where for the second equality we have used the assumption that the true inertia matrix is constant. Assuming again constant M^{B}, $\frac{\mathrm{d}}{\mathrm{d}t}\mathrm{v}(\Delta M^{\mathrm{B}}) = \frac{\mathrm{d}}{\mathrm{d}t}\mathrm{v}(\widehat{M}^{\mathrm{B}})$, so evaluating equation (4.13), and using the relationship in equation (4.20), it follows that

$$\begin{aligned}
\dot{V} = &-(\boldsymbol{q}^{*}_{\mathrm{B/D}}(\boldsymbol{q}^{\mathsf{S}}_{\mathrm{B/D}} - \mathbf{1}^{\mathsf{S}})) \circ (K_p \star (\boldsymbol{q}^{*}_{\mathrm{B/D}}(\boldsymbol{q}^{\mathsf{S}}_{\mathrm{B/D}} - \mathbf{1}^{\mathsf{S}}))) - \boldsymbol{s}^{\mathsf{S}} \circ (K_d \star \boldsymbol{s}^{\mathsf{S}}) \\
&-\alpha \mathrm{v}(\Delta M^{\mathrm{B}})^{\mathrm{T}} \, \mathsf{P} \, \mathrm{v}(\Delta M^{\mathrm{B}}) \leq 0,
\end{aligned} \tag{4.21}$$

for all $(\boldsymbol{q}_{\mathrm{B/D}}, \boldsymbol{s}, \mathrm{v}(\Delta M^{\mathrm{B}})) \in \mathbb{H}^{u}_{d} \times \mathbb{H}^{v}_{d} \times \mathbb{R}^{7} \backslash \{\mathbf{1}, \mathbf{0}, 0_{7\times 1}\}$. Hence, the equilibrium point $(\boldsymbol{q}_{\mathrm{B/D}}, \boldsymbol{s}, \mathrm{v}(\Delta M^{\mathrm{B}})) = (+\mathbf{1}, \mathbf{0}, 0_{7\times 1})$ is uniformly stable and the solutions are uniformly bounded, i.e., $\boldsymbol{q}_{\mathrm{B/D}}$, $\boldsymbol{s}$, $\mathrm{v}(\Delta M^{\mathrm{B}})$, $\in \mathcal{L}_{\infty}$. Moreover, from equations (4.1) and (4.10) this also means that $\boldsymbol{\omega}^{\mathrm{B}}_{\mathrm{B/D}}, \mathrm{v}(\widehat{M}^{\mathrm{B}}) \in \mathcal{L}_{\infty}$. Since $V \geq 0$ and $\dot{V} \leq 0$, $\lim_{t\to\infty} V(t)$ exists and is finite. Hence, $\lim_{t\to\infty} \int_0^t \dot{V}(\tau)\,\mathrm{d}\tau = \lim_{t\to\infty} V(t) - V(0)$ also exists and is finite. Since $\boldsymbol{q}_{\mathrm{B/D}}, \boldsymbol{s}, \mathrm{v}(\Delta M^{\mathrm{B}}), \boldsymbol{\omega}^{\mathrm{B}}_{\mathrm{B/D}}, \mathrm{v}(\widehat{M}^{\mathrm{B}}), \dot{\boldsymbol{\omega}}^{\mathrm{D}}_{\mathrm{D/I}}, \boldsymbol{\omega}^{\mathrm{B}}_{\mathrm{D/I}}, \boldsymbol{q}_{\mathrm{D/I}} \in \mathcal{L}_{\infty}$, then from equations (2.38), (2.58) and (4.9) in combination with Lemma 53 in [50], $r^{\mathrm{B}}_{\mathrm{B/D}}, \dot{\boldsymbol{q}}_{\mathrm{B/D}}, \boldsymbol{f}^{\mathrm{B}}, \dot{\boldsymbol{\omega}}^{\mathrm{B}}_{\mathrm{B/D}}, \dot{\boldsymbol{s}} \in \mathcal{L}_{\infty}$, and hence $\ddot{V}$ is bounded. Then, by Barbalat's lemma, the system trajectories approach the set for which $\dot{V} = 0$. Since $K_p = \mathrm{diag}(0, \bar{K}_r, 0, \bar{K}_q)$, this implies that $\mathrm{vec}\big(\boldsymbol{q}^{*}_{\mathrm{B/D}}(\boldsymbol{q}^{\mathsf{S}}_{\mathrm{B/D}} - \mathbf{1}^{\mathsf{S}})\big) \to \mathbf{0}$, $\boldsymbol{s} \to \mathbf{0}$, and $\mathsf{P}^{1/2}\mathrm{v}(\Delta M^{\mathrm{B}}) \to 0_{7\times 1}$ as $t \to \infty$. By Lemma 12, $\mathrm{vec}\big(\boldsymbol{q}^{*}_{\mathrm{B/D}}(\boldsymbol{q}^{\mathsf{S}}_{\mathrm{B/D}} - \mathbf{1}^{\mathsf{S}})\big) \to \mathbf{0}$ as $t \to \infty$ implies $\boldsymbol{q}_{\mathrm{B/D}} \to \pm\mathbf{1}$ as $t \to \infty$. Furthermore, calculating the limit as $t \to \infty$ of both sides of equation (4.10) yields $\boldsymbol{\omega}^{\mathrm{B}}_{\mathrm{B/D}} \to \mathbf{0}$, which concludes the first part of the proof.

If, in addition, $\mathsf{P}(t)$ satisfies $\operatorname{rank}\mathsf{P}(t) = 7$, or equivalently $\mathsf{P}(t) > 0$, then $\dot{V} < 0$, which implies that $\operatorname{vec}\big(\boldsymbol{q}^{*}_{\text{B/D}}(\boldsymbol{q}^{\text{S}}_{\text{B/D}} - \mathbf{1}^{\text{S}})\big) \to \mathbf{0}$, $\boldsymbol{s} \to \mathbf{0}$, and $\text{v}(\Delta M^{\text{B}}) \to 0_{7\times 1}$ as $t \to \infty$. Through analogous arguments, we conclude that $\boldsymbol{q}_{\text{B/D}} \to \pm\mathbf{1}$, $\boldsymbol{\omega}^{\text{B}}_{\text{B/D}} \to \mathbf{0}$. Therefore, by the definition of ΔM^{B}, we can conclude that $\text{v}(\widehat{M}^{\text{B}}) \to \text{v}(M^{\text{B}})$ as $t \to \infty$.

■

Remark 4. For the case in which $\operatorname{rank}\mathsf{P}(t) = 7$, or equivalently $\mathsf{P}(t) > 0$, it is possible to directly prove that $\text{v}(\Delta M^{\text{B}}) \to 0_{7\times 1}$ because the term

$$-\alpha \text{v}(\Delta M^{\text{B}})^{\text{T}}\, \mathsf{P}(t)\, \text{v}(\Delta M^{\text{B}})$$

appears in the derivative of the Lyapunov function, which is the main contribution of the concurrent learning framework. Note that to do this, the manipulation of the dynamical system into the form of equation (4.5) was key.

Remark 5. The result provides *almost* global asymptotic stability since we can only ensure $\boldsymbol{q}_{\text{B/D}} \to \pm\mathbf{1}$ as $t \to \infty$, and not simply $\boldsymbol{q}_{\text{B/D}} \to \mathbf{1}$ as $t \to \infty$. The existence of an equilibrium point of the closed loop system at the unstable pole $\boldsymbol{q}_{\text{B/D}} \to -\mathbf{1}$ will give rise to the *unwinding phenomenon*, which was described in Chapter 1. For an approach to deal with this phenomenon, the reader is referred to [64], which proposes a robust, hybrid controller of similar form to that of [46, 141, 47].

Remark 6. The matrix $\mathsf{P}(t)$ is positive semi-definite (except at time $t-\tau$, when it is initialized) by construction. By this same token, the integration in equation (4.18) is unbounded. Appropriate monitoring of the rank condition must be enforced so that once the rank condition in equation (4.16) is satisfied, α can eventually be set to $\alpha = 0$ to avoid numerical problems in the control law. For this reason, the discrete concurrent learning which will be described in the next section is a reasonable substitute. Discretizing the collection of data allows bounding the growth of the largest singular values of $\mathsf{P}(t)$.

Remark 7. As pointed out in [133], linear and angular velocity measurements, among others, are inevitably corrupted by noise in real systems. This limitation is not considered in this work and will be the subject of future research. However, the concurrent learning framework has already been successfully tested experimentally in [113] to perform control. In practice, the derivatives of certain states might not be readily accessible through the measurements. This is the case, for example, with $\dot{\boldsymbol{\omega}}^{\mathrm{B}}_{\mathrm{B/D}}$. An optimal fixed-point smoother can be used to estimate these variables, as suggested in [113, 140]. A Butterworth filter applied to $\boldsymbol{\omega}^{\mathrm{B}}_{\mathrm{B/D}}$ has also been observed to capture the evolution of $\dot{\boldsymbol{\omega}}^{\mathrm{B}}_{\mathrm{B/D}}$ accurately when differentiated in the s-domain. Appropriate corrections for the lag introduced by the estimators or filters have to be made in this case.

Remark 8. The concurrent learning algorithm requires knowledge of the forces and torques applied about the center of mass of the body, i.e. knowledge of $\boldsymbol{f}^{\mathrm{B}} = f^{\mathrm{B}} + \epsilon\tau^{\mathrm{B}}$. In simulation, this quantity was obtained from the output of the controller. In practice, these quantities are not trivial to obtain and it will require that the actuators and body disturbances are properly characterized. Preliminary results for research on this topic have shown that taking the output of the controller in the case of mild, additive Gaussian disturbances at the input is a reasonable action to take. However, these findings have yet to be formalized and broadened.

4.3 Adaptive Control with Discrete Concurrent Learning

In this section we provide an adaptive pose-tracking controller that uses discrete concurrent learning to provide strong assurances on the convergence of the mass and the inertia matrix of the spacecraft when dynamical data is stored and used for estimation. As discussed in the previous section, bounding the growth of the regressor-like matrix P is important. In this section we develop a version of the controller that uses a discrete formulation of concurrent learning for incorporation of data into the adaptation of the inertia parameters. To do this, we evaluate the dynamic equation of motion given by equation (4.3) at $t = t_k$ to yield the

following relationship:

$$\boldsymbol{f}^{\text{B}}(t_k) = R_k(\dot{\boldsymbol{\omega}}^{\text{B}}_{\text{B/D}}, \boldsymbol{\omega}^{\text{B}}_{\text{B/D}}, \dot{\boldsymbol{\omega}}^{\text{D}}_{\text{D/I}}, \boldsymbol{\omega}^{\text{D}}_{\text{D/I}}, \boldsymbol{q}_{\text{B/D}})\text{v}(M^{\text{B}}) = R_k\text{v}(M^{\text{B}}), \tag{4.22}$$

where R_k is R sampled at $t = t_k$. Equivalently, we can evaluate the relationship $\varepsilon \triangleq R\text{v}(\widehat{M^{\text{B}}}) - \boldsymbol{f}^{\text{B}}$ at time $t = t_k$ to yield the error-like signal ε_k as

$$\varepsilon_k \triangleq R_k\text{v}(\widehat{M^{\text{B}}}) - \boldsymbol{f}^{\text{B}}(t_k). \tag{4.23}$$

Analogous to the analysis of ε in the previous section, we can manipulate ε_k as

$$\begin{aligned} \varepsilon_k &\triangleq R_k\text{v}(\widehat{M^{\text{B}}}) - \boldsymbol{f}^{\text{B}}(t_k) \\ &= R_k\text{v}(\widehat{M^{\text{B}}}) - R_k\text{v}(M^{\text{B}}) \\ &= R_k\text{v}(\Delta M^{\text{B}}), \end{aligned} \tag{4.24}$$

reinforcing the idea that ε_k provides a quantification of the error in the estimate of the dual inertia matrix.

Now define the sets $\mathcal{X} = \{(\dot{\boldsymbol{\omega}}^{\text{B}}_{\text{B/D}}, \boldsymbol{\omega}^{\text{B}}_{\text{B/D}}, \dot{\boldsymbol{\omega}}^{\text{D}}_{\text{D/I}}, \boldsymbol{\omega}^{\text{D}}_{\text{D/I}}, \boldsymbol{q}_{\text{B/D}})_j\}_{j=1}^{N_s}$ and $\mathcal{F} = \{(\boldsymbol{f}^{\text{B}})_j\}_{j=1}^{N_s}$ to contain recorded pairs of data as per equation (4.22) at times $\{t_j\}_{j=1}^{N_s}$. For our application, the cardinality of the sets $\mathcal{X}$ and $\mathcal{F}$ is $7 \leq N_s < \infty$, and is set by the user. It is worth emphasizing that these sets will be initially empty, and that data will be incorporated as they become available. An extended discussion on how to incorporate measurements and other implementation aspects of the discrete concurrent learning method will be thoroughly addressed in Chapter 9.

The next result closely follows the result provided in the previous section, but it uses a discrete version of concurrent learning.

Theorem 2. *Consider the relative kinematic and dynamic equations given by equation* (2.38)

and equation (2.58)*. Let the dual control force be defined by the feedback control law*

$$\boldsymbol{f}_c^{\mathrm{B}} = -\mathrm{vec}\big(\boldsymbol{q}_{\mathrm{B/D}}^*(\boldsymbol{q}_{\mathrm{B/D}}^{\mathsf{S}} - \mathbf{1}^{\mathsf{S}})\big) - K_d \star \boldsymbol{s}^{\mathsf{S}} + \boldsymbol{\omega}_{\mathrm{B/I}}^{\mathrm{B}} \times (\widehat{M^{\mathrm{B}}} \star (\boldsymbol{\omega}_{\mathrm{B/I}}^{\mathrm{B}})^{\mathsf{S}}) + \widehat{M^{\mathrm{B}}} \star (\boldsymbol{q}_{\mathrm{B/D}}^* \dot{\boldsymbol{\omega}}_{\mathrm{D/I}}^{\mathrm{D}} \boldsymbol{q}_{\mathrm{B/D}})^{\mathsf{S}} + \widehat{M^{\mathrm{B}}} \star (\boldsymbol{\omega}_{\mathrm{D/I}}^{\mathrm{B}} \times \boldsymbol{\omega}_{\mathrm{B/D}}^{\mathrm{B}})^{\mathsf{S}} - \widehat{M^{\mathrm{B}}} \star (K_p \star \frac{\mathrm{d}}{\mathrm{d}t}(\boldsymbol{q}_{\mathrm{B/D}}^*(\boldsymbol{q}_{\mathrm{B/D}}^{\mathsf{S}} - \mathbf{1}^{\mathsf{S}})))^{\mathsf{S}}, \quad (4.25)$$

where

$$\boldsymbol{s} = \boldsymbol{\omega}_{\mathrm{B/D}}^{\mathrm{B}} + (K_p \star (\boldsymbol{q}_{\mathrm{B/D}}^*(\boldsymbol{q}_{\mathrm{B/D}}^{\mathsf{S}} - \mathbf{1}^{\mathsf{S}})))^{\mathsf{S}}, \quad (4.26)$$

$$K_p = \begin{bmatrix} K_r & 0_{4\times4} \\ 0_{4\times4} & K_q \end{bmatrix},\ K_r = \begin{bmatrix} 0 & 0_{1\times3} \\ 0_{3\times1} & \bar{K}_r \end{bmatrix},\ K_q = \begin{bmatrix} 0 & 0_{1\times3} \\ 0_{3\times1} & \bar{K}_q \end{bmatrix}, \quad (4.27)$$

$$K_d = \begin{bmatrix} K_v & 0_{4\times4} \\ 0_{4\times4} & K_\omega \end{bmatrix},\ K_v = \begin{bmatrix} 0 & 0_{1\times3} \\ 0_{3\times1} & \bar{K}_v \end{bmatrix},\ K_\omega = \begin{bmatrix} 0 & 0_{1\times3} \\ 0_{3\times1} & \bar{K}_\omega \end{bmatrix}, \quad (4.28)$$

and $\bar{K}_r, \bar{K}_q, \bar{K}_v, \bar{K}_\omega \in \mathbb{R}^{3\times3}$ *are positive definite matrices,* $\widehat{M^{\mathrm{B}}}$ *is an estimate of* M^{B} *updated according to*

$$\frac{\mathrm{d}}{\mathrm{d}t}\mathrm{v}(\widehat{M^{\mathrm{B}}}) = -\alpha K_i \sum_{k=1}^{N_s} R_k^{\mathsf{T}} \varepsilon_k + K_i\big[-\mathrm{h}((\boldsymbol{s} \times \boldsymbol{\omega}_{\mathrm{B/I}}^{\mathrm{B}})^{\mathsf{S}}, (\boldsymbol{\omega}_{\mathrm{B/I}}^{\mathrm{B}})^{\mathsf{S}}) - \mathrm{h}(\boldsymbol{s}^{\mathsf{S}}, (\boldsymbol{q}_{\mathrm{B/D}}^* \dot{\boldsymbol{\omega}}_{\mathrm{D/I}}^{\mathrm{D}} \boldsymbol{q}_{\mathrm{B/D}})^{\mathsf{S}} + (\boldsymbol{\omega}_{\mathrm{D/I}}^{\mathrm{B}} \times \boldsymbol{\omega}_{\mathrm{B/D}}^{\mathrm{B}})^{\mathsf{S}} - K_p \star \frac{\mathrm{d}(\boldsymbol{q}_{\mathrm{B/D}}^*(\boldsymbol{q}_{\mathrm{B/D}}^{\mathsf{S}} - \mathbf{1}^{\mathsf{S}}))}{\mathrm{d}t})\big], \quad (4.29)$$

where $\alpha > 0$*,* $K_i \in \mathbb{R}^{7\times7}$ *is a positive definite matrix, the function* $\mathrm{h} : \mathbb{H}_d^v \times \mathbb{H}_d^v \to \mathbb{R}^7$ *is defined as* $\boldsymbol{a} \circ (M^B \star \boldsymbol{b}) = \mathrm{h}(\boldsymbol{a}, \boldsymbol{b})^{\mathsf{T}}\mathrm{v}(M^B) = \mathrm{v}(M^B)^{\mathsf{T}}\mathrm{h}(\boldsymbol{a}, \boldsymbol{b})$ *or, equivalently,* $\mathrm{h}(\boldsymbol{a}, \boldsymbol{b}) = [a_6b_6,\ a_7b_6{+}a_6b_7,\ a_8b_6{+}a_6b_8,\ a_7b_7,\ a_8b_7{+}a_7b_8,\ a_8b_8,\ a_2b_2{+}a_3b_3{+}a_4b_4]^{\mathsf{T}}$*, and* ε_k *is given by equation* (4.23)*, constructed from the data in the sets* $\mathcal{X}$ *and* $\mathcal{F}$*.*

Assume that $\boldsymbol{q}_{\mathrm{D/I}}, \boldsymbol{\omega}_{\mathrm{D/I}}^{\mathrm{D}}, \dot{\boldsymbol{\omega}}_{\mathrm{D/I}}^{\mathrm{D}} \in \mathcal{L}_\infty$*. Then, for all initial conditions,* $\lim_{t\to\infty} \boldsymbol{q}_{\mathrm{B/D}} = \pm\mathbf{1}$ *(i.e.,* $\lim_{t\to\infty} q_{\mathrm{B/D}} = \pm1$ *and* $\lim_{t\to\infty} r_{\mathrm{B/D}}^{\mathrm{B}} = 0$*), and* $\lim_{t\to\infty} \boldsymbol{\omega}_{\mathrm{B/D}}^{\mathrm{B}} = \mathbf{0}$ *(i.e.,* $\lim_{t\to\infty} \omega_{\mathrm{B/D}}^{\mathrm{B}} = 0$ *and* $\lim_{t\to\infty} v_{\mathrm{B/D}}^{\mathrm{B}} = 0$*).*

If, in addition,

$$\operatorname{rank} \sum_{k=1}^{N_s} R_k^{\intercal} R_k = 7, \tag{4.30}$$

then $\lim_{t\to\infty} \mathrm{v}(\widehat{M^{\mathrm{B}}}) = \mathrm{v}(M^{\mathrm{B}})$.

Proof. Note that $\boldsymbol{q}_{\mathrm{B/D}} = \pm\mathbf{1}$, $\boldsymbol{s} = \mathbf{0}$, and $\mathrm{v}(\Delta M^{\mathrm{B}}) = 0_{7\times 1}$ are the equilibrium conditions of the closed-loop system with dynamics given by equation (2.58), kinematics described by equation (2.38), feedback control law given by equation (4.25), and a dual inertia matrix update as in equation (4.29), with ε_k defined in equation (4.23). Consider now the following candidate Lyapunov function for the equilibrium point $(\boldsymbol{q}_{\mathrm{B/D}}, \boldsymbol{s}, \mathrm{v}(\Delta M^{\mathrm{B}})) = (+\mathbf{1}, \mathbf{0}, 0_{7\times 1})$:

$$\begin{aligned} V(\boldsymbol{q}_{\mathrm{B/D}}, \boldsymbol{s}, \mathrm{v}(\Delta M^{\mathrm{B}})) = (\boldsymbol{q}_{\mathrm{B/D}} - \mathbf{1}) \circ (\boldsymbol{q}_{\mathrm{B/D}} - \mathbf{1}) + \tfrac{1}{2}\boldsymbol{s}^{\mathsf{S}} \circ (M^{\mathrm{B}} \star \boldsymbol{s}^{\mathsf{S}}) \\ + \tfrac{1}{2}\mathrm{v}(\Delta M^{\mathrm{B}})^{\intercal} K_i^{-1} \mathrm{v}(\Delta M^{\mathrm{B}}). \end{aligned} \tag{4.31}$$

Note that V is a valid candidate Lyapunov function since

$$V(\boldsymbol{q}_{\mathrm{B/D}} = \mathbf{1}, \boldsymbol{s} = \mathbf{0}, \mathrm{v}(\Delta M^{\mathrm{B}}) = 0_{7\times 1}) = 0$$

and

$$V(\boldsymbol{q}_{\mathrm{B/D}}, \boldsymbol{s}, \mathrm{v}(\Delta M^{\mathrm{B}})) > 0 \; \forall (\boldsymbol{q}_{\mathrm{B/D}}, \boldsymbol{s}, \mathrm{v}(\Delta M^{\mathrm{B}})) \in \mathbb{H}_d^u \times \mathbb{H}_d^v \times \mathbb{R}^7 \backslash \{\mathbf{1}, \mathbf{0}, 0_{7\times 1}\}.$$

Following the same approach as in the proof of Theorem 1, and after introduction of the feedback control law given by equation (4.25) and simplification we obtain that

$$\begin{aligned} \dot{V} = & -(\boldsymbol{q}^*_{\mathrm{B/D}}(\boldsymbol{q}^{\mathsf{S}}_{\mathrm{B/D}} - \mathbf{1}^{\mathsf{S}})) \circ (K_p \star (\boldsymbol{q}^*_{\mathrm{B/D}}(\boldsymbol{q}^{\mathsf{S}}_{\mathrm{B/D}} - \mathbf{1}^{\mathsf{S}}))) + (\boldsymbol{s} \times \boldsymbol{\omega}^{\mathrm{B}}_{\mathrm{B/I}})^{\mathsf{S}} \circ (\Delta M^{\mathrm{B}} \star (\boldsymbol{\omega}^{\mathrm{B}}_{\mathrm{B/I}})^{\mathsf{S}}) \\ & + \boldsymbol{s}^{\mathsf{S}} \circ (\Delta M^{\mathrm{B}} \star (\boldsymbol{q}^*_{\mathrm{B/D}} \dot{\boldsymbol{\omega}}^{\mathrm{D}}_{\mathrm{D/I}} \boldsymbol{q}_{\mathrm{B/D}})^{\mathsf{S}} + \Delta M^{\mathrm{B}} \star (\boldsymbol{\omega}^{\mathrm{B}}_{\mathrm{D/I}} \times \boldsymbol{\omega}^{\mathrm{B}}_{\mathrm{B/D}})^{\mathsf{S}} - \Delta M^{\mathrm{B}} \star (K_p \star \frac{\mathrm{d}(\boldsymbol{q}^*_{\mathrm{B/D}}(\boldsymbol{q}^{\mathsf{S}}_{\mathrm{B/D}} - \mathbf{1}^{\mathsf{S}}))}{\mathrm{d}t})) \\ & - \boldsymbol{s}^{\mathsf{S}} \circ (K_d \star \boldsymbol{s}^{\mathsf{S}}) + \mathrm{v}(\Delta M^{\mathrm{B}})^{\intercal} K_i^{-1} \frac{\mathrm{d}}{\mathrm{d}t} \mathrm{v}(\Delta M^{\mathrm{B}}). \end{aligned}$$

Assuming constant M^{B}, $\frac{\mathrm{d}}{\mathrm{d}t}\mathrm{v}(\Delta M^{\mathrm{B}}) = \frac{\mathrm{d}}{\mathrm{d}t}\mathrm{v}(\widehat{M^{\mathrm{B}}})$, so evaluating equation (4.29), and using

the relationship in equation (4.24) to evaluate ε_k, it follows that

$$\begin{aligned}\dot{V}=&-(\boldsymbol{q}^*_{\text{B/D}}(\boldsymbol{q}^{\text{S}}_{\text{B/D}}-\mathbf{1}^{\text{S}}))\circ(K_p\star(\boldsymbol{q}^*_{\text{B/D}}(\boldsymbol{q}^{\text{S}}_{\text{B/D}}-\mathbf{1}^{\text{S}})))-\boldsymbol{s}^{\text{S}}\circ(K_d\star\boldsymbol{s}^{\text{S}})\\&-\alpha\text{v}(\Delta M^{\text{B}})^{\text{T}}\sum_{k=1}^{N_s}R_k^{\text{T}}R_k\text{v}(\Delta M^{\text{B}})\leq 0,\end{aligned}\tag{4.32}$$

for all $(\boldsymbol{q}_{\text{B/D}},\boldsymbol{s},\text{v}(\Delta M^{\text{B}}))\in\mathbb{H}_d^u\times\mathbb{H}_d^v\times\mathbb{R}^7\backslash\{\mathbf{1},\mathbf{0},0_{7\times1}\}$. Hence, the equilibrium point $(\boldsymbol{q}_{\text{B/D}},\boldsymbol{s},\text{v}(\Delta M^{\text{B}}))=(+\mathbf{1},\mathbf{0},0_{7\times1})$ is uniformly stable and the solutions are uniformly bounded, i.e., $\boldsymbol{q}_{\text{B/D}}$, $\boldsymbol{s}$, $\text{v}(\Delta M^{\text{B}})$, $\in\mathcal{L}_\infty$. Moreover, from equations (4.1) and (4.26) this also means that $\boldsymbol{\omega}^{\text{B}}_{\text{B/D}},\text{v}(\widehat{M}^{\text{B}})\in\mathcal{L}_\infty$. Since $V\geq0$ and $\dot{V}\leq0$, $\lim_{t\to\infty}V(t)$ exists and is finite. Hence, $\lim_{t\to\infty}\int_0^t\dot{V}(\tau)\,\text{d}\tau=\lim_{t\to\infty}V(t)-V(0)$ also exists and is finite. Since $\boldsymbol{q}_{\text{B/D}},\boldsymbol{s},\text{v}(\Delta M^{\text{B}}),\boldsymbol{\omega}^{\text{B}}_{\text{B/D}},\text{v}(\widehat{M}^{\text{B}}),\dot{\boldsymbol{\omega}}^{\text{D}}_{\text{D/I}},\boldsymbol{\omega}^{\text{B}}_{\text{D/I}},\boldsymbol{q}_{\text{D/I}}\in\mathcal{L}_\infty$, then from equations (2.38), (2.58) and (4.25) in combination with Lemma 53 in [50], $r^{\text{B}}_{\text{B/D}},\dot{\boldsymbol{q}}_{\text{B/D}},\boldsymbol{f}^{\text{B}},\dot{\boldsymbol{\omega}}^{\text{B}}_{\text{B/D}},\dot{\boldsymbol{s}}\in\mathcal{L}_\infty$, and hence $\ddot{V}$ is bounded. Then, by Barbalat's lemma, the system trajectories approach the set for which $\dot{V}=0$. Since $K_p=\text{diag}(0,\bar{K}_r,0,\bar{K}_q)$, this implies that $\text{vec}\big(\boldsymbol{q}^*_{\text{B/D}}(\boldsymbol{q}^{\text{S}}_{\text{B/D}}-\mathbf{1}^{\text{S}})\big)\to\mathbf{0}$, $\boldsymbol{s}\to\mathbf{0}$, and $\Big(\sum_{k=1}^{N_s}R_k^{\text{T}}R_k\Big)^{1/2}\text{v}(\Delta M^{\text{B}})\to0_{7\times1}$ as $t\to\infty$. By Lemma 12, $\text{vec}\big(\boldsymbol{q}^*_{\text{B/D}}(\boldsymbol{q}^{\text{S}}_{\text{B/D}}-\mathbf{1}^{\text{S}})\big)\to\mathbf{0}$ as $t\to\infty$ implies $\boldsymbol{q}_{\text{B/D}}\to\pm\mathbf{1}$ as $t\to\infty$. Furthermore, calculating the limit as $t\to\infty$ of both sides of equation (4.10) yields $\boldsymbol{\omega}^{\text{B}}_{\text{B/D}}\to\mathbf{0}$, which concludes the first part of the proof.

If, in addition, $\text{rank}\sum_{k=1}^{N_s}R_k^{\text{T}}R_k=7$, or equivalently $\sum_{k=1}^{N_s}R_k^{\text{T}}R_k>0$, then $\dot{V}<0$, which implies that $\text{vec}\big(\boldsymbol{q}^*_{\text{B/D}}(\boldsymbol{q}^{\text{S}}_{\text{B/D}}-\mathbf{1}^{\text{S}})\big)\to\mathbf{0}$, $\boldsymbol{s}\to\mathbf{0}$, and $\text{v}(\Delta M^{\text{B}})\to0_{7\times1}$ as $t\to\infty$. Through analogous arguments, we conclude that $\boldsymbol{q}_{\text{B/D}}\to\pm\mathbf{1}$, $\boldsymbol{\omega}^{\text{B}}_{\text{B/D}}\to\mathbf{0}$. Therefore, by the definition of ΔM^{B}, we can conclude that $\text{v}(\widehat{M}^{\text{B}})\to\text{v}(M^{\text{B}})$ as $t\to\infty$. ■

Remark 9. For the case $\text{rank}\sum_{k=1}^{N_s}R_k^{\text{T}}R_k=7$, or equivalently $\sum_{k=1}^{N_s}R_k^{\text{T}}R_k>0$, it is possible to prove that $\text{v}(\Delta M^{\text{B}})\to0_{7\times1}$ because the term

$$-\text{v}(\Delta M^{\text{B}})\sum_{j=1}^{N_s}R_k^{\text{T}}R_k\text{v}(\Delta M^{\text{B}})$$

appears in the derivative of the Lyapunov function, which again is the contribution of the

concurrent learning framework. Note that to do this, equation (4.24) was key, and that the matrix $\sum_{k=1}^{N_s} R_k^{\mathrm{T}} \varepsilon_k$ is constructed from collected data stored in the sets $\mathcal{X}$ and $\mathcal{F}$.

Remark 10. Chapter 6 in [140] addresses how the matrices $\mathcal{X}$ and $\mathcal{F}$ should be populated. Algorithm 6.2 therein, which aims to maximize the minimum singular value of $\sum_{j=1}^{N_s} R_k^{\mathrm{T}} R_k$, was selected for the implementation of the proposed controller. It is worth emphasizing that for the algorithm to work we only require that equation (4.30) is satisfied. The maximization of the minimum singular value just speeds up the convergence of the parameters.

4.4 Concurrent Learning as a Contributing Factor to Meet Persistency of Excitation Conditions

In this section we provide an approach to incorporate the concurrent learning rank conditions into the analysis of convergence of the estimation parameters in the context of persistency of excitation (PE).

Consider the system with kinematics dictated by equation (2.38) and relative dynamics given by equation (2.58). If we evaluate the control law proposed in Theorem 1 we obtain the closed-loop system described by the following set of equations:

$$\dot{\boldsymbol{q}}_{\mathrm{B/D}} = \tfrac{1}{2}\boldsymbol{q}_{\mathrm{B/D}}\boldsymbol{\omega}^{\mathrm{B}}_{\mathrm{B/D}} \tag{4.33}$$

$$\begin{aligned} M^{\mathrm{B}} \star (\dot{\boldsymbol{\omega}}^{\mathrm{B}}_{\mathrm{B/D}})^{\mathsf{S}} = & -\mathrm{vec}\big(\boldsymbol{q}^{*}_{\mathrm{B/D}}(\boldsymbol{q}^{\mathsf{S}}_{\mathrm{B/D}} - \mathbf{1}^{\mathsf{S}})\big) - K_d \star \boldsymbol{s}^{\mathsf{S}} + \boldsymbol{\omega}^{\mathrm{B}}_{\mathrm{B/I}} \times (\Delta M^{\mathrm{B}} \star (\boldsymbol{\omega}^{\mathrm{B}}_{\mathrm{B/I}})^{\mathsf{S}}) \\ & + \Delta M^{\mathrm{B}} \star (\boldsymbol{q}^{*}_{\mathrm{B/D}} \dot{\boldsymbol{\omega}}^{\mathrm{D}}_{\mathrm{D/I}} \boldsymbol{q}_{\mathrm{B/D}})^{\mathsf{S}} + \Delta M^{\mathrm{B}} \star (\boldsymbol{\omega}^{\mathrm{B}}_{\mathrm{D/I}} \times \boldsymbol{\omega}^{\mathrm{B}}_{\mathrm{B/D}})^{\mathsf{S}} - \widehat{M^{\mathrm{B}}} \star (K_p \star \frac{\mathrm{d}}{\mathrm{d}t}(\boldsymbol{q}^{*}_{\mathrm{B/D}}(\boldsymbol{q}^{\mathsf{S}}_{\mathrm{B/D}} - \mathbf{1}^{\mathsf{S}})))^{\mathsf{S}} \end{aligned} \tag{4.34}$$

with $\widehat{M^{\mathrm{B}}}$ updated as

$$\frac{\mathrm{d}}{\mathrm{d}t}\mathrm{v}(\widehat{M^{\mathrm{B}}}) = -\alpha K_i \mathsf{P}\mathrm{v}(\Delta M^{\mathrm{B}}) + K_i\Big[-\mathrm{h}((\boldsymbol{s}\times\boldsymbol{\omega}^{\mathrm{B}}_{\mathrm{B/I}})^{\mathsf{S}},(\boldsymbol{\omega}^{\mathrm{B}}_{\mathrm{B/I}})^{\mathsf{S}}) \\ -\mathrm{h}(\boldsymbol{s}^{\mathsf{S}},(\boldsymbol{q}^{*}_{\mathrm{B/D}}\dot{\boldsymbol{\omega}}^{\mathrm{D}}_{\mathrm{D/I}}\boldsymbol{q}_{\mathrm{B/D}})^{\mathsf{S}}+(\boldsymbol{\omega}^{\mathrm{B}}_{\mathrm{D/I}}\times\boldsymbol{\omega}^{\mathrm{B}}_{\mathrm{B/D}})^{\mathsf{S}}-K_p\star\frac{\mathrm{d}(\boldsymbol{q}^{*}_{\mathrm{B/D}}(\boldsymbol{q}^{\mathsf{S}}_{\mathrm{B/D}}-\mathbf{1}^{\mathsf{S}}))}{\mathrm{d}t})\Big], \quad (4.35)$$

where we have dropped the dependence of $\mathsf{P}(t)$ on time for the sake of exposition.

In the Lyapunov analysis provided in the proof of Theorem 1, we concluded that $\boldsymbol{\omega}^{\mathrm{B}}_{\mathrm{B/D}}\to\mathbf{0}$, $\boldsymbol{s}\to\mathbf{0}$, and $\boldsymbol{q}_{\mathrm{B/D}}\to\mathbf{1}$ as $t\to\infty$. We can prove that $\dot{\boldsymbol{\omega}}^{\mathrm{B}}_{\mathrm{B/D}}\to\mathbf{0}$ as follows. We know that

$$\lim_{t\to\infty}\int_0^t \dot{\boldsymbol{\omega}}^{\mathrm{B}}_{\mathrm{B/D}}\,\mathrm{d}t = \lim_{t\to\infty}\boldsymbol{\omega}^{\mathrm{B}}_{\mathrm{B/D}}(t)-\boldsymbol{\omega}^{\mathrm{B}}_{\mathrm{B/D}}(0) = -\boldsymbol{\omega}^{\mathrm{B}}_{\mathrm{B/D}}(0)$$

exists and is finite. Using the fact that $\boldsymbol{q}_{\mathrm{D/I}},\boldsymbol{\omega}^{\mathrm{D}}_{\mathrm{D/I}},\dot{\boldsymbol{\omega}}^{\mathrm{D}}_{\mathrm{D/I}},\ddot{\boldsymbol{\omega}}^{\mathrm{D}}_{\mathrm{D/I}},\dot{\boldsymbol{q}}_{\mathrm{B/D}},\ddot{\boldsymbol{q}}_{\mathrm{B/D}},\dot{\boldsymbol{\omega}}^{\mathrm{B}}_{\mathrm{B/D}},\frac{\mathrm{dv}(\widehat{M^{\mathrm{B}}})}{\mathrm{d}t}\in\mathcal{L}_\infty$, from which it follows that $\ddot{\boldsymbol{\omega}}^{\mathrm{B}}_{\mathrm{B/D}}\in\mathcal{L}_\infty$ by differentiating the dynamics equation (2.58). By Barbalat's Lemma, $\lim_{t\to\infty}\dot{\boldsymbol{\omega}}^{\mathrm{B}}_{\mathrm{B/D}}=\mathbf{0}$. Therefore, taking the limit as $t\to\infty$ of equation (4.34), we obtain

$$\mathbf{0}=\lim_{t\to\infty}\boldsymbol{\omega}^{\mathrm{D}}_{\mathrm{D/I}}\times(\Delta M^{\mathrm{B}}\star(\boldsymbol{\omega}^{\mathrm{D}}_{\mathrm{D/I}})^{\mathsf{S}})+\Delta M^{\mathrm{B}}\star(\dot{\boldsymbol{\omega}}^{\mathrm{D}}_{\mathrm{D/I}})^{\mathsf{S}}. \quad (4.36)$$

Following the notation used by Filipe in [50], we define $\mathrm{W}_{rb}:[0,\infty)\to\mathbb{R}^{8\times 7}$ as

$$\mathrm{W}_{rb}(t)\mathrm{v}(\Delta M^{\mathrm{B}}) \triangleq \boldsymbol{\omega}^{\mathrm{D}}_{\mathrm{D/I}}\times(\Delta M^{\mathrm{B}}\star(\boldsymbol{\omega}^{\mathrm{D}}_{\mathrm{D/I}})^{\mathsf{S}})+\Delta M^{\mathrm{B}}\star(\dot{\boldsymbol{\omega}}^{\mathrm{D}}_{\mathrm{D/I}})^{\mathsf{S}}. \quad (4.37)$$

Explicitly,

$$\mathrm{W}_{rb}(t) = \begin{bmatrix} 0_{4\times 6} & \dot{v}^{\mathrm{D}}_{\mathrm{D/I}}+\omega^{\mathrm{D}}_{\mathrm{D/I}}\times v^{\mathrm{D}}_{\mathrm{D/I}} \\ \mathrm{W}_{rb,I}(t) & 0_{4\times 1}\end{bmatrix},$$

where $\boldsymbol{\omega}^{\mathrm{D}}_{\mathrm{D/I}} = \omega^{\mathrm{D}}_{\mathrm{D/I}} + \epsilon v^{\mathrm{D}}_{\mathrm{D/I}} = (0, [p^{\mathrm{D}}_{\mathrm{D/I}}, q^{\mathrm{D}}_{\mathrm{D/I}}, r^{\mathrm{D}}_{\mathrm{D/I}}]^{\mathrm{T}}) + \epsilon v^{\mathrm{D}}_{\mathrm{D/I}}$ and

$$\mathrm{W}_{rb,I}(t)=\begin{bmatrix} 0 & 0 & 0 & 0 & 0 & 0 \\ \dot{p}^{\mathrm{D}}_{\mathrm{D/I}} & \dot{q}^{\mathrm{D}}_{\mathrm{D/I}}-p^{\mathrm{D}}_{\mathrm{D/I}}r^{\mathrm{D}}_{\mathrm{D/I}} & \dot{r}^{\mathrm{D}}_{\mathrm{D/I}}+p^{\mathrm{D}}_{\mathrm{D/I}}q^{\mathrm{D}}_{\mathrm{D/I}} & -q^{\mathrm{D}}_{\mathrm{D/I}}r^{\mathrm{D}}_{\mathrm{D/I}} & (q^{\mathrm{D}}_{\mathrm{D/I}})^2-(r^{\mathrm{D}}_{\mathrm{D/I}})^2 & q^{\mathrm{D}}_{\mathrm{D/I}}r^{\mathrm{D}}_{\mathrm{D/I}} \\ p^{\mathrm{D}}_{\mathrm{D/I}}r^{\mathrm{D}}_{\mathrm{D/I}} & \dot{p}^{\mathrm{D}}_{\mathrm{D/I}}+q^{\mathrm{D}}_{\mathrm{D/I}}r^{\mathrm{D}}_{\mathrm{D/I}} & (r^{\mathrm{D}}_{\mathrm{D/I}})^2-(p^{\mathrm{D}}_{\mathrm{D/I}})^2 & \dot{q}^{\mathrm{D}}_{\mathrm{D/I}} & \dot{r}^{\mathrm{D}}_{\mathrm{D/I}}-p^{\mathrm{D}}_{\mathrm{D/I}}q^{\mathrm{D}}_{\mathrm{D/I}} & -p^{\mathrm{D}}_{\mathrm{D/I}}r^{\mathrm{D}}_{\mathrm{D/I}} \\ -p^{\mathrm{D}}_{\mathrm{D/I}}q^{\mathrm{D}}_{\mathrm{D/I}} & (p^{\mathrm{D}}_{\mathrm{D/I}})^2-(q^{\mathrm{D}}_{\mathrm{D/I}})^2 & \dot{p}^{\mathrm{D}}_{\mathrm{D/I}}-q^{\mathrm{D}}_{\mathrm{D/I}}r^{\mathrm{D}}_{\mathrm{D/I}} & p^{\mathrm{D}}_{\mathrm{D/I}}q^{\mathrm{D}}_{\mathrm{D/I}} & \dot{q}^{\mathrm{D}}_{\mathrm{D/I}}+p^{\mathrm{D}}_{\mathrm{D/I}}r^{\mathrm{D}}_{\mathrm{D/I}} & \dot{r}^{\mathrm{D}}_{\mathrm{D/I}} \end{bmatrix}.$$

Thus, equation (4.36) can be expressed as

$$\mathbf{0}= \lim_{t\to\infty} \mathrm{W}_{rb}(t)\mathrm{v}(\Delta M^{\mathrm{B}}). \tag{4.38}$$

From Barbalat's Lemma in Theorem 1, we also concluded that $\mathsf{P}^{1/2}\mathrm{v}(\Delta M^{\mathrm{B}}) \to 0_{7\times 1}$ as $t \to \infty$. Therefore, equation (4.35) becomes identically zero at $t \to \infty$. If we preserve the term associated to concurrent learning, we obtain

$$0_{7\times 1} = \lim_{t\to\infty} \alpha K_i \mathsf{P}\mathrm{v}(\Delta M^{\mathrm{B}}) = \lim_{t\to\infty} \alpha \mathsf{P}\mathrm{v}(\Delta M^{\mathrm{B}}). \tag{4.39}$$

Equations (4.38) and (4.39) can be combined as

$$\begin{bmatrix} \mathbf{0} \\ 0_{7\times 1} \end{bmatrix} = \lim_{t\to\infty} \begin{bmatrix} \mathrm{W}_{rb}(t) \\ \alpha\mathsf{P} \end{bmatrix} \mathrm{v}(\Delta M^{\mathrm{B}}) \tag{4.40}$$

Therefore, the condition for persistency of excitation including participation of a concurrent learning term can be cast as

$$\int_{t_1}^{t_1+T_2} \begin{bmatrix} \mathrm{W}_{rb}(t) \\ \alpha\mathsf{P} \end{bmatrix}^{\mathrm{T}} \begin{bmatrix} \mathrm{W}_{rb}(t) \\ \alpha\mathsf{P} \end{bmatrix} \mathrm{d}t > 0, \tag{4.41}$$

for all $t > T_1$ for some $T_1 > 0$ and $T_2 > 0$, which can be equivalently rewritten as

$$\int_{t_1}^{t_1+T_2} \mathrm{W}_{rb}(t)^{\mathrm{T}}\mathrm{W}_{rb}(t) + \alpha^2 \mathsf{P}^{\mathrm{T}}\mathsf{P}\,\mathrm{d}t > 0. \tag{4.42}$$

Several remarks are in order.

Remark 11. It is clear from the form of equation (4.42) that the rank condition $\mathrm{rank}\,\mathsf{P} = 7$ in equation (4.16) immediately satisfies the persistency of excitation requirement.

Remark 12. For the estimation task, since $\mathsf{P} \geq 0$, the proposed adaptive controllers will perform at least the same, but likely better, than the baseline controller without concurrent learning. The rank of the matrix P depends on dynamical information of the system. Therefore, even for stabilizing tasks in which $\boldsymbol{\omega}^{\mathrm{D}}_{\mathrm{D/I}} = \mathbf{0}$ and $\mathrm{W}_{rb}(t) = 0_{8\times 7}$, the proposed adaptive controllers might still be able to achieve parameter convergence.

Remark 13. For the case $\alpha = 0$, which represents no contribution from the concurrent learning algorithm to the estimation of the mass parameters in equation (4.13), the requirement for parameter convergence given in equation (4.42) collapses to the better known requirement of persistency of excitation

$$\int_{t_1}^{t_1+T_2} \mathrm{W}_{rb}(t)^{\mathrm{T}}\mathrm{W}_{rb}(t)\,\mathrm{d}t > 0, \tag{4.43}$$

for all $t > T_1$ for some $T_1 > 0$ and $T_2 > 0$.

Remark 14. The matrix $\mathrm{W}_{rb}(t)$ can be obtained as

$$\mathrm{W}_{rb}(t) = R(\mathbf{0}, \mathbf{0}, \dot{\boldsymbol{\omega}}^{\mathrm{D}}_{\mathrm{D/I}}, \boldsymbol{\omega}^{\mathrm{D}}_{\mathrm{D/I}}, \mathbf{1}). \tag{4.44}$$

Remark 15. In [50], the persistency excitation condition is given for the more general

case, in which gravitational and J_2 effects are also captured in the dynamics, as

$$\int_{t_1}^{t_1+T_2} \mathrm{W}(t)^{\mathrm{T}}\mathrm{W}(t)\,\mathrm{d}t > 0, \tag{4.45}$$

for all $t > T_1$ for some $T_1 > 0$ and $T_2 > 0$ derived in a similar manner as was done here. The equivalent condition for the case that considers concurrent learning would be given as

$$\int_{t_1}^{t_1+T_2} (\mathrm{W}(t)^{\mathrm{T}}\mathrm{W}(t) + \alpha^2\mathsf{P}^{\mathrm{T}}\mathsf{P})\,\mathrm{d}t > 0, \tag{4.46}$$

for all $t > T_1$ for some $T_1 > 0$ and $T_2 > 0$.

4.5 Numerical Results

Both controllers were simulated using MATLAB R2017a and Simulink, and their performance was compared to that of the nominal controller proposed in [47]. The initial state of the system is given by $q_{\mathrm{B/D}}(0) = (0.8721, -[0.1178, 0.4621, 0.1097]^{\mathrm{T}})$, $\bar{r}^{\mathrm{B}}_{\mathrm{B/D}}(0) = [1, 2, 0.5]^{\mathrm{T}}$ (m), $\bar{\omega}^{\mathrm{B}}_{\mathrm{B/D}}(0) = [0.5, 1, 1]^{\mathrm{T}}$ (rad/s), $\bar{v}^{\mathrm{B}}_{\mathrm{B/D}}(0) = [0.5, -0.5, 1]^{\mathrm{T}}$ (m/s), $\mathrm{v}(M^{\mathrm{B}}) = [5, 2, 3, 5, 1, 4, 10]^{\mathrm{T}}$, $\mathrm{v}(\widehat{M}^{\mathrm{B}})(0) = 0_{7\times 1}$, with units of kg.m^2 and kg for the inertia elements and the mass respectively. The matrix gains were set to $\bar{K}_r = 0.74/3\mathbb{I}_3$, $\bar{K}_q = 0.2/3\mathbb{I}_3$, $\bar{K}_v = 84.37\mathbb{I}_3$, $\bar{K}_\omega = 15\mathbb{I}_3$, and $K_i = 10\mathbb{I}_7$. Both simulations were run for $T = 50$ s.

For the controller proposed in Theorem 1, which incorporates a continuous formulation of the concurrent learning framework, a time-varying reference is selected as $\bar{\omega}^{\mathrm{D}}_{\mathrm{D}/I}(t) = [0, \sin(t), 0]^{\mathrm{T}}$ and $\bar{v}^{\mathrm{D}}_{\mathrm{D}/I}(t) = [1, 0, 0]^{\mathrm{T}}$. The controller gain is set to $\alpha = 1$. For this particular

reference,

$$\mathrm{W}_{rb}(t) = \begin{bmatrix} 0 & 0 & 0 & 0 & 0 & 0 & 1 \\ 0 & 0 & 0 & 0 & 0 & 0 & 0 \\ 0 & 0 & 0 & 0 & 0 & 0 & -\sin(t) \\ 0 & 0 & 0 & 0 & 0 & 0 & 0 \\ 0 & \cos(t) & 0 & 0 & \sin(t)^2 & 0 & 0 \\ 0 & 0 & 0 & \cos(t) & 0 & 0 & 0 \\ 0 & -\sin(t)^2 & 0 & 0 & \cos(t) & 0 & 0 \\ 0 & 0 & 0 & 0 & 0 & 0 & 0 \end{bmatrix}, \tag{4.47}$$

and

$$\mathrm{W}_{rb}(t)^{\mathrm{T}}\mathrm{W}_{rb}(t) = \mathrm{diag}\left(0, \cos(t)^2 + \sin(t)^4, 0, \cos(t)^2, \cos(t)^2 + \sin(t)^4, 0, \sin(t)^2 + 1\right),$$

which has maximum rank 4. This means that for the baseline controller, the persistency of excitation condition will not be met since we require the condition in equation (4.43) to be satisfied.

The continuous controller was simulated using ODE45 with relative and absolute tolerances set to 10^{-10}. Figure 4.1 shows the pose of the spacecraft converging to the reference trajectory. It is worth emphasizing that the transients are less pronounced for the proposed controller. Figure 4.2 shows the evolution of the estimate of the dual inertia matrix. For the proposed controller, the parameters converge in under 3 seconds. In fact, $\mathsf{P} > 0$ from the fourth timestep corresponding to $t = 0.003$ s, but its minimum singular value only becomes $\sigma_{\min}(\mathsf{P}) = 0.1$ at $t = 0.45$ s. The singular values are shown as a function of time in Figure 4.3. Given the positive definiteness of P, the convergence of the inertia parameters is guaranteed early in the simulation for the proposed controller, while not all parameters converge for the baseline controller, since the persistency of excitation condition is not met.

Finally, Figure 4.4 shows the control effort (i.e., forces and torques) applied at the base of the spacecraft to achieve the control objective, exhibiting no meaningful differences.

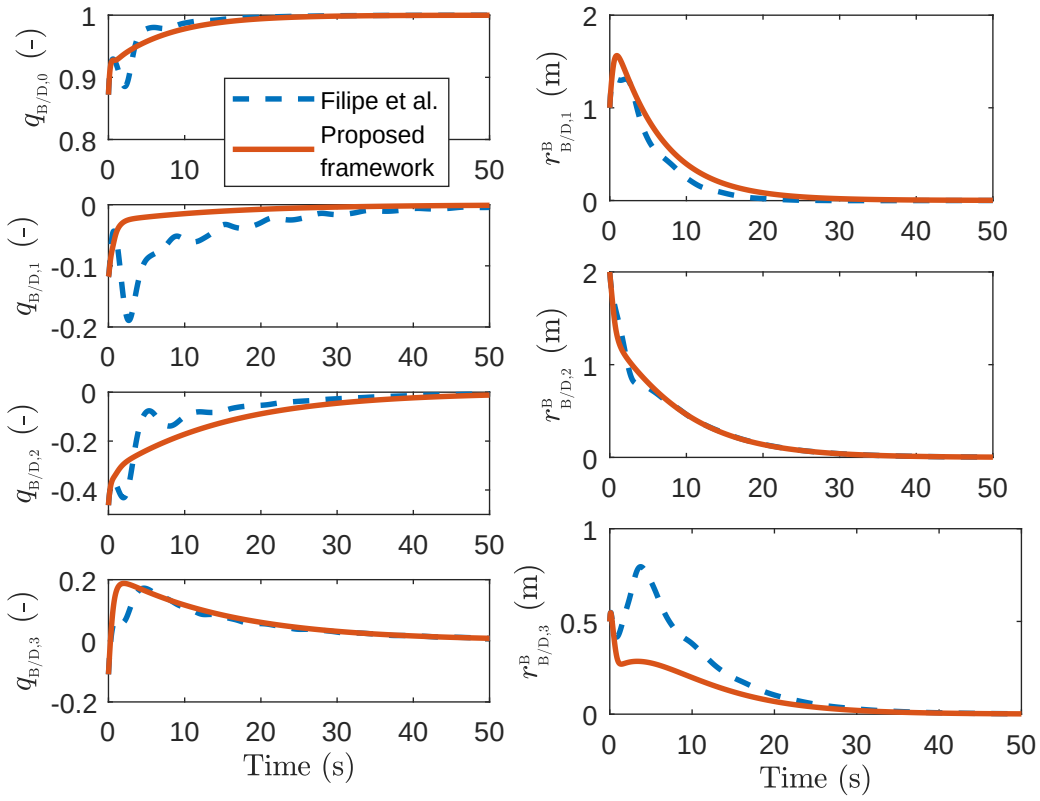

Figure 4.1: Attitude and position tracking error for continuous formulation.

For the simulation of the controller proposed in Theorem 2, which incorporates a discrete formulation of the concurrent learning framework, a constant reference is selected as $\bar{\omega}^{\mathrm{D}}_{\mathrm{D/I}}(t) = [1, 0, 0]^{\mathrm{T}}$ and $\bar{v}^{\mathrm{D}}_{\mathrm{D/I}}(t) = [1, 0, 0]^{\mathrm{T}}$. The controller gain is set to $\alpha = 0.005$. For this

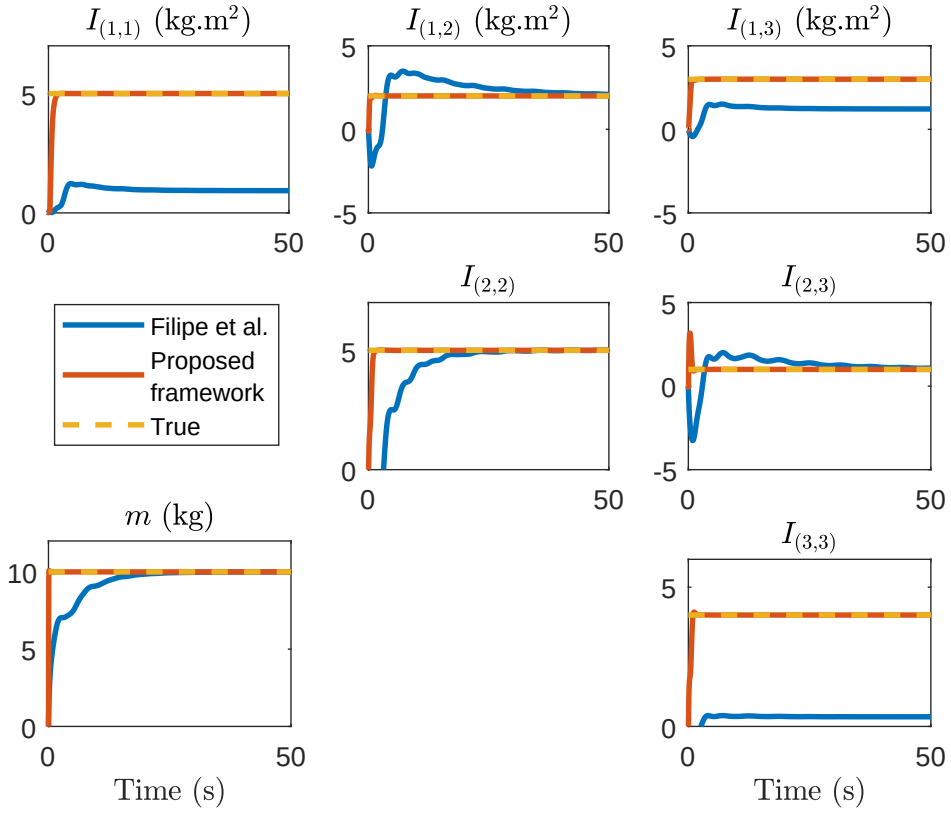

Figure 4.2: Evolution of estimated dual inertia matrix parameters for continuous formulation.

maneuver, we have

$$\mathrm{W}_{rb}(t) = \begin{bmatrix} 0 & 0 & 0 & 0 & 0 & 0 & 0 \\ 0 & 0 & 0 & 0 & 0 & 0 & 0 \\ 0 & 0 & 0 & 0 & 0 & 0 & 0 \\ 0 & 0 & 0 & 0 & 0 & 0 & 0 \\ 0 & 0 & 0 & 0 & 0 & 0 & 0 \\ 0 & 0 & -1 & 0 & 0 & 0 & 0 \\ 0 & 1 & 0 & 0 & 0 & 0 & 0 \\ 0 & 0 & 0 & 0 & 0 & 0 & 0 \end{bmatrix}. \tag{4.48}$$

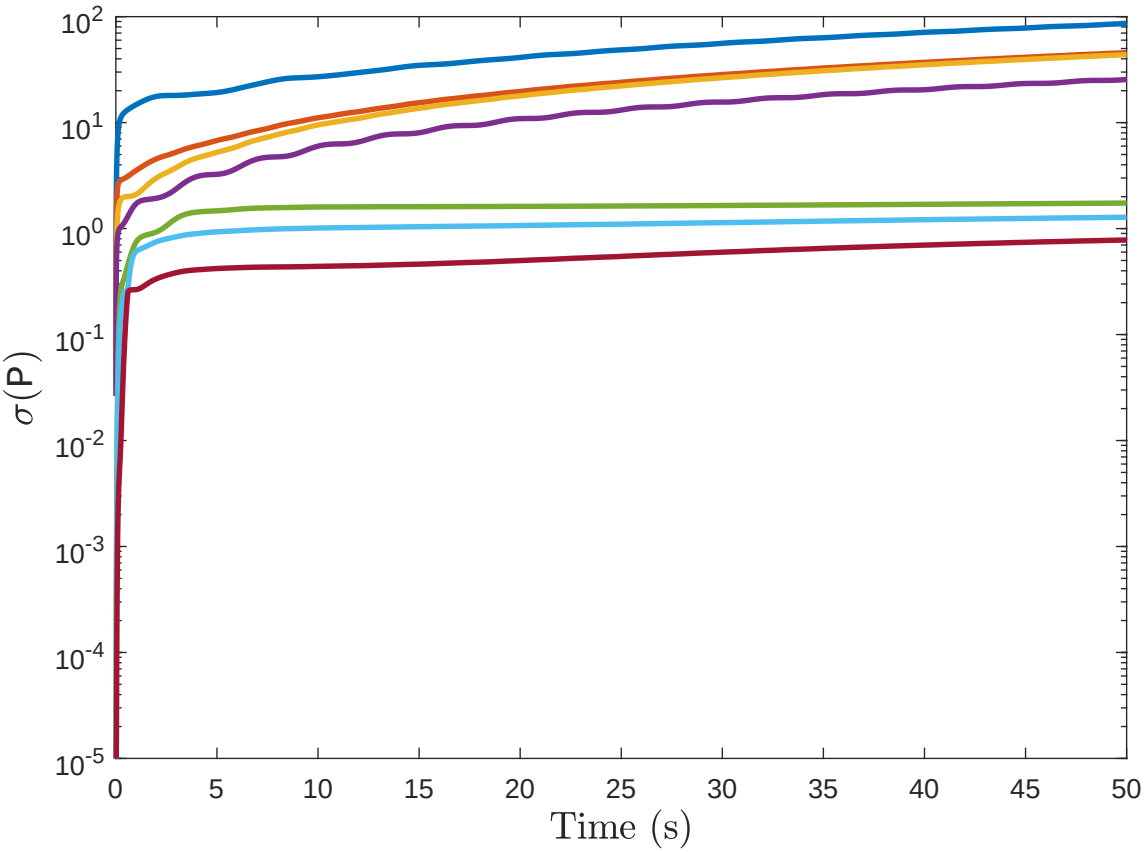

Figure 4.3: Singular values of matrix P as a function of time.

Thus, the persistency of excitation integrand for the baseline controller will be given by

$$\mathrm{W}_{rb}(t)^{\mathrm{T}}\mathrm{W}_{rb}(t) = \mathrm{diag}\left(0, 1, 1, 0, 0, 0, 0\right),$$

which has rank 2 for all time. Therefore, the convergence of parameters is not guaranteed by the baseline controller.

The parameters that concern the discrete implementation of the concurrent learning controller are set to $N_s = 50$, $\alpha = 0.0005$, and the minimum singular value of the sum of regressor matrices required to stop the search of new data points is set to a value of 20. The results are simulated using SIMULINK's implementation of RK4, called ODE4, with a 0.01 s timestep. Figure 4.5 shows the tracking error of the body frame relative to the desired frame. It is clear that both controllers are able to successfully track the 6-DOF reference,

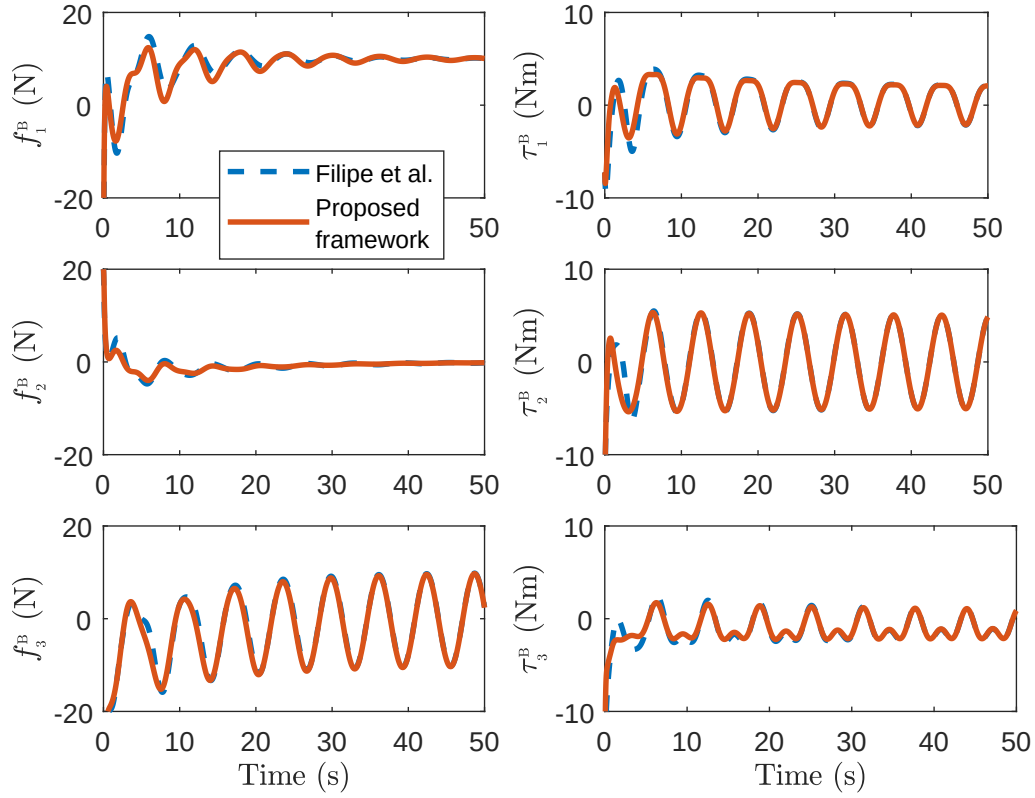

Figure 4.4: Control effort commanded by the controller for continuous formulation.

with no remarkable differences regarding the transient behavior. Figure 4.6 shows the evolution of the estimated mass properties as a function of time during the maneuver. The mass converges quickly for the concurrent learning controller, while the estimate of the baseline controller does not converge. Similarly, all of the inertia parameters converge for the proposed algorithm, but four of the estimates do not converge for the baseline controller from [47]. This behavior can be attributed to the lack of excitation induced by the desired linear and angular velocity references, which is corroborated by the rank deficiency of $\mathrm{W}_{rb}(t)^{\mathrm{T}}\mathrm{W}_{rb}(t)$. However, the rank condition detailed in equation (4.30) for the concurrent learning approach is satisfied even for such a non-exciting reference. In fact, the criterion is achieved at $t = 0.0177$ s. Additionally, we can point out the fact that the non-zero entries of $\mathrm{W}_{rb}(t)^{\mathrm{T}}\mathrm{W}_{rb}(t)$ indicate which components of the estimate will converge. In this case, the second diagonal entry corresponds to $I_{(1,2)}$, and the third diagonal entry corresponds to

$I_{(1,3)}$, both of which converge to the true value. Finally, Figure 4.7 shows the control effort applied on the spacecraft. They are both similar and within acceptable limits.

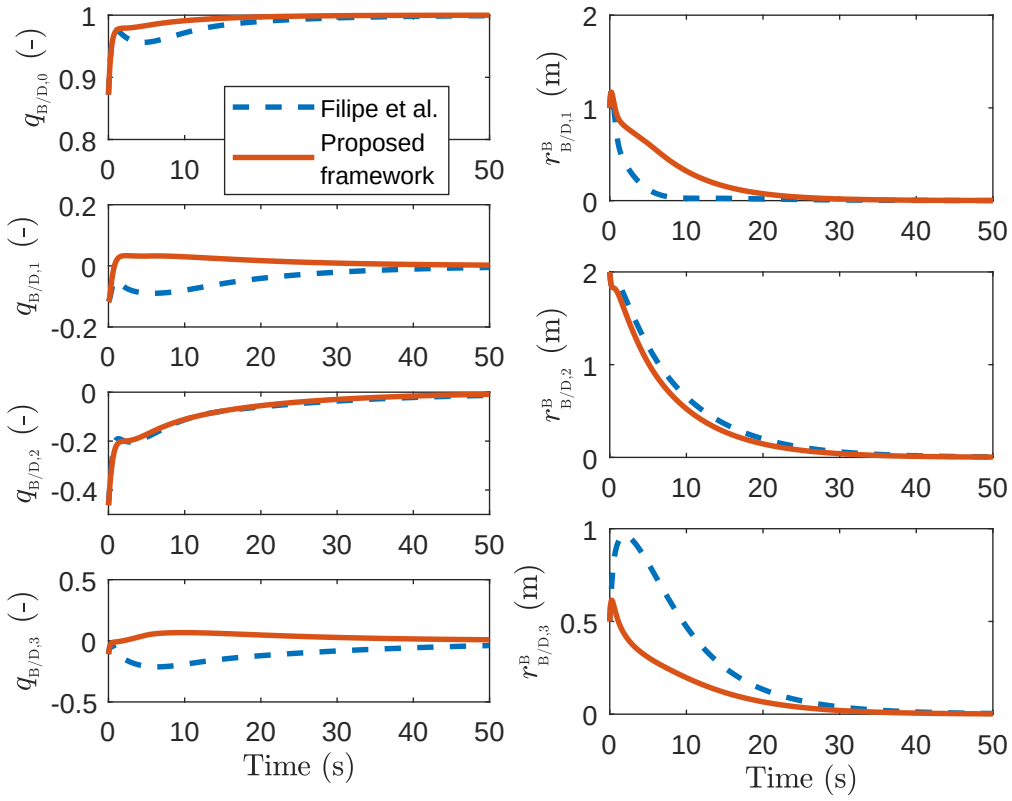

Figure 4.5: Attitude and position tracking error for discrete formulation.

These two example highlights the main advantage that the proposed controllers can provide when compared to others in terms of system identification and reliability in terms of tracking the desired reference trajectory. Finally, it is worth noting that the parameter N_s plays a significant role in the speed the algorithm. This issue will be addressed in a future chapter.

4.6 Conclusions

In this chapter we explored the use of concurrent learning for control of a rigid body spacecraft while estimating its mass properties. Two different controllers were provided. The

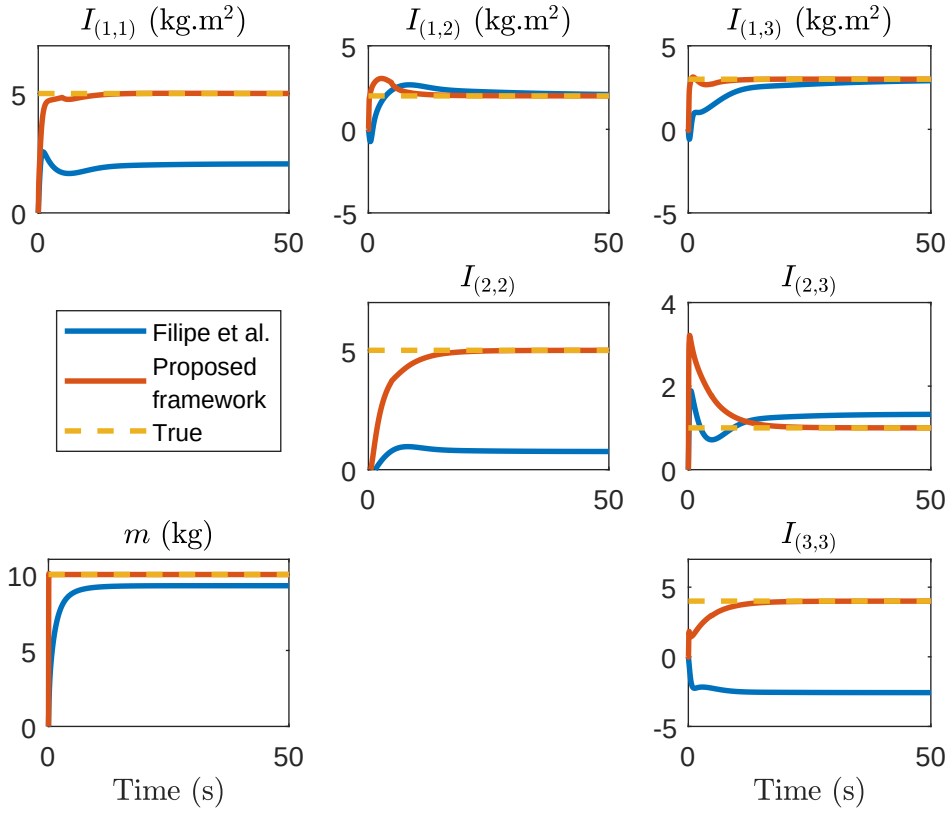

Figure 4.6: Evolution of estimated dual inertia matrix parameters for discrete formulation.

first one uses a continuous time formulation of the concurrent learning framework, while the second one uses a discrete version of the algorithm. In both cases, the adaptive controller is shown to provide tracking of the desired reference trajectory regardless of the estimate of the dual inertia matrix. Furthermore, an important connection was made between the rank condition that appears in concurrent learning, and the persistency of excitation requirement that is so common in adaptive control theory, which showed that these two conditions are one and the same. However, satisfying the rank condition in concurrent learning implies immediately satisfies persistent excitation, leading to parameter convergence. An important consequence of this is that it is no longer needed to evaluate the persistency of excitation integral for every interval of time. Instead, computing the rank of an appropriate matrix in the concurrent learning framework should be used as the first indicator to determine whether parameter convergence can be assured.

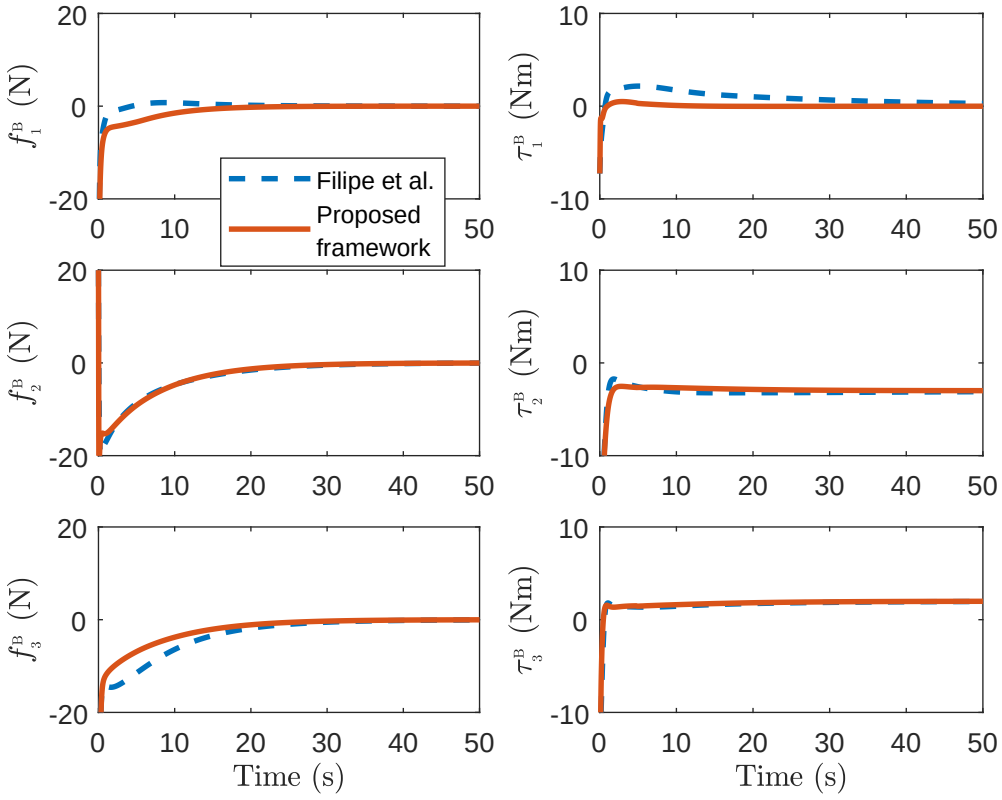

Figure 4.7: Control effort commanded by the controller for discrete formulation.

CHAPTER 5
DYNAMIC MODELING OF A ROBOTIC ARM ON A SATELLITE USING DUAL QUATERNIONS

In this chapter, the equations of motion for a given robotic arm configuration on a satellite base will be derived using two different approaches. Even though both methods will make use of Newton-Euler principles to model the dynamics, the first method, which we shall call the *decoupled* approach, treats the translational and rotational equations separately. The second approach, which we shall call the *dual quaternion (DQ)* approach, uses dual algebra to combine translational and rotational dynamics.

5.1 Dynamic System Modeling - Decoupled Formulation

This section will be dedicated to the derivation of the equations of motion for the robotic arm on the satellite base shown in Figure 5.1 using classical Newton-Euler techniques, as described in [94]. In Figure 5.2 we show the points of interest (including the centers of mass and joint locations), coordinate frames, and forces and torques applied on each body.

We know the motion of each of the four rigid bodies obeys the following equations

$$m_0\dot{\bar{v}}_{\mathfrak{o}_0/\mathcal{I}} + \bar{\omega}_{\mathfrak{o}_0/\mathcal{I}} \times m_0\bar{v}_{\mathfrak{o}_0/\mathcal{I}} = \bar{f}_{\mathfrak{o}_0} - \bar{f}_{1/0}, \tag{5.1}$$

$$I_0\dot{\bar{\omega}}_{\mathfrak{o}_0/\mathcal{I}} + \bar{\omega}_{\mathfrak{o}_0/\mathcal{I}} \times I_0\bar{\omega}_{\mathfrak{o}_0/\mathcal{I}} = \bar{\tau}_{\mathfrak{o}_0} - \bar{\tau}_{1/0} + \bar{r}_{0/\mathfrak{o}_0} \times (-\bar{f}_{1/0}) - \bar{\tau}_{\text{act},1}, \tag{5.2}$$

$$m_1\dot{\bar{v}}_{\mathfrak{o}_1/\mathcal{I}} + \bar{\omega}_{\mathfrak{o}_1/\mathcal{I}} \times m_1\bar{v}_{\mathfrak{o}_1/\mathcal{I}} = \bar{f}_{\mathfrak{o}_1} + \bar{f}_{1/0} - \bar{f}_{2/1}, \tag{5.3}$$

$$I_1\dot{\bar{\omega}}_{\mathfrak{o}_1/\mathcal{I}} + \bar{\omega}_{\mathfrak{o}_1/\mathcal{I}} \times I_1\bar{\omega}_{\mathfrak{o}_1/\mathcal{I}} = \bar{\tau}_{\mathfrak{o}_1} + \bar{\tau}_{1/0} - \bar{\tau}_{2/1} + \bar{r}_{0/\mathfrak{o}_1} \times \bar{f}_{1/0} + \bar{r}_{1/\mathfrak{o}_1} \times (-\bar{f}_{2/1}) + \bar{\tau}_{\text{act},1} - \bar{\tau}_{\text{act},2}, \tag{5.4}$$

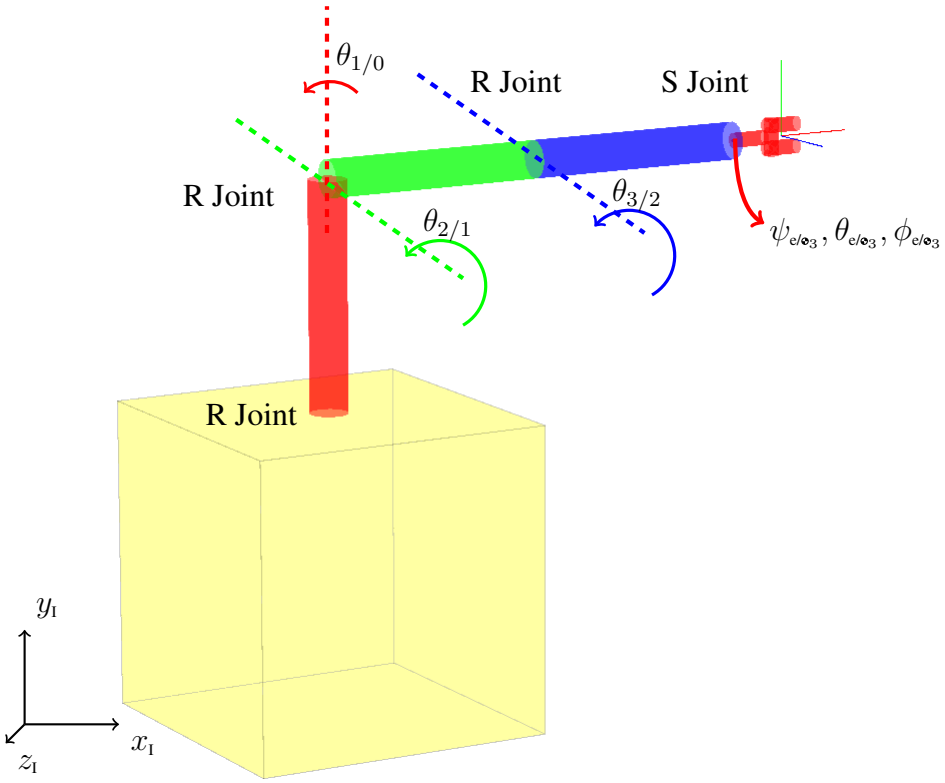

Figure 5.1: RRRS robotic arm in nominal configuration on a satellite base showing joint angle definition.

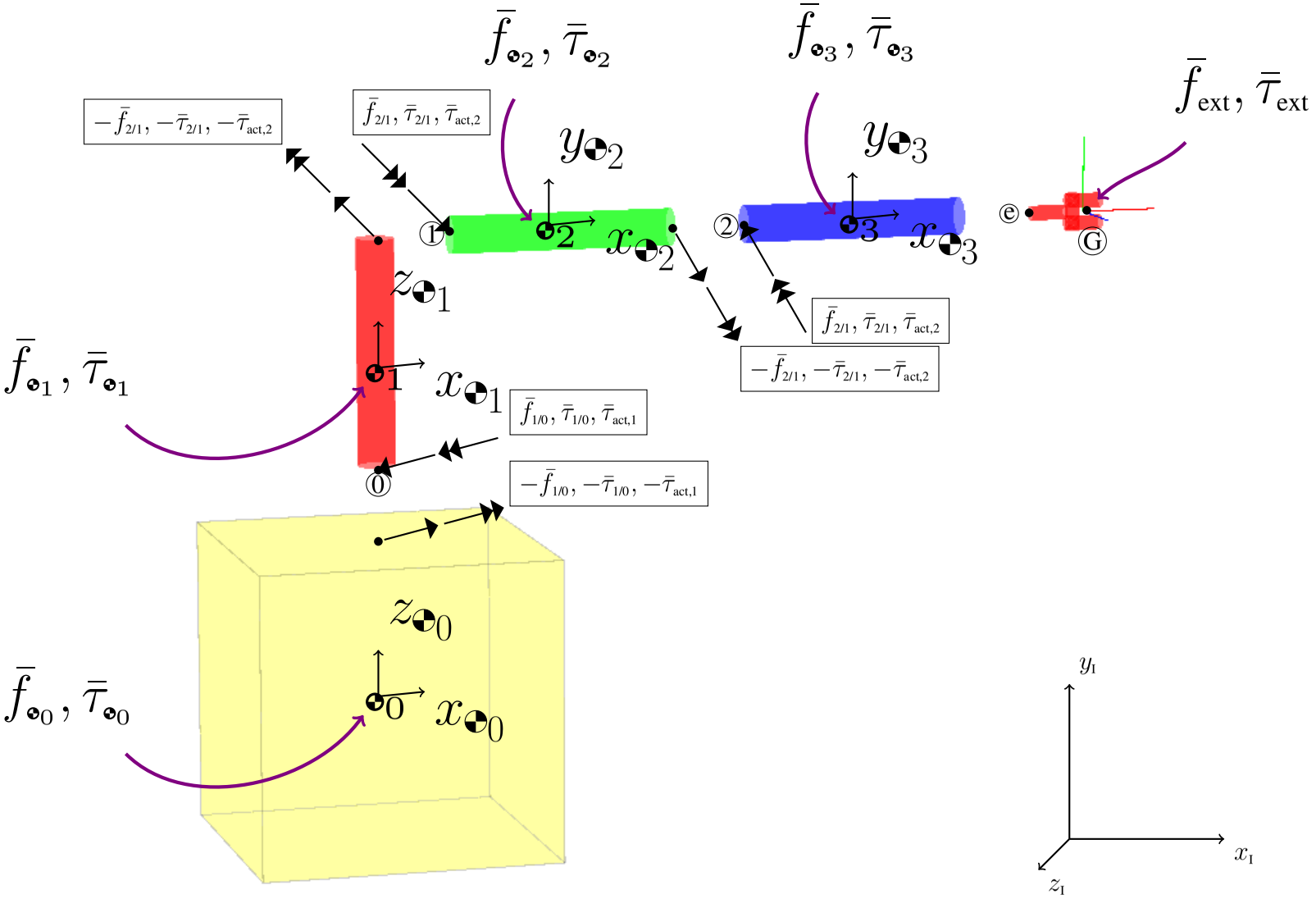

Figure 5.2: Exploded view showing internal forces, points of interest, and frame definition.

$$m_2\dot{\bar{v}}_{\mathbf{o}_2/\mathrm{I}} + \bar{\omega}_{\mathbf{o}_2/\mathrm{I}} \times m_2\bar{v}_{\mathbf{o}_2/\mathrm{I}} = \bar{f}_{\mathbf{o}_2} + \bar{f}_{2/1} - \bar{f}_{3/2}, \quad (5.5)$$

$$I_2\dot{\bar{\omega}}_{\mathbf{o}_2/\mathrm{I}} + \bar{\omega}_{\mathbf{o}_2/\mathrm{I}} \times I_2\bar{\omega}_{\mathbf{o}_2/\mathrm{I}} = \bar{\tau}_{\mathbf{o}_2} + \bar{\tau}_{2/1} - \bar{\tau}_{3/2} + \bar{r}_{1/\mathbf{o}_2} \times \bar{f}_{2/1} + \bar{r}_{2/\mathbf{o}_2} \times (-\bar{f}_{3/2}) + \bar{\tau}_{\mathrm{act},2} - \bar{\tau}_{\mathrm{act},3}, \quad (5.6)$$

and

$$m_3\dot{\bar{v}}_{\mathbf{o}_3/\mathrm{I}} + \bar{\omega}_{\mathbf{o}_3/\mathrm{I}} \times m_3\bar{v}_{\mathbf{o}_3/\mathrm{I}} = \bar{f}_{\mathbf{o}_3} + \bar{f}_{3/2} + \bar{f}_{\mathrm{ext}}, \quad (5.7)$$

$$I_3\dot{\bar{\omega}}_{\mathbf{o}_3/\mathrm{I}} + \bar{\omega}_{\mathbf{o}_3/\mathrm{I}} \times I_3\bar{\omega}_{\mathbf{o}_3/\mathrm{I}} = \bar{\tau}_{\mathbf{o}_3} + \bar{\tau}_{3/2} + \bar{\tau}_{\mathrm{ext}} + \bar{r}_{2/\mathbf{o}_3} \times \bar{f}_{3/2} + \bar{r}_{\mathrm{G}/\mathbf{o}_3} \times \bar{f}_{\mathrm{ext}} + \bar{\tau}_{\mathrm{act},3}, \quad (5.8)$$

where we have assumed that the end effector is massless for exposition purposes, and that any external forces applied on it, get transmitted accordingly to the spherical joint. In these equations, $\bar{v}_{\mathbf{o}_\mathrm{i}/\mathrm{I}}$ and $\bar{\omega}_{\mathbf{o}_\mathrm{i}/\mathrm{I}}$ are the linear and angular velocity of the frame $\mathbf{o}_\mathrm{i}$ with respect to frame I, and $\dot{\bar{v}}_{\mathbf{o}_\mathrm{i}/\mathrm{I}}$ and $\dot{\bar{\omega}}_{\mathbf{o}_\mathrm{i}/\mathrm{I}}$ are the corresponding linear and angular accelerations.

5.1.1 Frame Assignment to Each Variable

We will assign a coordinate frame to each of the variables in equations (5.1) to (5.8). We list these in Table 5.1. In particular, we are interested in providing the following quantities

Table 5.1: Frame assignment for relevant variables.

	Motion	External	Reaction	Joint Actuation	Geometry
Frame $\mathbf{o}_1$	$\bar{v}^{\mathbf{o}_0}_{\mathbf{o}_0/\mathrm{I}}, \bar{\omega}^{\mathbf{o}_0}_{\mathbf{o}_0/\mathrm{I}}$	$\bar{f}^{\mathbf{o}_0}_{\mathbf{o}_0}, \bar{\tau}^{\mathbf{o}_0}_{\mathbf{o}_0}$			$\bar{r}^{\mathbf{o}_0}_{0/\mathbf{o}_0}$
Frame $\mathbf{o}_1$	$\bar{v}^{\mathbf{o}_1}_{\mathbf{o}_1/\mathrm{I}}, \bar{\omega}^{\mathbf{o}_1}_{\mathbf{o}_1/\mathrm{I}}$	$\bar{f}^{\mathbf{o}_1}_{\mathbf{o}_1}, \bar{\tau}^{\mathbf{o}_1}_{\mathbf{o}_1}$	$\bar{f}^{\mathbf{o}_1}_{1/0}, \bar{\tau}^{\mathbf{o}_1}_{1/0}$	$\bar{\tau}^{\mathbf{o}_1}_{\mathrm{act},1}$	$\bar{r}^{\mathbf{o}_1}_{0/\mathbf{o}_1}, \bar{r}^{\mathbf{o}_1}_{1/\mathbf{o}_1}$
Frame $\mathbf{o}_2$	$\bar{v}^{\mathbf{o}_2}_{\mathbf{o}_2/\mathrm{I}}, \bar{\omega}^{\mathbf{o}_2}_{\mathbf{o}_2/\mathrm{I}}$	$\bar{f}^{\mathbf{o}_2}_{\mathbf{o}_2}, \bar{\tau}^{\mathbf{o}_2}_{\mathbf{o}_2}$	$\bar{f}^{2/1}_{\mathbf{o}_2}, \bar{\tau}^{\mathbf{o}_2}_{2/1}$	$\bar{\tau}^{\mathbf{o}_2}_{\mathrm{act},2}$	$\bar{r}^{\mathbf{o}_2}_{1/\mathbf{o}_2}, \bar{r}^{\mathbf{o}_2}_{2/\mathbf{o}_2}$
Frame $\mathbf{o}_3$	$\bar{v}^{\mathbf{o}_3}_{\mathbf{o}_3/\mathrm{I}}, \bar{\omega}^{\mathbf{o}_3}_{\mathbf{o}_3/\mathrm{I}}$	$\bar{f}^{\mathbf{o}_3}_{\mathbf{o}_3}, \bar{\tau}^{\mathbf{o}_3}_{\mathbf{o}_3}$	$\bar{f}^{3/2}_{\mathbf{o}_3}, \bar{\tau}^{\mathbf{o}_3}_{3/2}$	$\bar{\tau}^{\mathbf{o}_3}_{\mathrm{act},3}$	$\bar{r}^{\mathbf{o}_3}_{2/\mathbf{o}_3}, \bar{r}^{\mathbf{o}_3}_{\mathrm{e}/\mathbf{o}_3}$
Frame G		$\bar{f}^{\mathrm{G}}_{\mathrm{ext}}, \bar{\tau}^{\mathrm{G}}_{\mathrm{ext}}$			

explicitly:

$$\bar{\tau}^{\mathfrak{o}_1}_{1/0} = \begin{bmatrix} \left(\bar{\tau}^{\mathfrak{o}_1}_{1/0}\right)_x \\ \left(\bar{\tau}^{\mathfrak{o}_1}_{1/0}\right)_y \\ 0 \end{bmatrix}, \qquad \bar{\tau}^{\mathfrak{o}_1}_{\text{act},1} = \begin{bmatrix} 0 \\ 0 \\ \left(\bar{\tau}^{\mathfrak{o}_1}_{\text{act},1}\right)_z \end{bmatrix} \tag{5.9}$$

$$\bar{\tau}^{\mathfrak{o}_2}_{2/1} = \begin{bmatrix} \left(\bar{\tau}^{\mathfrak{o}_2}_{2/1}\right)_x \\ \left(\bar{\tau}^{\mathfrak{o}_2}_{2/1}\right)_y \\ 0 \end{bmatrix}, \qquad \bar{\tau}^{\mathfrak{o}_2}_{\text{act},2} = \begin{bmatrix} 0 \\ 0 \\ \left(\bar{\tau}^{\mathfrak{o}_2}_{\text{act},2}\right)_z \end{bmatrix} \tag{5.10}$$

$$\bar{\tau}^{\mathfrak{o}_3}_{3/2} = \begin{bmatrix} \left(\bar{\tau}^{\mathfrak{o}_3}_{3/2}\right)_x \\ \left(\bar{\tau}^{\mathfrak{o}_3}_{3/2}\right)_y \\ 0 \end{bmatrix}, \qquad \bar{\tau}^{\mathfrak{o}_3}_{\text{act},3} = \begin{bmatrix} 0 \\ 0 \\ \left(\bar{\tau}^{\mathfrak{o}_3}_{\text{act},3}\right)_z \end{bmatrix} \tag{5.11}$$

5.1.2 Constraints

We now consider kinematic constraints. Four rigid bodies possess a total of 24 degrees of freedom (DOF). However, our robot only has nine degrees of freedom (six for the motion of the base, and three associated to each of the joints of the arm). Thus, we need 15 ($= 24 - 9$) constraint equations, nine of which will come from linear velocity constraints at the joints, and 6 from angular velocity constraints. While the constraints can be given as a set of algebraic equations, and the problem could be treated as a descriptor system (see Ref. [142]), we will obtain second order derivatives to incorporate the constraints as differential equations. The latter approach has the advantage that it immediately allows solving for the reaction forces and torques at each time step.

Linear Constraints

Linear velocity constraints are based on the fact that at the joint, the two bodies will move with the same velocity. Thus, their accelerations are also the same. We start by deriving the position constraint, followed by an inertial derivative of this relationship to yield a velocity

constraint, and then another inertial derivative to yield our desired acceleration relationship. We know from the geometry of the problem that

$$\bar{r}_{\mathfrak{o}_0/\mathrm{I}} + \bar{r}_{0/\mathfrak{o}_0} = \bar{r}_{\mathfrak{o}_1/\mathrm{I}} + \bar{r}_{0/\mathfrak{o}_1}. \tag{5.12}$$

Taking the inertial time derivative:

$$\frac{{}^{\mathrm{I}}\mathrm{d}}{\mathrm{d}t}(\bar{r}_{\mathfrak{o}_0/\mathrm{I}} + \bar{r}_{0/\mathfrak{o}_0}) = \frac{{}^{\mathrm{I}}\mathrm{d}}{\mathrm{d}t}(\bar{r}_{\mathfrak{o}_1/\mathrm{I}} + \bar{r}_{0/\mathfrak{o}_1}) \tag{5.13}$$

$$\bar{v}_{\mathfrak{o}_0/\mathrm{I}} + \frac{{}^{\mathfrak{o}_0}\mathrm{d}}{\mathrm{d}t}(\bar{r}_{0/\mathfrak{o}_0}) + \bar{\omega}_{\mathfrak{o}_0/\mathrm{I}} \times \bar{r}_{0/\mathfrak{o}_0} = \bar{v}_{\mathfrak{o}_1/\mathrm{I}} + \frac{{}^{\mathfrak{o}_1}\mathrm{d}}{\mathrm{d}t}(\bar{r}_{0/\mathfrak{o}_1}) + \bar{\omega}_{\mathfrak{o}_1/\mathrm{I}} \times \bar{r}_{0/\mathfrak{o}_1} \tag{5.14}$$

$$\bar{v}_{\mathfrak{o}_0/\mathrm{I}} + \bar{\omega}_{\mathfrak{o}_0/\mathrm{I}} \times \bar{r}_{0/\mathfrak{o}_0} = \bar{v}_{\mathfrak{o}_1/\mathrm{I}} + \bar{\omega}_{\mathfrak{o}_1/\mathrm{I}} \times \bar{r}_{0/\mathfrak{o}_1}. \tag{5.15}$$

Taking a second inertial time derivative:

$$\frac{{}^{\mathrm{I}}\mathrm{d}}{\mathrm{d}t}(\bar{v}_{\mathfrak{o}_0/\mathrm{I}} + \bar{\omega}_{\mathfrak{o}_0/\mathrm{I}} \times \bar{r}_{0/\mathfrak{o}_0}) = \frac{{}^{\mathrm{I}}\mathrm{d}}{\mathrm{d}t}(\bar{v}_{\mathfrak{o}_1/\mathrm{I}} + \bar{\omega}_{\mathfrak{o}_1/\mathrm{I}} \times \bar{r}_{0/\mathfrak{o}_1}) \tag{5.16}$$

$$\bar{a}_{\mathfrak{o}_0/\mathrm{I}} + \frac{{}^{\mathfrak{o}_0}\mathrm{d}}{\mathrm{d}t}(\bar{\omega}_{\mathfrak{o}_0/\mathrm{I}} \times \bar{r}_{0/\mathfrak{o}_0}) + \bar{\omega}_{\mathfrak{o}_0/\mathrm{I}} \times (\bar{\omega}_{\mathfrak{o}_0/\mathrm{I}} \times \bar{r}_{0/\mathfrak{o}_0}) = \bar{a}_{\mathfrak{o}_1/\mathrm{I}} + \frac{{}^{\mathfrak{o}_1}\mathrm{d}}{\mathrm{d}t}(\bar{\omega}_{\mathfrak{o}_1/\mathrm{I}} \times \bar{r}_{0/\mathfrak{o}_1}) + \bar{\omega}_{\mathfrak{o}_1/\mathrm{I}} \times (\bar{\omega}_{\mathfrak{o}_1/\mathrm{I}} \times \bar{r}_{0/\mathfrak{o}_1}) \tag{5.17}$$

$$\bar{a}_{\mathfrak{o}_0/\mathrm{I}} + \dot{\bar{\omega}}_{\mathfrak{o}_0/\mathrm{I}} \times \bar{r}_{0/\mathfrak{o}_0} + \bar{\omega}_{\mathfrak{o}_0/\mathrm{I}} \times (\bar{\omega}_{\mathfrak{o}_0/\mathrm{I}} \times \bar{r}_{0/\mathfrak{o}_0}) = \bar{a}_{\mathfrak{o}_1/\mathrm{I}} + \dot{\bar{\omega}}_{\mathfrak{o}_1/\mathrm{I}} \times \bar{r}_{0/\mathfrak{o}_1} + \bar{\omega}_{\mathfrak{o}_1/\mathrm{I}} \times (\bar{\omega}_{\mathfrak{o}_1/\mathrm{I}} \times \bar{r}_{0/\mathfrak{o}_1}). \tag{5.18}$$

Assigning coordinates yields

$$\bar{a}^{\mathfrak{o}_0}_{\mathfrak{o}_0/\mathrm{I}} + \dot{\bar{\omega}}^{\mathfrak{o}_0}_{\mathfrak{o}_0/\mathrm{I}} \times \bar{r}^{\mathfrak{o}_0}_{0/\mathfrak{o}_0} + \bar{\omega}^{\mathfrak{o}_0}_{\mathfrak{o}_0/\mathrm{I}} \times (\bar{\omega}^{\mathfrak{o}_0}_{\mathfrak{o}_0/\mathrm{I}} \times \bar{r}^{\mathfrak{o}_0}_{0/\mathfrak{o}_0}) = R^{\mathrm{T}}_{\mathfrak{o}_1/\mathfrak{o}_0}\left(\bar{a}^{\mathfrak{o}_1}_{\mathfrak{o}_1/\mathrm{I}} + \dot{\bar{\omega}}^{\mathfrak{o}_1}_{\mathfrak{o}_1/\mathrm{I}} \times \bar{r}^{\mathfrak{o}_1}_{0/\mathfrak{o}_1} + \bar{\omega}^{\mathfrak{o}_1}_{\mathfrak{o}_1/\mathrm{I}} \times (\bar{\omega}^{\mathfrak{o}_1}_{\mathfrak{o}_1/\mathrm{I}} \times \bar{r}^{\mathfrak{o}_1}_{0/\mathfrak{o}_1})\right), \tag{5.19}$$

where $R_{\mathrm{Y/X}} \in \mathrm{SO}(3)$ is the rotation matrix that transforms coordinates from the X-frame to the Y-frame. Finally, using $\bar{a}^{\mathfrak{o}_0}_{\mathfrak{o}_0/\mathrm{I}} = \dot{\bar{v}}^{\mathfrak{o}_0}_{\mathfrak{o}_0/\mathrm{I}} + \bar{\omega}^{\mathfrak{o}_0}_{\mathfrak{o}_0/\mathrm{I}} \times \bar{v}^{\mathfrak{o}_0}_{\mathfrak{o}_0/\mathrm{I}}$, where $\dot{\bar{v}}^{\mathfrak{o}_0}_{\mathfrak{o}_0/\mathrm{I}}$ is the time derivative of the components expressed in the local coordinate system, in this case $\mathfrak{o}_0$, and the analogous

expression for $\bar{a}^{\mathfrak{o}_1}_{\mathfrak{o}_1/\mathrm{I}}$,

$$\dot{\bar{v}}^{\mathfrak{o}_0}_{\mathfrak{o}_0/\mathrm{I}}+\bar{\omega}^{\mathfrak{o}_0}_{\mathfrak{o}_0/\mathrm{I}}\times\bar{v}^{\mathfrak{o}_0}_{\mathfrak{o}_0/\mathrm{I}}+\dot{\bar{\omega}}^{\mathfrak{o}_0}_{\mathfrak{o}_0/\mathrm{I}}\times\bar{r}^{\mathfrak{o}_0}_{0/\mathfrak{o}_0}+\bar{\omega}^{\mathfrak{o}_0}_{\mathfrak{o}_0/\mathrm{I}}\times\left(\bar{\omega}^{\mathfrak{o}_0}_{\mathfrak{o}_0/\mathrm{I}}\times\bar{r}^{\mathfrak{o}_0}_{0/\mathfrak{o}_0}\right)= \tag{5.20}$$
$$R^{\mathrm{T}}_{\mathfrak{o}_1/\mathfrak{o}_0}\left(\dot{\bar{v}}^{\mathfrak{o}_1}_{\mathfrak{o}_1/\mathrm{I}}+\bar{\omega}^{\mathfrak{o}_1}_{\mathfrak{o}_1/\mathrm{I}}\times\bar{v}^{\mathfrak{o}_1}_{\mathfrak{o}_1/\mathrm{I}}+\dot{\bar{\omega}}^{\mathfrak{o}_1}_{\mathfrak{o}_1/\mathrm{I}}\times\bar{r}^{\mathfrak{o}_1}_{0/\mathfrak{o}_1}+\bar{\omega}^{\mathfrak{o}_1}_{\mathfrak{o}_1/\mathrm{I}}\times\left(\bar{\omega}^{\mathfrak{o}_1}_{\mathfrak{o}_1/\mathrm{I}}\times\bar{r}^{\mathfrak{o}_1}_{0/\mathfrak{o}_1}\right)\right).$$

Equivalently, the linear acceleration constraints at points 1, and 2 are given by

$$\dot{\bar{v}}^{\mathfrak{o}_1}_{\mathfrak{o}_1/\mathrm{I}}+\bar{\omega}^{\mathfrak{o}_1}_{\mathfrak{o}_1/\mathrm{I}}\times\bar{v}^{\mathfrak{o}_1}_{\mathfrak{o}_1/\mathrm{I}}+\dot{\bar{\omega}}^{\mathfrak{o}_1}_{\mathfrak{o}_1/\mathrm{I}}\times\bar{r}^{\mathfrak{o}_1}_{1/\mathfrak{o}_1}+\bar{\omega}^{\mathfrak{o}_1}_{\mathfrak{o}_1/\mathrm{I}}\times\left(\bar{\omega}^{\mathfrak{o}_1}_{\mathfrak{o}_1/\mathrm{I}}\times\bar{r}^{\mathfrak{o}_1}_{1/\mathfrak{o}_1}\right)= \tag{5.21}$$
$$R^{\mathrm{T}}_{\mathfrak{o}_2/\mathfrak{o}_1}\left(\dot{\bar{v}}^{\mathfrak{o}_2}_{\mathfrak{o}_2/\mathrm{I}}+\bar{\omega}^{\mathfrak{o}_2}_{\mathfrak{o}_2/\mathrm{I}}\times\bar{v}^{\mathfrak{o}_2}_{\mathfrak{o}_2/\mathrm{I}}+\dot{\bar{\omega}}^{\mathfrak{o}_2}_{\mathfrak{o}_2/\mathrm{I}}\times\bar{r}^{\mathfrak{o}_2}_{1/\mathfrak{o}_2}+\bar{\omega}^{\mathfrak{o}_2}_{\mathfrak{o}_2/\mathrm{I}}\times\left(\bar{\omega}^{\mathfrak{o}_2}_{\mathfrak{o}_2/\mathrm{I}}\times\bar{r}^{\mathfrak{o}_2}_{1/\mathfrak{o}_2}\right)\right),$$

and

$$\dot{\bar{v}}^{\mathfrak{o}_2}_{\mathfrak{o}_2/\mathrm{I}}+\bar{\omega}^{\mathfrak{o}_2}_{\mathfrak{o}_2/\mathrm{I}}\times\bar{v}^{\mathfrak{o}_2}_{\mathfrak{o}_2/\mathrm{I}}+\dot{\bar{\omega}}^{\mathfrak{o}_2}_{\mathfrak{o}_2/\mathrm{I}}\times\bar{r}^{\mathfrak{o}_2}_{2/\mathfrak{o}_2}+\bar{\omega}^{\mathfrak{o}_2}_{\mathfrak{o}_2/\mathrm{I}}\times\left(\bar{\omega}^{\mathfrak{o}_2}_{\mathfrak{o}_2/\mathrm{I}}\times\bar{r}^{\mathfrak{o}_2}_{2/\mathfrak{o}_2}\right)= \tag{5.22}$$
$$R^{\mathrm{T}}_{\mathfrak{o}_3/\mathfrak{o}_2}\left(\dot{\bar{v}}^{\mathfrak{o}_3}_{\mathfrak{o}_3/\mathrm{I}}+\bar{\omega}^{\mathfrak{o}_3}_{\mathfrak{o}_3/\mathrm{I}}\times\bar{v}^{\mathfrak{o}_3}_{\mathfrak{o}_3/\mathrm{I}}+\dot{\bar{\omega}}^{\mathfrak{o}_3}_{\mathfrak{o}_3/\mathrm{I}}\times\bar{r}^{\mathfrak{o}_3}_{2/\mathfrak{o}_3}+\bar{\omega}^{\mathfrak{o}_3}_{\mathfrak{o}_3/\mathrm{I}}\times\left(\bar{\omega}^{\mathfrak{o}_3}_{\mathfrak{o}_3/\mathrm{I}}\times\bar{r}^{\mathfrak{o}_3}_{2/\mathfrak{o}_3}\right)\right).$$

Angular Constraints

Similar relationships can be derived for the angular acceleration relationship between connected joints. In particular, we first study the angular relationship at joint 0, where the following relationship holds,

$$\bar{\omega}_{\mathfrak{o}_1/\mathrm{I}}=\bar{\omega}_{\mathfrak{o}_0/\mathrm{I}}+\bar{\omega}_{\mathfrak{o}_1/\mathfrak{o}_0}, \tag{5.23}$$

and

$$\bar{\omega}^{\mathfrak{o}_1}_{\mathfrak{o}_1/\mathfrak{o}_0}=\bar{\omega}^{\mathfrak{o}_0}_{\mathfrak{o}_1/\mathfrak{o}_0}=\left[0,0,\dot{\theta}_{1/0}\right]^{\mathrm{T}}. \tag{5.24}$$

Taking the inertial time derivative to obtain an angular acceleration relationship yields

$$\frac{{}^{\mathrm{I}}\mathrm{d}}{\mathrm{d}t}(\bar{\omega}_{\mathfrak{o}_1/\mathrm{I}})=\frac{{}^{\mathrm{I}}\mathrm{d}}{\mathrm{d}t}(\bar{\omega}_{\mathfrak{o}_0/\mathrm{I}}+\bar{\omega}_{\mathfrak{o}_1/\mathfrak{o}_0}) \tag{5.25}$$
$$\dot{\bar{\omega}}_{\mathfrak{o}_1/\mathrm{I}}=\dot{\bar{\omega}}_{\mathfrak{o}_0/\mathrm{I}}+\frac{{}^{\mathfrak{o}_0}\mathrm{d}}{\mathrm{d}t}(\bar{\omega}_{\mathfrak{o}_1/\mathfrak{o}_0})+\bar{\omega}_{\mathfrak{o}_0/\mathrm{I}}\times\bar{\omega}_{\mathfrak{o}_1/\mathfrak{o}_0} \tag{5.26}$$

Assigning coordinates, and using the facts that

$$\dot{\bar{\omega}}_{\mathfrak{o}_1/\mathfrak{o}_0} = \frac{{}^{\mathfrak{o}_0}\mathrm{d}}{\mathrm{d}t}(\bar{\omega}_{\mathfrak{o}_1/\mathfrak{o}_0}) = \frac{{}^{\mathfrak{o}_1}\mathrm{d}}{\mathrm{d}t}(\bar{\omega}_{\mathfrak{o}_1/\mathfrak{o}_0}) \tag{5.27}$$

$$\dot{\bar{\omega}}^{\mathfrak{o}_0}_{\mathfrak{o}_1/\mathfrak{o}_0} = \dot{\bar{\omega}}^{\mathfrak{o}_1}_{\mathfrak{o}_1/\mathfrak{o}_0} = \begin{bmatrix} 0 \\ 0 \\ \ddot{\theta}_{1/0} \end{bmatrix}, \tag{5.28}$$

we obtain

$$\dot{\bar{\omega}}^{\mathfrak{o}_1}_{\mathfrak{o}_1/\mathrm{I}} = R_{\mathfrak{o}_1/\mathfrak{o}_0}\left(\dot{\bar{\omega}}^{\mathfrak{o}_0}_{\mathfrak{o}_0/\mathrm{I}} + \bar{\omega}^{\mathfrak{o}_0}_{\mathfrak{o}_0/\mathrm{I}} \times \bar{\omega}^{\mathfrak{o}_0}_{\mathfrak{o}_1/\mathfrak{o}_0}\right) + \begin{bmatrix} 0 \\ 0 \\ \ddot{\theta}_{1/0} \end{bmatrix}^{\mathfrak{o}_1}. \tag{5.29}$$

An analogous procedure for the angular relationships at joints 1 and 2 yields

$$\dot{\bar{\omega}}^{\mathfrak{o}_2}_{\mathfrak{o}_2/\mathrm{I}} = R_{\mathfrak{o}_2/\mathfrak{o}_1}\left(\dot{\bar{\omega}}^{\mathfrak{o}_1}_{\mathfrak{o}_1/\mathrm{I}} + \bar{\omega}^{\mathfrak{o}_1}_{\mathfrak{o}_1/\mathrm{I}} \times \bar{\omega}^{\mathfrak{o}_1}_{\mathfrak{o}_2/\mathfrak{o}_1}\right) + \begin{bmatrix} 0 \\ 0 \\ \ddot{\theta}_{2/1} \end{bmatrix}^{\mathfrak{o}_2}, \tag{5.30}$$

and

$$\dot{\bar{\omega}}^{\mathfrak{o}_3}_{\mathfrak{o}_3/\mathrm{I}} = R_{\mathfrak{o}_3/\mathfrak{o}_2}\left(\dot{\bar{\omega}}^{\mathfrak{o}_2}_{\mathfrak{o}_2/\mathrm{I}} + \bar{\omega}^{\mathfrak{o}_2}_{\mathfrak{o}_2/\mathrm{I}} \times \bar{\omega}^{\mathfrak{o}_2}_{\mathfrak{o}_3/\mathfrak{o}_2}\right) + \begin{bmatrix} 0 \\ 0 \\ \ddot{\theta}_{3/2} \end{bmatrix}^{\mathfrak{o}_3}, \tag{5.31}$$

where now we have that

$$\bar{\omega}^{\mathfrak{o}_1}_{\mathfrak{o}_2/\mathfrak{o}_1} = \begin{bmatrix} 0 \\ -\dot{\theta}_{2/1} \\ 0 \end{bmatrix} \quad \text{and} \quad \bar{\omega}^{\mathfrak{o}_2}_{\mathfrak{o}_3/\mathfrak{o}_2} = \begin{bmatrix} 0 \\ 0 \\ \dot{\theta}_{3/2} \end{bmatrix}. \tag{5.32}$$

The acceleration of the joint angles ($\ddot{\theta}$) is dependent upon the angular accelerations of each of the bodies ($\dot{\bar{\omega}}$). This dependency must be removed from the equations. Thus, for each constraint equation, it will suffice to ignore the coordinate in which the joint acceleration appears. By design for revolute joints, the joint acceleration appears in the third coordinate when expressed in the joint frame (because joints actuate about body Z-axis) for each of our constraint equations. Thus, we will only use the first two coordinates of equations (5.29) to (5.31). Our final constraint equations are given by

$$E_{23}\dot{\bar{\omega}}^{\mathfrak{o}_1}_{\mathfrak{o}_1/\mathcal{I}} = E_{23}R_{\mathfrak{o}_1/\mathfrak{o}_0}\left(\dot{\bar{\omega}}^{\mathfrak{o}_0}_{\mathfrak{o}_0/\mathcal{I}} + \bar{\omega}^{\mathfrak{o}_0}_{\mathfrak{o}_0/\mathcal{I}} \times \bar{\omega}^{\mathfrak{o}_0}_{\mathfrak{o}_1/\mathfrak{o}_0}\right), \tag{5.33}$$

$$E_{23}\dot{\bar{\omega}}^{\mathfrak{o}_2}_{\mathfrak{o}_2/\mathcal{I}} = E_{23}R_{\mathfrak{o}_2/\mathfrak{o}_1}\left(\dot{\bar{\omega}}^{\mathfrak{o}_1}_{\mathfrak{o}_1/\mathcal{I}} + \bar{\omega}^{\mathfrak{o}_1}_{\mathfrak{o}_1/\mathcal{I}} \times \bar{\omega}^{\mathfrak{o}_1}_{\mathfrak{o}_2/\mathfrak{o}_1}\right), \tag{5.34}$$

$$E_{23}\dot{\bar{\omega}}^{\mathfrak{o}_3}_{\mathfrak{o}_3/\mathcal{I}} = E_{23}R_{\mathfrak{o}_3/\mathfrak{o}_2}\left(\dot{\bar{\omega}}^{\mathfrak{o}_2}_{\mathfrak{o}_2/\mathcal{I}} + \bar{\omega}^{\mathfrak{o}_2}_{\mathfrak{o}_2/\mathcal{I}} \times \bar{\omega}^{\mathfrak{o}_2}_{\mathfrak{o}_3/\mathfrak{o}_2}\right), \tag{5.35}$$

where

$$E_{23} = \begin{bmatrix} 1 & 0 & 0 \\ 0 & 1 & 0 \end{bmatrix}. \tag{5.36}$$

5.1.3 Attitude Kinematics

The kinematics are given by one of two possible formulations. The first formulation describes the attitude of each of the bodies through propagation of the four different quaternions. That is,

$$\dot{q}_{\mathfrak{o}_i/\mathcal{I}} = \tfrac{1}{2} q_{\mathfrak{o}_i/\mathcal{I}} \omega^{\mathfrak{o}_i}_{\mathfrak{o}_i/\mathcal{I}}, \qquad i \in \{0, \ldots, 3\}. \tag{5.37}$$

The second approach propagates the attitude of the base, but only keeps track of the joint angles for the other bodies. This is done as follows:

$$\dot{q}_{\mathfrak{o}_0/\mathcal{I}} = \tfrac{1}{2} q_{\mathfrak{o}_0/\mathcal{I}} \omega^{\mathfrak{o}_0}_{\mathfrak{o}_0/\mathcal{I}}, \tag{5.38}$$

$$\dot{\theta}_{1/0} = [0,0,1](\bar{\omega}^{\mathfrak{o}_1}_{\mathfrak{o}_1/\mathcal{I}} - \bar{\omega}^{\mathfrak{o}_1}_{\mathfrak{o}_0/\mathcal{I}}), \tag{5.39}$$

$$\dot{\theta}_{2/1} = [0,0,1](\bar{\omega}^{\mathfrak{o}_2}_{\mathfrak{o}_2/\mathcal{I}} - \bar{\omega}^{\mathfrak{o}_2}_{\mathfrak{o}_1/\mathcal{I}}), \tag{5.40}$$

$$\dot{\theta}_{3/2} = [0,0,1](\bar{\omega}^{\mathfrak{o}_3}_{\mathfrak{o}_3/\mathcal{I}} - \bar{\omega}^{\mathfrak{o}_3}_{\mathfrak{o}_2/\mathcal{I}}). \tag{5.41}$$

5.1.4 Position Kinematics

Similar to the development given in Section 5.1.3, there are two approaches to providing position information for each of the bodies. One is integrating the velocity of each body, while the other one is based on the fact that the links will have a set position given the base position, and joint angles. Therefore, we use the following relationship to only find the position of the base

$$\dot{\bar{r}}^{\mathrm{I}}_{\mathfrak{o}_0/\mathcal{I}} = R^{\mathrm{T}}_{\mathfrak{o}_0/\mathrm{I}} \bar{v}^{\mathfrak{o}_0}_{\mathfrak{o}_0/\mathcal{I}} \tag{5.42}$$

5.1.5 State Definition

The overall state of the system $x \in \mathbb{R}^{34}$ to be propagated at every iteration will be defined as

$$\begin{aligned} x \triangleq \big[&(\bar{r}^{\mathrm{I}}_{\mathfrak{o}_0/\mathcal{I}})^{\mathrm{T}}, (q_{\mathfrak{o}_0/\mathcal{I}})^{\mathrm{T}}, \theta_{1/0}, \theta_{2/1}, \theta_{3/2}, (\bar{\omega}^{\mathfrak{o}_0}_{\mathfrak{o}_0/\mathcal{I}})^{\mathrm{T}}, (\bar{v}^{\mathfrak{o}_0}_{\mathfrak{o}_0/\mathcal{I}})^{\mathrm{T}}, \dots \\ &(\bar{\omega}^{\mathfrak{o}_1}_{\mathfrak{o}_1/\mathcal{I}})^{\mathrm{T}}, (\bar{v}^{\mathfrak{o}_1}_{\mathfrak{o}_1/\mathcal{I}})^{\mathrm{T}}, (\bar{\omega}^{\mathfrak{o}_2}_{\mathfrak{o}_2/\mathcal{I}})^{\mathrm{T}}, (\bar{v}^{\mathfrak{o}_2}_{\mathfrak{o}_2/\mathcal{I}})^{\mathrm{T}}, (\bar{\omega}^{\mathfrak{o}_3}_{\mathfrak{o}_3/\mathcal{I}})^{\mathrm{T}}, (\bar{v}^{\mathfrak{o}_3}_{\mathfrak{o}_3/\mathcal{I}})^{\mathrm{T}} \big]^{\mathrm{T}}. \end{aligned} \tag{5.43}$$

For convenience purposes, we will also define the following sub-state $y \in \mathbb{R}^{24}$, which contains only linear and angular velocity quantities:

$$y \triangleq \left[(\bar{v}^{\mathfrak{o}_0}_{\mathfrak{o}_0/\mathcal{I}})^{\mathrm{T}}, (\bar{v}^{\mathfrak{o}_1}_{\mathfrak{o}_1/\mathcal{I}})^{\mathrm{T}}, (\bar{v}^{\mathfrak{o}_2}_{\mathfrak{o}_2/\mathcal{I}})^{\mathrm{T}}, (\bar{v}^{\mathfrak{o}_3}_{\mathfrak{o}_3/\mathcal{I}})^{\mathrm{T}}, (\bar{\omega}^{\mathfrak{o}_0}_{\mathfrak{o}_0/\mathcal{I}})^{\mathrm{T}}, (\bar{\omega}^{\mathfrak{o}_1}_{\mathfrak{o}_1/\mathcal{I}})^{\mathrm{T}}, (\bar{\omega}^{\mathfrak{o}_2}_{\mathfrak{o}_2/\mathcal{I}})^{\mathrm{T}}, (\bar{\omega}^{\mathfrak{o}_3}_{\mathfrak{o}_3/\mathcal{I}})^{\mathrm{T}} \right]^{\mathrm{T}}. \tag{5.44}$$

Now, define a larger vector $\mathcal{Y} \in \mathbb{R}^{39}$, which also includes *internal* forces and torques, as

$$\mathcal{Y} \triangleq \begin{bmatrix} \dot{y} \\ \mathcal{T} \end{bmatrix} = \left[\dot{y}^{\mathrm{T}}, (\bar{f}_{1/0}^{\mathfrak{o}_1})^{\mathrm{T}}, (\bar{f}_{2/1}^{\mathfrak{o}_2})^{\mathrm{T}}, (\bar{f}_{3/2}^{\mathfrak{o}_3})^{\mathrm{T}}, (\bar{\tau}_{1/0})_x, (\bar{\tau}_{1/0})_y, (\bar{\tau}_{2/1})_x, (\bar{\tau}_{2/1})_y, (\bar{\tau}_{3/2})_x, (\bar{\tau}_{3/2})_y \right]^{\mathrm{T}}. \tag{5.45}$$

Finally, we can cast equations (5.1) to (5.8), (5.20) to (5.22) and (5.33) to (5.35) in the form

$$\mathcal{S}\mathcal{Y} = \mathcal{B}, \tag{5.46}$$

$$\begin{bmatrix} \mathcal{S}_{11} & \mathcal{S}_{12} \\ \mathcal{S}_{21} & \mathcal{S}_{22} \end{bmatrix} \begin{bmatrix} \dot{y} \\ \mathcal{T} \end{bmatrix} = \begin{bmatrix} \mathcal{B}_1 \\ \mathcal{B}_2 \end{bmatrix}, \tag{5.47}$$

and solve for $\mathcal{Y}$ at every time-step, yielding the unknown derivatives of vector x from equation (5.43), and internal torques generated at a given state. Notice that only internal reaction forces and torques are contained in $\mathcal{Y}$. All other forces are assumed to be known, and thus, contained in $\mathcal{B}$. After solving for $\dot{y}$ in equation (5.47), we obtain the derivative of the other components of the vector x using equations (5.38) to (5.41) for the attitude kinematics of the base and the joint angles, and equation (5.42) for the translation of the base. This procedure composes a system of ordinary differential equations that describes the time evolution of the state vector x.

5.2 Dual Quaternion Formulation

In this section, the equations of motion for the same robot architecture on a spacecraft base will be derived using the dual quaternion formalism.

5.2.1 Wrenches

The use of wrenches will be pervasive in this implementation due to how naturally these transform using dual quaternions. Next, we introduce all wrenches to avoid confusion. The wrenches arising due to external forces applied to the center of mass of each of the bodies

are given in the body's coordinates. Their source is denoted as $\mathbb{o}_i$, for $i \in \{0, 1, 2, 3\}$:

$$\begin{aligned} \boldsymbol{W}^{\mathbb{o}_0}_{\mathbb{o}_0}(O_{\mathbb{o}_0}) &= f^{\mathbb{o}_0}_{\mathbb{o}_0} + \epsilon\tau^{\mathbb{o}_0}_{\mathbb{o}_0}, \qquad \boldsymbol{W}^{\mathbb{o}_1}_{\mathbb{o}_1}(O_{\mathbb{o}_1}) = f^{\mathbb{o}_1}_{\mathbb{o}_1} + \epsilon\tau^{\mathbb{o}_1}_{\mathbb{o}_1}, \\ \boldsymbol{W}^{\mathbb{o}_2}_{\mathbb{o}_2}(O_{\mathbb{o}_2}) &= f^{\mathbb{o}_2}_{\mathbb{o}_2} + \epsilon\tau^{\mathbb{o}_2}_{\mathbb{o}_2}, \qquad \boldsymbol{W}^{\mathbb{o}_3}_{\mathbb{o}_3}(O_{\mathbb{o}_3}) = f^{\mathbb{o}_3}_{\mathbb{o}_3} + \epsilon\tau^{\mathbb{o}_3}_{\mathbb{o}_3}. \end{aligned} \tag{5.48}$$

Next, the reaction wrenches are given in body coordinates of the distal body, and their point of application is the location of the joint. That is, the possible points of application are the origin of the frames associated to the joints $\{O_0, O_1, O_2\}$. In particular, we have that

$$\boldsymbol{W}^{\mathbb{o}_1}_{1/0}(O_0) = f^{\mathbb{o}_1}_{1/0} + \epsilon\tau^{\mathbb{o}_1}_{1/0}, \qquad \boldsymbol{W}^{\mathbb{o}_2}_{2/1}(O_1) = f^{\mathbb{o}_2}_{2/1} + \epsilon\tau^{\mathbb{o}_2}_{2/1}, \qquad \boldsymbol{W}^{\mathbb{o}_3}_{3/2}(O_2) = f^{\mathbb{o}_3}_{3/2} + \epsilon\tau^{\mathbb{o}_3}_{3/2}. \tag{5.49}$$

Furthermore, the wrench associated to the actuation of the joints is given merely by a pure torque wrench, applied at the joints, in body coordinates of the distal body. These are given by

$$\boldsymbol{W}^{\mathbb{o}_1}_{\text{act},1}(O_0) = 0 + \epsilon\tau^{\mathbb{o}_1}_{\text{act},1}, \qquad \boldsymbol{W}^{\mathbb{o}_2}_{\text{act},2}(O_1) = 0 + \epsilon\tau^{\mathbb{o}_2}_{\text{act},2}, \qquad \boldsymbol{W}^{\mathbb{o}_3}_{\text{act},3}(O_2) = 0 + \epsilon\tau^{\mathbb{o}_3}_{\text{act},3}. \tag{5.50}$$

Finally, we have that the external wrench applied on the end effector will be given by

$$\boldsymbol{W}^{\text{G}}_{\text{ext}}(O_{\text{G}}) = f^{\text{G}}_{\text{ext}} + \epsilon\tau^{\text{G}}_{\text{ext}}. \tag{5.51}$$

5.2.2 Robot Geometry in Dual Quaternions

Several important dual quaternions will be defined in order to facilitate the transformation of wrenches from the joints, or the end effector, onto a point of application which is more conducive to the derivation of the equations of motion. In all cases, this point of interest will be the center of mass of the corresponding body.

Satellite Base

Defining the dual quaternions pertaining to the satellite base, or body 0, we get:

$$\boldsymbol{q}_{0/\mathfrak{o}_0} = (1 + \epsilon\tfrac{1}{2} r^{\mathfrak{o}_0}_{0/\mathfrak{o}_0})(q_{0/\mathfrak{o}_0} + \epsilon 0) = q_{0/\mathfrak{o}_0} + \epsilon\tfrac{1}{2} r^{\mathfrak{o}_0}_{0/\mathfrak{o}_0} q_{0/\mathfrak{o}_0} \tag{5.52}$$

$$= q_{\mathfrak{o}_1/\mathfrak{o}_0} + \epsilon\tfrac{1}{2} r^{\mathfrak{o}_0}_{0/\mathfrak{o}_0} q_{\mathfrak{o}_1/\mathfrak{o}_0}, \tag{5.53}$$

where the last equality holds because the orientation of the frame at joint 0 is the same as the orientation of the frame at $\mathfrak{o}_1$, that is $q_{0/\mathfrak{o}_0} = q_{\mathfrak{o}_1/\mathfrak{o}_0}$. This type of frame relationship will be formalized in a future section.

Link 1

We now define the dual quaternion transformations pertaining to link 1:

$$\boldsymbol{q}_{\mathfrak{o}_1/0} = (1 + \epsilon\tfrac{1}{2} r^{\mathfrak{o}_1}_{\mathfrak{o}_1/0})(1 + \epsilon 0) = 1 + \epsilon\tfrac{1}{2} r^{\mathfrak{o}_1}_{\mathfrak{o}_1/0}, \tag{5.54}$$

and

$$\boldsymbol{q}_{1/\mathfrak{o}_1} = (1 + \epsilon\tfrac{1}{2} r^{\mathfrak{o}_1}_{1/\mathfrak{o}_1})(q_{1/\mathfrak{o}_1} + \epsilon 0) = q_{1/\mathfrak{o}_1} + \epsilon\tfrac{1}{2} r^{\mathfrak{o}_1}_{1/\mathfrak{o}_1} q_{1/\mathfrak{o}_1} \tag{5.55}$$

$$= q_{\mathfrak{o}_2/\mathfrak{o}_1} + \epsilon\tfrac{1}{2} r^{\mathfrak{o}_1}_{1/\mathfrak{o}_1} q_{\mathfrak{o}_2/\mathfrak{o}_1}, \tag{5.56}$$

since the orientation of the frame at joint 1 is the same as the orientation of the frame at $\mathfrak{o}_2$, that is $q_{1/\mathfrak{o}_1} = q_{\mathfrak{o}_2/\mathfrak{o}_1}$.

Link 2

We now define the dual quaternion transformations pertaining to link 2:

$$\boldsymbol{q}_{\mathfrak{o}_2/1} = (1 + \epsilon\tfrac{1}{2} r^{\mathfrak{o}_2}_{\mathfrak{o}_2/1})(1 + \epsilon 0) = 1 + \epsilon\tfrac{1}{2} r^{\mathfrak{o}_2}_{\mathfrak{o}_2/1}, \tag{5.57}$$

and

$$\boldsymbol{q}_{2/\mathbf{o}_2} = (1 + \epsilon\tfrac{1}{2} r^{\mathbf{o}_2}_{2/\mathbf{o}_2})(q_{2/\mathbf{o}_2} + \epsilon 0) = q_{2/\mathbf{o}_2} + \epsilon\tfrac{1}{2} r^{\mathbf{o}_2}_{2/\mathbf{o}_2} q_{2/\mathbf{o}_2} \tag{5.58}$$

$$= q_{\mathbf{o}_3/\mathbf{o}_2} + \epsilon\tfrac{1}{2} r^{\mathbf{o}_2}_{1/\mathbf{o}_2} q_{\mathbf{o}_3/\mathbf{o}_2}, \tag{5.59}$$

since the orientation of the frame at joint 2 is the same as the orientation of the frame at $\mathbf{o}_3$, that is $q_{2/\mathbf{o}_1} = q_{\mathbf{o}_3/\mathbf{o}_2}$.

Link 3

We now define the dual quaternion transformations pertaining to link 3. From the frame at joint 2 to the center of mass of body three, identified by $\mathbf{o}_3$

$$\boldsymbol{q}_{\mathbf{o}_3/2} = (1 + \epsilon\tfrac{1}{2} r^{\mathbf{o}_3}_{\mathbf{o}_3/2})(1 + \epsilon 0) = 1 + \epsilon\tfrac{1}{2} r^{\mathbf{o}_3}_{\mathbf{o}_3/2}. \tag{5.60}$$

To determine the relative pose between frame $\mathbf{o}_3$ and e, which is attached to end effector with its origin at the joint, the rotation of the spherical joint must be parametrized accordingly. As shown in Figure 5.1, we have parametrized the motion of the end-effector using three Euler angles. In particular, we use a 3-2-1 rotation[1], where yaw is denoted by $\psi_{e/\mathbf{o}_3}$, pitch by $\theta_{e/\mathbf{o}_3}$, and roll by $\phi_{e/\mathbf{o}_3}$. In particular, we have that the frame transformation from $\mathbf{o}_3$ to the frame e is given by

$$\boldsymbol{q}_{e/\mathbf{o}_3} = (1 + \epsilon\tfrac{1}{2} r^{\mathbf{o}_3}_{e/\mathbf{o}_3})(q_{e/\mathbf{o}_3} + \epsilon 0) = q_{e/\mathbf{o}_3} + \epsilon\tfrac{1}{2} r^{\mathbf{o}_3}_{e/\mathbf{o}_3} q_{e/\mathbf{o}_3}, \tag{5.61}$$

[1] Yaw is applied first about the 3-axis, followed by pitch about the 1-axis, followed by roll about the 1-axis.

where

$$q_{e/\mathfrak{o}_3} = \begin{bmatrix} \cos(\phi_{e/\mathfrak{o}_3}/2)\cos(\theta_{e/\mathfrak{o}_3}/2)\cos(\psi_{e/\mathfrak{o}_3}/2) + \sin(\phi_{e/\mathfrak{o}_3}/2)\sin(\theta_{e/\mathfrak{o}_3}/2)\sin(\psi_{e/\mathfrak{o}_3}/2) \\ \sin(\phi_{e/\mathfrak{o}_3}/2)\cos(\theta_{e/\mathfrak{o}_3}/2)\cos(\psi_{e/\mathfrak{o}_3}/2) - \cos(\phi_{e/\mathfrak{o}_3}/2)\sin(\theta_{e/\mathfrak{o}_3}/2)\sin(\psi_{e/\mathfrak{o}_3}/2) \\ \cos(\phi_{e/\mathfrak{o}_3}/2)\sin(\theta_{e/\mathfrak{o}_3}/2)\cos(\psi_{e/\mathfrak{o}_3}/2) + \sin(\phi_{e/\mathfrak{o}_3}/2)\cos(\theta_{e/\mathfrak{o}_3}/2)\sin(\psi_{e/\mathfrak{o}_3}/2) \\ \cos(\phi_{e/\mathfrak{o}_3}/2)\cos(\theta_{e/\mathfrak{o}_3}/2)\sin(\psi_{e/\mathfrak{o}_3}/2) - \sin(\phi_{e/\mathfrak{o}_3}/2)\sin(\theta_{e/\mathfrak{o}_3}/2)\cos(\psi_{e/\mathfrak{o}_3}/2) \end{bmatrix}. \tag{5.62}$$

5.2.3 Robot Dynamic Equations in Dual Quaternion Form

Applying equation (2.56) to each of our four bodies shown in Figure 5.2 we get the following set of expressions.

$$\begin{aligned} M_{\mathfrak{o}_0} \star (\dot{\boldsymbol{\omega}}^{\mathfrak{o}_0}_{\mathfrak{o}_0/I})^{\mathsf{s}} + \boldsymbol{\omega}^{\mathfrak{o}_0}_{\mathfrak{o}_0/I} \times \left(M_{\mathfrak{o}_0} \star (\boldsymbol{\omega}^{\mathfrak{o}_0}_{\mathfrak{o}_0/I})^{\mathsf{s}}\right) &= \boldsymbol{W}^{\mathfrak{o}_0}_{0}(O_{\mathfrak{o}_0}) \\ &= \boldsymbol{W}^{\mathfrak{o}_0}_{\mathfrak{o}_0}(O_{\mathfrak{o}_0}) - \boldsymbol{W}^{\mathfrak{o}_0}_{1/0}(O_{\mathfrak{o}_0}) - \boldsymbol{W}^{\mathfrak{o}_0}_{\text{act},1}(O_{\mathfrak{o}_0}), \end{aligned} \tag{5.63}$$

$$\begin{aligned} M_{\mathfrak{o}_1} \star (\dot{\boldsymbol{\omega}}^{\mathfrak{o}_1}_{\mathfrak{o}_1/I})^{\mathsf{s}} + \boldsymbol{\omega}^{\mathfrak{o}_1}_{\mathfrak{o}_1/I} \times \left(M_{\mathfrak{o}_1} \star (\boldsymbol{\omega}^{\mathfrak{o}_1}_{\mathfrak{o}_1/I})^{\mathsf{s}}\right) &= \boldsymbol{W}^{\mathfrak{o}_1}_{1}(O_{\mathfrak{o}_1}) \\ &= \boldsymbol{W}^{\mathfrak{o}_1}_{\mathfrak{o}_1}(O_{\mathfrak{o}_1}) + \boldsymbol{W}^{\mathfrak{o}_1}_{1/0}(O_{\mathfrak{o}_1}) + \boldsymbol{W}^{\mathfrak{o}_1}_{\text{act},1}(O_{\mathfrak{o}_1}) \\ &\quad - \boldsymbol{W}^{\mathfrak{o}_1}_{2/1}(O_{\mathfrak{o}_1}) - \boldsymbol{W}^{\mathfrak{o}_1}_{\text{act},2}(O_{\mathfrak{o}_1}), \end{aligned} \tag{5.64}$$

$$\begin{aligned} M_{\mathfrak{o}_2} \star (\dot{\boldsymbol{\omega}}^{\mathfrak{o}_2}_{\mathfrak{o}_2/I})^{\mathsf{s}} + \boldsymbol{\omega}^{\mathfrak{o}_2}_{\mathfrak{o}_2/I} \times \left(M_{\mathfrak{o}_2} \star (\boldsymbol{\omega}^{\mathfrak{o}_2}_{\mathfrak{o}_2/I})^{\mathsf{s}}\right) &= \boldsymbol{W}^{\mathfrak{o}_2}_{2}(O_{\mathfrak{o}_2}) \\ &= \boldsymbol{W}^{\mathfrak{o}_2}_{\mathfrak{o}_2}(O_{\mathfrak{o}_2}) + \boldsymbol{W}^{\mathfrak{o}_2}_{2/1}(O_{\mathfrak{o}_2}) + \boldsymbol{W}^{\mathfrak{o}_2}_{\text{act},2}(O_{\mathfrak{o}_2}) \\ &\quad - \boldsymbol{W}^{\mathfrak{o}_2}_{3/2}(O_{\mathfrak{o}_2}) - \boldsymbol{W}^{\mathfrak{o}_2}_{\text{act},3}(O_{\mathfrak{o}_2}), \end{aligned} \tag{5.65}$$

$$M_{\mathfrak{s}_3} \star (\dot{\boldsymbol{\omega}}^{\mathfrak{s}_3}_{\mathfrak{s}_3/\mathrm{I}})^{\mathsf{S}} + \boldsymbol{\omega}^{\mathfrak{s}_3}_{\mathfrak{s}_3/\mathrm{I}} \times \left(M_{\mathfrak{s}_3} \star (\boldsymbol{\omega}^{\mathfrak{s}_3}_{\mathfrak{s}_3/\mathrm{I}})^{\mathsf{S}}\right) = \boldsymbol{W}^{\mathfrak{s}_3}_{3}(O_{\mathfrak{s}_3})$$
$$= \boldsymbol{W}^{\mathfrak{s}_3}_{\mathfrak{s}_3}(O_{\mathfrak{s}_3}) + \boldsymbol{W}^{\mathfrak{s}_3}_{3/2}(O_{\mathfrak{s}_3}) + \boldsymbol{W}^{\mathfrak{s}_3}_{\mathrm{ext}}(O_{\mathfrak{s}_3}) + \boldsymbol{W}^{\mathfrak{s}_3}_{\mathrm{act},3}(O_{\mathfrak{s}_3}). \tag{5.66}$$

We now use the shifting law introduced in Section 2.3.1 to transform the canonical wrenches defined in Section 5.2.1. For each body we obtain the following expressions

$$M_{\mathfrak{s}_0} \star (\dot{\boldsymbol{\omega}}^{\mathfrak{s}_0}_{\mathfrak{s}_0/\mathrm{I}})^{\mathsf{S}} + \boldsymbol{\omega}^{\mathfrak{s}_0}_{\mathfrak{s}_0/\mathrm{I}} \times \left(M_{\mathfrak{s}_0} \star (\boldsymbol{\omega}^{\mathfrak{s}_0}_{\mathfrak{s}_0/\mathrm{I}})^{\mathsf{S}}\right) = \boldsymbol{W}^{\mathfrak{s}_0}_{\mathfrak{s}_0}(O_{\mathfrak{s}_0}) - \boldsymbol{q}_{0/\mathfrak{s}_0} \boldsymbol{W}^{\mathfrak{s}_1}_{1/0}(O_0) \boldsymbol{q}^*_{0/\mathfrak{s}_0} - \boldsymbol{q}_{0/\mathfrak{s}_0} \boldsymbol{W}^{\mathfrak{s}_1}_{\mathrm{act},1}(O_0) \boldsymbol{q}^*_{0/\mathfrak{s}_0}, \tag{5.67}$$

$$\begin{aligned} M_{\mathfrak{s}_1} \star (\dot{\boldsymbol{\omega}}^{\mathfrak{s}_1}_{\mathfrak{s}_1/\mathrm{I}})^{\mathsf{S}} + \boldsymbol{\omega}^{\mathfrak{s}_1}_{\mathfrak{s}_1/\mathrm{I}} \times \left(M_{\mathfrak{s}_1} \star (\boldsymbol{\omega}^{\mathfrak{s}_1}_{\mathfrak{s}_1/\mathrm{I}})^{\mathsf{S}}\right) &= \boldsymbol{W}^{\mathfrak{s}_1}_{\mathfrak{s}_1}(O_{\mathfrak{s}_1}) \\ &+ \boldsymbol{q}^*_{\mathfrak{s}_1/0} \boldsymbol{W}^{\mathfrak{s}_1}_{1/0}(O_0) \boldsymbol{q}_{\mathfrak{s}_1/0} + \boldsymbol{q}^*_{\mathfrak{s}_1/0} \boldsymbol{W}^{\mathfrak{s}_1}_{\mathrm{act},1}(O_0) \boldsymbol{q}_{\mathfrak{s}_1/0} \\ &- \boldsymbol{q}_{1/\mathfrak{s}_1} \boldsymbol{W}^{\mathfrak{s}_2}_{2/1}(O_1) \boldsymbol{q}^*_{1/\mathfrak{s}_1} - \boldsymbol{q}_{1/\mathfrak{s}_1} \boldsymbol{W}^{\mathfrak{s}_2}_{\mathrm{act},2}(O_1) \boldsymbol{q}^*_{1/\mathfrak{s}_1}, \end{aligned} \tag{5.68}$$

$$\begin{aligned} M_{\mathfrak{s}_2} \star (\dot{\boldsymbol{\omega}}^{\mathfrak{s}_2}_{\mathfrak{s}_2/\mathrm{I}})^{\mathsf{S}} + \boldsymbol{\omega}^{\mathfrak{s}_2}_{\mathfrak{s}_2/\mathrm{I}} \times \left(M_{\mathfrak{s}_2} \star (\boldsymbol{\omega}^{\mathfrak{s}_2}_{\mathfrak{s}_2/\mathrm{I}})^{\mathsf{S}}\right) &= \boldsymbol{W}^{\mathfrak{s}_2}_{\mathfrak{s}_2}(O_{\mathfrak{s}_2}) \\ &+ \boldsymbol{q}^*_{\mathfrak{s}_2/1} \boldsymbol{W}^{\mathfrak{s}_2}_{2/1}(O_1) \boldsymbol{q}_{\mathfrak{s}_2/1} + \boldsymbol{q}^*_{\mathfrak{s}_2/1} \boldsymbol{W}^{\mathfrak{s}_2}_{\mathrm{act},2}(O_1) \boldsymbol{q}_{\mathfrak{s}_2/1} \\ &- \boldsymbol{q}_{2/\mathfrak{s}_2} \boldsymbol{W}^{\mathfrak{s}_3}_{3/2}(O_2) \boldsymbol{q}^*_{2/\mathfrak{s}_2} - \boldsymbol{q}_{2/\mathfrak{s}_2} \boldsymbol{W}^{\mathfrak{s}_3}_{\mathrm{act},3}(O_2) \boldsymbol{q}^*_{2/\mathfrak{s}_2}, \end{aligned} \tag{5.69}$$

$$\begin{aligned} M_{\mathfrak{s}_3} \star (\dot{\boldsymbol{\omega}}^{\mathfrak{s}_3}_{\mathfrak{s}_3/\mathrm{I}})^{\mathsf{S}} + \boldsymbol{\omega}^{\mathfrak{s}_3}_{\mathfrak{s}_3/\mathrm{I}} \times \left(M_{\mathfrak{s}_3} \star (\boldsymbol{\omega}^{\mathfrak{s}_3}_{\mathfrak{s}_3/\mathrm{I}})^{\mathsf{S}}\right) &= \boldsymbol{W}^{\mathfrak{s}_3}_{\mathfrak{s}_3}(O_{\mathfrak{s}_3}) \\ &+ \boldsymbol{q}^*_{\mathfrak{s}_3/2} \boldsymbol{W}^{\mathfrak{s}_3}_{3/2}(O_2) \boldsymbol{q}_{\mathfrak{s}_3/2} + \boldsymbol{q}^*_{\mathfrak{s}_3/2} \boldsymbol{W}^{\mathfrak{s}_3}_{\mathrm{act},3}(O_2) \boldsymbol{q}_{\mathfrak{s}_3/2} \\ &+ \boldsymbol{q}_{\mathrm{G}/\mathfrak{s}_3} \boldsymbol{W}^{\mathrm{G}}_{\mathrm{ext}}(O_{\mathrm{G}}) \boldsymbol{q}^*_{\mathrm{G}/\mathfrak{s}_3}. \end{aligned} \tag{5.70}$$

5.2.4 Relative Kinematics and Joint Motion

This section will display the dual velocities that appear in the development of the equations of motion. Additionally, it provides expressions for the dual velocity and acceleration for

each of the joints in the system.

Kinematics at Link 1 and Joint 0

Since the frame at joint 0 and the frame at $\mathfrak{o}_1$ are attached to the same rigid body, the following expressions hold:

$$\boldsymbol{\omega}^{\mathfrak{o}_1}_{\mathfrak{o}_1/0} = \omega^{\mathfrak{o}_1}_{\mathfrak{o}_1/0} + \epsilon(v^{\mathfrak{o}_1}_{\mathfrak{o}_1/0} + \omega^{\mathfrak{o}_1}_{\mathfrak{o}_1/0} \times r^{\mathfrak{o}_1}_{\mathfrak{o}_1/\mathfrak{o}_1}) = \mathbf{0}, \tag{5.71}$$

$$\boldsymbol{\omega}^{\mathfrak{o}_0}_{\mathfrak{o}_1/0} = \omega^{\mathfrak{o}_0}_{\mathfrak{o}_1/0} + \epsilon(v^{\mathfrak{o}_0}_{\mathfrak{o}_1/0} + \omega^{\mathfrak{o}_0}_{\mathfrak{o}_1/0} \times r^{\mathfrak{o}_0}_{\mathfrak{o}_0/\mathfrak{o}_1}) = \mathbf{0}, \tag{5.72}$$

$$\dot{\boldsymbol{q}}_{\mathfrak{o}_1/0} = \tfrac{1}{2}\boldsymbol{q}_{\mathfrak{o}_1/0}\boldsymbol{\omega}^{\mathfrak{o}_1}_{\mathfrak{o}_1/0} = \mathbf{0}. \tag{5.73}$$

Additionally, expressing the joint dual velocity and acceleration as dual quaternions we get

$$\boldsymbol{\omega}^{0}_{0/\mathfrak{o}_0} = \left(0, \left[0,\ 0,\ \dot{\theta}_{1/0}\right]^{\mathrm{T}}\right) + \epsilon 0, \tag{5.74}$$

$$\dot{\boldsymbol{\omega}}^{0}_{0/\mathfrak{o}_0} = \left(0, \left[0,\ 0,\ \ddot{\theta}_{1/0}\right]^{\mathrm{T}}\right) + \epsilon 0. \tag{5.75}$$

At joint 0, we also have that

$$\boldsymbol{\omega}^{\mathfrak{o}_0}_{0/\mathfrak{o}_0} = \omega^{\mathfrak{o}_0}_{0/\mathfrak{o}_0} + \epsilon(v^{\mathfrak{o}_0}_{0/\mathfrak{o}_0} + \omega^{\mathfrak{o}_0}_{0/\mathfrak{o}_0} \times r^{\mathfrak{o}_0}_{\mathfrak{o}_0/0}) = \omega^{\mathfrak{o}_0}_{0/\mathfrak{o}_0} + \epsilon 0, \tag{5.76}$$

where $\omega^{\mathfrak{o}_0}_{0/\mathfrak{o}_0} = \left(0, [0, 0, \dot{\theta}_{1/0}]^{\mathrm{T}}\right)$ and $v^{\mathfrak{o}_0}_{0/\mathfrak{o}_0} = 0$.

Kinematics at Link 2 and Joint 1

Since the frame at joint 1 and the frame at $\mathfrak{o}_2$ are attached to the same rigid body, the following expressions hold:

$$\boldsymbol{\omega}^{\mathfrak{o}_2}_{\mathfrak{o}_2/1} = \omega^{\mathfrak{o}_2}_{\mathfrak{o}_2/1} + \epsilon(v^{\mathfrak{o}_2}_{\mathfrak{o}_2/1} + \omega^{\mathfrak{o}_2}_{\mathfrak{o}_2/1} \times r^{\mathfrak{o}_2}_{\mathfrak{o}_2/\mathfrak{o}_2}) = \mathbf{0}, \tag{5.77}$$

$$\boldsymbol{\omega}^{\mathfrak{o}_1}_{\mathfrak{o}_2/1} = \omega^{\mathfrak{o}_1}_{\mathfrak{o}_2/1} + \epsilon(v^{\mathfrak{o}_1}_{\mathfrak{o}_2/1} + \omega^{\mathfrak{o}_1}_{\mathfrak{o}_2/1} \times r^{\mathfrak{o}_1}_{\mathfrak{o}_1/\mathfrak{o}_2}) = \mathbf{0}, \tag{5.78}$$

$$\dot{\boldsymbol{q}}_{\mathfrak{o}_2/1} = \tfrac{1}{2}\boldsymbol{q}_{\mathfrak{o}_2/1}\boldsymbol{\omega}^{\mathfrak{o}_2}_{\mathfrak{o}_2/1} = \mathbf{0}. \tag{5.79}$$

Additionally, expressing the joint dual velocity and acceleration as dual quaternions we get

$$\boldsymbol{\omega}^{1}_{1/\mathfrak{o}_1} = \left(0, \left[0,\ 0,\ \dot{\theta}_{2/1}\right]^{\mathrm{T}}\right) + \epsilon 0, \tag{5.80}$$

$$\dot{\boldsymbol{\omega}}^{1}_{1/\mathfrak{o}_1} = \left(0, \left[0,\ 0,\ \ddot{\theta}_{2/1}\right]^{\mathrm{T}}\right) + \epsilon 0. \tag{5.81}$$

At joint 1, we also have that

$$\boldsymbol{\omega}^{\mathfrak{o}_1}_{1/\mathfrak{o}_1} = \omega^{\mathfrak{o}_1}_{1/\mathfrak{o}_1} + \epsilon(v^{\mathfrak{o}_1}_{1/\mathfrak{o}_1} + \omega^{\mathfrak{o}_1}_{1/\mathfrak{o}_1} \times r^{\mathfrak{o}_1}_{\mathfrak{o}_1/1}) = \omega^{\mathfrak{o}_1}_{1/\mathfrak{o}_1} + \epsilon\omega^{\mathfrak{o}_1}_{1/\mathfrak{o}_1} \times r^{\mathfrak{o}_1}_{\mathfrak{o}_1/1}, \tag{5.82}$$

where $\omega^{\mathfrak{o}_1}_{1/\mathfrak{o}_1} = \left(0, [0, -\dot{\theta}_{2/1}, 0]^{\mathrm{T}}\right)$ and $v^{\mathfrak{o}_1}_{1/\mathfrak{o}_1} = 0$.

Kinematics at Link 3 and Joint 2

Since the frame at joint 2 and the frame at $\mathfrak{o}_3$ are attached to the same rigid body, the following expressions hold:

$$\boldsymbol{\omega}^{\mathfrak{o}_3}_{\mathfrak{o}_3/2} = \omega^{\mathfrak{o}_3}_{\mathfrak{o}_3/2} + \epsilon(v^{\mathfrak{o}_3}_{\mathfrak{o}_3/2} + \omega^{\mathfrak{o}_3}_{\mathfrak{o}_3/2} \times r^{\mathfrak{o}_3}_{\mathfrak{o}_3/\mathfrak{o}_3}) = \mathbf{0} \tag{5.83}$$

$$\boldsymbol{\omega}^{\mathfrak{o}_2}_{\mathfrak{o}_3/2} = \omega^{\mathfrak{o}_2}_{\mathfrak{o}_3/2} + \epsilon(v^{\mathfrak{o}_2}_{\mathfrak{o}_3/2} + \omega^{\mathfrak{o}_2}_{\mathfrak{o}_3/2} \times r^{\mathfrak{o}_2}_{\mathfrak{o}_2/\mathfrak{o}_3}) = \mathbf{0} \tag{5.84}$$

$$\dot{\boldsymbol{q}}_{\mathfrak{o}_3/2} = \tfrac{1}{2}\boldsymbol{q}_{\mathfrak{o}_3/2}\boldsymbol{\omega}^{\mathfrak{o}_3}_{\mathfrak{o}_3/2} = \mathbf{0} \tag{5.85}$$

Additionally, expressing the joint dual velocity and acceleration as dual quaternions we get

$$\boldsymbol{\omega}^{2}_{2/\mathfrak{o}_2} = \left(0, \left[0,\ 0,\ \dot{\theta}_{3/2}\right]^{\mathrm{T}}\right) + \epsilon 0, \tag{5.86}$$

$$\dot{\boldsymbol{\omega}}^{2}_{2/\mathfrak{o}_2} = \left(0, \left[0,\ 0,\ \ddot{\theta}_{3/2}\right]^{\mathrm{T}}\right) + \epsilon 0. \tag{5.87}$$

At joint 2, we also have that

$$\boldsymbol{\omega}^{\mathfrak{o}_2}_{2/\mathfrak{o}_2}=\omega^{\mathfrak{o}_2}_{2/\mathfrak{o}_2}+\epsilon(v^{\mathfrak{o}_2}_{2/\mathfrak{o}_2}+\omega^{\mathfrak{o}_2}_{2/\mathfrak{o}_2}\times r^{\mathfrak{o}_2}_{\mathfrak{o}_2/2})=\omega^{\mathfrak{o}_2}_{2/\mathfrak{o}_2}+\epsilon\omega^{\mathfrak{o}_2}_{2/\mathfrak{o}_2}\times r^{\mathfrak{o}_2}_{\mathfrak{o}_2/2}, \tag{5.88}$$

where $\omega^{\mathfrak{o}_2}_{2/\mathfrak{o}_2}=\left(0,[0,0,\dot{\theta}_{3/2}]^{\mathrm{T}}\right)$ and $v^{\mathfrak{o}_2}_{2/\mathfrak{o}_2}=0$.

Kinematics at Joint e

The end-effector motion is due to a spherical joint. We select to parametrize the motion as a 3-2-1 Euler angle sequence. The dual velocity is computed in terms of the angular rates $\dot{\psi}_{\mathrm{e}/\mathfrak{o}_3}$, $\dot{\theta}_{\mathrm{e}/\mathfrak{o}_3}$ and $\dot{\phi}_{\mathrm{e}/\mathfrak{o}_3}$. From our dual velocity relationship given in equation (2.36), we know that

$$\boldsymbol{\omega}^{\mathrm{e}}_{\mathrm{e}/\mathfrak{o}_3}=\omega^{\mathrm{e}}_{\mathrm{e}/\mathfrak{o}_3}+\epsilon(v^{\mathrm{e}}_{\mathrm{e}/\mathfrak{o}_3}+\omega^{\mathrm{e}}_{\mathrm{e}/\mathfrak{o}_3}\times r^{\mathrm{e}}_{\mathrm{e}/\mathrm{e}}) \tag{5.89}$$

$$=\omega^{\mathrm{e}}_{\mathrm{e}/\mathfrak{o}_3}+\epsilon 0, \tag{5.90}$$

where we used that $r^{\mathrm{e}}_{\mathrm{e}/\mathrm{e}}=0$ and $v^{\mathrm{e}}_{\mathrm{e}/\mathfrak{o}_3}=0$. Finally, we know that $\omega^{\mathrm{e}}_{\mathrm{e}/\mathfrak{o}_3}=(0,\bar{\omega}^{\mathrm{e}}_{\mathrm{e}/\mathfrak{o}_3})$ where from basic kinematics we have

$$\bar{\omega}^{\mathrm{e}}_{\mathrm{e}/\mathfrak{o}_3}=\begin{bmatrix}1 & 0 & -\sin(\theta_{\mathrm{e}/\mathfrak{o}_3})\\ 0 & \cos(\phi_{\mathrm{e}/\mathfrak{o}_3}) & \cos(\theta_{\mathrm{e}/\mathfrak{o}_3})\sin(\phi_{\mathrm{e}/\mathfrak{o}_3})\\ 0 & -\sin(\phi_{\mathrm{e}/\mathfrak{o}_3}) & \cos(\theta_{\mathrm{e}/\mathfrak{o}_3})\cos(\phi_{\mathrm{e}/\mathfrak{o}_3})\end{bmatrix}\begin{bmatrix}\dot{\phi}_{\mathrm{e}/\mathfrak{o}_3}\\ \dot{\theta}_{\mathrm{e}/\mathfrak{o}_3}\\ \dot{\psi}_{\mathrm{e}/\mathfrak{o}_3}\end{bmatrix}. \tag{5.91}$$

At this point it is worth emphasizing that Euler angles and their associated singularities can be avoided by use of quaternions. For this work, we choose to use Euler angles to maintain uniformity with the methodology developed for the other types of joints.

5.2.5 Derivation of Kinematic Constraints Using Dual Quaternions

This section aims to develop the kinematic constraint equations obtained through the use of dual quaternions. For this, we relate the dual velocity of bodies 0 (the satellite base) and

1 (link 1) as follows:

$$\begin{aligned}\boldsymbol{\omega}_{\mathfrak{e}_1/\mathrm{I}}^{\mathfrak{e}_1} &= \boldsymbol{\omega}_{\mathfrak{e}_1/0}^{\mathfrak{e}_1} + \boldsymbol{\omega}_{0/\mathfrak{e}_0}^{\mathfrak{e}_1} + \boldsymbol{\omega}_{\mathfrak{e}_0/\mathrm{I}}^{\mathfrak{e}_1} \\ &= \boldsymbol{\omega}_{\mathfrak{e}_1/0}^{\mathfrak{e}_1} + \boldsymbol{q}_{\mathfrak{e}_1/0}^{*}\boldsymbol{\omega}_{0/\mathfrak{e}_0}^{0}\boldsymbol{q}_{\mathfrak{e}_1/0} + \boldsymbol{q}_{\mathfrak{e}_1/\mathfrak{e}_0}^{*}\boldsymbol{\omega}_{\mathfrak{e}_0/\mathrm{I}}^{\mathfrak{e}_0}\boldsymbol{q}_{\mathfrak{e}_1/\mathfrak{e}_0} \\ &= \boldsymbol{q}_{\mathfrak{e}_1/0}^{*}\boldsymbol{\omega}_{0/\mathfrak{e}_0}^{0}\boldsymbol{q}_{\mathfrak{e}_1/0} + \boldsymbol{q}_{\mathfrak{e}_1/\mathfrak{e}_0}^{*}\boldsymbol{\omega}_{\mathfrak{e}_0/\mathrm{I}}^{\mathfrak{e}_0}\boldsymbol{q}_{\mathfrak{e}_1/\mathfrak{e}_0}, \end{aligned} \tag{5.92}$$

where the last equality uses equation (5.71). Taking time derivatives on both sides, and using equation (5.73)

$$\begin{aligned}\dot{\boldsymbol{\omega}}_{\mathfrak{e}_1/\mathrm{I}}^{\mathfrak{e}_1} &= \boldsymbol{q}_{\mathfrak{e}_1/0}^{*}\dot{\boldsymbol{\omega}}_{0/\mathfrak{e}_0}^{0}\boldsymbol{q}_{\mathfrak{e}_1/0} + \frac{\mathrm{d}}{\mathrm{d}t}\left(\boldsymbol{q}_{\mathfrak{e}_1/\mathfrak{e}_0}^{*}\boldsymbol{\omega}_{\mathfrak{e}_0/\mathrm{I}}^{\mathfrak{e}_0}\boldsymbol{q}_{\mathfrak{e}_1/\mathfrak{e}_0}\right) \\ &= \boldsymbol{q}_{\mathfrak{e}_1/0}^{*}\dot{\boldsymbol{\omega}}_{0/\mathfrak{e}_0}^{0}\boldsymbol{q}_{\mathfrak{e}_1/0} + \boldsymbol{q}_{\mathfrak{e}_1/\mathfrak{e}_0}^{*}\left(\dot{\boldsymbol{\omega}}_{\mathfrak{e}_0/\mathrm{I}}^{\mathfrak{e}_0} + \boldsymbol{\omega}_{\mathfrak{e}_0/\mathrm{I}}^{\mathfrak{e}_0} \times \boldsymbol{\omega}_{\mathfrak{e}_1/\mathfrak{e}_0}^{\mathfrak{e}_0}\right)\boldsymbol{q}_{\mathfrak{e}_1/\mathfrak{e}_0}, \end{aligned}$$

and since $\boldsymbol{\omega}_{\mathfrak{e}_1/\mathfrak{e}_0}^{\mathfrak{e}_0} = \boldsymbol{\omega}_{\mathfrak{e}_1/0}^{\mathfrak{e}_0} + \boldsymbol{\omega}_{0/\mathfrak{e}_0}^{\mathfrak{e}_0} = \mathbf{0} + \boldsymbol{\omega}_{0/\mathfrak{e}_0}^{\mathfrak{e}_0} = \boldsymbol{\omega}_{0/\mathfrak{e}_0}^{\mathfrak{e}_0}$, we get as our acceleration relationship

$$\dot{\boldsymbol{\omega}}_{\mathfrak{e}_1/\mathrm{I}}^{\mathfrak{e}_1} = \boldsymbol{q}_{\mathfrak{e}_1/0}^{*}\dot{\boldsymbol{\omega}}_{0/\mathfrak{e}_0}^{0}\boldsymbol{q}_{\mathfrak{e}_1/0} + \boldsymbol{q}_{\mathfrak{e}_1/\mathfrak{e}_0}^{*}\left(\dot{\boldsymbol{\omega}}_{\mathfrak{e}_0/\mathrm{I}}^{\mathfrak{e}_0} + \boldsymbol{\omega}_{\mathfrak{e}_0/\mathrm{I}}^{\mathfrak{e}_0} \times \boldsymbol{\omega}_{0/\mathfrak{e}_0}^{\mathfrak{e}_0}\right)\boldsymbol{q}_{\mathfrak{e}_1/\mathfrak{e}_0}.$$

Finally, in order to expose the joint acceleration $\ddot{\theta}_{1/0}$ shown in equation (5.75), we clear $\dot{\boldsymbol{\omega}}_{0/\mathfrak{e}_0}^{0}$ of any transformations as follows

$$\boldsymbol{q}_{\mathfrak{e}_1/0}\dot{\boldsymbol{\omega}}_{\mathfrak{e}_1/\mathrm{I}}^{\mathfrak{e}_1}\boldsymbol{q}_{\mathfrak{e}_1/0}^{*} = \dot{\boldsymbol{\omega}}_{0/\mathfrak{e}_0}^{0} + \boldsymbol{q}_{\mathfrak{e}_1/0}\boldsymbol{q}_{\mathfrak{e}_1/\mathfrak{e}_0}^{*}\left(\dot{\boldsymbol{\omega}}_{\mathfrak{e}_0/\mathrm{I}}^{\mathfrak{e}_0} + \boldsymbol{\omega}_{\mathfrak{e}_0/\mathrm{I}}^{\mathfrak{e}_0} \times \boldsymbol{\omega}_{0/\mathfrak{e}_0}^{\mathfrak{e}_0}\right)\boldsymbol{q}_{\mathfrak{e}_1/\mathfrak{e}_0}\boldsymbol{q}_{\mathfrak{e}_1/0}^{*}, \tag{5.93}$$

which yields both linear and rotational constraint equations in a compact manner:

$$\boldsymbol{q}_{\mathfrak{e}_1/0}\dot{\boldsymbol{\omega}}_{\mathfrak{e}_1/\mathrm{I}}^{\mathfrak{e}_1}\boldsymbol{q}_{\mathfrak{e}_1/0}^{*} = \dot{\boldsymbol{\omega}}_{0/\mathfrak{e}_0}^{0} + \boldsymbol{q}_{0/\mathfrak{e}_0}^{*}\left(\dot{\boldsymbol{\omega}}_{\mathfrak{e}_0/\mathrm{I}}^{\mathfrak{e}_0} + \boldsymbol{\omega}_{\mathfrak{e}_0/\mathrm{I}}^{\mathfrak{e}_0} \times \boldsymbol{\omega}_{0/\mathfrak{e}_0}^{\mathfrak{e}_0}\right)\boldsymbol{q}_{0/\mathfrak{e}_0}. \tag{5.94}$$

Following an analogous process, we can use the dual velocity relationships that arise at

joints 1 and 2 given by

$$\boldsymbol{\omega}^{\mathfrak{o}_2}_{\mathfrak{o}_2/\mathrm{I}} = \boldsymbol{q}^*_{\mathfrak{o}_2/1}\boldsymbol{\omega}^1_{1/\mathfrak{o}_1}\boldsymbol{q}_{\mathfrak{o}_2/1} + \boldsymbol{q}^*_{\mathfrak{o}_2/\mathfrak{o}_1}\boldsymbol{\omega}^{\mathfrak{o}_1}_{\mathfrak{o}_1/\mathrm{I}}\boldsymbol{q}_{\mathfrak{o}_2/\mathfrak{o}_1}, \tag{5.95}$$

$$\boldsymbol{\omega}^{\mathfrak{o}_3}_{\mathfrak{o}_3/\mathrm{I}} = \boldsymbol{q}^*_{\mathfrak{o}_3/2}\boldsymbol{\omega}^2_{2/\mathfrak{o}_2}\boldsymbol{q}_{\mathfrak{o}_3/2} + \boldsymbol{q}^*_{\mathfrak{o}_3/\mathfrak{o}_2}\boldsymbol{\omega}^{\mathfrak{o}_2}_{\mathfrak{o}_2/\mathrm{I}}\boldsymbol{q}_{\mathfrak{o}_3/\mathfrak{o}_2}, \tag{5.96}$$

to derive the dual acceleration relationships that we need. These are given by

$$\boldsymbol{q}_{\mathfrak{o}_2/1}\dot{\boldsymbol{\omega}}^{\mathfrak{o}_2}_{\mathfrak{o}_2/\mathrm{I}}\boldsymbol{q}^*_{\mathfrak{o}_2/1} = \dot{\boldsymbol{\omega}}^1_{1/\mathfrak{o}_1} + \boldsymbol{q}^*_{1/\mathfrak{o}_1}\left(\dot{\boldsymbol{\omega}}^{\mathfrak{o}_1}_{\mathfrak{o}_1/\mathrm{I}} + \boldsymbol{\omega}^{\mathfrak{o}_1}_{\mathfrak{o}_1/\mathrm{I}} \times \boldsymbol{\omega}^{\mathfrak{o}_1}_{1/\mathfrak{o}_1}\right)\boldsymbol{q}_{1/\mathfrak{o}_1}, \tag{5.97}$$

and

$$\boldsymbol{q}_{\mathfrak{o}_3/2}\dot{\boldsymbol{\omega}}^{\mathfrak{o}_3}_{\mathfrak{o}_3/\mathrm{I}}\boldsymbol{q}^*_{\mathfrak{o}_3/2} = \dot{\boldsymbol{\omega}}^2_{2/\mathfrak{o}_2} + \boldsymbol{q}^*_{2/\mathfrak{o}_2}\left(\dot{\boldsymbol{\omega}}^{\mathfrak{o}_2}_{\mathfrak{o}_2/\mathrm{I}} + \boldsymbol{\omega}^{\mathfrak{o}_2}_{\mathfrak{o}_2/\mathrm{I}} \times \boldsymbol{\omega}^{\mathfrak{o}_2}_{2/\mathfrak{o}_2}\right)\boldsymbol{q}_{2/\mathfrak{o}_2}. \tag{5.98}$$

Thus, in general, the constraint at the i-th joint can be written as

$$\boldsymbol{q}_{\mathfrak{o}_{i+1}/i}\dot{\boldsymbol{\omega}}^{\mathfrak{o}_{i+1}}_{\mathfrak{o}_{i+1}/\mathrm{I}}\boldsymbol{q}^*_{\mathfrak{o}_{i+1}/i} = \dot{\boldsymbol{\omega}}^{i}_{i/\mathfrak{o}_i} + \boldsymbol{q}^*_{i/\mathfrak{o}_i}\left(\dot{\boldsymbol{\omega}}^{\mathfrak{o}_i}_{\mathfrak{o}_i/\mathrm{I}} + \boldsymbol{\omega}^{\mathfrak{o}_i}_{\mathfrak{o}_i/\mathrm{I}} \times \boldsymbol{\omega}^{\mathfrak{o}_i}_{i/\mathfrak{o}_i}\right)\boldsymbol{q}_{i/\mathfrak{o}_i}. \tag{5.99}$$

It is worth emphasizing that expressing this constraint equation in the i coordinate system allows for the generalized coordinates, velocities and accelerations to be "exposed", or free of transformations. This will be particularly useful when trying to eliminate redundant degrees of freedom from the overall system of equations.

5.2.6 Dual Quaternion Kinematics

Even though we could integrate the kinematics for each of the bodies independently using the equations

$$\dot{\boldsymbol{q}}_{\mathfrak{o}_i/\mathrm{I}} = \tfrac{1}{2}\boldsymbol{q}_{\mathfrak{o}_i/\mathrm{I}}\boldsymbol{\omega}^{\mathfrak{o}_i}_{\mathfrak{o}_i/\mathrm{I}}, \tag{5.100}$$

this is more computationally intensive and less numerically accurate than simply integrating the kinematics of the base, and the joint generalized velocities to obtain the generalized coordinates. Thus, our kinematics will be given in this form only for the base by

$$\dot{\boldsymbol{q}}_{\mathfrak{o}_0/\mathrm{I}} = \tfrac{1}{2}\boldsymbol{q}_{\mathfrak{o}_0/\mathrm{I}}\boldsymbol{\omega}^{\mathfrak{o}_0}_{\mathfrak{o}_0/\mathrm{I}}, \tag{5.101}$$

while joint kinematics are simply derived from equations (5.92), (5.95) and (5.96), and the definition of $\boldsymbol{\omega}^0_{0/\mathfrak{o}_0}$ given in equation (5.74),

$$\boldsymbol{\omega}^0_{0/\mathfrak{o}_0} = \boldsymbol{q}_{\mathfrak{o}_1/0}\boldsymbol{\omega}^{\mathfrak{o}_1}_{\mathfrak{o}_1/\mathrm{I}}\boldsymbol{q}^*_{\mathfrak{o}_1/0} - \boldsymbol{q}^*_{0/\mathfrak{o}_0}\boldsymbol{\omega}^{\mathfrak{o}_0}_{\mathfrak{o}_0/\mathrm{I}}\boldsymbol{q}_{0/\mathfrak{o}_0}, \tag{5.102}$$

$$\boldsymbol{\omega}^1_{1/\mathfrak{o}_1} = \boldsymbol{q}_{\mathfrak{o}_2/1}\boldsymbol{\omega}^{\mathfrak{o}_2}_{\mathfrak{o}_2/\mathrm{I}}\boldsymbol{q}^*_{\mathfrak{o}_2/1} - \boldsymbol{q}^*_{1/\mathfrak{o}_1}\boldsymbol{\omega}^{\mathfrak{o}_1}_{\mathfrak{o}_1/\mathrm{I}}\boldsymbol{q}_{1/\mathfrak{o}_1}, \tag{5.103}$$

$$\boldsymbol{\omega}^2_{2/\mathfrak{o}_2} = \boldsymbol{q}_{\mathfrak{o}_3/2}\boldsymbol{\omega}^{\mathfrak{o}_3}_{\mathfrak{o}_3/\mathrm{I}}\boldsymbol{q}^*_{\mathfrak{o}_3/2} - \boldsymbol{q}^*_{2/\mathfrak{o}_2}\boldsymbol{\omega}^{\mathfrak{o}_2}_{\mathfrak{o}_2/\mathrm{I}}\boldsymbol{q}_{2/\mathfrak{o}_2}. \tag{5.104}$$

Finally, if we assume we can represent a dual quaternion as a vector in $\mathbb{R}^8$, we obtain the joint velocity by selecting the appropriate entry:

$$\begin{aligned}\dot{\theta}_{1/0} &= [0,0,0,1,0,0,0,0]\boldsymbol{\omega}^0_{0/\mathfrak{o}_0} \\ &= [0,0,0,1,0,0,0,0]\left(\boldsymbol{q}_{\mathfrak{o}_1/0}\boldsymbol{\omega}^{\mathfrak{o}_1}_{\mathfrak{o}_1/\mathrm{I}}\boldsymbol{q}^*_{\mathfrak{o}_1/0} - \boldsymbol{q}^*_{0/\mathfrak{o}_0}\boldsymbol{\omega}^{\mathfrak{o}_0}_{\mathfrak{o}_0/\mathrm{I}}\boldsymbol{q}_{0/\mathfrak{o}_0}\right),\end{aligned} \tag{5.105}$$

$$\begin{aligned}\dot{\theta}_{2/1} &= [0,0,0,1,0,0,0,0]\boldsymbol{\omega}^1_{1/\mathfrak{o}_1} \\ &= [0,0,0,1,0,0,0,0]\left(\boldsymbol{q}_{\mathfrak{o}_2/1}\boldsymbol{\omega}^{\mathfrak{o}_2}_{\mathfrak{o}_2/\mathrm{I}}\boldsymbol{q}^*_{\mathfrak{o}_2/1} - \boldsymbol{q}^*_{1/\mathfrak{o}_1}\boldsymbol{\omega}^{\mathfrak{o}_1}_{\mathfrak{o}_1/\mathrm{I}}\boldsymbol{q}_{1/\mathfrak{o}_1}\right),\end{aligned} \tag{5.106}$$

$$\begin{aligned}\dot{\theta}_{3/2} &= [0,0,0,1,0,0,0,0]\boldsymbol{\omega}^2_{2/\mathfrak{o}_2} \\ &= [0,0,0,1,0,0,0,0]\left(\boldsymbol{q}_{\mathfrak{o}_{3/2}}\boldsymbol{\omega}^{\mathfrak{o}_3}_{\mathfrak{o}_3/1}\boldsymbol{q}^*_{\mathfrak{o}_{3/2}} - \boldsymbol{q}^*_{2/\mathfrak{o}_2}\boldsymbol{\omega}^{\mathfrak{o}_2}_{\mathfrak{o}_2/1}\boldsymbol{q}_{2/\mathfrak{o}_2}\right). \end{aligned} \tag{5.107}$$

It is worth emphasizing that if instead we had a prismatic joint, the multiplying vector would be $[0,0,0,0,0,0,0,1]$ instead, and similar mapping relationships can be derived for different types of joints. Explicit expressions will be provided in a future section.

5.2.7 Dual Quaternion Formulation Implementation

Analogous to the decoupled formulation derived in previous subsections, the unknown quantities are the linear and angular accelerations of each of the bodies, as well as the reactions forces and torques that these bodies experience due to their attachment to a particular type of joint. To solve for these unknown quantities using dual quaternions, we will again cast our dynamics formulation as a linear system of the form

$$\boldsymbol{\mathcal{S}}\boldsymbol{\mathcal{Y}} = \boldsymbol{\mathcal{B}}, \tag{5.108}$$

where $\boldsymbol{\mathcal{Y}}$ is the unknown variable that contains the dual accelerations and wrenches, and $\boldsymbol{\mathcal{S}}$ and $\boldsymbol{\mathcal{B}}$ are configuration-dependendent matrices that can be constructed from the knowledge of all non-reaction wrenches. In this section, we construct the $\boldsymbol{\mathcal{S}}$, $\boldsymbol{\mathcal{Y}}$, and $\boldsymbol{\mathcal{B}}$ matrices.

To cast the system in the form of equation (5.108), we need to express the transformations of the dual accelerations and reaction forces as an affine transformation with respect to $\boldsymbol{\mathcal{Y}}$. Using the notation introduced in equations (2.28) and (2.48) and moving terms with unknown quantities to the left hand side, and all others to the right-hand side, equation (5.67)

becomes

$$\begin{aligned}
&\mathrm{H}\,(M_{\mathfrak{o}_0}) \star \dot{\boldsymbol{\omega}}^{\mathfrak{o}_0}_{\mathfrak{o}_0/\mathrm{I}} + \left[\!\left[\boldsymbol{q}_{0/\mathfrak{o}_0} \right]\!\right]_{\mathrm{L}} \left[\!\left[\boldsymbol{q}^*_{0/\mathfrak{o}_0} \right]\!\right]_{\mathrm{R}} \star \boldsymbol{W}^{\mathfrak{o}_1}_{1/0}(O_0) \\
&\qquad = -\boldsymbol{\omega}^{\mathfrak{o}_0}_{\mathfrak{o}_0/\mathrm{I}} \times \left(M_{\mathfrak{o}_0} \star (\boldsymbol{\omega}^{\mathfrak{o}_0}_{\mathfrak{o}_0/\mathrm{I}})^{\mathsf{S}} \right) + \boldsymbol{W}^{\mathfrak{o}_0}_{\mathfrak{o}_0}(O_{\mathfrak{o}_0}) \\
&\qquad\quad - \boldsymbol{q}_{0/\mathfrak{o}_0} \boldsymbol{W}^{\mathfrak{o}_1}_{\mathrm{act},1}(O_0) \boldsymbol{q}^*_{0/\mathfrak{o}_0},
\end{aligned} \tag{5.109}$$

equation (5.68) becomes

$$\begin{aligned}
&\mathrm{H}\,(M_{\mathfrak{o}_1}) \star \dot{\boldsymbol{\omega}}^{\mathfrak{o}_1}_{\mathfrak{o}_1/\mathrm{I}} - \left[\!\left[\boldsymbol{q}^*_{\mathfrak{o}_1/0} \right]\!\right]_{\mathrm{L}} \left[\!\left[\boldsymbol{q}_{\mathfrak{o}_1/0} \right]\!\right]_{\mathrm{R}} \star \boldsymbol{W}^{\mathfrak{o}_1}_{1/0}(O_0) + \left[\!\left[\boldsymbol{q}_{1/\mathfrak{o}_1} \right]\!\right]_{\mathrm{L}} \left[\!\left[\boldsymbol{q}^*_{1/\mathfrak{o}_1} \right]\!\right]_{\mathrm{R}} \star \boldsymbol{W}^{\mathfrak{o}_2}_{2/1}(O_1) \\
&\qquad = -\boldsymbol{\omega}^{\mathfrak{o}_1}_{\mathfrak{o}_1/\mathrm{I}} \times \left(M_{\mathfrak{o}_1} \star (\boldsymbol{\omega}^{\mathfrak{o}_1}_{\mathfrak{o}_1/\mathrm{I}})^{\mathsf{S}} \right) + \boldsymbol{W}^{\mathfrak{o}_1}_{\mathfrak{o}_1}(O_{\mathfrak{o}_1}) \\
&\qquad\quad + \boldsymbol{q}^*_{\mathfrak{o}_1/0} \boldsymbol{W}^{\mathfrak{o}_1}_{\mathrm{act},1}(O_0) \boldsymbol{q}_{\mathfrak{o}_1/0} - \boldsymbol{q}_{1/\mathfrak{o}_1} \boldsymbol{W}^{\mathfrak{o}_2}_{\mathrm{act},2}(O_1) \boldsymbol{q}^*_{1/\mathfrak{o}_1},
\end{aligned} \tag{5.110}$$

equation (5.69) becomes

$$\begin{aligned}
&\mathrm{H}\,(M_{\mathfrak{o}_2}) \star \dot{\boldsymbol{\omega}}^{\mathfrak{o}_2}_{\mathfrak{o}_2/\mathrm{I}} - \left[\!\left[\boldsymbol{q}^*_{\mathfrak{o}_2/1} \right]\!\right]_{\mathrm{L}} \left[\!\left[\boldsymbol{q}_{\mathfrak{o}_2/1} \right]\!\right]_{\mathrm{R}} \star \boldsymbol{W}^{\mathfrak{o}_2}_{2/1}(O_1) + \left[\!\left[\boldsymbol{q}_{2/\mathfrak{o}_2} \right]\!\right]_{\mathrm{L}} \left[\!\left[\boldsymbol{q}^*_{2/\mathfrak{o}_2} \right]\!\right]_{\mathrm{R}} \star \boldsymbol{W}^{\mathfrak{o}_3}_{3/2}(O_2) \\
&\qquad = -\boldsymbol{\omega}^{\mathfrak{o}_2}_{\mathfrak{o}_2/\mathrm{I}} \times \left(M_{\mathfrak{o}_2} \star (\boldsymbol{\omega}^{\mathfrak{o}_2}_{\mathfrak{o}_2/\mathrm{I}})^{\mathsf{S}} \right) + \boldsymbol{W}^{\mathfrak{o}_2}_{\mathfrak{o}_2}(O_{\mathfrak{o}_2}) \\
&\qquad\quad + \boldsymbol{q}^*_{\mathfrak{o}_2/1} \boldsymbol{W}^{\mathfrak{o}_2}_{\mathrm{act},2}(O_1) \boldsymbol{q}_{\mathfrak{o}_2/1} - \boldsymbol{q}_{2/\mathfrak{o}_2} \boldsymbol{W}^{\mathfrak{o}_3}_{\mathrm{act},3}(O_2) \boldsymbol{q}^*_{2/\mathfrak{o}_2},
\end{aligned} \tag{5.111}$$

and equation (5.70) is cast as

$$\begin{aligned}
&\mathrm{H}\,(M_{\mathfrak{o}_3}) \star \dot{\boldsymbol{\omega}}^{\mathfrak{o}_3}_{\mathfrak{o}_3/\mathrm{I}} - \left[\!\left[\boldsymbol{q}^*_{\mathfrak{o}_3/2} \right]\!\right]_{\mathrm{L}} \left[\!\left[\boldsymbol{q}_{\mathfrak{o}_3/2} \right]\!\right]_{\mathrm{R}} \star \boldsymbol{W}^{\mathfrak{o}_3}_{3/2}(O_2) \\
&\qquad = -\boldsymbol{\omega}^{\mathfrak{o}_3}_{\mathfrak{o}_3/\mathrm{I}} \times \left(M_{\mathfrak{o}_3} \star (\boldsymbol{\omega}^{\mathfrak{o}_3}_{\mathfrak{o}_3/\mathrm{I}})^{\mathsf{S}} \right) + \boldsymbol{W}^{\mathfrak{o}_3}_{\mathfrak{o}_3}(O_{\mathfrak{o}_3}) \\
&\qquad\quad + \boldsymbol{q}^*_{\mathfrak{o}_3/2} \boldsymbol{W}^{\mathfrak{o}_3}_{\mathrm{act},3}(O_2) \boldsymbol{q}_{\mathfrak{o}_3/2} \\
&\qquad\quad + \boldsymbol{q}_{\mathrm{G}/\mathfrak{o}_3} \boldsymbol{W}^{\mathrm{G}}_{\mathrm{ext}}(O_G) \boldsymbol{q}^*_{\mathrm{G}/\mathfrak{o}_3}.
\end{aligned} \tag{5.112}$$

Now, we must take into account the fact that we are not trying to solve for all of $\boldsymbol{W}^{\mathfrak{o}_1}_{1/0}(O_0)$, $\boldsymbol{W}^{\mathfrak{o}_2}_{2/1}(O_1)$, or $\boldsymbol{W}^{\mathfrak{o}_3}_{3/2}(O_2)$. The first and fifth entries are zero because wrenches are dual

vector quaternions, and so are their adjoints. The eight entry is zero because it corresponds to the degree of freedom of the joint. If the joint were prismatic, or cylindrical, and the translational degree of freedom aligned with the local Z-axis, then the fourth entry would also be zero. The non-zero components of the wrench form the *reduced* wrench, and for reaction wrenches that correspond to revolute-type joints, we obtain

$$\tilde{\boldsymbol{W}}^{\mathbb{o}_1}_{1/0}(O_0) \triangleq \begin{bmatrix} (\bar{f}^{\mathbb{o}_1}_{1/0})_x \\ (\bar{f}^{\mathbb{o}_1}_{1/0})_y \\ (\bar{f}^{\mathbb{o}_1}_{1/0})_z \\ (\bar{\tau}^{\mathbb{o}_1}_{1/0})_x \\ (\bar{\tau}^{\mathbb{o}_1}_{1/0})_y \end{bmatrix}, \quad \tilde{\boldsymbol{W}}^{\mathbb{o}_2}_{2/1}(O_1) \triangleq \begin{bmatrix} (\bar{f}^{\mathbb{o}_2}_{2/1})_x \\ (\bar{f}^{\mathbb{o}_2}_{2/1})_y \\ (\bar{f}^{\mathbb{o}_2}_{2/1})_z \\ (\bar{\tau}^{\mathbb{o}_2}_{2/1})_x \\ (\bar{\tau}^{\mathbb{o}_2}_{2/1})_y \end{bmatrix}, \quad \text{and} \quad \tilde{\boldsymbol{W}}^{\mathbb{o}_3}_{3/2}(O_2) \triangleq \begin{bmatrix} (\bar{f}^{\mathbb{o}_3}_{3/2})_x \\ (\bar{f}^{\mathbb{o}_3}_{3/2})_y \\ (\bar{f}^{\mathbb{o}_3}_{3/2})_z \\ (\bar{\tau}^{\mathbb{o}_3}_{3/2})_x \\ (\bar{\tau}^{\mathbb{o}_3}_{3/2})_y \end{bmatrix}. \quad (5.113)$$

Thus, we define the mapping matrix

$$\boldsymbol{E}^{\mathrm{T}}_{158} \triangleq \begin{bmatrix} 0 & 0 & 0 & 0 & 0 \\ 1 & 0 & 0 & 0 & 0 \\ 0 & 1 & 0 & 0 & 0 \\ 0 & 0 & 1 & 0 & 0 \\ 0 & 0 & 0 & 0 & 0 \\ 0 & 0 & 0 & 1 & 0 \\ 0 & 0 & 0 & 0 & 1 \\ 0 & 0 & 0 & 0 & 0 \end{bmatrix}, \quad (5.114)$$

and use it in equations (5.109) to (5.112) to introduce the reduced reaction wrenches as

follows

$$\begin{aligned}
&\mathrm{H}\left(M_{\mathfrak{o}_0}\right) \star \dot{\boldsymbol{\omega}}^{\mathfrak{o}_0}_{\mathfrak{o}_0/\mathrm{I}} + \left[\!\left[\boldsymbol{q}_{0/\mathfrak{o}_0} \right]\!\right]_{\mathrm{L}} \left[\!\left[\boldsymbol{q}^*_{0/\mathfrak{o}_0} \right]\!\right]_{\mathrm{R}} \boldsymbol{E}^{\mathrm{T}}_{158} \tilde{\boldsymbol{W}}^{\mathfrak{o}_1}_{1/0}(O_0) \\
&\qquad = -\boldsymbol{\omega}^{\mathfrak{o}_0}_{\mathfrak{o}_0/\mathrm{I}} \times \left(M_{\mathfrak{o}_0} \star (\boldsymbol{\omega}^{\mathfrak{o}_0}_{\mathfrak{o}_0/\mathrm{I}})^{\mathsf{s}}\right) + \boldsymbol{W}^{\mathfrak{o}_0}_{\mathfrak{o}_0}(O_{\mathfrak{o}_0}) \\
&\qquad\quad - \boldsymbol{q}_{0/\mathfrak{o}_0} \boldsymbol{W}^{\mathfrak{o}_1}_{\mathrm{act},1}(O_0) \boldsymbol{q}^*_{0/\mathfrak{o}_0},
\end{aligned} \tag{5.115}$$

$$\begin{aligned}
&\mathrm{H}\left(M_{\mathfrak{o}_1}\right) \star \dot{\boldsymbol{\omega}}^{\mathfrak{o}_1}_{\mathfrak{o}_1/\mathrm{I}} - \left[\!\left[\boldsymbol{q}^*_{\mathfrak{o}_1/0} \right]\!\right]_{\mathrm{L}} \left[\!\left[\boldsymbol{q}_{\mathfrak{o}_1/0} \right]\!\right]_{\mathrm{R}} \boldsymbol{E}^{\mathrm{T}}_{158} \tilde{\boldsymbol{W}}^{\mathfrak{o}_1}_{1/0}(O_0) + \left[\!\left[\boldsymbol{q}_{1/\mathfrak{o}_1} \right]\!\right]_{\mathrm{L}} \left[\!\left[\boldsymbol{q}^*_{1/\mathfrak{o}_1} \right]\!\right]_{\mathrm{R}} \boldsymbol{E}^{\mathrm{T}}_{158} \tilde{\boldsymbol{W}}^{\mathfrak{o}_2}_{2/1}(O_1) \\
&\qquad = -\boldsymbol{\omega}^{\mathfrak{o}_1}_{\mathfrak{o}_1/\mathrm{I}} \times \left(M_{\mathfrak{o}_1} \star (\boldsymbol{\omega}^{\mathfrak{o}_1}_{\mathfrak{o}_1/\mathrm{I}})^{\mathsf{s}}\right) + \boldsymbol{W}^{\mathfrak{o}_1}_{\mathfrak{o}_1}(O_{\mathfrak{o}_1}) \\
&\qquad\quad + \boldsymbol{q}^*_{\mathfrak{o}_1/0} \boldsymbol{W}^{\mathfrak{o}_1}_{\mathrm{act},1}(O_0) \boldsymbol{q}_{\mathfrak{o}_1/0} - \boldsymbol{q}_{1/\mathfrak{o}_1} \boldsymbol{W}^{\mathfrak{o}_2}_{\mathrm{act},2}(O_1) \boldsymbol{q}^*_{1/\mathfrak{o}_1},
\end{aligned} \tag{5.116}$$

$$\begin{aligned}
&\mathrm{H}\left(M_{\mathfrak{o}_2}\right) \star \dot{\boldsymbol{\omega}}^{\mathfrak{o}_2}_{\mathfrak{o}_2/\mathrm{I}} - \left[\!\left[\boldsymbol{q}^*_{\mathfrak{o}_2/1} \right]\!\right]_{\mathrm{L}} \left[\!\left[\boldsymbol{q}_{\mathfrak{o}_2/1} \right]\!\right]_{\mathrm{R}} \boldsymbol{E}^{\mathrm{T}}_{158} \tilde{\boldsymbol{W}}^{\mathfrak{o}_2}_{2/1}(O_1) + \left[\!\left[\boldsymbol{q}_{2/\mathfrak{o}_2} \right]\!\right]_{\mathrm{L}} \left[\!\left[\boldsymbol{q}^*_{2/\mathfrak{o}_2} \right]\!\right]_{\mathrm{R}} \boldsymbol{E}^{\mathrm{T}}_{158} \tilde{\boldsymbol{W}}^{\mathfrak{o}_3}_{3/2}(O_2) \\
&\qquad = -\boldsymbol{\omega}^{\mathfrak{o}_2}_{\mathfrak{o}_2/\mathrm{I}} \times \left(M_{\mathfrak{o}_2} \star (\boldsymbol{\omega}^{\mathfrak{o}_2}_{\mathfrak{o}_2/\mathrm{I}})^{\mathsf{s}}\right) + \boldsymbol{W}^{\mathfrak{o}_2}_{\mathfrak{o}_2}(O_{\mathfrak{o}_2}) \\
&\qquad\quad + \boldsymbol{q}^*_{\mathfrak{o}_2/1} \boldsymbol{W}^{\mathfrak{o}_2}_{\mathrm{act},2}(O_1) \boldsymbol{q}_{\mathfrak{o}_2/1} - \boldsymbol{q}_{2/\mathfrak{o}_2} \boldsymbol{W}^{\mathfrak{o}_3}_{\mathrm{act},3}(O_2) \boldsymbol{q}^*_{2/\mathfrak{o}_2},
\end{aligned} \tag{5.117}$$

$$\begin{aligned}
&\mathrm{H}\left(M_{\mathfrak{o}_3}\right) \star \dot{\boldsymbol{\omega}}^{\mathfrak{o}_3}_{\mathfrak{o}_3/\mathrm{I}} - \left[\!\left[\boldsymbol{q}^*_{\mathfrak{o}_3/2} \right]\!\right]_{\mathrm{L}} \left[\!\left[\boldsymbol{q}_{\mathfrak{o}_3/2} \right]\!\right]_{\mathrm{R}} \boldsymbol{E}^{\mathrm{T}}_{158} \tilde{\boldsymbol{W}}^{\mathfrak{o}_3}_{3/2}(O_2) \\
&\qquad = -\boldsymbol{\omega}^{\mathfrak{o}_3}_{\mathfrak{o}_3/\mathrm{I}} \times \left(M_{\mathfrak{o}_3} \star (\boldsymbol{\omega}^{\mathfrak{o}_3}_{\mathfrak{o}_3/\mathrm{I}})^{\mathsf{s}}\right) + \boldsymbol{W}^{\mathfrak{o}_3}_{\mathfrak{o}_3}(O_{\mathfrak{o}_3}) \\
&\qquad\quad + \boldsymbol{q}^*_{\mathfrak{o}_3/2} \boldsymbol{W}^{\mathfrak{o}_3}_{\mathrm{act},3}(O_2) \boldsymbol{q}_{\mathfrak{o}_3/2} \\
&\qquad\quad + \boldsymbol{q}_{\mathrm{G}/\mathfrak{o}_3} \boldsymbol{W}^{G}_{\mathrm{ext}}(O_G) \boldsymbol{q}^*_{\mathrm{G}/\mathfrak{o}_3}.
\end{aligned} \tag{5.118}$$

Notice that the $\star$ operator has now been omitted for $\tilde{\boldsymbol{W}}$ since we can simply take it to be a five-dimensional vector multiplying an appropriately sized matrix.

It is worth emphasizing that in the case of a prismatic joint, the matrix that would

provide such a mapping for the appropriate reduced reaction wrench coordinates would be

$$\boldsymbol{E}_{145}^{\mathrm{T}} \triangleq \begin{bmatrix} 0 & 0 & 0 & 0 & 0 \\ 1 & 0 & 0 & 0 & 0 \\ 0 & 1 & 0 & 0 & 0 \\ 0 & 0 & 0 & 0 & 0 \\ 0 & 0 & 0 & 0 & 0 \\ 0 & 0 & 1 & 0 & 0 \\ 0 & 0 & 0 & 1 & 0 \\ 0 & 0 & 0 & 0 & 1 \end{bmatrix}. \tag{5.119}$$

We will now modify the constraints to incorporate them into the proposed framework. In this case, equation (5.94) becomes

$$\left[\!\left[\boldsymbol{q}_{\mathfrak{o}_1/0} \right]\!\right]_{\mathrm{L}} \left[\!\left[\boldsymbol{q}^*_{\mathfrak{o}_1/0} \right]\!\right]_{\mathrm{R}} \star \dot{\boldsymbol{\omega}}^{\mathfrak{o}_1}_{\mathfrak{o}_1/\mathrm{I}} - \left[\!\left[\boldsymbol{q}^*_{0/\mathfrak{o}_0} \right]\!\right]_{\mathrm{L}} \left[\!\left[\boldsymbol{q}_{0/\mathfrak{o}_0} \right]\!\right]_{\mathrm{R}} \star \dot{\boldsymbol{\omega}}^{\mathfrak{o}_0}_{\mathfrak{o}_0/\mathrm{I}} = \dot{\boldsymbol{\omega}}^{0}_{0/\mathfrak{o}_0} + \boldsymbol{q}^*_{0/\mathfrak{o}_0} \left(\boldsymbol{\omega}^{\mathfrak{o}_0}_{\mathfrak{o}_0/\mathrm{I}} \times \boldsymbol{\omega}^{\mathfrak{o}_0}_{0/\mathfrak{o}_0} \right) \boldsymbol{q}_{0/\mathfrak{o}_0} \tag{5.120}$$

Analogously, equations (5.97) and (5.98) respectively become

$$\left[\!\left[\boldsymbol{q}_{\mathfrak{o}_2/1} \right]\!\right]_{\mathrm{L}} \left[\!\left[\boldsymbol{q}^*_{\mathfrak{o}_2/1} \right]\!\right]_{\mathrm{R}} \star \dot{\boldsymbol{\omega}}^{\mathfrak{o}_2}_{\mathfrak{o}_2/\mathrm{I}} - \left[\!\left[\boldsymbol{q}^*_{1/\mathfrak{o}_1} \right]\!\right]_{\mathrm{L}} \left[\!\left[\boldsymbol{q}_{1/\mathfrak{o}_1} \right]\!\right]_{\mathrm{R}} \star \dot{\boldsymbol{\omega}}^{\mathfrak{o}_1}_{\mathfrak{o}_1/\mathrm{I}} = \dot{\boldsymbol{\omega}}^{1}_{1/\mathfrak{o}_1} + \boldsymbol{q}^*_{1/\mathfrak{o}_1} \left(\boldsymbol{\omega}^{\mathfrak{o}_1}_{\mathfrak{o}_1/\mathrm{I}} \times \boldsymbol{\omega}^{\mathfrak{o}_1}_{1/\mathfrak{o}_1} \right) \boldsymbol{q}_{1/\mathfrak{o}_1} \tag{5.121}$$

$$\left[\!\left[\boldsymbol{q}_{\mathfrak{o}_3/2} \right]\!\right]_{\mathrm{L}} \left[\!\left[\boldsymbol{q}^*_{\mathfrak{o}_3/2} \right]\!\right]_{\mathrm{R}} \star \dot{\boldsymbol{\omega}}^{\mathfrak{o}_3}_{\mathfrak{o}_3/\mathrm{I}} - \left[\!\left[\boldsymbol{q}^*_{2/\mathfrak{o}_2} \right]\!\right]_{\mathrm{L}} \left[\!\left[\boldsymbol{q}_{2/\mathfrak{o}_2} \right]\!\right]_{\mathrm{R}} \star \dot{\boldsymbol{\omega}}^{\mathfrak{o}_2}_{\mathfrak{o}_2/\mathrm{I}} = \dot{\boldsymbol{\omega}}^{2}_{2/\mathfrak{o}_2} + \boldsymbol{q}^*_{2/\mathfrak{o}_2} \left(\boldsymbol{\omega}^{\mathfrak{o}_2}_{\mathfrak{o}_2/\mathrm{I}} \times \boldsymbol{\omega}^{\mathfrak{o}_2}_{2/\mathfrak{o}_2} \right) \boldsymbol{q}_{2/\mathfrak{o}_2}. \tag{5.122}$$

Finally, the scalar part of the dual quaternions (first and fifth entries) of equations (5.120) to (5.122) are zero since the adjoint of a dual velocity is itself a dual velocity, which is a vector dual quaternion. Additionally, we want to eliminate the redundant information introduced by the joint angular acceleration through the annihilation of the appropriate

dual quaternion entry. Thus, we multiply these equations by

$$\boldsymbol{E}_{145} = \begin{bmatrix} 0 & 1 & 0 & 0 & 0 & 0 & 0 & 0 \\ 0 & 0 & 1 & 0 & 0 & 0 & 0 & 0 \\ 0 & 0 & 0 & 0 & 0 & 1 & 0 & 0 \\ 0 & 0 & 0 & 0 & 0 & 0 & 1 & 0 \\ 0 & 0 & 0 & 0 & 0 & 0 & 0 & 1 \end{bmatrix}, \tag{5.123}$$

which leads to

$$\boldsymbol{E}_{145}\left[\!\left[\boldsymbol{q}_{\mathfrak{o}_1/0} \right]\!\right]_{\mathrm{L}} \left[\!\left[\boldsymbol{q}^*_{\mathfrak{o}_1/0} \right]\!\right]_{\mathrm{R}} \star \dot{\boldsymbol{\omega}}^{\mathfrak{o}_1}_{\mathfrak{o}_1/\mathrm{I}} - \boldsymbol{E}_{145}\left[\!\left[\boldsymbol{q}^*_{0/\mathfrak{o}_0} \right]\!\right]_{\mathrm{L}} \left[\!\left[\boldsymbol{q}_{0/\mathfrak{o}_0} \right]\!\right]_{\mathrm{R}} \star \dot{\boldsymbol{\omega}}^{\mathfrak{o}_0}_{\mathfrak{o}_0/\mathrm{I}} = \boldsymbol{E}_{145} \boldsymbol{q}^*_{0/\mathfrak{o}_0} \left(\boldsymbol{\omega}^{\mathfrak{o}_0}_{\mathfrak{o}_0/\mathrm{I}} \times \boldsymbol{\omega}^{\mathfrak{o}_0}_{0/\mathfrak{o}_0} \right) \boldsymbol{q}_{0/\mathfrak{o}_0}, \tag{5.124}$$

$$\boldsymbol{E}_{145}\left[\!\left[\boldsymbol{q}_{\mathfrak{o}_2/1} \right]\!\right]_{\mathrm{L}} \left[\!\left[\boldsymbol{q}^*_{\mathfrak{o}_2/1} \right]\!\right]_{\mathrm{R}} \star \dot{\boldsymbol{\omega}}^{\mathfrak{o}_2}_{\mathfrak{o}_2/\mathrm{I}} - \boldsymbol{E}_{145}\left[\!\left[\boldsymbol{q}^*_{1/\mathfrak{o}_1} \right]\!\right]_{\mathrm{L}} \left[\!\left[\boldsymbol{q}_{1/\mathfrak{o}_1} \right]\!\right]_{\mathrm{R}} \star \dot{\boldsymbol{\omega}}^{\mathfrak{o}_1}_{\mathfrak{o}_1/\mathrm{I}} = \boldsymbol{E}_{145} \boldsymbol{q}^*_{1/\mathfrak{o}_1} \left(\boldsymbol{\omega}^{\mathfrak{o}_1}_{\mathfrak{o}_1/\mathrm{I}} \times \boldsymbol{\omega}^{\mathfrak{o}_1}_{1/\mathfrak{o}_1} \right) \boldsymbol{q}_{1/\mathfrak{o}_1}, \tag{5.125}$$

$$\boldsymbol{E}_{145}\left[\!\left[\boldsymbol{q}_{\mathfrak{o}_3/2} \right]\!\right]_{\mathrm{L}} \left[\!\left[\boldsymbol{q}^*_{\mathfrak{o}_3/2} \right]\!\right]_{\mathrm{R}} \star \dot{\boldsymbol{\omega}}^{\mathfrak{o}_3}_{\mathfrak{o}_3/\mathrm{I}} - \boldsymbol{E}_{145}\left[\!\left[\boldsymbol{q}^*_{2/\mathfrak{o}_2} \right]\!\right]_{\mathrm{L}} \left[\!\left[\boldsymbol{q}_{2/\mathfrak{o}_2} \right]\!\right]_{\mathrm{R}} \star \dot{\boldsymbol{\omega}}^{\mathfrak{o}_2}_{\mathfrak{o}_2/\mathrm{I}} = \boldsymbol{E}_{145} \boldsymbol{q}^*_{2/\mathfrak{o}_2} \left(\boldsymbol{\omega}^{\mathfrak{o}_2}_{\mathfrak{o}_2/\mathrm{I}} \times \boldsymbol{\omega}^{\mathfrak{o}_2}_{2/\mathfrak{o}_2} \right) \boldsymbol{q}_{2/\mathfrak{o}_2}. \tag{5.126}$$

It is worth emphasizing that if the corresponding joint is prismatic, we would instead multiply by $\boldsymbol{E}_{158}$, which has been defined above.

Let us now define the following quantities

$$\boldsymbol{y} \triangleq \begin{bmatrix} \boldsymbol{\omega}^{\mathfrak{o}_0}_{\mathfrak{o}_0/\mathrm{I}} \\ \boldsymbol{\omega}^{\mathfrak{o}_1}_{\mathfrak{o}_1/\mathrm{I}} \\ \boldsymbol{\omega}^{\mathfrak{o}_2}_{\mathfrak{o}_2/\mathrm{I}} \\ \boldsymbol{\omega}^{\mathfrak{o}_3}_{\mathfrak{o}_3/\mathrm{I}} \end{bmatrix}, \quad \dot{\boldsymbol{y}} = \begin{bmatrix} \dot{\boldsymbol{\omega}}^{\mathfrak{o}_0}_{\mathfrak{o}_0/\mathrm{I}} \\ \dot{\boldsymbol{\omega}}^{\mathfrak{o}_1}_{\mathfrak{o}_1/\mathrm{I}} \\ \dot{\boldsymbol{\omega}}^{\mathfrak{o}_2}_{\mathfrak{o}_2/\mathrm{I}} \\ \dot{\boldsymbol{\omega}}^{\mathfrak{o}_3}_{\mathfrak{o}_3/\mathrm{I}} \end{bmatrix}, \tag{5.127}$$

$$\boldsymbol{\mathcal{T}} \triangleq \begin{bmatrix} \tilde{\boldsymbol{W}}_{1/0}^{\circledcirc_1}(O_0) \\ \tilde{\boldsymbol{W}}_{2/1}^{\circledcirc_2}(O_1) \\ \tilde{\boldsymbol{W}}_{3/2}^{\circledcirc_3}(O_2) \end{bmatrix}, \tag{5.128}$$

and

$$\boldsymbol{\mathcal{Y}} = \begin{bmatrix} \dot{\boldsymbol{y}} \\ \boldsymbol{\mathcal{T}} \end{bmatrix}. \tag{5.129}$$

Then, we can arrange equations (5.115) to (5.118) and equations (5.124) to (5.126) into the following block-matrix form

$$\boldsymbol{\mathcal{S}}\boldsymbol{\mathcal{Y}} = \boldsymbol{\mathcal{B}} \tag{5.130}$$

$$\begin{bmatrix} \boldsymbol{\mathcal{S}}_{11} & \boldsymbol{\mathcal{S}}_{12} \\ \boldsymbol{\mathcal{S}}_{21} & \boldsymbol{\mathcal{S}}_{22} \end{bmatrix} \begin{bmatrix} \dot{\boldsymbol{y}} \\ \boldsymbol{\mathcal{T}} \end{bmatrix} = \begin{bmatrix} \boldsymbol{\mathcal{B}}_1 \\ \boldsymbol{\mathcal{B}}_2 \end{bmatrix} \tag{5.131}$$

where

$$\boldsymbol{\mathcal{S}}_{11} = \operatorname{diag}\left(\mathrm{H}\left(M_{\circledcirc_0}\right), \mathrm{H}\left(M_{\circledcirc_1}\right), \mathrm{H}\left(M_{\circledcirc_2}\right), \mathrm{H}\left(M_{\circledcirc_3}\right)\right), \tag{5.132}$$

$$\boldsymbol{\mathcal{S}}_{22} = 0_{15\times 15}, \tag{5.133}$$

$$\boldsymbol{\mathcal{S}}_{12} = \begin{bmatrix} \left[\!\left[\boldsymbol{q}_{0/\circledcirc_0}\right]\!\right]_{\mathrm{L}} \left[\!\left[\boldsymbol{q}_{0/\circledcirc_0}^*\right]\!\right]_{\mathrm{R}} \boldsymbol{E}_{158}^{\mathrm{T}} & 0_{8\times 5} & 0_{8\times 5} \\ -\left[\!\left[\boldsymbol{q}_{\circledcirc_1/0}^*\right]\!\right]_{\mathrm{L}} \left[\!\left[\boldsymbol{q}_{\circledcirc_1/0}\right]\!\right]_{\mathrm{R}} \boldsymbol{E}_{158}^{\mathrm{T}} & \left[\!\left[\boldsymbol{q}_{1/\circledcirc_1}\right]\!\right]_{\mathrm{L}} \left[\!\left[\boldsymbol{q}_{1/\circledcirc_1}^*\right]\!\right]_{\mathrm{R}} \boldsymbol{E}_{158}^{\mathrm{T}} & 0_{8\times 5} \\ 0_{8\times 5} & -\left[\!\left[\boldsymbol{q}_{\circledcirc_2/1}^*\right]\!\right]_{\mathrm{L}} \left[\!\left[\boldsymbol{q}_{\circledcirc_2/1}\right]\!\right]_{\mathrm{R}} \boldsymbol{E}_{158}^{\mathrm{T}} & \left[\!\left[\boldsymbol{q}_{2/\circledcirc_2}\right]\!\right]_{\mathrm{L}} \left[\!\left[\boldsymbol{q}_{2/\circledcirc_2}^*\right]\!\right]_{\mathrm{R}} \boldsymbol{E}_{158}^{\mathrm{T}} \\ 0_{8\times 5} & 0_{8\times 5} & -\left[\!\left[\boldsymbol{q}_{\circledcirc_3/2}^*\right]\!\right]_{\mathrm{L}} \left[\!\left[\boldsymbol{q}_{\circledcirc_3/2}\right]\!\right]_{\mathrm{R}} \boldsymbol{E}_{158}^{\mathrm{T}} \end{bmatrix}, \tag{5.134}$$

$$\boldsymbol{\mathcal{S}}_{21} = \begin{bmatrix} -\boldsymbol{E}_{145}\left[\!\left[\boldsymbol{q}^{*}_{0/\mathfrak{o}_0} \right]\!\right]_{\mathrm{L}} \left[\!\left[\boldsymbol{q}_{0/\mathfrak{o}_0} \right]\!\right]_{\mathrm{R}} & \boldsymbol{E}_{145}\left[\!\left[\boldsymbol{q}_{\mathfrak{o}_1/0} \right]\!\right]_{\mathrm{L}} \left[\!\left[\boldsymbol{q}^{*}_{\mathfrak{o}_1/0} \right]\!\right]_{\mathrm{R}} & & \\ 0_{5\times 8} & -\boldsymbol{E}_{145}\left[\!\left[\boldsymbol{q}^{*}_{1/\mathfrak{o}_1} \right]\!\right]_{\mathrm{L}} \left[\!\left[\boldsymbol{q}_{1/\mathfrak{o}_1} \right]\!\right]_{\mathrm{R}} & \cdots & \\ 0_{5\times 8} & 0_{5\times 8} & & \end{bmatrix}$$

$$\begin{bmatrix} 0_{5\times 8} & 0_{5\times 8} \\ \cdots \quad \boldsymbol{E}_{145}\left[\!\left[\boldsymbol{q}_{\mathfrak{o}_2/1} \right]\!\right]_{\mathrm{L}} \left[\!\left[\boldsymbol{q}^{*}_{\mathfrak{o}_2/1} \right]\!\right]_{\mathrm{R}} & 0_{5\times 8} \\ -\boldsymbol{E}_{145}\left[\!\left[\boldsymbol{q}^{*}_{2/\mathfrak{o}_2} \right]\!\right]_{\mathrm{L}} \left[\!\left[\boldsymbol{q}_{2/\mathfrak{o}_2} \right]\!\right]_{\mathrm{R}} & \boldsymbol{E}_{145}\left[\!\left[\boldsymbol{q}_{\mathfrak{o}_3/2} \right]\!\right]_{\mathrm{L}} \left[\!\left[\boldsymbol{q}^{*}_{\mathfrak{o}_3/2} \right]\!\right]_{\mathrm{R}} \end{bmatrix}, \quad (5.135)$$

$$\boldsymbol{\mathcal{B}}_1 = \begin{bmatrix} -\boldsymbol{\omega}^{\mathfrak{o}_0}_{\mathfrak{o}_0/\mathrm{I}} \times \left(M_{\mathfrak{o}_0} \star (\boldsymbol{\omega}^{\mathfrak{o}_0}_{\mathfrak{o}_0/\mathrm{I}})^{\mathsf{s}} \right) + \boldsymbol{W}^{\mathfrak{o}_0}_{\mathfrak{o}_0}(O_{\mathfrak{o}_0}) - \boldsymbol{q}_{0/\mathfrak{o}_0} \boldsymbol{W}^{\mathfrak{o}_1}_{\mathrm{act},1}(O_0) \boldsymbol{q}^{*}_{0/\mathfrak{o}_0} \\ -\boldsymbol{\omega}^{\mathfrak{o}_1}_{\mathfrak{o}_1/\mathrm{I}} \times \left(M_{\mathfrak{o}_1} \star (\boldsymbol{\omega}^{\mathfrak{o}_1}_{\mathfrak{o}_1/\mathrm{I}})^{\mathsf{s}} \right) + \boldsymbol{W}^{\mathfrak{o}_1}_{\mathfrak{o}_1}(O_{\mathfrak{o}_1}) + \boldsymbol{q}^{*}_{\mathfrak{o}_1/0} \boldsymbol{W}^{\mathfrak{o}_1}_{\mathrm{act},1}(O_0) \boldsymbol{q}_{\mathfrak{o}_1/0} - \boldsymbol{q}_{1/\mathfrak{o}_1} \boldsymbol{W}^{\mathfrak{o}_2}_{\mathrm{act},2}(O_1) \boldsymbol{q}^{*}_{1/\mathfrak{o}_1} \\ -\boldsymbol{\omega}^{\mathfrak{o}_2}_{\mathfrak{o}_2/\mathrm{I}} \times \left(M_{\mathfrak{o}_2} \star (\boldsymbol{\omega}^{\mathfrak{o}_2}_{\mathfrak{o}_2/\mathrm{I}})^{\mathsf{s}} \right) + \boldsymbol{W}^{\mathfrak{o}_2}_{\mathfrak{o}_2}(O_{\mathfrak{o}_2}) + \boldsymbol{q}^{*}_{\mathfrak{o}_2/1} \boldsymbol{W}^{\mathfrak{o}_2}_{\mathrm{act},2}(O_1) \boldsymbol{q}_{\mathfrak{o}_2/1} - \boldsymbol{q}_{2/\mathfrak{o}_2} \boldsymbol{W}^{\mathfrak{o}_3}_{\mathrm{act},3}(O_2) \boldsymbol{q}^{*}_{2/\mathfrak{o}_2} \\ -\boldsymbol{\omega}^{\mathfrak{o}_3}_{\mathfrak{o}_3/\mathrm{I}} \times \left(M_{\mathfrak{o}_3} \star (\boldsymbol{\omega}^{\mathfrak{o}_3}_{\mathfrak{o}_3/\mathrm{I}})^{\mathsf{s}} \right) + \boldsymbol{W}^{\mathfrak{o}_3}_{\mathfrak{o}_3}(O_{\mathfrak{o}_3}) + \boldsymbol{q}^{*}_{\mathfrak{o}_3/2} \boldsymbol{W}^{\mathfrak{o}_3}_{\mathrm{act},3}(O_2) \boldsymbol{q}_{\mathfrak{o}_3/2} + \boldsymbol{q}_{\mathrm{G}/\mathfrak{o}_3} \boldsymbol{W}^{\mathrm{G}}_{\mathrm{ext}}(O_{\mathrm{G}}) \boldsymbol{q}^{*}_{\mathrm{G}/\mathfrak{o}_3} \end{bmatrix}, \quad (5.136)$$

and

$$\boldsymbol{\mathcal{B}}_2 = \begin{bmatrix} \boldsymbol{E}_{145} \boldsymbol{q}^{*}_{0/\mathfrak{o}_0} \left(\boldsymbol{\omega}^{\mathfrak{o}_0}_{\mathfrak{o}_0/\mathrm{I}} \times \boldsymbol{\omega}^{\mathfrak{o}_0}_{0/\mathfrak{o}_0} \right) \boldsymbol{q}_{0/\mathfrak{o}_0} \\ \boldsymbol{E}_{145} \boldsymbol{q}^{*}_{1/\mathfrak{o}_1} \left(\boldsymbol{\omega}^{\mathfrak{o}_1}_{\mathfrak{o}_1/\mathrm{I}} \times \boldsymbol{\omega}^{\mathfrak{o}_1}_{1/\mathfrak{o}_1} \right) \boldsymbol{q}_{1/\mathfrak{o}_1} \\ \boldsymbol{E}_{145} \boldsymbol{q}^{*}_{2/\mathfrak{o}_2} \left(\boldsymbol{\omega}^{\mathfrak{o}_2}_{\mathfrak{o}_2/\mathrm{I}} \times \boldsymbol{\omega}^{\mathfrak{o}_2}_{2/\mathfrak{o}_2} \right) \boldsymbol{q}_{2/\mathfrak{o}_2} \end{bmatrix}. \quad (5.137)$$

Finally, since $\boldsymbol{\mathcal{S}}_{11}$ is always invertible we can avoid inverting $\boldsymbol{\mathcal{S}}$, which is a large matrix. Through algebraic manipulation of the system given in equation (5.130), and using the fact that $\boldsymbol{\mathcal{S}}_{22} = 0_{15\times 15}$, we can determine the following relationships:

$$\boldsymbol{\mathcal{T}} = (\boldsymbol{\mathcal{S}}_{21} \boldsymbol{\mathcal{S}}_{11}^{-1} \boldsymbol{\mathcal{S}}_{12})^{-1} (\boldsymbol{\mathcal{S}}_{21} \boldsymbol{\mathcal{S}}_{11}^{-1} \boldsymbol{\mathcal{B}}_1 - \boldsymbol{\mathcal{B}}_2), \quad (5.138)$$

$$\dot{\boldsymbol{y}} = -\boldsymbol{\mathcal{S}}_{11}^{-1} \boldsymbol{\mathcal{S}}_{12} \boldsymbol{\mathcal{T}} + \boldsymbol{\mathcal{S}}_{11}^{-1} \boldsymbol{\mathcal{B}}_1 = -\boldsymbol{\mathcal{S}}_{11}^{-1} \boldsymbol{\mathcal{S}}_{12} (\boldsymbol{\mathcal{S}}_{21} \boldsymbol{\mathcal{S}}_{11}^{-1} \boldsymbol{\mathcal{S}}_{12})^{-1} (\boldsymbol{\mathcal{S}}_{21} \boldsymbol{\mathcal{S}}_{11}^{-1} \boldsymbol{\mathcal{B}}_1 - \boldsymbol{\mathcal{B}}_2) + \boldsymbol{\mathcal{S}}_{11}^{-1} \boldsymbol{\mathcal{B}}_1. \quad (5.139)$$

5.3 Results

To ensure that the model described in Section 5.2 is valid, a simple simulation was run using MATLAB R2017a's ODE45. The integrator's option AbsTol (absolute tolerance)

was set to 1×10^{-14} and RelTol (relative tolerance) was set to 2.220×10^{-14}; the final time was set to $t_f = 70$ s. To evaluate center of mass, linear momentum, and angular momentum conservation, only internal (joint) wrenches were applied. The generalized forces, which correspond to the non-zero components of the actuation wrenches described in equation (5.50),

$$\begin{aligned}
\boldsymbol{W}^{\circ_1}_{\text{act},1}(O_0) &= \mathsf{0} + \epsilon(0, [0, 0, (\bar{\tau}_{\text{act},1})_z]^{\mathrm{T}}), \\
\boldsymbol{W}^{\circ_2}_{\text{act},2}(O_1) &= \mathsf{0} + \epsilon(0, [0, 0, (\bar{\tau}_{\text{act},2})_z]^{\mathrm{T}}), \\
\boldsymbol{W}^{\circ_3}_{\text{act},3}(O_2) &= \mathsf{0} + \epsilon(0, [0, 0, (\bar{\tau}_{\text{act},3})_z]^{\mathrm{T}}),
\end{aligned} \tag{5.140}$$

were set to

$$\begin{aligned}
(\bar{\tau}_{\text{act},1})_z &= \begin{cases} 0.5 \sin(t-2)\ \text{N}, & 2\ \text{s} < t < 5\ \text{s}, \\ 0, & \text{otherwise}, \end{cases} \\
(\bar{\tau}_{\text{act},2})_z &= \begin{cases} 0.5 \sin(t-10)\ \text{N}, & 10\ \text{s} < t < 12\ \text{s}, \\ 0, & \text{otherwise}, \end{cases} \\
(\bar{\tau}_{\text{act},3})_z &= \begin{cases} 0.5 \sin(t-20)\ \text{N}, & 20\ \text{s} < t < 22\ \text{s}, \\ 0, & \text{otherwise}. \end{cases}
\end{aligned} \tag{5.141}$$

The deviation of the center of mass of the system with respect to its initial position is shown in Figure 5.3. The total kinetic energy of the system is shown in Figure 5.4, and the condition number for matrix $\boldsymbol{\mathcal{S}}$, used in equation (5.108), is plotted in Figure 5.5 for every evaluation of the dynamics.

Next, the numerical performance differences between the dual quaternion approach (DQ), and the decoupled formulation (Decoupled) of the dynamics described at the beginning of this chapter, were evaluated for the same set of inputs. Figure 5.6 shows the comparison between the norm of the change of the center of mass of the system with respect to its initial position as a function of time. Next, the conservation of the linear and

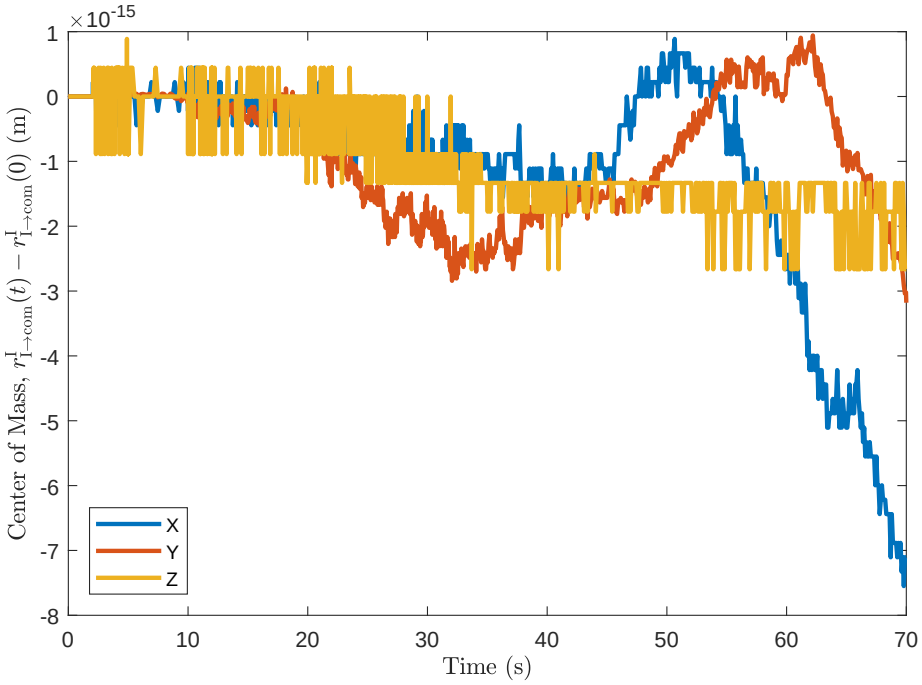

Figure 5.3: Center of mass deviation from initial position.

angular momenta of both systems is compared as shown in Figures 5.7 and 5.8. As expected, the dual quaternion formulation possesses a numerical advantage since they more naturally account for the coupling between the rigid bodies' translational and rotational motion.

However, the performance decays when discontinuous inputs are applied. A simulation was run with discontinuous inputs given by

$$
\begin{aligned}
(\bar{\tau}_{\text{act},1})_z &= \begin{cases} 0.5 \text{ N}, & 2 \text{ s} < t < 5 \text{ s}, \\ 0, & \text{otherwise}, \end{cases} \\
(\bar{\tau}_{\text{act},2})_z &= \begin{cases} 0.5 \text{ N}, & 10 \text{ s} < t < 12 \text{ s}, \\ 0, & \text{otherwise}, \end{cases} \\
(\bar{\tau}_{\text{act},3})_z &= \begin{cases} 0.5 \text{ N}, & 20 \text{ s} < t < 22 \text{ s}, \\ 0, & \text{otherwise}. \end{cases}
\end{aligned}
\tag{5.142}
$$

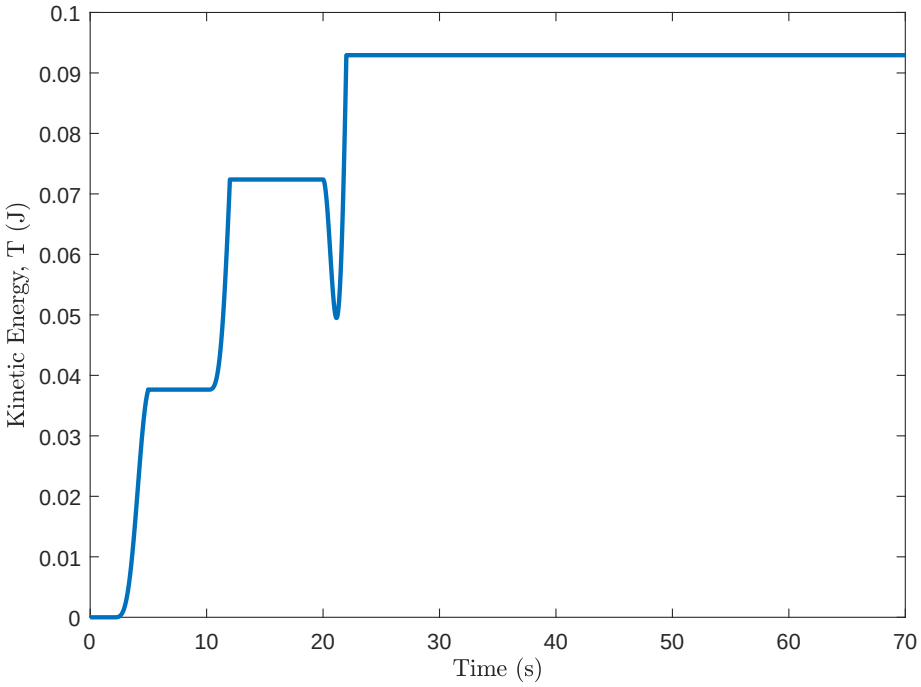

Figure 5.4: Kinetic energy of the system.

Analogous to the previous scenario, Figures 5.9 to 5.11 show the conservation of the location of the center of mass, linear momentum, and angular momentum. In this case we observe that the dual quaternion framework does not provide an advantage over the decoupled formulation. This is expected since the dual quaternion framework must enforce two constraints. This is more manageable by the integrator with continuous inputs such as those described in equation (5.141). Integration of systems evolving on manifolds is not a trivial task. For this reason, variational integrators may be proposed. In particular, the approaches in [143, 144] for multibody systems and in [145] for dual quaternion rigid body motion (or [146] for a similar approach in the context of rotational motion) are highly relevant to address the issues of numerical performance.

In order to compare the time impact in performance associated to using the dual quaternion formulation, 100 simulations with the control sequence provided in equation (5.141) were run with different absolute and relative tolerance levels. Table 5.2 shows a summary of the results when the comparisons are run in MATLAB's native ODE45 solver, while

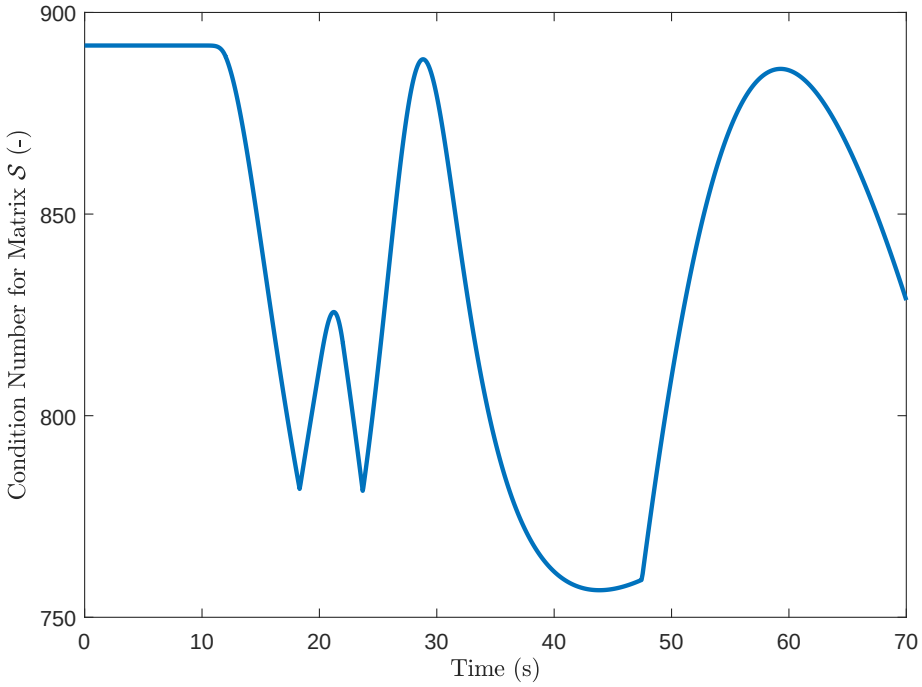

Figure 5.5: Condition number of $\boldsymbol{\mathcal{S}}$.

Table 5.3 shows the run times when these simulations are performed using the SIMULINK environment with ODE45 as the solver.

Table 5.2: Average and variance of run times for 100 simulations for two different dynamics formulations using MATLAB.

Tolerance	Average Time Decoupled (s)	Average Time DQ (s)	Percentage Increase	Variance Time Decoupled (s)	Variance Time DQ (s)
10^{-9}	8.173e-01	9.171e-01	12.21	4.157e-05	4.603e-05
10^{-10}	1.098e+00	1.254e+00	14.24	2.884e-05	2.957e-05
10^{-11}	1.543e+00	1.738e+00	12.68	4.480e-05	6.865e-05
10^{-12}	2.081e+00	2.537e+00	21.89	9.763e-05	7.187e-05
10^{-13}	3.082e+00	3.605e+00	16.99	1.806e-04	3.901e-04

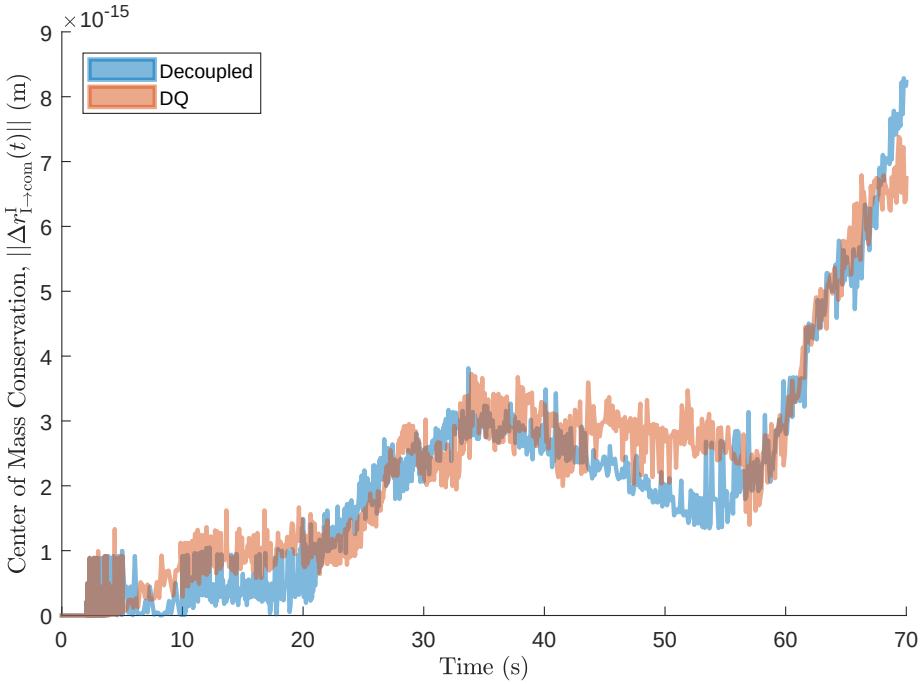

Figure 5.6: Movement of the center of mass of the system as a function of time with respect to position at $t = 0$ s.

Table 5.3: Average and variance of run times for 100 simulations for two different dynamics formulations using SIMULINK.

Tolerance	Average Time Decoupled (s)	Average Time DQ (s)	Percentage Increase	Variance Time Decoupled (s)	Variance Time DQ (s)
10^{-9}	2.115e-01	2.426e-01	14.69	2.953e-03	2.232e-04
10^{-10}	2.120e-01	2.792e-01	31.65	1.042e-04	2.069e-04
10^{-11}	2.468e-01	3.283e-01	33.03	1.059e-04	2.182e-04
10^{-12}	2.850e-01	4.184e-01	46.83	1.225e-04	1.422e-03
10^{-13}	3.554e-01	5.350e-01	50.55	1.350e-04	2.052e-04

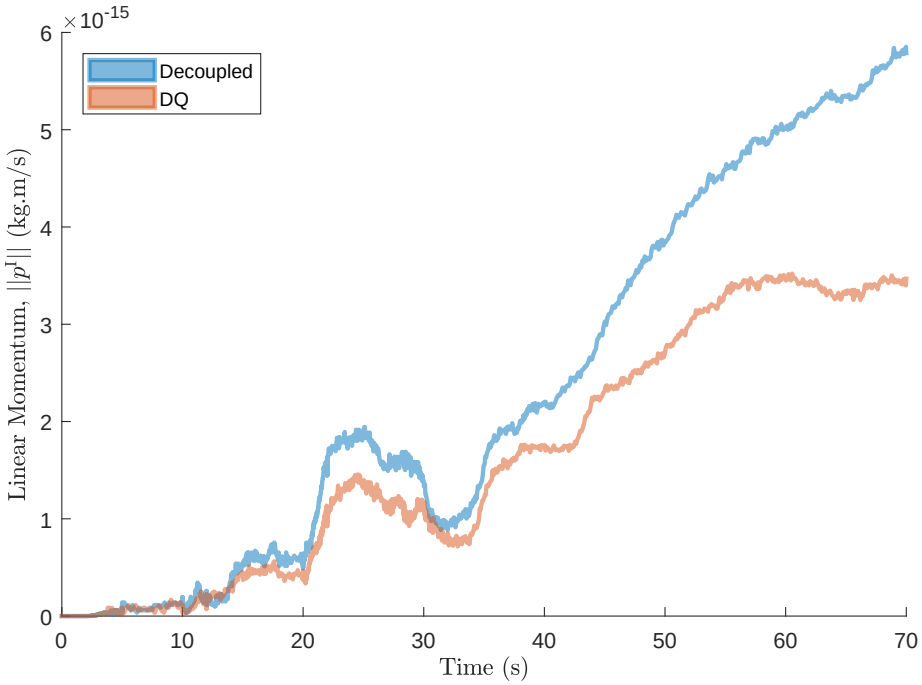

Figure 5.7: Linear momentum comparison between decoupled and dual quaternion formulation.

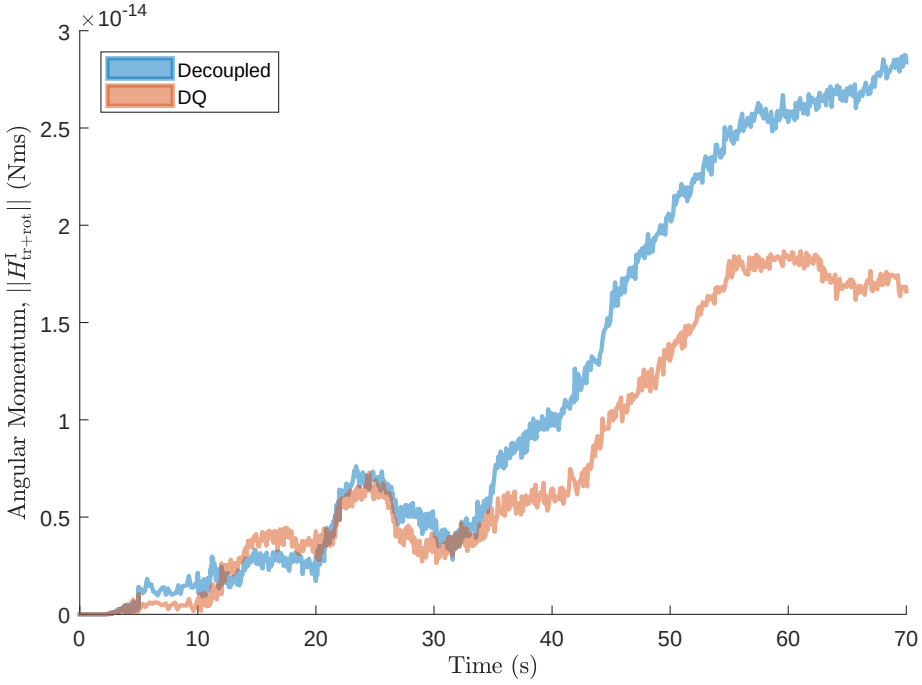

Figure 5.8: Angular momentum comparison between decoupled and dual quaternion formulation.

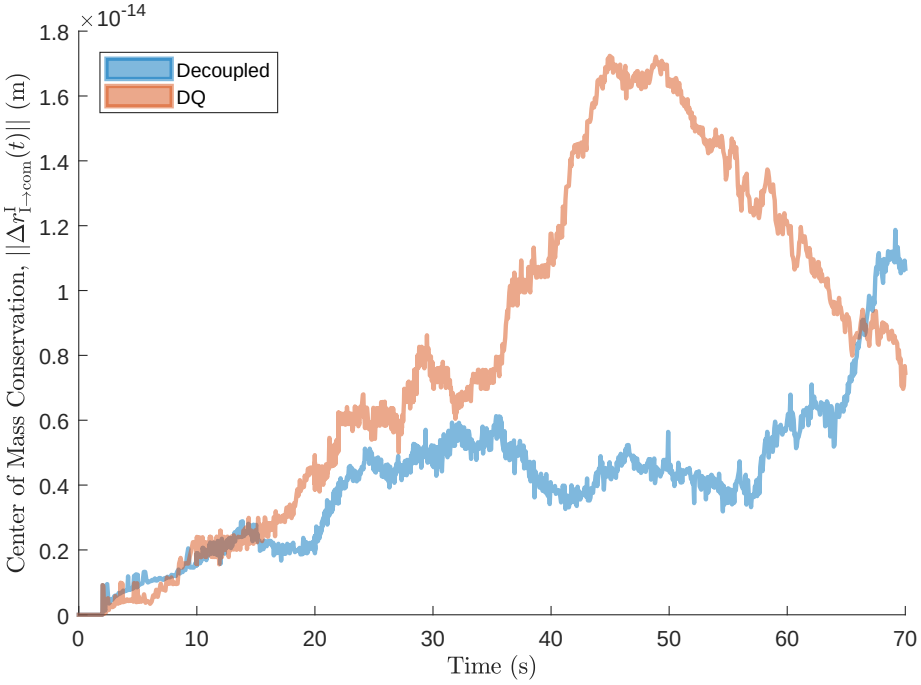

Figure 5.9: Movement of the center of mass of the system as a function of time with respect to position at $t = 0$ s for discontinuous inputs.

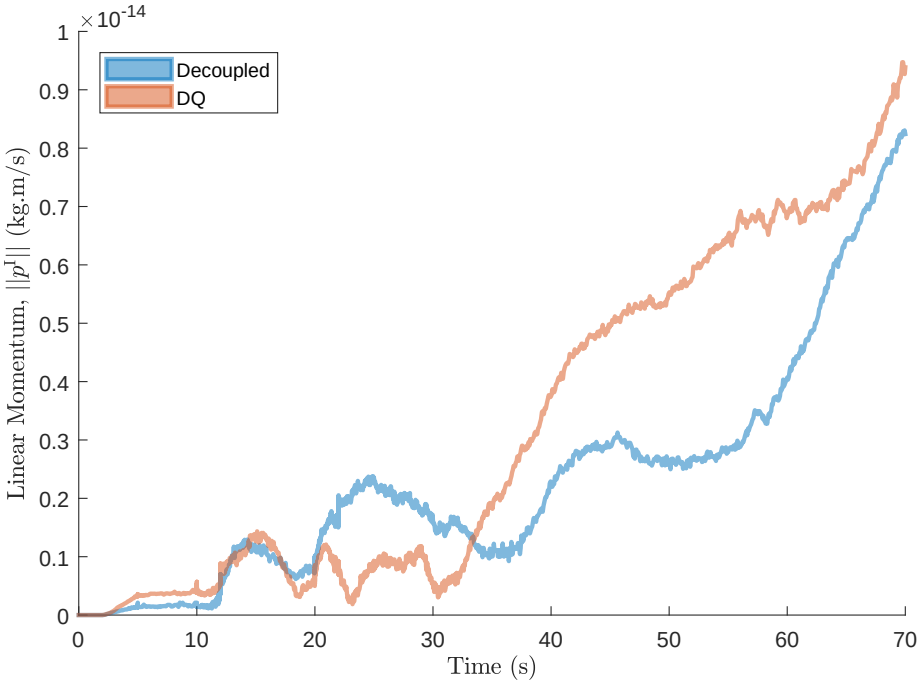

Figure 5.10: Linear momentum comparison between decoupled and dual quaternion formulation for discontinuous inputs.

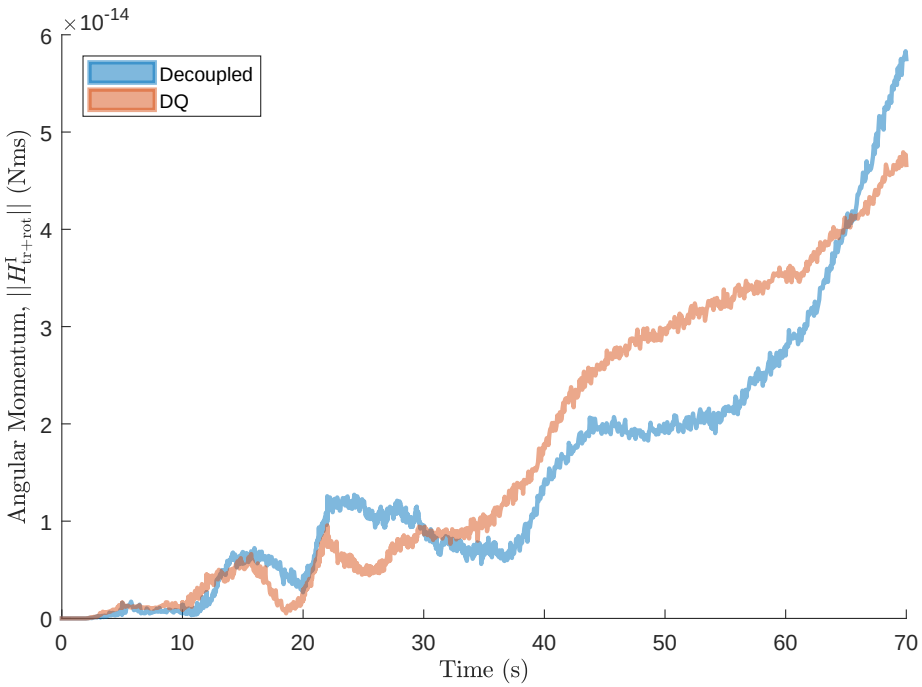

Figure 5.11: Angular momentum comparison between decoupled and dual quaternion formulation for discontinuous inputs.

CHAPTER 6
DYNAMICS FRAMEWORK GENERALIZATION

This chapter aims to provide a generalized dual quaternion framework to model kinematics and dynamics of spacecraft-mounted multibody systems. The framework expands upon the approach introduced in Chapter 5 for joints of the following types:

1. Revolute (R)
2. Prismatic (P)
3. Spherical (S)
4. Cylindrical (C)
5. Cartesian (U).

The approach is aimed towards characterizing spacecraft with one or more serial robotic arms having varying lengths. The framework, in fact, will hold for robotic arms that branch out themselves, while preserving a rooted tree structure, with the satellite base being the root.

As in previous sections, we will use roman variables for frames, subscripts and superscripts of physical quantities. We will use standard math font for the labeling of physical components, like bodies and joints. For example, body i will have its center of mass at $\mathbf{o}_\mathrm{i}$.

6.1 Variable Definition and Conventions

We will model the spacecraft as a graph $\mathcal{G}(v, e)$, where v is the number of vertices, and e represents the number of edges. This graph, in particular, will correspond to that of a directed and rooted tree with arborescent branching, that is, a graph with tree structure where direction of the edges matters, and these in general point away from the root.

For our specific application, the nodes of the graph will be the different rigid bodies composing the serial manipulator(s), and the edges will be the different joints of the manipulator(s). Figure 6.1 shows an example of the labeling for the different rigid bodies composing a two-arm configuration on a satellite. The same configuration is shown in Figure 6.2 with the labeling of the vertices (nodes) and edges accordingly. As is common in

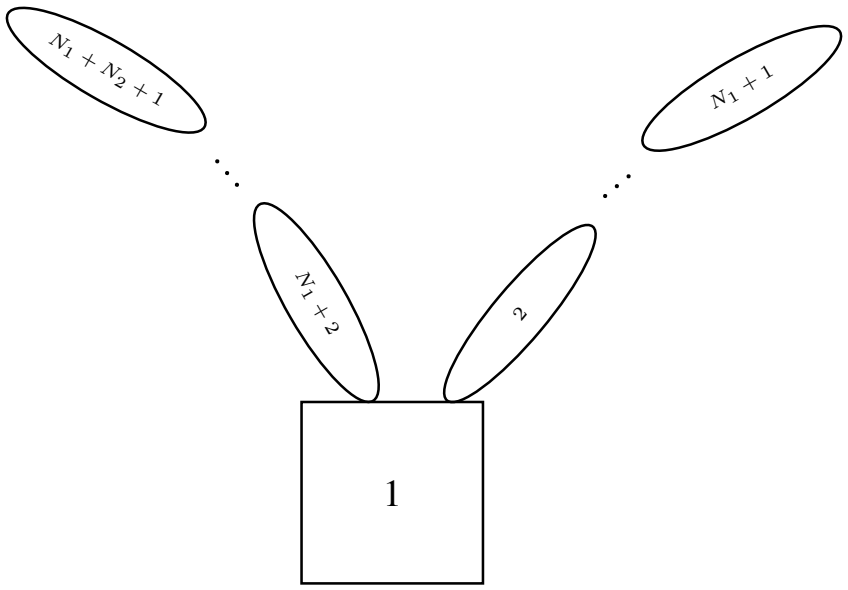

Figure 6.1: Spacecraft configuration with robotic arms of arbitrary length. Rigid body numbering shown.

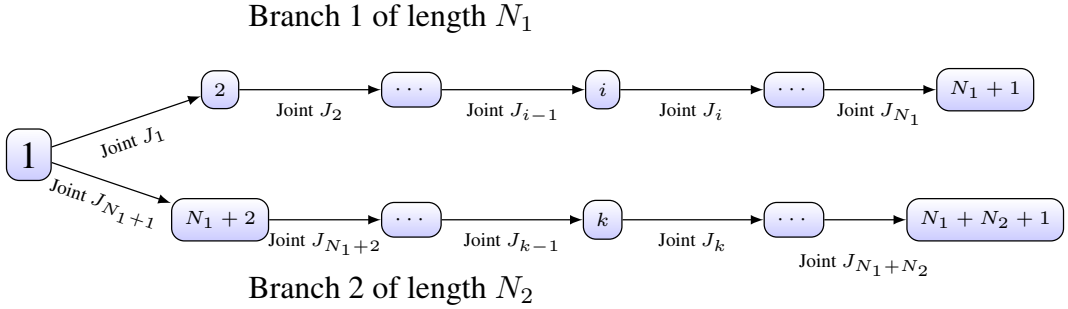

Figure 6.2: Tree structure representation of robotic satellite with two arms of lengths N_1 and N_2 showing joint labeling.

graph theory, matrices will aid in the description of the system's topology. Two matrices will be particularly useful in this generalization: the incidence matrix, denoted by C, and

the branch termination vector, denoted as B. The incidence matrix contains information about the connectivity between the joints and the bodies. The columns of the incidence matrix represent rigid bodies, while the rows represent joints. Thus, entry C_{ij} indicates the relationship between joint i and rigid body j as follows

$$(C)_{i,j} = c_{ij} \triangleq \begin{cases} 1, & \text{if joint } i \text{ is proximal, body } j \text{ is distal,} \\ 0, & \text{if joint } i \text{ is not connected to body } j, \\ -1, & \text{if joint } i \text{ is distal, body } j \text{ is proximal,} \end{cases} \tag{6.1}$$

where the relative positions are with respect to the satellite base.

The branch termination vector, B denotes whether the given body is the end of a branch. The body will most likely be an end-effector and external wrenches due to interaction with the environment may be applied on it. We define the vector B as

$$(B)_i = b_i \triangleq \begin{cases} 1, & \text{if body } i \text{ ends a branch,} \\ 0, & \text{otherwise.} \end{cases} \tag{6.2}$$

We will define the functions $N(\cdot), P(\cdot)$ as follows. Given a row or column of matrix C, or vector B, they output the indices of the "-1" entries, and the indices of the "+1" entries, respectively. Additionally, we will use the notation $C(:, j)$ to identify the j-th column of C, $C(i, :)$ to identify the i-th row of matrix C. It is worth emphasizing that each row will contain exactly one "-1" entry and exactly one "+1" entry, although, in general, columns can have several "-1" or "1" entries[1].

Example 2. The incidence and branch termination matrices for the architecture shown in

[1]The column corresponding to the satellite base will only have "-1" values, since no joint is proximal. The columns corresponding to end-effector bodies will only possess "+1" values since end-effectors are all distal with respect to their corresponding joint.

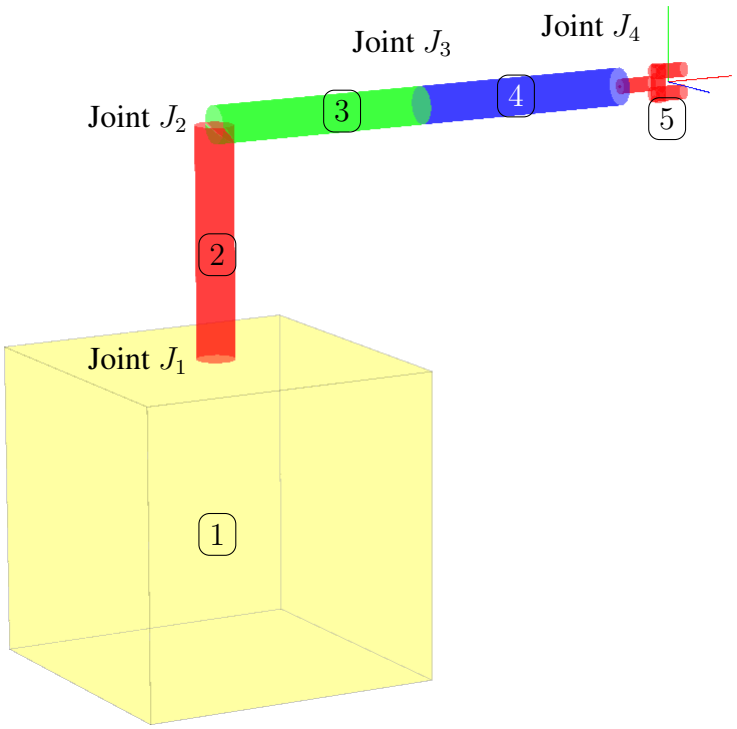

Figure 6.3: Robotic arm configuration on a satellite base.

Figure 6.3 are given by

$$C = \begin{array}{c} \\ \text{Joint } J_1 \\ \text{Joint } J_2 \\ \text{Joint } J_3 \\ \text{Joint } J_4 \end{array} \begin{array}{c} \begin{array}{ccccc} \boxed{1} & \boxed{2} & \boxed{3} & \boxed{4} & \boxed{5} \end{array} \\ \begin{bmatrix} -1 & 1 & 0 & 0 & 0 \\ 0 & -1 & 1 & 0 & 0 \\ 0 & 0 & -1 & 1 & 0 \\ 0 & 0 & 0 & -1 & 1 \end{bmatrix} \end{array} \tag{6.3}$$

$$B = \begin{matrix} \textcircled{1} \\ \textcircled{2} \\ \textcircled{3} \\ \textcircled{4} \\ \textcircled{5} \end{matrix} \begin{bmatrix} 0 \\ 0 \\ 0 \\ 0 \\ 1 \end{bmatrix}. \tag{6.4}$$

As example of the usage of the functions $N(\cdot)$ and $P(\cdot)$, we have

$$N(C(1,:)) = N(\text{row 1 of matrix C}) = \{1\}, \tag{6.5}$$

$$P(C(1,:)) = P(\text{row 1 of matrix C}) = \{2\}, \tag{6.6}$$

$$P(B) = P(\text{vector } B) = \{5\}. \tag{6.7}$$

Let N_i be the length of branch i, d_i be the degrees of freedom of joint J_i, J the total number of joints, and B the total number of rigid bodies. Therefore, $\mathrm{B} = 1 + \mathrm{J}$, and $\mathrm{J} = \sum_{i \in \text{Branches}} N_i$. Using this notation, matrix $C \in \mathbb{R}^{\mathrm{J}\times\mathrm{B}}$ and vector $B \in \mathbb{R}^{\mathrm{B}}$. We will define D as the total number of degrees of freedom added by the joints, which can be computed as $\mathrm{D} = \sum_{i \in \text{Joints}} d_i$. Exploiting the duality between degrees of freedom at a joint, d_i, and the dimensionality of the reaction wrench, r_i, we will define $\mathrm{R} = \sum_{i \in \text{Joints}} r_i = \sum_{i \in \text{Joints}} 6 - d_i$.

The vector $\boldsymbol{y} \in \mathbb{R}^{8\mathrm{B}}$ is defined as the collection of dual velocities, given by

$$\boldsymbol{y} \triangleq \begin{bmatrix} \boldsymbol{\omega}^{\circ_1}_{\circ_1/I} \\ \vdots \\ \boldsymbol{\omega}^{\circ_i}_{\circ_i/I} \\ \vdots \\ \boldsymbol{\omega}^{\circ_B}_{\circ_B/I} \end{bmatrix}. \tag{6.8}$$

The vector of generalized coordinates $\Gamma \in \mathbb{R}^{\mathrm{D}}$ represents the generalized coordinates of

the joints and it is defined as

$$\Gamma \triangleq \begin{bmatrix} \Gamma_{\mathrm{J_1}} \\ \vdots \\ \Gamma_{\mathrm{J_i}} \\ \vdots \\ \Gamma_{\mathrm{J_J}} \end{bmatrix}, \tag{6.9}$$

where the form of $\Gamma_{\mathrm{J_i}}$ is dependent upon the type of joint J_i. Table 6.1 lists the parametrization used for each type of joint. Here it is worth noting that the generalized coordinates parametrize the motion of the i frame (fixed to the distal body with respect to the joint) with respect to the proximal body, which is captured by the index k, where $k = N(C(i,:))$. In particular, S joints are modeled with an Eulerian 3-2-1 (yaw ψ, pitch θ, roll ϕ) rotation

Table 6.1: Generalized coordinates $\Gamma_{\mathrm{J_i}}$ for joint J_i depending on its type.

Joint Type	Generalized Coordinate Parametrization	d_i (DOF)
R	$\theta_{\mathrm{i/o_k}} \in \mathbb{R}^1$	1
P	$z_{\mathrm{i/o_k}} \in \mathbb{R}^1$	1
S	$[\phi_{\mathrm{i/o_k}}, \theta_{\mathrm{i/o_k}}, \psi_{\mathrm{i/o_k}}]^{\mathrm{T}} \in \mathbb{R}^3$	3
C	$[\theta_{\mathrm{i/o_k}}, z_{\mathrm{i/o_k}}]^{\mathrm{T}} \in \mathbb{R}^2$	2
U	$[x_{\mathrm{i/o_k}}, y_{\mathrm{i/o_k}}, z_{\mathrm{i/o_k}}]^{\mathrm{T}} \in \mathbb{R}^3$	3
$k = N(C(i,:))$		

sequence.

Thus, the state vector for any given spacecraft-robotic arm configuration will be given by

$$\boldsymbol{x} \triangleq \begin{bmatrix} \boldsymbol{q}_{\mathrm{o_1/I}} \\ \Gamma \\ \boldsymbol{y} \end{bmatrix}, \tag{6.10}$$

where $\boldsymbol{q}_{\mathrm{o_1/I}} \in \mathbb{H}_d$ is the pose of the base.

Figure 6.4 shows joint J_i with its associated frame i; the frame $\mathrm{o_{i+1}}$, which has the same

orientation as frame i but its origin is at the center of mass of body $i+1$; and the frame at the center of mass of the proximal body denoted by $\mathfrak{o}_{\mathrm{k}}$, where $k = N(C(i,:))$. The origin of the i frame is positioned at the physical interface between the two adjoining bodies. Figure 6.4 also shows three types of wrenches. The reaction and actuation wrenches appear at the joint, with their point of application being the origin of the joint frame O_{i}, and their coordinates expressed in the i frame. We additionally show the body wrench $\boldsymbol{W}^{\mathfrak{o}_{\mathrm{i+1}}}_{\mathfrak{o}_{\mathrm{i+1}}}(O_{\mathfrak{o}_{\mathrm{i+1}}})$. Joint actuation wrenches $\boldsymbol{W}^{\mathrm{i}}_{\mathrm{act,i}}(O_{\mathrm{i}})$ induce motion about the degrees of freedom of the joint. Reaction wrenches $\boldsymbol{W}^{\mathrm{i}}_{\mathrm{i+1/k}}(O_{\mathrm{i}})$ arise due to physical constraints at the joints, and they are dual in nature to the joint actuation wrenches. Body wrenches, which are assumed to act at the center of mass of the body, come from control sources or other natural phenomena such as gravitational effects, or atmospheric drag. It will be assumed that the degrees of

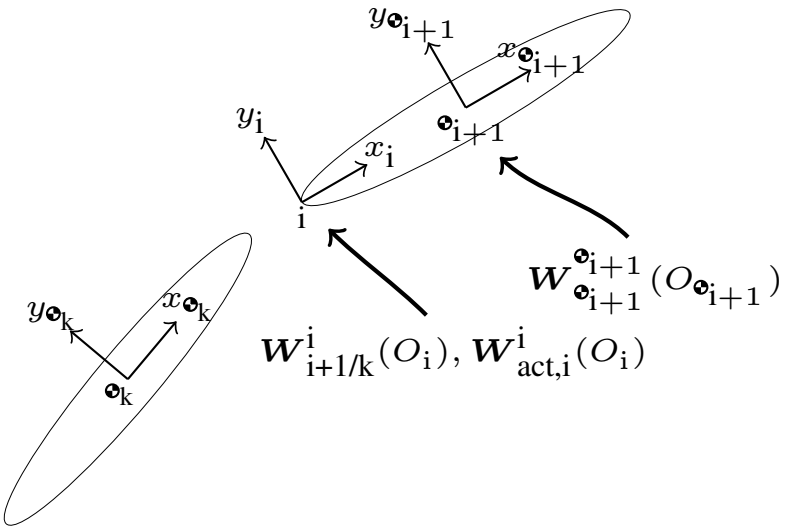

Figure 6.4: Body frame labeling and wrench definition at joint J_i between bodies $i+1$ and $k = N(C(i,:))$.

freedom of the joints are along the Z_{i}-axis, which is a common assumption in the field of robotics, while the X_{i} and Y_{i} axes can be selected according to any predetermined set of rules, such as those laid out in Chapter 5 of [121]. The exceptions are the universal and spherical joints, both of which have three degrees of freedom, and for which an orientation of the axes must be assumed a priori. For the cartesian joint, the local coordinate system is

defined such that it is parallel to the physical axes of motion. For the spherical joint, one suggestion is to define the X_{i} pointing towards the $i+1^{\mathrm{th}}$ rigid body, while the Y_{i} and Z_{i} complete the orthogonal axis system.

We will define $\boldsymbol{\mathcal{T}} \in \mathbb{R}^{\mathrm{R}}$, the collection of reduced reaction wrenches, as

$$\boldsymbol{\mathcal{T}} \triangleq \begin{bmatrix} \tilde{\boldsymbol{W}}^{1}_{2/1}(O_1) \\ \vdots \\ \tilde{\boldsymbol{W}}^{\mathrm{i}}_{\mathrm{i+1/N(C(i,:))}}(O_{\mathrm{i}}) \\ \tilde{\boldsymbol{W}}^{\mathrm{i+1}}_{\mathrm{i+2/N(C(i+1,:))}}(O_{\mathrm{i+1}}) \\ \vdots \\ \tilde{\boldsymbol{W}}^{\mathrm{B}}_{\mathrm{B+1/N(C(B,:))}}(O_{\mathrm{B}}) \end{bmatrix}, \tag{6.11}$$

where $\tilde{\boldsymbol{W}}^{\mathrm{i}}_{\mathrm{i+1/N(C(i,:))}} \in \mathbb{R}^{r_i}$ is obtained from $\boldsymbol{W}^{\mathrm{i}}_{\mathrm{i+1/N(C(i,:))}} \in \mathbb{H}_d$ by eliminating the entries that correspond to the generalized coordinate of the joint, since there are no reaction forces or torques applied on the bodies about that generalized coordinate. In general, we can obtain $\tilde{\boldsymbol{W}}^{\mathrm{i}}_{\mathrm{i+1/N(C(i,:))}}$ from $\boldsymbol{W}^{\mathrm{i}}_{\mathrm{i+1/N(C(i,:))}}$ using the relationship $\boldsymbol{W}^{\mathrm{i}}_{\mathrm{i+1/N(C(i,:))}} = V_i \tilde{\boldsymbol{W}}^{\mathrm{i}}_{\mathrm{i+1/N(C(i,:))}}$, the form of the matrix $V_i \in \mathbb{R}^{8\times r_i}$ depending on the type of joint. Table 6.2 lists the general wrench $\boldsymbol{W}^{\mathrm{i}}_{\mathrm{i+1/N(C(i,:))}}$, the reduced wrench $\tilde{\boldsymbol{W}}^{\mathrm{i}}_{\mathrm{i+1/N(C(i,:))}}$, and the mapping matrix V_i for each of the joints considered. The matrix $\boldsymbol{E}_{\pi(1,2,3,4,5,6,7,8;i)}$ is formed by removing rows $\pi(1,2,3,4,5,6,7,8;i)$

Table 6.2: Form of reduced reaction wrenches for different joint types.

Joint Type	$\boldsymbol{W}^{\mathrm{i}}_{\mathrm{i+1/i}}$	$\tilde{\boldsymbol{W}}^{\mathrm{i}}_{\mathrm{i+1/i}}$	V_i	Λ_i
R	$(0,[f_x,f_y,f_z]^{\mathrm{T}}) + \epsilon(0,[\tau_x,\tau_y,0]^{\mathrm{T}})$	$[f_x,f_y,f_z,\tau_x,\tau_y]^{\mathrm{T}}$	$\boldsymbol{E}^{\mathrm{T}}_{158}$	$\boldsymbol{E}_{145}$
P	$(0,[f_x,f_y,0]^{\mathrm{T}}) + \epsilon(0,[\tau_x,\tau_y,\tau_z]^{\mathrm{T}})$	$[f_x,f_y,\tau_x,\tau_y,\tau_z]^{\mathrm{T}}$	$\boldsymbol{E}^{\mathrm{T}}_{145}$	$\boldsymbol{E}_{158}$
S	$(0,[f_x,f_y,f_z]^{\mathrm{T}}) + \epsilon(0,[0,0,0]^{\mathrm{T}})$	$[f_x,f_y,f_z]^{\mathrm{T}}$	$\boldsymbol{E}^{\mathrm{T}}_{15678}$	$\boldsymbol{E}_{12345}$
C	$(0,[f_x,f_y,0]^{\mathrm{T}}) + \epsilon(0,[\tau_x,\tau_y,0]^{\mathrm{T}})$	$[f_x,f_y,\tau_x,\tau_y]^{\mathrm{T}}$	$\boldsymbol{E}^{\mathrm{T}}_{1458}$	$\boldsymbol{E}_{1458}$
U	$(0,[0,0,0]^{\mathrm{T}}) + \epsilon(0,[\tau_x,\tau_y,\tau_z]^{\mathrm{T}})$	$[\tau_x,\tau_y,\tau_z]^{\mathrm{T}}$	$\boldsymbol{E}^{\mathrm{T}}_{12345}$	$\boldsymbol{E}_{15678}$

from the eight-by-eight identity matrix, $\mathbb{I}_8$. The function $\pi(\cdot;i)$ selects an ordered subset of $\{1,2,3,4,5,6,7,8\}$ based on the type of joint i. The matrices Λ_i are provided for compact-

ness, as they will be used in a future section as a way of eliminating a degree of freedom from a constraint equation for a given type of joint. Also, for completion purposes, we provide the form of the actuation wrenches in Table 6.3 and its corresponding mapping matrix from reduced actuation wrenches, identified by $V_{\text{act,i}}$.

Table 6.3: Form of actuation wrenches for different joint types.

Joint Type	$\boldsymbol{W}^{\text{i}}_{\text{act,i}}$	$V_{\text{act,i}}$
R	$(0,[0,0,0]^{\text{T}}) + \epsilon(0,[0,0,\tau_z]^{\text{T}})$	$\boldsymbol{E}^{\text{T}}_{1234567}$
P	$(0,[0,0,f_z]^{\text{T}}) + \epsilon(0,[0,0,0]^{\text{T}})$	$\boldsymbol{E}^{\text{T}}_{1235678}$
S	$(0,[0,0,0]^{\text{T}}) + \epsilon(0,[\tau_x,\tau_y,\tau_z]^{\text{T}})$	$\boldsymbol{E}^{\text{T}}_{12345}$
C	$(0,[0,0,f_z]^{\text{T}}) + \epsilon(0,[0,0,\tau_z]^{\text{T}})$	$\boldsymbol{E}^{\text{T}}_{123567}$
U	$(0,[f_x,f_y,f_z]^{\text{T}}) + \epsilon(0,[0,0,0]^{\text{T}})$	$\boldsymbol{E}^{\text{T}}_{15678}$

6.2 Kinematics

The kinematics of the system are fully characterized by the kinematics of the satellite base, and the kinematics of the joint generalized coordinates. The pose of the satellite base evolves as

$$\dot{\boldsymbol{q}}_{\mathfrak{o}_1/\text{I}} = \tfrac{1}{2}\boldsymbol{q}_{\mathfrak{o}_1/\text{I}}\boldsymbol{\omega}^{\mathfrak{o}_1}_{\mathfrak{o}_1/\text{I}}. \tag{6.12}$$

The joint dual velocity expressed in joint coordinates can be determined from

$$\boldsymbol{\omega}^{\text{i}}_{\text{i}/\mathfrak{o}_\text{k}} = \boldsymbol{q}_{\mathfrak{o}_{\text{i}+1}/\text{i}}\boldsymbol{\omega}^{\mathfrak{o}_{\text{i}+1}}_{\mathfrak{o}_{\text{i}+1}/\text{I}}\boldsymbol{q}^*_{\mathfrak{o}_{\text{i}+1}/\text{i}} - \boldsymbol{q}^*_{\text{i}/\mathfrak{o}_\text{k}}\boldsymbol{\omega}^{\mathfrak{o}_\text{k}}_{\mathfrak{o}_\text{k}/\text{I}}\boldsymbol{q}_{\text{i}/\mathfrak{o}_\text{k}}, \quad k = N(C(i,:)), \tag{6.13}$$

while the generalized coordinates of the joints can be determined to evolve as

$$\dot{\Gamma}_{\text{J}_\text{i}} = L_{\text{J}_\text{i}}\boldsymbol{\omega}^{\text{i}}_{\text{i}/\mathfrak{o}_\text{k}} = L_{\text{J}_\text{i}}(\boldsymbol{q}_{\mathfrak{o}_{\text{i}+1}/\text{i}}\boldsymbol{\omega}^{\mathfrak{o}_{\text{i}+1}}_{\mathfrak{o}_{\text{i}+1}/\text{I}}\boldsymbol{q}^*_{\mathfrak{o}_{\text{i}+1}/\text{i}} - \boldsymbol{q}^*_{\text{i}/\mathfrak{o}_\text{k}}\boldsymbol{\omega}^{\mathfrak{o}_\text{k}}_{\mathfrak{o}_\text{k}/\text{I}}\boldsymbol{q}_{\text{i}/\mathfrak{o}_\text{k}}), \quad k = N(C(i,:)). \tag{6.14}$$

The matrix L_{J_i} depends on the joint type, and these are listed in Table 6.4.

Furthermore, from equation (6.13), we can derive an acceleration-level relationship at

Table 6.4: Mapping matrix from angular velocity to generalized coordinates.

Joint Type	$L_{\mathrm{J_i}}$
R	$\begin{bmatrix}0,0,0,1,0,0,0,0\end{bmatrix}$
P	$\begin{bmatrix}0,0,0,0,0,0,0,1\end{bmatrix}$
S	$\begin{bmatrix} 0 & 1 & \tan(\theta_{\mathrm{i}/\mathfrak{o}_\mathrm{k}})\sin(\phi_{\mathrm{i}/\mathfrak{o}_\mathrm{k}}) & \cos(\phi_{\mathrm{i}/\mathfrak{o}_\mathrm{k}})\tan(\theta_{\mathrm{i}/\mathfrak{o}_\mathrm{k}}) & 0 & 0 & 0 & 0 \\ 0 & 0 & \cos(\phi_{\mathrm{i}/\mathfrak{o}_\mathrm{k}}) & -\sin(\phi_{\mathrm{i}/\mathfrak{o}_\mathrm{k}}) & 0 & 0 & 0 & 0 \\ 0 & 0 & \sin(\phi_{\mathrm{i}/\mathfrak{o}_\mathrm{k}})/\cos(\theta_{\mathrm{i}/\mathfrak{o}_\mathrm{k}}) & \cos(\phi_{\mathrm{i}/\mathfrak{o}_\mathrm{k}})/\cos(\theta_{\mathrm{i}/\mathfrak{o}_\mathrm{k}}) & 0 & 0 & 0 & 0 \end{bmatrix}$
C	$\begin{bmatrix}0,0,0,1,0,0,0,0\\0,0,0,0,0,0,0,1\end{bmatrix}$
U	$\begin{bmatrix}0,0,0,0,0,0,1,0\\0,0,0,0,0,0,0,1\\0,0,0,0,0,0,0,1\end{bmatrix}$

each joint given by

$$\dot{\boldsymbol{\omega}}^{\mathrm{i}}_{\mathrm{i}/\mathfrak{o}_\mathrm{k}} = \boldsymbol{q}_{\mathfrak{o}_{\mathrm{i}+1}/\mathrm{i}}\dot{\boldsymbol{\omega}}^{\mathfrak{o}_{\mathrm{i}+1}}_{\mathfrak{o}_{\mathrm{i}+1}/\mathrm{I}}\boldsymbol{q}^*_{\mathfrak{o}_{\mathrm{i}+1}/\mathrm{i}} - \boldsymbol{q}^*_{\mathrm{i}/\mathfrak{o}_\mathrm{k}}\dot{\boldsymbol{\omega}}^{\mathfrak{o}_\mathrm{k}}_{\mathfrak{o}_\mathrm{k}/\mathrm{I}}\boldsymbol{q}_{\mathrm{i}/\mathfrak{o}_\mathrm{k}} - \boldsymbol{q}^*_{\mathrm{i}/\mathfrak{o}_\mathrm{k}}(\boldsymbol{\omega}^{\mathfrak{o}_\mathrm{k}}_{\mathfrak{o}_\mathrm{k}/\mathrm{I}} \times \boldsymbol{\omega}^{\mathfrak{o}_\mathrm{k}}_{\mathrm{i}/\mathfrak{o}_\mathrm{k}})\boldsymbol{q}_{\mathrm{i}/\mathfrak{o}_\mathrm{k}}, \quad k = N(C(i,:)), \quad (6.15)$$

resulting in

$$\mathbf{0} = \Lambda_i\boldsymbol{q}_{\mathfrak{o}_{\mathrm{i}+1}/\mathrm{i}}\dot{\boldsymbol{\omega}}^{\mathfrak{o}_{\mathrm{i}+1}}_{\mathfrak{o}_{\mathrm{i}+1}/\mathrm{I}}\boldsymbol{q}^*_{\mathfrak{o}_{\mathrm{i}+1}/\mathrm{i}} - \Lambda_i\boldsymbol{q}^*_{\mathrm{i}/\mathfrak{o}_\mathrm{k}}\dot{\boldsymbol{\omega}}^{\mathfrak{o}_\mathrm{k}}_{\mathfrak{o}_\mathrm{k}/\mathrm{I}}\boldsymbol{q}_{\mathrm{i}/\mathfrak{o}_\mathrm{k}} - \Lambda_i\boldsymbol{q}^*_{\mathrm{i}/\mathfrak{o}_\mathrm{k}}(\boldsymbol{\omega}^{\mathfrak{o}_\mathrm{k}}_{\mathfrak{o}_\mathrm{k}/\mathrm{I}} \times \boldsymbol{\omega}^{\mathfrak{o}_\mathrm{k}}_{\mathrm{i}/\mathfrak{o}_\mathrm{k}})\boldsymbol{q}_{\mathrm{i}/\mathfrak{o}_\mathrm{k}}, \quad k = N(C(i,:)), \quad (6.16)$$

where we have used the fact that $\Lambda_i\dot{\boldsymbol{\omega}}^{\mathrm{i}}_{\mathrm{i}/\mathfrak{o}_\mathrm{k}} = \mathbf{0}$, by construction of Λ_i, defined in Table 6.2.

6.3 Dynamics

We will now generalize the rigid body Newton-Euler dynamics to that of a spacecraft with multiple serial robotic manipulators. We will show that the equations of motion can be cast

in the form

$$\begin{bmatrix} \boldsymbol{\mathcal{S}}_{11} & \boldsymbol{\mathcal{S}}_{12} \\ \boldsymbol{\mathcal{S}}_{21} & \boldsymbol{\mathcal{S}}_{22} \end{bmatrix} \begin{bmatrix} \dot{\boldsymbol{y}} \\ \boldsymbol{\mathcal{T}} \end{bmatrix} = \begin{bmatrix} \boldsymbol{\mathcal{B}}_1 \\ \boldsymbol{\mathcal{B}}_2 \end{bmatrix}. \tag{6.17}$$

We will define each of the blocks $\boldsymbol{\mathcal{S}}_{11} \in \mathbb{R}^{8\mathrm{B}\times 8\mathrm{B}}$, $\boldsymbol{\mathcal{S}}_{12} \in \mathbb{R}^{8\mathrm{B}\times \mathrm{R}}$, $\boldsymbol{\mathcal{S}}_{21} \in \mathbb{R}^{\mathrm{R}\times 8\mathrm{B}}$, $\boldsymbol{\mathcal{S}}_{22} \in \mathbb{R}^{\mathrm{R}\times \mathrm{R}}$, $\boldsymbol{\mathcal{B}}_1 \in \mathbb{R}^{8\mathrm{B}}$, and $\boldsymbol{\mathcal{B}}_2 \in \mathbb{R}^{\mathrm{R}}$ independently.

The block $\boldsymbol{\mathcal{S}}_{11}$ is composed of the dual inertia matrix for each of the bodies. It is given by

$$\boldsymbol{\mathcal{S}}_{11} = \begin{bmatrix} \mathrm{H}\left(M_{\mathfrak{o}_1}\right) & & & \dots & 0_{8\times 8} \\ & \ddots & & & \vdots \\ & & \mathrm{H}\left(M_{\mathfrak{o}_\mathrm{i}}\right) & & \\ \vdots & & & \ddots & \\ 0_{8\times 8} & \dots & & & \mathrm{H}\left(M_{\mathfrak{o}_\mathrm{B}}\right) \end{bmatrix}. \tag{6.18}$$

Notice that since this matrix is block diagonal, its inverse can be easily computed as the inverse of its sub-blocks, which exist as proven in Lemma 3. Thus, in cases when there are no moving mechanical components, fluid slosh, or fuel consumption, the inverse of $\boldsymbol{\mathcal{S}}_{11}$ can be pre-computed and stored in memory to speed up computations. The block $\boldsymbol{\mathcal{S}}_{22} \in \mathbb{R}^{\mathrm{R}\times \mathrm{R}}$ represents the effect of the reaction wrenches on the constraint equations. Since wrenches do not appear in the constraint equations, this block is composed of zeros. Explicitly, this block is given by

$$\boldsymbol{\mathcal{S}}_{22} = 0_{\mathrm{R}\times \mathrm{R}}. \tag{6.19}$$

The block $\boldsymbol{\mathcal{S}}_{12} \in \mathbb{R}^{8\mathrm{B}\times \mathrm{R}}$ couples the reaction wrenches with the dynamics of each body. These wrenches initially appear on the right-hand side of the Newton-Euler equation and are moved to the left-hand side as an unknown. The point of application of the wrench and the frame of reference are shifted to the center of mass of the body for which the equation is being derived. The matrix is composed of blocks of size $(\boldsymbol{\mathcal{S}}_{12})_{ij} \in \mathbb{R}^{8\times r_j}$, corresponding

to the attachment of body i to joint j, where each of these blocks is specified as

$$(\boldsymbol{\mathcal{S}}_{12})_{ij} = \begin{cases} -\left[\!\left[\boldsymbol{q}^{*}_{\mathfrak{o}_\mathrm{i}/\mathrm{j}} \right]\!\right]_{\mathrm{L}} \left[\!\left[\boldsymbol{q}_{\mathfrak{o}_\mathrm{i}/\mathrm{j}} \right]\!\right]_{\mathrm{R}} V_j, & \text{if } c_{ji} = 1, \\ 0_{8\times r_j}, & \text{if } c_{ji} = 0, \\ \left[\!\left[\boldsymbol{q}_{\mathrm{j}/\mathfrak{o}_\mathrm{i}} \right]\!\right]_{\mathrm{L}} \left[\!\left[\boldsymbol{q}^{*}_{\mathrm{j}/\mathfrak{o}_\mathrm{i}} \right]\!\right]_{\mathrm{R}} V_j, & \text{if } c_{ji} = -1. \end{cases} \tag{6.20}$$

The form of matrix V_j depends on the type of joint as was detailed in Table 6.2. The block $\boldsymbol{\mathcal{S}}_{21} \in \mathbb{R}^{\mathrm{R}\times 8\mathrm{B}}$ introduces the dual accelerations of each body into the constraint equations. The matrix is composed of blocks $(\boldsymbol{\mathcal{S}}_{21})_{ij} \in \mathbb{R}^{r_i\times 8}$, corresponding to the constraint at joint i and its relationship with body j as described by equation (6.16). These sub-blocks are specified as

$$(\boldsymbol{\mathcal{S}}_{21})_{ij} = \begin{cases} \Lambda_i \left[\!\left[\boldsymbol{q}_{\mathfrak{o}_\mathrm{j}/\mathrm{i}} \right]\!\right]_{\mathrm{L}} \left[\!\left[\boldsymbol{q}^{*}_{\mathfrak{o}_\mathrm{j}/\mathrm{i}} \right]\!\right]_{\mathrm{R}}, & \text{if } c_{ij} = 1, \\ 0_{r_i\times 8}, & \text{if } c_{ij} = 0, \\ -\Lambda_i \left[\!\left[\boldsymbol{q}^{*}_{\mathrm{i}/\mathfrak{o}_\mathrm{j}} \right]\!\right]_{\mathrm{L}} \left[\!\left[\boldsymbol{q}_{\mathrm{i}/\mathfrak{o}_\mathrm{j}} \right]\!\right]_{\mathrm{R}}, & \text{if } c_{ij} = -1. \end{cases} \tag{6.21}$$

The form of matrix Λ_i depends on the type of joint and it is provided in Table 6.2.

The vector $\boldsymbol{\mathcal{B}}_1 \in \mathbb{R}^{8\mathrm{B}}$ corresponds to the right hand side of the Newton-Euler equation. In particular, it contains the non-linear term $\boldsymbol{\omega} \times (M \star \boldsymbol{\omega}^{\mathsf{s}})$, the known wrenches applied at the center of mass, and the wrenches due to joint actuation. If the body ends a branch, it is assumed that it can interact with the environment at a specific point in the body. This is included in $\boldsymbol{\mathcal{B}}_1$ as well through "external" wrenches. External wrenches for branch i will be assumed to act at frame $\mathrm{G_i}$, the frame assigned to the end-effector of branch-terminating body i, and they will be denoted by $\boldsymbol{W}^{\mathrm{G_i}}_{\mathrm{ext,i}}(O_{\mathrm{G_i}})$. The vector is composed of sub-vectors $(\boldsymbol{\mathcal{B}}_1)_i \in \mathbb{R}^8$ given by

$$\begin{aligned} (\boldsymbol{\mathcal{B}}_1)_i = &-\boldsymbol{\omega}^{\mathfrak{o}_\mathrm{i}}_{\mathfrak{o}_\mathrm{i}/\mathrm{I}} \times (M_{\mathfrak{o}_\mathrm{i}} \star (\boldsymbol{\omega}^{\mathfrak{o}_\mathrm{i}}_{\mathfrak{o}_\mathrm{i}/\mathrm{I}})^{\mathsf{s}}) + \boldsymbol{W}^{\mathfrak{o}_\mathrm{i}}_{\mathfrak{o}_\mathrm{i}}(O_{\mathfrak{o}_\mathrm{i}}) + b_i \boldsymbol{q}_{\mathrm{G_i}/\mathfrak{o}_\mathrm{i}} \boldsymbol{W}^{\mathrm{G_i}}_{\mathrm{ext},i}(O_{\mathrm{G_i}}) \boldsymbol{q}^{*}_{\mathrm{G_i}/\mathfrak{o}_\mathrm{i}} \\ &- \sum_{j\in N(C(:,i))} \boldsymbol{q}_{\mathrm{j}/\mathfrak{o}_\mathrm{i}} \boldsymbol{W}^{\mathrm{j}}_{\mathrm{act,j}}(O_{\mathrm{j}}) \boldsymbol{q}^{*}_{\mathrm{j}/\mathfrak{o}_\mathrm{i}} + \sum_{j\in P(C(:,i))} \boldsymbol{q}^{*}_{\mathfrak{o}_\mathrm{i}/\mathrm{j}} \boldsymbol{W}^{\mathrm{j}}_{\mathrm{act,j}}(O_{\mathrm{j}}) \boldsymbol{q}_{\mathfrak{o}_\mathrm{i}/\mathrm{j}}. \end{aligned} \tag{6.22}$$

The vector $\boldsymbol{\mathcal{B}}_2 \in \mathbb{R}^{\mathrm{R}}$ corresponds to the right-hand-side of the constraint equations for each of the joints. In particular, it contains a cross term of dual velocities that arises when taking the derivative of the dual velocity constraint to yield a dual acceleration constraint, detailed in equation (6.16). The vector is composed of sub-vectors $(\boldsymbol{\mathcal{B}}_2)_i \in \mathbb{R}^{r_i}$ given by

$$(\boldsymbol{\mathcal{B}}_2)_i = \Lambda_i \boldsymbol{q}^*_{\mathrm{i}/\mathcal{O}_\mathrm{k}} (\boldsymbol{\omega}^{\mathcal{O}_\mathrm{k}}_{\mathcal{O}_\mathrm{k}/\mathrm{I}} \times \boldsymbol{\omega}^{\mathcal{O}_\mathrm{k}}_{\mathrm{i}/\mathcal{O}_\mathrm{k}}) \boldsymbol{q}_{\mathrm{i}/\mathcal{O}_\mathrm{k}} = \Lambda_i \boldsymbol{q}^*_{\mathrm{i}/\mathcal{O}_\mathrm{k}} \boldsymbol{\omega}^{\mathcal{O}_\mathrm{k}}_{\mathcal{O}_\mathrm{k}/\mathrm{I}} \boldsymbol{q}_{\mathrm{i}/\mathcal{O}_\mathrm{k}} \times \boldsymbol{\omega}^{\mathrm{i}}_{\mathrm{i}/\mathcal{O}_\mathrm{k}}, \quad k = N(C(i,:)), \tag{6.23}$$

where in the last equality we used the invariance of the dual quaternion cross product, proven in Lemma 1.

Finally, since $\boldsymbol{\mathcal{S}}_{11}$ is always invertible and $\boldsymbol{\mathcal{S}}_{22} = 0_{\mathrm{R}\times\mathrm{R}}$, we can avoid inverting the large matrix on the left-hand-side of equation (6.17) by using the Schur complement. Thus, if

$$\boldsymbol{\mathcal{S}} \triangleq \begin{bmatrix} \boldsymbol{\mathcal{S}}_{11} & \boldsymbol{\mathcal{S}}_{12} \\ \boldsymbol{\mathcal{S}}_{21} & \boldsymbol{\mathcal{S}}_{22} \end{bmatrix} = \begin{bmatrix} \boldsymbol{\mathcal{S}}_{11} & \boldsymbol{\mathcal{S}}_{12} \\ \boldsymbol{\mathcal{S}}_{21} & 0_{\mathrm{R}\times\mathrm{R}} \end{bmatrix}, \tag{6.24}$$

we define the Schur complement of block $\boldsymbol{\mathcal{S}}_{11}$ as $\boldsymbol{\mathcal{S}}/\boldsymbol{\mathcal{S}}_{11} \triangleq -\boldsymbol{\mathcal{S}}_{21}\boldsymbol{\mathcal{S}}_{11}^{-1}\boldsymbol{\mathcal{S}}_{12}$. Therefore, the inverse of $\boldsymbol{\mathcal{S}}$ is given by

$$\boldsymbol{\mathcal{S}}^{-1} = \begin{bmatrix} \boldsymbol{\mathcal{S}}_{11}^{-1} + \boldsymbol{\mathcal{S}}_{11}^{-1}\boldsymbol{\mathcal{S}}_{12}(\boldsymbol{\mathcal{S}}/\boldsymbol{\mathcal{S}}_{11})^{-1}\boldsymbol{\mathcal{S}}_{21}\boldsymbol{\mathcal{S}}_{11}^{-1} & -\boldsymbol{\mathcal{S}}_{11}^{-1}\boldsymbol{\mathcal{S}}_{12}(\boldsymbol{\mathcal{S}}/\boldsymbol{\mathcal{S}}_{11})^{-1} \\ -(\boldsymbol{\mathcal{S}}/\boldsymbol{\mathcal{S}}_{11})^{-1}\boldsymbol{\mathcal{S}}_{21}\boldsymbol{\mathcal{S}}_{11}^{-1} & (\boldsymbol{\mathcal{S}}/\boldsymbol{\mathcal{S}}_{11})^{-1} \end{bmatrix}. \tag{6.25}$$

Hence, we can solve for the unknowns as

$$\begin{bmatrix} \dot{\boldsymbol{y}} \\ \boldsymbol{\mathcal{T}} \end{bmatrix} = \boldsymbol{\mathcal{S}}^{-1} \begin{bmatrix} \boldsymbol{\mathcal{B}}_1 \\ \boldsymbol{\mathcal{B}}_2 \end{bmatrix}, \tag{6.26}$$

which upon expansion, yields

$$\begin{aligned}\boldsymbol{\mathcal{T}} &= (\boldsymbol{\mathcal{S}}_{21}\boldsymbol{\mathcal{S}}_{11}^{-1}\boldsymbol{\mathcal{S}}_{12})^{-1}(\boldsymbol{\mathcal{S}}_{21}\boldsymbol{\mathcal{S}}_{11}^{-1}\boldsymbol{\mathcal{B}}_1 - \boldsymbol{\mathcal{B}}_2),\\ \dot{\boldsymbol{y}} &= -\boldsymbol{\mathcal{S}}_{11}^{-1}\boldsymbol{\mathcal{S}}_{12}\boldsymbol{\mathcal{T}} + \boldsymbol{\mathcal{S}}_{11}^{-1}\boldsymbol{\mathcal{B}}_1 = -\boldsymbol{\mathcal{S}}_{11}^{-1}\boldsymbol{\mathcal{S}}_{12}(\boldsymbol{\mathcal{S}}_{21}\boldsymbol{\mathcal{S}}_{11}^{-1}\boldsymbol{\mathcal{S}}_{12})^{-1}(\boldsymbol{\mathcal{S}}_{21}\boldsymbol{\mathcal{S}}_{11}^{-1}\boldsymbol{\mathcal{B}}_1 - \boldsymbol{\mathcal{B}}_2) + \boldsymbol{\mathcal{S}}_{11}^{-1}\boldsymbol{\mathcal{B}}_1.\end{aligned} \tag{6.27}$$

6.4 Locking or Prescribing Joint Motion

In some instances, it is desirable to lock a certain degree a freedom or prescribe its generalized coordinate, while still being able to determine the reaction wrenches produced by this motion. Additionally, knowledge of the required actuation wrench can provide insight into the holding torque that a given motor must provide, or exert during specific smaneuvers. A straight-forward modification of the equations provided herein can yield this information.

Let the admissible dual velocity and acceleration of the prescribed-motion for joint J_i be given by

$$\begin{aligned}\boldsymbol{\omega}^{\mathrm{i}}_{\mathrm{i}/\mathcal{O}_k} &= \boldsymbol{\omega}_{\mathrm{pres}}, \quad k = N(C(i,:)),\\ \dot{\boldsymbol{\omega}}^{\mathrm{i}}_{\mathrm{i}/\mathcal{O}_k} &= \dot{\boldsymbol{\omega}}_{\mathrm{pres}}.\end{aligned} \tag{6.28}$$

The generalized speed is still mapped as follows

$$\dot{\Gamma}_{\mathrm{J_i}} = L_{\mathrm{J_i}}\boldsymbol{\omega}^{\mathrm{i}}_{\mathrm{i}/\mathcal{O}_k}. \tag{6.29}$$

Assuming knowledge of the proximal body's dual acceleration $\dot{\boldsymbol{\omega}}^{\mathcal{O}_k}_{\mathcal{O}_k/\mathrm{I}}$, which must be solved for in tandem with all other dual accelerations and reaction wrenches, and since all velocity-level quantities are known, the distal body's dual velocity and acceleration are fully de-

scribed by the kinematic relationships

$$\text{Dual Velocity:} \quad \boldsymbol{\omega}^{\mathfrak{e}_{i+1}}_{\mathfrak{e}_{i+1}/\mathrm{I}} = \boldsymbol{q}^{*}_{\mathfrak{e}_{i+1}/\mathfrak{i}} \boldsymbol{\omega}^{\mathfrak{i}}_{\mathfrak{i}/\mathfrak{e}_k} \boldsymbol{q}_{\mathfrak{e}_{i+1}/\mathfrak{i}} + \boldsymbol{q}^{*}_{\mathfrak{e}_{i+1}/\mathfrak{e}_k} \boldsymbol{\omega}^{\mathfrak{e}_k}_{\mathfrak{e}_k/\mathrm{I}} \boldsymbol{q}_{\mathfrak{e}_{i+1}/\mathfrak{e}_k} \tag{6.30}$$

$$\text{Dual Acceleration:} \quad \dot{\boldsymbol{\omega}}^{\mathfrak{e}_{i+1}}_{\mathfrak{e}_{i+1}/\mathrm{I}} = \boldsymbol{q}^{*}_{\mathfrak{e}_{i+1}/\mathfrak{i}} \dot{\boldsymbol{\omega}}^{\mathfrak{i}}_{\mathfrak{i}/\mathfrak{e}_k} \boldsymbol{q}_{\mathfrak{e}_{i+1}/\mathfrak{i}} + \boldsymbol{q}^{*}_{\mathfrak{e}_{i+1}/\mathfrak{e}_k} (\dot{\boldsymbol{\omega}}^{\mathfrak{e}_k}_{\mathfrak{e}_k/\mathrm{I}} + \boldsymbol{\omega}^{\mathfrak{e}_k}_{\mathfrak{e}_k/\mathrm{I}} \times \boldsymbol{\omega}^{\mathfrak{e}_k}_{\mathfrak{i}/\mathfrak{e}_k}) \boldsymbol{q}_{\mathfrak{e}_{i+1}/\mathfrak{e}_k}, \tag{6.31}$$

both of which can be easily derived from equation (6.13) and equation (6.15). Since the dual acceleration $\dot{\boldsymbol{\omega}}^{\mathfrak{e}_{i+1}}_{\mathfrak{e}_{i+1}/\mathrm{I}}$ is no longer an unknown, we must remove the corresponding equations from the system of equations presented in equation (6.17). To do this, we remove $\dot{\boldsymbol{\omega}}^{\mathfrak{e}_{i+1}}_{\mathfrak{e}_{i+1}/\mathrm{I}}$ from the vector of unknowns $\dot{\boldsymbol{y}}$, and block-matrices $(\boldsymbol{\mathcal{S}}_{11})_{\{:,i+1\}}$, $(\boldsymbol{\mathcal{S}}_{\mathbf{21}})_{\{:,i+1\}}$, which are the corresponding coefficients of $\dot{\boldsymbol{\omega}}^{\mathfrak{e}_{i+1}}_{\mathfrak{e}_{i+1}/\mathrm{I}}$ that appear in both Newton-Euler, and constraint equations. For the sake of exposition, let us rename these modified variables as $\hat{\dot{\boldsymbol{y}}}$, $\hat{\boldsymbol{\mathcal{S}}}_{11}$, and $\hat{\boldsymbol{\mathcal{S}}}_{21}$.

Next, we need to manipulate the modified Newton-Euler equation for bodies $i+1$ and $k = N(C(i,:))$, since both are connected to joint J_i, to include the actuation wrench as part of the vector of unknowns. In general terms, this equation is given by

$$\boldsymbol{q}^{*}_{\mathfrak{e}_{i+1}/\mathfrak{i}} \boldsymbol{W}^{\mathfrak{i}}_{\text{act,i}}(O_{\mathfrak{i}}) \boldsymbol{q}_{\mathfrak{e}_{i+1}/\mathfrak{i}} = (\hat{\boldsymbol{\mathcal{S}}}_{11})_{\{i+1,:\}} \hat{\dot{\boldsymbol{y}}} + (\boldsymbol{\mathcal{S}}_{12})_{\{i+1,:\}} \boldsymbol{\mathcal{T}} - (\boldsymbol{\mathcal{B}}_1)_{\{i+1,0,i\}} \tag{6.32}$$

and

$$-\boldsymbol{q}_{\mathfrak{i}/\mathfrak{e}_k} \boldsymbol{W}^{\mathfrak{i}}_{\text{act,i}}(O_{\mathfrak{i}}) \boldsymbol{q}^{*}_{\mathfrak{i}/\mathfrak{e}_k} = (\hat{\boldsymbol{\mathcal{S}}}_{11})_{\{k,:\}} \hat{\dot{\boldsymbol{y}}} + (\boldsymbol{\mathcal{S}}_{12})_{\{k,:\}} \boldsymbol{\mathcal{T}} - (\boldsymbol{\mathcal{B}}_1)_{\{k,i,0\}} \tag{6.33}$$

where we have defined

$$\begin{aligned}(\boldsymbol{\mathcal{B}}_1)_{\{i,p,r\}} \triangleq\ & -\boldsymbol{\omega}^{\mathfrak{e}_{\mathfrak{i}}}_{\mathfrak{e}_{\mathfrak{i}}/\mathrm{I}} \times (M_{\mathfrak{e}_{\mathfrak{i}}} \star (\boldsymbol{\omega}^{\mathfrak{e}_{\mathfrak{i}}}_{\mathfrak{e}_{\mathfrak{i}}/\mathrm{I}})^{\mathsf{s}}) + \boldsymbol{W}^{\mathfrak{e}_{\mathfrak{i}}}_{\mathfrak{e}_{\mathfrak{i}}}(O_{\mathfrak{e}_{\mathfrak{i}}}) + b_i \boldsymbol{q}_{\mathrm{G}_{\mathfrak{i}}/\mathfrak{e}_{\mathfrak{i}}} \boldsymbol{W}^{\mathrm{G}_{\mathfrak{i}}}_{\text{ext},i}(O_{\mathrm{G}_{\mathfrak{i}}}) \boldsymbol{q}^{*}_{\mathrm{G}_{\mathfrak{i}}/\mathfrak{e}_{\mathfrak{i}}} \\ & - \sum_{\substack{j \in N(C(:,i)) \\ j \neq p}} \boldsymbol{q}_{\mathfrak{j}/\mathfrak{e}_{\mathfrak{i}}} \boldsymbol{W}^{\mathfrak{j}}_{\text{act,j}}(O_{\mathfrak{j}}) \boldsymbol{q}^{*}_{\mathfrak{j}/\mathfrak{e}_{\mathfrak{i}}} + \sum_{\substack{j \in P(C(:,i)) \\ j \neq r}} \boldsymbol{q}^{*}_{\mathfrak{e}_{\mathfrak{j}}/\mathfrak{j}} \boldsymbol{W}^{\mathfrak{j}}_{\text{act,j}}(O_{\mathfrak{j}}) \boldsymbol{q}_{\mathfrak{e}_{\mathfrak{j}}/\mathfrak{j}}. \end{aligned} \tag{6.34}$$

By manipulating equation (6.32) and equation (6.33), we obtain

$$(\hat{\boldsymbol{\mathcal{S}}}_{11})_{\{i+1,:\}}\hat{\dot{\boldsymbol{y}}} + (\boldsymbol{\mathcal{S}}_{12})_{\{i+1,:\}}\boldsymbol{\mathcal{T}} - \Big[\!\Big[\boldsymbol{q}^{*}_{\mathfrak{o}_{i+1}/\mathfrak{i}} \Big]\!\Big]_{\mathrm{L}} \Big[\!\Big[\boldsymbol{q}_{\mathfrak{o}_{i+1}/\mathfrak{i}} \Big]\!\Big]_{\mathrm{R}} V_{\mathrm{act,i}} \tilde{\boldsymbol{W}}^{\mathrm{i}}_{\mathrm{act,i}}(O_{\mathrm{i}}) = (\boldsymbol{\mathcal{B}}_1)_{\{i+1,0,i\}}, \quad (6.35)$$

and

$$(\hat{\boldsymbol{\mathcal{S}}}_{11})_{\{k,:\}}\hat{\dot{\boldsymbol{y}}} + (\boldsymbol{\mathcal{S}}_{12})_{\{k,:\}}\boldsymbol{\mathcal{T}} + \Big[\!\Big[\boldsymbol{q}_{\mathrm{i}/\mathfrak{o}_k} \Big]\!\Big]_{\mathrm{L}} \Big[\!\Big[\boldsymbol{q}^{*}_{\mathrm{i}/\mathfrak{o}_k} \Big]\!\Big]_{\mathrm{R}} V_{\mathrm{act,i}} \tilde{\boldsymbol{W}}^{\mathrm{i}}_{\mathrm{act,i}}(O_{\mathrm{i}}) = (\boldsymbol{\mathcal{B}}_1)_{\{k,i,0\}}. \quad (6.36)$$

Further manipulation of equation (6.35) allows clearing $\tilde{\boldsymbol{W}}^{\mathrm{i}}_{\mathrm{act,i}}(O_{\mathrm{i}})$ of transformations as

$$\begin{aligned} V^{\mathrm{T}}_{\mathrm{act,i}} \Big[\!\Big[\boldsymbol{q}_{\mathfrak{o}_{i+1}/\mathfrak{i}} \Big]\!\Big]_{\mathrm{L}} \Big[\!\Big[\boldsymbol{q}^{*}_{\mathfrak{o}_{i+1}/\mathfrak{i}} \Big]\!\Big]_{\mathrm{R}} (\hat{\boldsymbol{\mathcal{S}}}_{11})_{\{i+1,:\}}\hat{\dot{\boldsymbol{y}}} + V^{\mathrm{T}}_{\mathrm{act,i}} \Big[\!\Big[\boldsymbol{q}_{\mathfrak{o}_{i+1}/\mathfrak{i}} \Big]\!\Big]_{\mathrm{L}} \Big[\!\Big[\boldsymbol{q}^{*}_{\mathfrak{o}_{i+1}/\mathfrak{i}} \Big]\!\Big]_{\mathrm{R}} (\boldsymbol{\mathcal{S}}_{12})_{\{i+1,:\}}\boldsymbol{\mathcal{T}} \\ - \tilde{\boldsymbol{W}}^{\mathrm{i}}_{\mathrm{act,i}}(O_{\mathrm{i}}) = V^{\mathrm{T}}_{\mathrm{act,i}} \Big[\!\Big[\boldsymbol{q}_{\mathfrak{o}_{i+1}/\mathfrak{i}} \Big]\!\Big]_{\mathrm{L}} \Big[\!\Big[\boldsymbol{q}^{*}_{\mathfrak{o}_{i+1}/\mathfrak{i}} \Big]\!\Big]_{\mathrm{R}} (\boldsymbol{\mathcal{B}}_1)_{\{i+1,0,i\}}, \end{aligned} \quad (6.37)$$

where we have used Lemma 2 and the fact that $V^{\mathrm{T}}_{\mathrm{act,i}} V_{\mathrm{act,i}} = \mathbb{I}_{d_i}$ for $\tilde{\boldsymbol{W}}^{\mathrm{i}}_{\mathrm{act,i}}(O_{\mathrm{i}}) \in \mathbb{R}^{d_i}$.

The resulting system of equations will be of the form

$$\begin{bmatrix} \Upsilon\hat{\boldsymbol{\mathcal{S}}}_{11} & \Upsilon\boldsymbol{\mathcal{S}}_{12} & \boldsymbol{\mathcal{S}}_{\mathrm{act,i},1} \\ \hat{\boldsymbol{\mathcal{S}}}_{21} & \boldsymbol{\mathcal{S}}_{22} & \boldsymbol{\mathcal{S}}_{\mathrm{act,i},2} \end{bmatrix} \begin{bmatrix} \hat{\dot{\boldsymbol{y}}} \\ \boldsymbol{\mathcal{T}} \\ \tilde{\boldsymbol{W}}^{\mathrm{i}}_{\mathrm{act,i}}(O_{\mathrm{i}}) \end{bmatrix} = \begin{bmatrix} \Upsilon\hat{\boldsymbol{\mathcal{B}}}_1 \\ \boldsymbol{\mathcal{B}}_2 \end{bmatrix}. \quad (6.38)$$

Here we have that

$$\boldsymbol{\mathcal{S}}_{\mathrm{act,i},2} = 0_{\mathrm{R}\times d_i}, \quad (6.39)$$

while $\boldsymbol{\mathcal{S}}_{\mathrm{act,i},1} \in \mathbb{R}^{(8(\mathrm{B}-1)+d_i)\times d_i}$ is described by

$$(\boldsymbol{\mathcal{S}}_{\mathrm{act,i},1})_j = \begin{cases} -\mathbb{I}_{d_i} & \text{if } j = i, \\ 0_{8\times d_i} & \text{if } j \neq i, j \neq k, \\ +\Big[\!\Big[\boldsymbol{q}_{\mathrm{i}/\mathfrak{o}_k} \Big]\!\Big]_{\mathrm{L}} \Big[\!\Big[\boldsymbol{q}^{*}_{\mathrm{i}/\mathfrak{o}_k} \Big]\!\Big]_{\mathrm{R}} V_{\mathrm{act,i}} & \text{if } j = k. \end{cases} \quad (6.40)$$

The vectors $\hat{\boldsymbol{\mathcal{B}}}_1$ and $\boldsymbol{\mathcal{B}}_1$ are identical, except the $(i+1)$-th and k-th entries, which are computed as

$$\begin{aligned}(\hat{\boldsymbol{\mathcal{B}}}_1)_{i+1} &:= (\boldsymbol{\mathcal{B}}_1)_{\{i+1,0,i\}} \\ (\hat{\boldsymbol{\mathcal{B}}}_1)_{k} &:= (\boldsymbol{\mathcal{B}}_1)_{\{k,i,0\}}.\end{aligned} \tag{6.41}$$

Additionally, the block diagonal matrix Υ is described as

$$(\Upsilon)_{(j,j)} = \begin{cases} V_{\text{act,i}}^{\text{T}} \left[\!\left[\boldsymbol{q}_{\mathfrak{e}_{\text{i+1}}/\text{i}} \right]\!\right]_{\text{L}} \left[\!\left[\boldsymbol{q}^{*}_{\mathfrak{e}_{\text{i+1}}/\text{i}} \right]\!\right]_{\text{R}} & \text{if } j = i,\ i \text{ is prescribed} \\ \mathbb{I}_8 & \text{if } j \neq i. \end{cases} \tag{6.42}$$

It is worth emphasizing that the resulting matrix

$$\begin{bmatrix} \Upsilon\hat{\boldsymbol{\mathcal{S}}}_{11} & \Upsilon\boldsymbol{\mathcal{S}}_{12} & \boldsymbol{\mathcal{S}}_{\text{act,i,1}} \\ \hat{\boldsymbol{\mathcal{S}}}_{21} & \boldsymbol{\mathcal{S}}_{22} & \boldsymbol{\mathcal{S}}_{\text{act,i,2}} \end{bmatrix} \tag{6.43}$$

belongs to $\mathbb{R}^{(8(\text{B}-1)+R+d_i)\times(8(\text{B}-1)+R+d_i)}$ and thus, it is square and invertible.

6.5 Framework Summary

Algorithm 1 provides a detailed description of how to implement the kinematics and dynamics framework introduced in the previous sections.

Algorithm 1 Kinematics and dynamics of spacecraft-mounted robotic systems.

Given: $\boldsymbol{x}(0)$, T B, C, V_i, $V_{\text{act,i}}$, Λ_i and $\boldsymbol{q}_{\mathfrak{o}_{i+1}/\mathfrak{i}}$ from geometry
Optionally given: Index j, $\boldsymbol{\omega}_{\text{pres}}, \dot{\boldsymbol{\omega}}_{\text{pres}}$
While $t < T$
  Extract $\boldsymbol{q}_{\mathfrak{o}_1/\mathfrak{I}}$, Γ, $\boldsymbol{y}$ from $\boldsymbol{x}$
    Extract $\Gamma_{\mathfrak{J}_i}$ from Γ
      Compute $\boldsymbol{q}_{\mathfrak{i}/\mathfrak{o}_k}$ from $\Gamma_{\mathfrak{J}_i}$, where $k = N(C(i,:))$, for all i
    Extract $\boldsymbol{\omega}^{\mathfrak{o}_i}_{\mathfrak{o}_i/\mathfrak{I}}$ from $\boldsymbol{y}$ for all i
      Compute $\boldsymbol{\omega}^{\mathfrak{i}}_{\mathfrak{i}/\mathfrak{o}_k}$ using equation (6.13) for all i
    If Joint j is prescribed
      Compute $\boldsymbol{\omega}^{\mathfrak{o}_{j+1}}_{\mathfrak{o}_{j+1}/\mathfrak{I}}$ from equation (6.30)
      Compute $\boldsymbol{\omega}^{\mathfrak{o}_{i+1}}_{\mathfrak{o}_{i+1}/\mathfrak{I}}$ using joint velocities $\boldsymbol{\omega}^{\mathfrak{i}}_{\mathfrak{i}/\mathfrak{o}_k}$ for all outboard bodies $i+1 > j+1$ on same branch
    End If
  Compute $\dot{\boldsymbol{q}}_{\mathfrak{o}_1/\mathfrak{I}}$ from equation (6.12)
  Compute $\dot{\Gamma}_{\mathfrak{J}_i}$ from equation (6.14) for all i
  Assemble $\boldsymbol{\mathcal{S}}_{11}$, $\boldsymbol{\mathcal{S}}_{12}$, $\boldsymbol{\mathcal{S}}_{21}$, $\boldsymbol{\mathcal{S}}_{22}$, $\boldsymbol{\mathcal{B}}_1$, $\boldsymbol{\mathcal{B}}_2$
  If Joint j is prescribed
    Compute $\hat{\boldsymbol{\mathcal{S}}}_{11}$ from $\boldsymbol{\mathcal{S}}_{11}$, $\hat{\boldsymbol{\mathcal{S}}}_{21}$ from $\hat{\boldsymbol{\mathcal{S}}}_{21}$
    Compute $\hat{\boldsymbol{\mathcal{B}}}_1$ from $\boldsymbol{\mathcal{B}}_1$ using equation (6.41)
    Compute Υ from equation (6.42)
    Solve for $\hat{\dot{\boldsymbol{y}}}$, $\boldsymbol{\mathcal{T}}$ and $\tilde{\boldsymbol{W}}^{\mathfrak{j}}_{\text{act,j}}(O_{\mathfrak{j}})$ using equation (6.38)
    Compute $\dot{\boldsymbol{\omega}}^{\mathfrak{o}_{j+1}}_{\mathfrak{o}_{j+1}/\mathfrak{I}}$ from equation (6.31)
    Assemble $\dot{\boldsymbol{y}}$ from $\hat{\dot{\boldsymbol{y}}}$ and $\dot{\boldsymbol{\omega}}^{\mathfrak{o}_{j+1}}_{\mathfrak{o}_{j+1}/\mathfrak{I}}$
  Else
    Solve for $\dot{\boldsymbol{y}}$ and $\boldsymbol{\mathcal{T}}$ using equation (6.27)
  End If
  Assemble $\dot{\boldsymbol{x}}$ from $\dot{\boldsymbol{q}}_{\mathfrak{o}_1/\mathfrak{I}}$, $\dot{\Gamma}$, $\dot{\boldsymbol{y}}$
  Integrate $\dot{\boldsymbol{x}}$
End While

CHAPTER 7

TWO-MANIPULATOR SATELLITE

7.1 System Architecture and Frame Definition for Satellite with Two Manipulators

We lay out the architecture of the satellite in Figures 7.1 and 7.2. In Figure 7.3 we provide a schematic to show the coordinate frames to be used in the description of the problem, as well as the wrenches. It is worth emphasizing that reaction wrenches and actuation wrenches are assumed positive as applied on the body on which they are shown, and negative on the proximal body relative to the joint.

7.2 Auxiliary Matrices for Two Arm Architecture

The incidence matrix $C \in \mathbb{R}^{\mathrm{J}\times\mathrm{B}}$, which provides information about body-joint connectivity, is given by

$$C = \begin{bmatrix} -1 & 1 & 0 & 0 & 0 & 0 & 0 & 0 & 0 & 0 & 0 \\ 0 & -1 & 1 & 0 & 0 & 0 & 0 & 0 & 0 & 0 & 0 \\ 0 & 0 & -1 & 1 & 0 & 0 & 0 & 0 & 0 & 0 & 0 \\ 0 & 0 & 0 & -1 & 1 & 0 & 0 & 0 & 0 & 0 & 0 \\ 0 & 0 & 0 & 0 & -1 & 1 & 0 & 0 & 0 & 0 & 0 \\ -1 & 0 & 0 & 0 & 0 & 0 & 1 & 0 & 0 & 0 & 0 \\ 0 & 0 & 0 & 0 & 0 & 0 & -1 & 1 & 0 & 0 & 0 \\ 0 & 0 & 0 & 0 & 0 & 0 & 0 & -1 & 1 & 0 & 0 \\ 0 & 0 & 0 & 0 & 0 & 0 & 0 & 0 & -1 & 1 & 0 \\ 0 & 0 & 0 & 0 & 0 & 0 & 0 & 0 & 0 & -1 & 1 \end{bmatrix} \tag{7.1}$$

The branch termination matrix $B \in \mathbb{R}^{\mathrm{B}}$, which indicates whether the body ends a

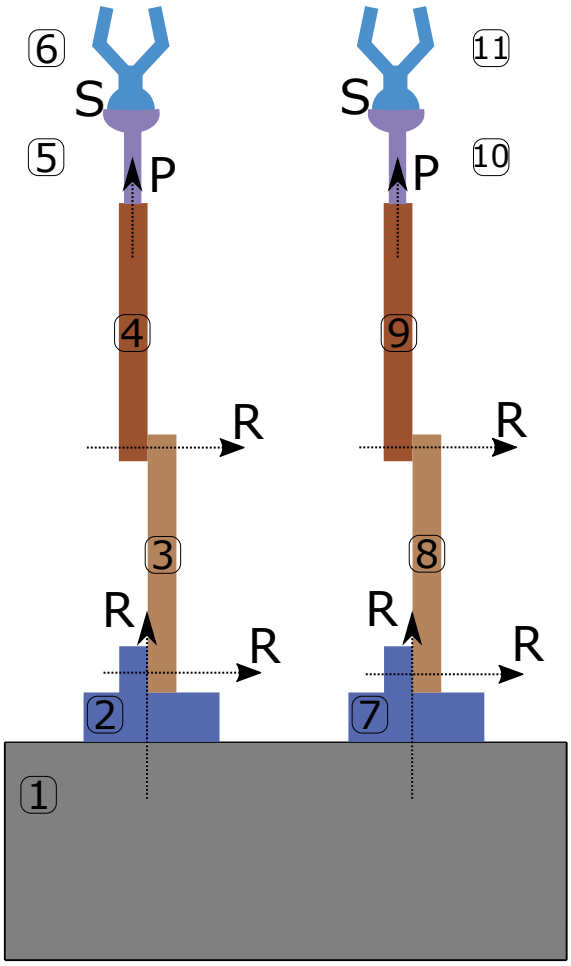

Figure 7.1: Proposed architecture with joint types in nominal configuration and body labeling.

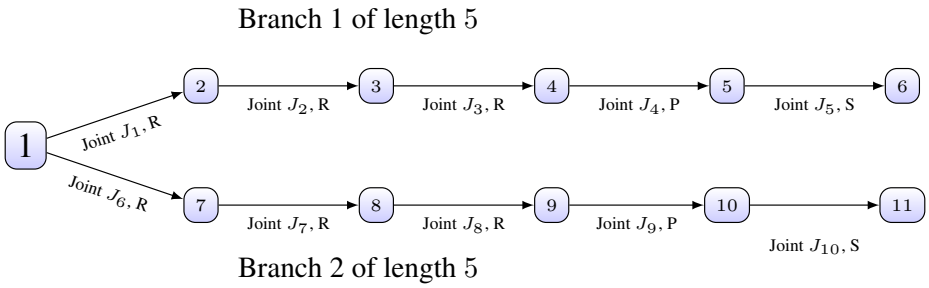

Figure 7.2: Tree structure for proposed two-arm architecture showing body and joint labeling, as well as joint type.

branch, is given by

$$B = \begin{bmatrix} 0 & 0 & 0 & 0 & 0 & 1 & 0 & 0 & 0 & 0 & 1 \end{bmatrix} \tag{7.2}$$

Finally, the results of applying the functions P() and N() to the rows and columns of C that are of interest in our derivation are given in Tables 7.1 and 7.2

Table 7.1: $P(\cdot)$ and $N(\cdot)$ functions applied to the columns of C for two-arm satellite topology.

Column Number i	$P(C(:,i))$	$N(C(:,i))$
1	$\{\}$	$\{1,\ 6\}$
2	$\{1\}$	$\{2\}$
3	$\{2\}$	$\{3\}$
4	$\{3\}$	$\{4\}$
5	$\{4\}$	$\{5\}$
6	$\{5\}$	$\{\}$
7	$\{6\}$	$\{7\}$
8	$\{7\}$	$\{8\}$
9	$\{8\}$	$\{9\}$
10	$\{9\}$	$\{10\}$
11	$\{10\}$	$\{\}$

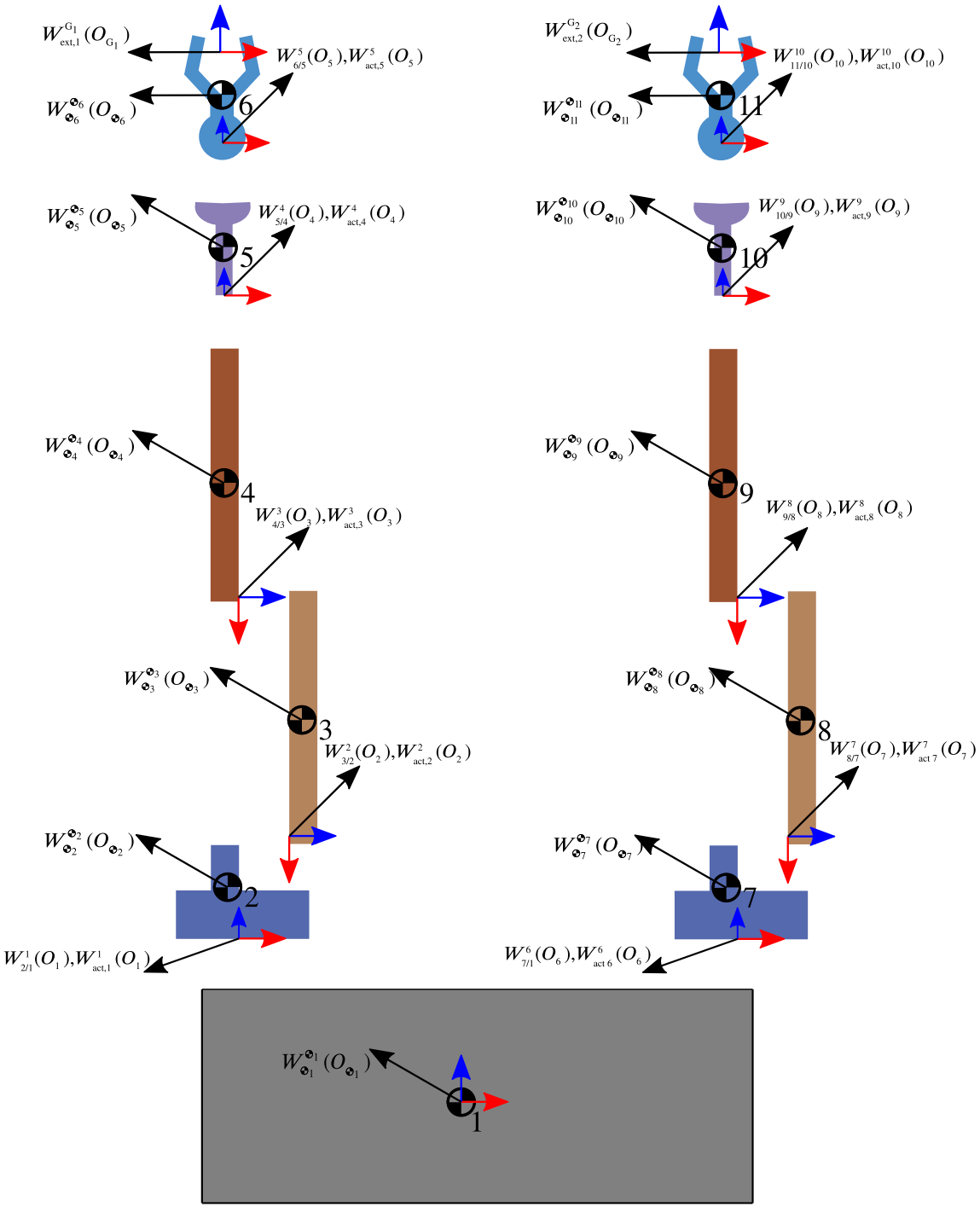

Figure 7.3: Coordinate system definition and wrenches for two arm satellite architecture.

Table 7.2: $N(\cdot)$ function applied to the rows of C for two-arm satellite topology.

Row Number i	$N(C(i,:))$
1	$\{1\}$
2	$\{2\}$
3	$\{3\}$
4	$\{4\}$
5	$\{5\}$
6	$\{1\}$
7	$\{7\}$
8	$\{8\}$
9	$\{9\}$
10	$\{10\}$

7.3 Variable Definition for Two Arm Architecture

To characterize the degrees of freedom at each joint, and the dimensionality of the reaction wrenches that appear at each joint we use Table 7.3. On this spacecraft, we will have a total amount of degrees of freedom added by the joints of $\mathrm{D} = \sum_{i \in \text{Joints}} \mathrm{d}_i = 14$. The spacecraft will have two branches of lengths $N_1 = N_2 = 5$, leading to a total amount of joints $\mathrm{J} = \sum_{i \in \text{Branches}} N_i = 10$. This implies that the total number of rigid bodies is $\mathrm{B} = 1 + \mathrm{J} = 11$. Finally, we can compute the dimensionality of all reaction wrenches appearing in the system as $\mathrm{R} = \sum_{i \in \text{Joints}} r_i = \sum_{i \in \text{Joints}} 6 - d_i = 46$.

We will define our state vector to be

$$\boldsymbol{x} = \begin{bmatrix} \boldsymbol{q}_{\mathcal{B}_0/\mathcal{I}} \\ \Gamma \\ \boldsymbol{y} \end{bmatrix} \in \mathbb{H}_d \times \mathbb{R}^{14} \times \mathbb{R}^{88}. \tag{7.3}$$

Table 7.3: Joint characterization for two-arm spacecraft.

Joint Label	Type	Motion DOF d_i	Reaction Wrench Dimension $\mathrm{r}_i = 6 - d_i$
J_1	R	1	5
J_2	R	1	5
J_3	R	1	5
J_4	P	1	5
J_5	S	3	3
J_6	R	1	5
J_7	R	1	5
J_8	R	1	5
J_9	P	1	5
J_{10}	S	3	3

The vector of generalized coordinates $\Gamma \in \mathbb{R}^{\mathrm{D}} = \mathbb{R}^{14}$ is given by

$$\Gamma \triangleq \left[\Gamma_{\mathrm{J}_1}^{\mathrm{T}},\ \Gamma_{\mathrm{J}_2}^{\mathrm{T}},\ \Gamma_{\mathrm{J}_3}^{\mathrm{T}},\ \Gamma_{\mathrm{J}_4}^{\mathrm{T}},\ \Gamma_{\mathrm{J}_5}^{\mathrm{T}},\ \Gamma_{\mathrm{J}_6}^{\mathrm{T}},\ \Gamma_{\mathrm{J}_7}^{\mathrm{T}},\ \Gamma_{\mathrm{J}_8}^{\mathrm{T}},\ \Gamma_{\mathrm{J}_9}^{\mathrm{T}},\ \Gamma_{\mathrm{J}_{10}}^{\mathrm{T}},\right]^{\mathrm{T}}, \tag{7.4}$$

where

$$\Gamma_{\mathrm{J}_1} = \theta_{1/\mathfrak{o}_1} \qquad \Gamma_{\mathrm{J}_6} = \theta_{6/\mathfrak{o}_1}$$

$$\Gamma_{\mathrm{J}_2} = \theta_{2/\mathfrak{o}_2} \qquad \Gamma_{\mathrm{J}_7} = \theta_{7/\mathfrak{o}_7}$$

$$\Gamma_{\mathrm{J}_3} = \theta_{3/\mathfrak{o}_3} \qquad \Gamma_{\mathrm{J}_8} = \theta_{8/\mathfrak{o}_8}$$

$$\Gamma_{\mathrm{J}_4} = z_{4/\mathfrak{o}_4} \qquad \Gamma_{\mathrm{J}_9} = z_{9/\mathfrak{o}_9}$$

$$\Gamma_{\mathrm{J}_5} = \left[\phi_{5/\mathfrak{o}_5},\ \theta_{5/\mathfrak{o}_5},\ \psi_{5/\mathfrak{o}_5}\right]^{\mathrm{T}} \qquad \Gamma_{\mathrm{J}_{10}} = \left[\phi_{10/\mathfrak{o}_{10}},\ \theta_{10/\mathfrak{o}_{10}},\ \psi_{10/\mathfrak{o}_{10}}\right]^{\mathrm{T}}.$$

The dual velocities $\boldsymbol{y} \in \mathbb{R}^{8\mathrm{B}} = \mathbb{R}^{88}$ of the system are given by

$$\begin{aligned}\boldsymbol{y} = \big[&(\boldsymbol{\omega}^{\mathfrak{o}_1}_{\mathfrak{o}_1/\mathrm{I}})^{\mathrm{T}},\ (\boldsymbol{\omega}^{\mathfrak{o}_2}_{\mathfrak{o}_2/\mathrm{I}})^{\mathrm{T}},\ (\boldsymbol{\omega}^{\mathfrak{o}_3}_{\mathfrak{o}_3/\mathrm{I}})^{\mathrm{T}},\ (\boldsymbol{\omega}^{\mathfrak{o}_4}_{\mathfrak{o}_4/\mathrm{I}})^{\mathrm{T}},\ (\boldsymbol{\omega}^{\mathfrak{o}_5}_{\mathfrak{o}_5/\mathrm{I}})^{\mathrm{T}},\ (\boldsymbol{\omega}^{\mathfrak{o}_6}_{\mathfrak{o}_6/\mathrm{I}})^{\mathrm{T}}, \ldots \\ &(\boldsymbol{\omega}^{\mathfrak{o}_7}_{\mathfrak{o}_7/\mathrm{I}})^{\mathrm{T}},\ (\boldsymbol{\omega}^{\mathfrak{o}_8}_{\mathfrak{o}_8/\mathrm{I}})^{\mathrm{T}},\ (\boldsymbol{\omega}^{\mathfrak{o}_9}_{\mathfrak{o}_9/\mathrm{I}})^{\mathrm{T}},\ (\boldsymbol{\omega}^{\mathfrak{o}_{10}}_{\mathfrak{o}_{10}/\mathrm{I}})^{\mathrm{T}},\ (\boldsymbol{\omega}^{\mathfrak{o}_{11}}_{\mathfrak{o}_{11}/\mathrm{I}})^{\mathrm{T}}\big]^{\mathrm{T}},\end{aligned} \tag{7.5}$$

while the collection of reduced wrenches $\mathcal{T} \in \mathbb{R}^{\mathrm{R}} = \mathbb{R}^{46}$ is given by

$$\boldsymbol{\mathcal{T}} = \Big[(\tilde{\boldsymbol{W}}^{1}_{2/1}(O_1))^{\mathrm{T}},\ (\tilde{\boldsymbol{W}}^{2}_{3/2}(O_2))^{\mathrm{T}},\ (\tilde{\boldsymbol{W}}^{3}_{4/3}(O_3))^{\mathrm{T}},\ (\tilde{\boldsymbol{W}}^{4}_{5/4}(O_4))^{\mathrm{T}},\ (\tilde{\boldsymbol{W}}^{5}_{6/5}(O_5))^{\mathrm{T}}, \ldots$$
$$(\tilde{\boldsymbol{W}}^{6}_{7/1}(O_6))^{\mathrm{T}}, (\tilde{\boldsymbol{W}}^{7}_{8/7}(O_7))^{\mathrm{T}},\ (\tilde{\boldsymbol{W}}^{8}_{9/8}(O_8))^{\mathrm{T}},\ (\tilde{\boldsymbol{W}}^{9}_{10/9}(O_9))^{\mathrm{T}},\ (\tilde{\boldsymbol{W}}^{10}_{11/10}(O_{10}))^{\mathrm{T}}\Big]^{\mathrm{T}}. \tag{7.6}$$

The reaction wrenches are determined from the reduced reaction wrenches by the relationship $\boldsymbol{W}^{\mathrm{i}}_{\mathrm{i+1/N(C(i,:))}} = V_i \tilde{\boldsymbol{W}}^{\mathrm{i}}_{\mathrm{i+1/N(C(i,:))}}$. Since we have three different types of joints (R, P, and S), we will have three different forms for the matrix V_i. For revolute joints, we will have $V_1 = V_2 = V_3 = V_6 = V_7 = V_8 = \boldsymbol{E}^{\mathrm{T}}_{158}$. For prismatic joints, we will have $V_4 = V_9 = \boldsymbol{E}^{\mathrm{T}}_{145}$, and for spherical joints we will have $V_5 = V_{10} = \boldsymbol{E}^{\mathrm{T}}_{15678}$.

For the type of joints in our application, the reaction wrenches and reduced reaction wrenches will satisfy the following relationships:

Finally, in a similar manner we will define the Λ_i matrices as

7.4 Kinematics for Two Arm Architecture

In this section we provide the kinematics for the two-arm manipulator system. We know the kinematics of the satellite base are given by

$$\dot{\boldsymbol{q}}_{\mathfrak{o}_1/\mathrm{I}} = \tfrac{1}{2}\boldsymbol{q}_{\mathfrak{o}_1/\mathrm{I}}\boldsymbol{\omega}^{\mathfrak{o}_1}_{\mathfrak{o}_1/\mathrm{I}} \tag{7.7}$$

Next, we provide the generalized speeds for each of our joint coordinates. In particular,

Revolute: $\boldsymbol{W}^{\text{i}}_{\text{i+1/N(C(i,:))}} = \begin{bmatrix} 0 \\ f_x \\ f_y \\ f_z \\ 0 \\ \tau_x \\ \tau_y \\ 0 \end{bmatrix} = \begin{bmatrix} 0\,0\,0\,0\,0 \\ 1\,0\,0\,0\,0 \\ 0\,1\,0\,0\,0 \\ 0\,0\,1\,0\,0 \\ 0\,0\,0\,0\,0 \\ 0\,0\,0\,1\,0 \\ 0\,0\,0\,0\,1 \\ 0\,0\,0\,0\,0 \end{bmatrix} \begin{bmatrix} f_x \\ f_y \\ f_z \\ \tau_x \\ \tau_y \end{bmatrix} = \boldsymbol{E}^{\text{T}}_{158} \tilde{\boldsymbol{W}}^{\text{i}}_{\text{i+1/N(C(i,:))}}$

Prismatic: $\boldsymbol{W}^{\text{i}}_{\text{i+1/N(C(i,:))}} = \begin{bmatrix} 0 \\ f_x \\ f_y \\ 0 \\ 0 \\ \tau_x \\ \tau_y \\ \tau_z \end{bmatrix} = \begin{bmatrix} 0\,0\,0\,0\,0 \\ 1\,0\,0\,0\,0 \\ 0\,1\,0\,0\,0 \\ 0\,0\,0\,0\,0 \\ 0\,0\,0\,0\,0 \\ 0\,0\,1\,0\,0 \\ 0\,0\,0\,1\,0 \\ 0\,0\,0\,0\,1 \end{bmatrix} \begin{bmatrix} f_x \\ f_y \\ \tau_x \\ \tau_y \\ \tau_z \end{bmatrix} = \boldsymbol{E}^{\text{T}}_{145} \tilde{\boldsymbol{W}}^{\text{i}}_{\text{i+1/N(C(i,:))}}$

Spherical: $\boldsymbol{W}^{\text{i}}_{\text{i+1/N(C(i,:))}} = \begin{bmatrix} 0 \\ f_x \\ f_y \\ f_z \\ 0 \\ 0 \\ 0 \\ 0 \end{bmatrix} = \begin{bmatrix} 0\,0\,0 \\ 1\,0\,0 \\ 0\,1\,0 \\ 0\,0\,1 \\ 0\,0\,0 \\ 0\,0\,0 \\ 0\,0\,0 \\ 0\,0\,0 \end{bmatrix} \begin{bmatrix} f_x \\ f_y \\ f_z \end{bmatrix} = \boldsymbol{E}^{\text{T}}_{15678} \tilde{\boldsymbol{W}}^{\text{i}}_{\text{i+1/N(C(i,:))}}$

Revolute : $\Lambda_1 = \Lambda_2 = \Lambda_3 = \Lambda_6 = \Lambda_7 = \Lambda_8 = \boldsymbol{E}_{145}$

Prismatic: $\Lambda_4 = \Lambda_9 = \boldsymbol{E}_{158}$

Spherical: $\Lambda_5 = \Lambda_{10} = \boldsymbol{E}_{12345}$

we have

$$
\begin{aligned}
\dot{\Gamma}_{\mathrm{J}_1} &= L_{\mathrm{J}_1}\boldsymbol{\omega}^{1}_{1/\mathbf{o}_1} = L_{\mathrm{J}_1}(\boldsymbol{q}_{\mathbf{o}_2/1}\boldsymbol{\omega}^{\mathbf{o}_2}_{\mathbf{o}_2/\mathrm{I}}\boldsymbol{q}^{*}_{\mathbf{o}_2/1} - \boldsymbol{q}^{*}_{1/\mathbf{o}_1}\boldsymbol{\omega}^{\mathbf{o}_1}_{\mathbf{o}_1/\mathrm{I}}\boldsymbol{q}_{1/\mathbf{o}_1}) \\
\dot{\Gamma}_{\mathrm{J}_2} &= L_{\mathrm{J}_2}\boldsymbol{\omega}^{2}_{2/\mathbf{o}_2} = L_{\mathrm{J}_2}(\boldsymbol{q}_{\mathbf{o}_3/2}\boldsymbol{\omega}^{\mathbf{o}_3}_{\mathbf{o}_3/\mathrm{I}}\boldsymbol{q}^{*}_{\mathbf{o}_3/2} - \boldsymbol{q}^{*}_{2/\mathbf{o}_2}\boldsymbol{\omega}^{\mathbf{o}_2}_{\mathbf{o}_2/\mathrm{I}}\boldsymbol{q}_{2/\mathbf{o}_2}) \\
\dot{\Gamma}_{\mathrm{J}_3} &= L_{\mathrm{J}_3}\boldsymbol{\omega}^{3}_{3/\mathbf{o}_3} = L_{\mathrm{J}_3}(\boldsymbol{q}_{\mathbf{o}_4/3}\boldsymbol{\omega}^{\mathbf{o}_4}_{\mathbf{o}_4/\mathrm{I}}\boldsymbol{q}^{*}_{\mathbf{o}_4/3} - \boldsymbol{q}^{*}_{3/\mathbf{o}_3}\boldsymbol{\omega}^{\mathbf{o}_3}_{\mathbf{o}_3/\mathrm{I}}\boldsymbol{q}_{3/\mathbf{o}_3}) \\
\dot{\Gamma}_{\mathrm{J}_4} &= L_{\mathrm{J}_4}\boldsymbol{\omega}^{4}_{4/\mathbf{o}_4} = L_{\mathrm{J}_4}(\boldsymbol{q}_{\mathbf{o}_5/4}\boldsymbol{\omega}^{\mathbf{o}_5}_{\mathbf{o}_5/\mathrm{I}}\boldsymbol{q}^{*}_{\mathbf{o}_5/4} - \boldsymbol{q}^{*}_{4/\mathbf{o}_4}\boldsymbol{\omega}^{\mathbf{o}_4}_{\mathbf{o}_4/\mathrm{I}}\boldsymbol{q}_{4/\mathbf{o}_4}) \\
\dot{\Gamma}_{\mathrm{J}_5} &= L_{\mathrm{J}_5}\boldsymbol{\omega}^{5}_{5/\mathbf{o}_5} = L_{\mathrm{J}_5}(\boldsymbol{q}_{\mathbf{o}_6/5}\boldsymbol{\omega}^{\mathbf{o}_6}_{\mathbf{o}_6/\mathrm{I}}\boldsymbol{q}^{*}_{\mathbf{o}_6/5} - \boldsymbol{q}^{*}_{5/\mathbf{o}_5}\boldsymbol{\omega}^{\mathbf{o}_5}_{\mathbf{o}_5/\mathrm{I}}\boldsymbol{q}_{5/\mathbf{o}_5}) \\
\dot{\Gamma}_{\mathrm{J}_6} &= L_{\mathrm{J}_6}\boldsymbol{\omega}^{6}_{6/\mathbf{o}_1} = L_{\mathrm{J}_6}(\boldsymbol{q}_{\mathbf{o}_7/6}\boldsymbol{\omega}^{\mathbf{o}_7}_{\mathbf{o}_7/\mathrm{I}}\boldsymbol{q}^{*}_{\mathbf{o}_7/6} - \boldsymbol{q}^{*}_{6/\mathbf{o}_1}\boldsymbol{\omega}^{\mathbf{o}_1}_{\mathbf{o}_1/\mathrm{I}}\boldsymbol{q}_{6/\mathbf{o}_1}) \\
\dot{\Gamma}_{\mathrm{J}_7} &= L_{\mathrm{J}_7}\boldsymbol{\omega}^{7}_{7/\mathbf{o}_7} = L_{\mathrm{J}_7}(\boldsymbol{q}_{\mathbf{o}_8/7}\boldsymbol{\omega}^{\mathbf{o}_8}_{\mathbf{o}_8/\mathrm{I}}\boldsymbol{q}^{*}_{\mathbf{o}_8/7} - \boldsymbol{q}^{*}_{7/\mathbf{o}_7}\boldsymbol{\omega}^{\mathbf{o}_7}_{\mathbf{o}_7/\mathrm{I}}\boldsymbol{q}_{7/\mathbf{o}_7}) \\
\dot{\Gamma}_{\mathrm{J}_8} &= L_{\mathrm{J}_8}\boldsymbol{\omega}^{8}_{8/\mathbf{o}_8} = L_{\mathrm{J}_8}(\boldsymbol{q}_{\mathbf{o}_9/8}\boldsymbol{\omega}^{\mathbf{o}_9}_{\mathbf{o}_9/\mathrm{I}}\boldsymbol{q}^{*}_{\mathbf{o}_9/8} - \boldsymbol{q}^{*}_{8/\mathbf{o}_8}\boldsymbol{\omega}^{\mathbf{o}_8}_{\mathbf{o}_8/\mathrm{I}}\boldsymbol{q}_{8/\mathbf{o}_8}) \\
\dot{\Gamma}_{\mathrm{J}_9} &= L_{\mathrm{J}_9}\boldsymbol{\omega}^{9}_{9/\mathbf{o}_9} = L_{\mathrm{J}_9}(\boldsymbol{q}_{\mathbf{o}_{10}/9}\boldsymbol{\omega}^{\mathbf{o}_{10}}_{\mathbf{o}_{10}/\mathrm{I}}\boldsymbol{q}^{*}_{\mathbf{o}_{10}/9} - \boldsymbol{q}^{*}_{9/\mathbf{o}_9}\boldsymbol{\omega}^{\mathbf{o}_9}_{\mathbf{o}_9/\mathrm{I}}\boldsymbol{q}_{9/\mathbf{o}_9}) \\
\dot{\Gamma}_{\mathrm{J}_{10}} &= L_{\mathrm{J}_{10}}\boldsymbol{\omega}^{10}_{10/\mathbf{o}_{10}} = L_{\mathrm{J}_{10}}(\boldsymbol{q}_{\mathbf{o}_{11}/10}\boldsymbol{\omega}^{\mathbf{o}_{11}}_{\mathbf{o}_{11}/\mathrm{I}}\boldsymbol{q}^{*}_{\mathbf{o}_{11}/10} - \boldsymbol{q}^{*}_{10/\mathbf{o}_{10}}\boldsymbol{\omega}^{\mathbf{o}_{10}}_{\mathbf{o}_{10}/\mathrm{I}}\boldsymbol{q}_{10/\mathbf{o}_{10}})
\end{aligned}
\quad . \tag{7.8}
$$

The matrices $L_{\mathrm{J}_\mathrm{i}}$ are dependent on the type of joint, and they are given by

Revolute : $L_{\mathrm{J}_1} = L_{\mathrm{J}_2} = L_{\mathrm{J}_3} = L_{\mathrm{J}_6} = L_{\mathrm{J}_7} = L_{\mathrm{J}_8} = [\,0\;0\;0\;1\;0\;0\;0\;0\,]$

Prismatic: $L_{\mathrm{J}_4} = L_{\mathrm{J}_9} = [\,0\;0\;0\;0\;0\;0\;0\;1\,]$

Spherical:

$$
L_{\mathrm{J}_5} = \begin{bmatrix}
0 & 1 & \tan(\theta_{5/\mathbf{o}_5})\sin(\phi_{5/\mathbf{o}_5}) & \cos(\phi_{5/\mathbf{o}_5})\tan(\theta_{5/\mathbf{o}_5}) & 0 & 0 & 0 & 0 \\
0 & 0 & \cos(\phi_{5/\mathbf{o}_5}) & -\sin(\phi_{5/\mathbf{o}_5}) & 0 & 0 & 0 & 0 \\
0 & 0 & \sin(\phi_{5/\mathbf{o}_5})/\cos(\theta_{5/\mathbf{o}_5}) & \cos(\phi_{5/\mathbf{o}_5})/\cos(\theta_{5/\mathbf{o}_5}) & 0 & 0 & 0 & 0
\end{bmatrix}
$$

$$
L_{\mathrm{J}_{10}} = \begin{bmatrix}
0 & 1 & \tan(\theta_{10/\mathbf{o}_{10}})\sin(\phi_{10/\mathbf{o}_{10}}) & \cos(\phi_{10/\mathbf{o}_{10}})\tan(\theta_{10/\mathbf{o}_{10}}) & 0 & 0 & 0 & 0 \\
0 & 0 & \cos(\phi_{10/\mathbf{o}_{10}}) & -\sin(\phi_{10/\mathbf{o}_{10}}) & 0 & 0 & 0 & 0 \\
0 & 0 & \sin(\phi_{10/\mathbf{o}_{10}})/\cos(\theta_{10/\mathbf{o}_{10}}) & \cos(\phi_{10/\mathbf{o}_{10}})/\cos(\theta_{10/\mathbf{o}_{10}}) & 0 & 0 & 0 & 0
\end{bmatrix}
$$

7.5 Dynamics for Two Arm Architecture

In this section, we describe the sub-blocks of matrix $\mathcal{S}$ and vector $\mathcal{B}$ used in our problem formulation to solve for the dual acceleration for each of the bodies, and the reduced reaction wrenches at the joints. In particular, we are looking to provide explicit expressions for each of the block matrices and block vectors of the expression

$$\begin{bmatrix} \boldsymbol{\mathcal{S}}_{11} & \boldsymbol{\mathcal{S}}_{12} \\ \boldsymbol{\mathcal{S}}_{21} & \boldsymbol{\mathcal{S}}_{22} \end{bmatrix} \begin{bmatrix} \dot{\boldsymbol{y}} \\ \boldsymbol{\mathcal{T}} \end{bmatrix} = \begin{bmatrix} \boldsymbol{\mathcal{B}}_1 \\ \boldsymbol{\mathcal{B}}_2 \end{bmatrix}. \tag{7.9}$$

7.5.1 Matrices $\boldsymbol{\mathcal{S}_{11}}$ and $\boldsymbol{\mathcal{S}_{22}}$

The matrix $\boldsymbol{\mathcal{S}_{11}}$ contains the coefficients of the unknown dual accelerations that appear in the Newton-Euler form of the equations. In our case, $\boldsymbol{\mathcal{S}_{11}} \in \mathbb{R}^{88\times 88}$ is given as

$$\begin{aligned} \boldsymbol{\mathcal{S}_{11}} = \operatorname{diag}\big(&\mathrm{H}\left(M_{\bullet_1}\right), \mathrm{H}\left(M_{\bullet_2}\right), \mathrm{H}\left(M_{\bullet_3}\right), \mathrm{H}\left(M_{\bullet_4}\right), \mathrm{H}\left(M_{\bullet_5}\right), \mathrm{H}\left(M_{\bullet_6}\right), \\ &\mathrm{H}\left(M_{\bullet_7}\right), \mathrm{H}\left(M_{\bullet_8}\right), \mathrm{H}\left(M_{\bullet_9}\right), \mathrm{H}\left(M_{\bullet_{10}}\right), \mathrm{H}\left(M_{\bullet_{11}}\right)\big). \end{aligned} \tag{7.10}$$

The matrix $\boldsymbol{\mathcal{S}_{22}}$ contains the coefficients of the reduced wrenches in the joint constraint equations. Since the reduced wrenches do not appear in the constraint equations, this matrix is a zero block. More specifically, $\boldsymbol{\mathcal{S}_{22}} \in \mathbb{R}^{46}$ is given by

$$\boldsymbol{\mathcal{S}_{22}} = 0_{46\times 46}. \tag{7.11}$$

7.5.2 Matrix $\boldsymbol{\mathcal{S}_{12}}$

The matrix $\boldsymbol{\mathcal{S}_{12}}$ contains the coefficients of the unknown reduced wrenches that appear in the Newton-Euler form of the equations. For this given architecture, its mathematical description is given as follows.

i	j	Entry $c_{j,i}$	Block $(\boldsymbol{\mathcal{S}}_{12})_{ij}$
i	j	$c_{j,i} = -1$	$[\![\boldsymbol{q}_{\mathrm{j}/\boldsymbol{\circ}_{\mathrm{i}}}]\!]_{\mathrm{L}} [\![\boldsymbol{q}^*_{\mathrm{j}/\boldsymbol{\circ}_{\mathrm{i}}}]\!]_{\mathrm{R}} V_j$
1	1	$c_{1,1} = -1$	$[\![\boldsymbol{q}_{1/\boldsymbol{\circ}_1}]\!]_{\mathrm{L}} [\![\boldsymbol{q}^*_{1/\boldsymbol{\circ}_1}]\!]_{\mathrm{R}} V_1$
2	2	$c_{2,2} = -1$	$[\![\boldsymbol{q}_{2/\boldsymbol{\circ}_2}]\!]_{\mathrm{L}} [\![\boldsymbol{q}^*_{2/\boldsymbol{\circ}_2}]\!]_{\mathrm{R}} V_2$
3	3	$c_{3,3} = -1$	$[\![\boldsymbol{q}_{3/\boldsymbol{\circ}_3}]\!]_{\mathrm{L}} [\![\boldsymbol{q}^*_{3/\boldsymbol{\circ}_3}]\!]_{\mathrm{R}} V_3$
4	4	$c_{4,4} = -1$	$[\![\boldsymbol{q}_{4/\boldsymbol{\circ}_4}]\!]_{\mathrm{L}} [\![\boldsymbol{q}^*_{4/\boldsymbol{\circ}_4}]\!]_{\mathrm{R}} V_4$
5	5	$c_{5,5} = -1$	$[\![\boldsymbol{q}_{5/\boldsymbol{\circ}_5}]\!]_{\mathrm{L}} [\![\boldsymbol{q}^*_{5/\boldsymbol{\circ}_5}]\!]_{\mathrm{R}} V_5$
1	6	$c_{6,1} = -1$	$[\![\boldsymbol{q}_{6/\boldsymbol{\circ}_1}]\!]_{\mathrm{L}} [\![\boldsymbol{q}^*_{6/\boldsymbol{\circ}_1}]\!]_{\mathrm{R}} V_6$
7	7	$c_{7,7} = -1$	$[\![\boldsymbol{q}_{7/\boldsymbol{\circ}_7}]\!]_{\mathrm{L}} [\![\boldsymbol{q}^*_{7/\boldsymbol{\circ}_7}]\!]_{\mathrm{R}} V_7$
8	8	$c_{8,8} = -1$	$[\![\boldsymbol{q}_{8/\boldsymbol{\circ}_8}]\!]_{\mathrm{L}} [\![\boldsymbol{q}^*_{8/\boldsymbol{\circ}_8}]\!]_{\mathrm{R}} V_8$
9	9	$c_{9,9} = -1$	$[\![\boldsymbol{q}_{9/\boldsymbol{\circ}_9}]\!]_{\mathrm{L}} [\![\boldsymbol{q}^*_{9/\boldsymbol{\circ}_9}]\!]_{\mathrm{R}} V_9$
10	10	$c_{10,10} = -1$	$[\![\boldsymbol{q}_{10/\boldsymbol{\circ}_{10}}]\!]_{\mathrm{L}} [\![\boldsymbol{q}^*_{10/\boldsymbol{\circ}_{10}}]\!]_{\mathrm{R}} V_{10}$

i	j	Entry $c_{j,i}$	Block $(\boldsymbol{\mathcal{S}}_{12})_{ij}$
i	j	$c_{j,i} = 1$	$-[\![\boldsymbol{q}^*_{\boldsymbol{\circ}_{\mathrm{i}}/\mathrm{j}}]\!]_{\mathrm{L}} [\![\boldsymbol{q}_{\boldsymbol{\circ}_{\mathrm{i}}/\mathrm{j}}]\!]_{\mathrm{R}} V_j$
2	1	$c_{1,2} = 1$	$-[\![\boldsymbol{q}^*_{\boldsymbol{\circ}_2/1}]\!]_{\mathrm{L}} [\![\boldsymbol{q}_{\boldsymbol{\circ}_2/1}]\!]_{\mathrm{R}} V_1$
3	2	$c_{2,3} = 1$	$-[\![\boldsymbol{q}^*_{\boldsymbol{\circ}_3/2}]\!]_{\mathrm{L}} [\![\boldsymbol{q}_{\boldsymbol{\circ}_3/2}]\!]_{\mathrm{R}} V_2$
4	3	$c_{3,4} = 1$	$-[\![\boldsymbol{q}^*_{\boldsymbol{\circ}_4/3}]\!]_{\mathrm{L}} [\![\boldsymbol{q}_{\boldsymbol{\circ}_4/3}]\!]_{\mathrm{R}} V_3$
5	4	$c_{4,5} = 1$	$-[\![\boldsymbol{q}^*_{\boldsymbol{\circ}_5/4}]\!]_{\mathrm{L}} [\![\boldsymbol{q}_{\boldsymbol{\circ}_5/4}]\!]_{\mathrm{R}} V_4$
6	5	$c_{5,6} = 1$	$-[\![\boldsymbol{q}^*_{\boldsymbol{\circ}_6/5}]\!]_{\mathrm{L}} [\![\boldsymbol{q}_{\boldsymbol{\circ}_6/5}]\!]_{\mathrm{R}} V_5$
7	6	$c_{6,7} = 1$	$-[\![\boldsymbol{q}^*_{\boldsymbol{\circ}_7/6}]\!]_{\mathrm{L}} [\![\boldsymbol{q}_{\boldsymbol{\circ}_7/6}]\!]_{\mathrm{R}} V_6$
8	7	$c_{7,8} = 1$	$-[\![\boldsymbol{q}^*_{\boldsymbol{\circ}_8/7}]\!]_{\mathrm{L}} [\![\boldsymbol{q}_{\boldsymbol{\circ}_8/7}]\!]_{\mathrm{R}} V_7$
9	8	$c_{8,9} = 1$	$-[\![\boldsymbol{q}^*_{\boldsymbol{\circ}_9/8}]\!]_{\mathrm{L}} [\![\boldsymbol{q}_{\boldsymbol{\circ}_9/8}]\!]_{\mathrm{R}} V_8$
10	9	$c_{9,10} = 1$	$-[\![\boldsymbol{q}^*_{\boldsymbol{\circ}_{10}/9}]\!]_{\mathrm{L}} [\![\boldsymbol{q}_{\boldsymbol{\circ}_{10}/9}]\!]_{\mathrm{R}} V_9$
11	10	$c_{10,11} = 1$	$-[\![\boldsymbol{q}^*_{\boldsymbol{\circ}_{11}/10}]\!]_{\mathrm{L}} [\![\boldsymbol{q}_{\boldsymbol{\circ}_{11}/10}]\!]_{\mathrm{R}} V_{10}$

7.5.3 Matrix $\boldsymbol{\mathcal{S}_{21}}$

The sub-matrix $\boldsymbol{\mathcal{S}_{21}}$ contains the coefficients of the unknown dual accelerations in the constraint equations that arise from relating the body accelerations of two bodies in combination with the joint generalized acceleration. For this given architecture, its mathematical description is given as follows.

i	j	Entry $c_{i,j}$	Block $(\boldsymbol{\mathcal{S}}_{21})_{ij}$
i	j	$c_{i,j} = -1$	$-\Lambda_i \left[\!\left[\boldsymbol{q}^*_{\mathrm{i}/\mathrm{o_j}} \right]\!\right]_{\mathrm{L}} \left[\!\left[\boldsymbol{q}_{\mathrm{i}/\mathrm{o_j}} \right]\!\right]_{\mathrm{R}}$
1	1	$c_{1,1} = -1$	$-\Lambda_1 \left[\!\left[\boldsymbol{q}^*_{1/\mathrm{o}_1} \right]\!\right]_{\mathrm{L}} \left[\!\left[\boldsymbol{q}_{1/\mathrm{o}_1} \right]\!\right]_{\mathrm{R}}$
2	2	$c_{2,2} = -1$	$-\Lambda_2 \left[\!\left[\boldsymbol{q}^*_{2/\mathrm{o}_2} \right]\!\right]_{\mathrm{L}} \left[\!\left[\boldsymbol{q}_{2/\mathrm{o}_2} \right]\!\right]_{\mathrm{R}}$
3	3	$c_{3,3} = -1$	$-\Lambda_3 \left[\!\left[\boldsymbol{q}^*_{3/\mathrm{o}_3} \right]\!\right]_{\mathrm{L}} \left[\!\left[\boldsymbol{q}_{3/\mathrm{o}_3} \right]\!\right]_{\mathrm{R}}$
4	4	$c_{4,4} = -1$	$-\Lambda_4 \left[\!\left[\boldsymbol{q}^*_{4/\mathrm{o}_4} \right]\!\right]_{\mathrm{L}} \left[\!\left[\boldsymbol{q}_{4/\mathrm{o}_4} \right]\!\right]_{\mathrm{R}}$
5	5	$c_{5,5} = -1$	$-\Lambda_5 \left[\!\left[\boldsymbol{q}^*_{5/\mathrm{o}_5} \right]\!\right]_{\mathrm{L}} \left[\!\left[\boldsymbol{q}_{5/\mathrm{o}_5} \right]\!\right]_{\mathrm{R}}$
6	1	$c_{6,1} = -1$	$-\Lambda_6 \left[\!\left[\boldsymbol{q}^*_{6/\mathrm{o}_1} \right]\!\right]_{\mathrm{L}} \left[\!\left[\boldsymbol{q}_{6/\mathrm{o}_1} \right]\!\right]_{\mathrm{R}}$
7	7	$c_{7,7} = -1$	$-\Lambda_7 \left[\!\left[\boldsymbol{q}^*_{7/\mathrm{o}_7} \right]\!\right]_{\mathrm{L}} \left[\!\left[\boldsymbol{q}_{7/\mathrm{o}_7} \right]\!\right]_{\mathrm{R}}$
8	8	$c_{8,8} = -1$	$-\Lambda_8 \left[\!\left[\boldsymbol{q}^*_{8/\mathrm{o}_8} \right]\!\right]_{\mathrm{L}} \left[\!\left[\boldsymbol{q}_{8/\mathrm{o}_8} \right]\!\right]_{\mathrm{R}}$
9	9	$c_{9,9} = -1$	$-\Lambda_9 \left[\!\left[\boldsymbol{q}^*_{9/\mathrm{o}_9} \right]\!\right]_{\mathrm{L}} \left[\!\left[\boldsymbol{q}_{9/\mathrm{o}_9} \right]\!\right]_{\mathrm{R}}$
10	10	$c_{10,10} = -1$	$-\Lambda_{10} \left[\!\left[\boldsymbol{q}^*_{10/\mathrm{o}_{10}} \right]\!\right]_{\mathrm{L}} \left[\!\left[\boldsymbol{q}_{10/\mathrm{o}_{10}} \right]\!\right]_{\mathrm{R}}$

i	j	Entry $c_{i,j}$	Block $(\boldsymbol{\mathcal{S}}_{21})_{ij}$
i	j	$c_{i,j} = 1$	$\Lambda_i \left[\!\left[\boldsymbol{q}_{\mathrm{o_j}/\mathrm{i}} \right]\!\right]_{\mathrm{L}} \left[\!\left[\boldsymbol{q}^*_{\mathrm{o_j}/\mathrm{i}} \right]\!\right]_{\mathrm{R}}$
1	2	$c_{1,2} = 1$	$\Lambda_1 \left[\!\left[\boldsymbol{q}_{\mathrm{o}_2/1} \right]\!\right]_{\mathrm{L}} \left[\!\left[\boldsymbol{q}^*_{\mathrm{o}_2/1} \right]\!\right]_{\mathrm{R}}$
2	3	$c_{2,3} = 1$	$\Lambda_2 \left[\!\left[\boldsymbol{q}_{\mathrm{o}_3/2} \right]\!\right]_{\mathrm{L}} \left[\!\left[\boldsymbol{q}^*_{\mathrm{o}_3/2} \right]\!\right]_{\mathrm{R}}$
3	4	$c_{3,4} = 1$	$\Lambda_3 \left[\!\left[\boldsymbol{q}_{\mathrm{o}_4/3} \right]\!\right]_{\mathrm{L}} \left[\!\left[\boldsymbol{q}^*_{\mathrm{o}_4/3} \right]\!\right]_{\mathrm{R}}$
4	5	$c_{4,5} = 1$	$\Lambda_4 \left[\!\left[\boldsymbol{q}_{\mathrm{o}_5/4} \right]\!\right]_{\mathrm{L}} \left[\!\left[\boldsymbol{q}^*_{\mathrm{o}_5/4} \right]\!\right]_{\mathrm{R}}$
5	6	$c_{5,6} = 1$	$\Lambda_5 \left[\!\left[\boldsymbol{q}_{\mathrm{o}_6/5} \right]\!\right]_{\mathrm{L}} \left[\!\left[\boldsymbol{q}^*_{\mathrm{o}_6/5} \right]\!\right]_{\mathrm{R}}$

6	7	$c_{6,7} = 1$	$\Lambda_6 \left[\!\left[\boldsymbol{q}_{\mathfrak{o}_7/6} \right]\!\right]_{\mathrm{L}} \left[\!\left[\boldsymbol{q}^*_{\mathfrak{o}_7/6} \right]\!\right]_{\mathrm{R}}$
7	8	$c_{7,8} = 1$	$\Lambda_7 \left[\!\left[\boldsymbol{q}_{\mathfrak{o}_8/7} \right]\!\right]_{\mathrm{L}} \left[\!\left[\boldsymbol{q}^*_{\mathfrak{o}_8/7} \right]\!\right]_{\mathrm{R}}$
8	9	$c_{8,9} = 1$	$\Lambda_8 \left[\!\left[\boldsymbol{q}_{\mathfrak{o}_9/8} \right]\!\right]_{\mathrm{L}} \left[\!\left[\boldsymbol{q}^*_{\mathfrak{o}_9/8} \right]\!\right]_{\mathrm{R}}$
9	10	$c_{9,10} = 1$	$\Lambda_9 \left[\!\left[\boldsymbol{q}_{\mathfrak{o}_{10}/9} \right]\!\right]_{\mathrm{L}} \left[\!\left[\boldsymbol{q}^*_{\mathfrak{o}_{10}/9} \right]\!\right]_{\mathrm{R}}$
10	11	$c_{10,11} = 1$	$\Lambda_{10} \left[\!\left[\boldsymbol{q}_{\mathfrak{o}_{11}/10} \right]\!\right]_{\mathrm{L}} \left[\!\left[\boldsymbol{q}^*_{\mathfrak{o}_{11}/10} \right]\!\right]_{\mathrm{R}}$

7.5.4 Vector $\boldsymbol{\mathcal{B}_1}$

The vector $\boldsymbol{\mathcal{B}_1}$ can be associated to the right-hand side of the Newton-Euler equations of motion. It contains all known wrenches, transformed to the center of mass of the body in question; it includes the $-\boldsymbol{\omega} \times (M \star \boldsymbol{\omega}^{\mathsf{s}})$ term that originally appears on the left-hand side of the Newton-Euler equation; and it excludes the effect of reaction wrenches, since these are unknown. The general form of the $(\boldsymbol{\mathcal{B}}_1)_i$ term is given by

$$(\boldsymbol{\mathcal{B}}_1)_i = -\boldsymbol{\omega}^{\mathfrak{o}_{\mathrm{i}}}_{\mathfrak{o}_{\mathrm{i}}/\mathrm{I}} \times (M_{\mathfrak{o}_{\mathrm{i}}} \star (\boldsymbol{\omega}^{\mathfrak{o}_{\mathrm{i}}}_{\mathfrak{o}_{\mathrm{i}}/\mathrm{I}})^{\mathsf{s}}) + \boldsymbol{W}^{\mathfrak{o}_{\mathrm{i}}}_{\mathfrak{o}_{\mathrm{i}}}(O_{\mathfrak{o}_{\mathrm{i}}}) + b_i \boldsymbol{q}_{\mathrm{G_i}/\mathfrak{o}_{\mathrm{i}}} \boldsymbol{W}^{\mathrm{G_i}}_{\mathrm{ext,i}}(O_{\mathrm{G_i}}) \boldsymbol{q}^*_{\mathrm{G_i}/\mathfrak{o}_{\mathrm{i}}} + \sum_{j \in P(C(:,i))} \boldsymbol{q}^*_{\mathfrak{o}_{\mathrm{i}}/\mathrm{j}} \boldsymbol{W}^{\mathrm{j}}_{\mathrm{act,j}}(O_{\mathrm{j}}) \boldsymbol{q}_{\mathfrak{o}_{\mathrm{i}}/\mathrm{j}} - \sum_{j \in N(C(:,i))} \boldsymbol{q}_{\mathrm{j}/\mathfrak{o}_{\mathrm{i}}} \boldsymbol{W}^{\mathrm{j}}_{\mathrm{act,j}}(O_{\mathrm{j}}) \boldsymbol{q}^*_{\mathrm{j}/\mathfrak{o}_{\mathrm{i}}}. \tag{7.12}$$

There is one sub-vector $(\boldsymbol{\mathcal{B}}_1)_i$ associated to each body. These are given as follows.

$$
\begin{aligned}
(\boldsymbol{\mathcal{B}}_1)_1 &= -\boldsymbol{\omega}^{\circ_1}_{\circ_1/\mathrm{I}} \times (M_{\circ_1} \star (\boldsymbol{\omega}^{\circ_1}_{\circ_1/\mathrm{I}})^{\mathsf{S}}) + \boldsymbol{W}^{\circ_1}_{\circ_1}(O_{\circ_1}) \\
&\qquad - \sum_{j \in \{1,6\}} \boldsymbol{q}_{\mathrm{j}/\circ_1} \boldsymbol{W}^{\mathrm{j}}_{\mathrm{act,j}}(O_{\mathrm{j}}) \boldsymbol{q}^*_{\mathrm{j}/\circ_1} \\
(\boldsymbol{\mathcal{B}}_1)_2 &= -\boldsymbol{\omega}^{\circ_2}_{\circ_2/\mathrm{I}} \times (M_{\circ_2} \star (\boldsymbol{\omega}^{\circ_2}_{\circ_2/\mathrm{I}})^{\mathsf{S}}) + \boldsymbol{W}^{\circ_2}_{\circ_2}(O_{\circ_2}) \\
&\qquad + \sum_{j \in \{1\}} \boldsymbol{q}^*_{\circ_2/\mathrm{j}} \boldsymbol{W}^{\mathrm{j}}_{\mathrm{act,j}}(O_{\mathrm{j}}) \boldsymbol{q}_{\circ_2/\mathrm{j}} - \sum_{j \in \{2\}} \boldsymbol{q}_{\mathrm{j}/\circ_2} \boldsymbol{W}^{\mathrm{j}}_{\mathrm{act,j}}(O_{\mathrm{j}}) \boldsymbol{q}^*_{\mathrm{j}/\circ_2} \\
(\boldsymbol{\mathcal{B}}_1)_3 &= -\boldsymbol{\omega}^{\circ_3}_{\circ_3/\mathrm{I}} \times (M_{\circ_3} \star (\boldsymbol{\omega}^{\circ_3}_{\circ_3/\mathrm{I}})^{\mathsf{S}}) + \boldsymbol{W}^{\circ_3}_{\circ_3}(O_{\circ_3}) \\
&\qquad + \sum_{j \in \{2\}} \boldsymbol{q}^*_{\circ_3/\mathrm{j}} \boldsymbol{W}^{\mathrm{j}}_{\mathrm{act,j}}(O_{\mathrm{j}}) \boldsymbol{q}_{\circ_3/\mathrm{j}} - \sum_{j \in \{3\}} \boldsymbol{q}_{\mathrm{j}/\circ_3} \boldsymbol{W}^{\mathrm{j}}_{\mathrm{act,j}}(O_{\mathrm{j}}) \boldsymbol{q}^*_{\mathrm{j}/\circ_3} \\
(\boldsymbol{\mathcal{B}}_1)_4 &= -\boldsymbol{\omega}^{\circ_4}_{\circ_4/\mathrm{I}} \times (M_{\circ_4} \star (\boldsymbol{\omega}^{\circ_4}_{\circ_4/\mathrm{I}})^{\mathsf{S}}) + \boldsymbol{W}^{\circ_4}_{\circ_4}(O_{\circ_4}) \\
&\qquad + \sum_{j \in \{3\}} \boldsymbol{q}^*_{\circ_4/\mathrm{j}} \boldsymbol{W}^{\mathrm{j}}_{\mathrm{act,j}}(O_{\mathrm{j}}) \boldsymbol{q}_{\circ_4/\mathrm{j}} - \sum_{j \in \{4\}} \boldsymbol{q}_{\mathrm{j}/\circ_4} \boldsymbol{W}^{\mathrm{j}}_{\mathrm{act,j}}(O_{\mathrm{j}}) \boldsymbol{q}^*_{\mathrm{j}/\circ_4} \\
(\boldsymbol{\mathcal{B}}_1)_5 &= -\boldsymbol{\omega}^{\circ_5}_{\circ_5/\mathrm{I}} \times (M_{\circ_5} \star (\boldsymbol{\omega}^{\circ_5}_{\circ_5/\mathrm{I}})^{\mathsf{S}}) + \boldsymbol{W}^{\circ_5}_{\circ_5}(O_{\circ_5}) \\
&\qquad + \sum_{j \in \{4\}} \boldsymbol{q}^*_{\circ_5/\mathrm{j}} \boldsymbol{W}^{\mathrm{j}}_{\mathrm{act,j}}(O_{\mathrm{j}}) \boldsymbol{q}_{\circ_5/\mathrm{j}} - \sum_{j \in \{5\}} \boldsymbol{q}_{\mathrm{j}/\circ_5} \boldsymbol{W}^{\mathrm{j}}_{\mathrm{act,j}}(O_{\mathrm{j}}) \boldsymbol{q}^*_{\mathrm{j}/\circ_5} \\
(\boldsymbol{\mathcal{B}}_1)_6 &= -\boldsymbol{\omega}^{\circ_6}_{\circ_6/\mathrm{I}} \times (M_{\circ_6} \star (\boldsymbol{\omega}^{\circ_6}_{\circ_6/\mathrm{I}})^{\mathsf{S}}) + \boldsymbol{W}^{\circ_6}_{\circ_6}(O_{\circ_6}) + \boldsymbol{q}_{\mathrm{G}_1/\circ_6} \boldsymbol{W}^{\mathrm{G}_1}_{\mathrm{ext,1}}(O_{\mathrm{G}_1}) \boldsymbol{q}^*_{\mathrm{G}_1/\circ_6} \\
&\qquad + \sum_{j \in \{5\}} \boldsymbol{q}^*_{\circ_6/\mathrm{j}} \boldsymbol{W}^{\mathrm{j}}_{\mathrm{act,j}}(O_{\mathrm{j}}) \boldsymbol{q}_{\circ_6/\mathrm{j}} \\
(\boldsymbol{\mathcal{B}}_1)_7 &= -\boldsymbol{\omega}^{\circ_7}_{\circ_7/\mathrm{I}} \times (M_{\circ_7} \star (\boldsymbol{\omega}^{\circ_7}_{\circ_7/\mathrm{I}})^{\mathsf{S}}) + \boldsymbol{W}^{\circ_7}_{\circ_7}(O_{\circ_7}) \\
&\qquad + \sum_{j \in \{6\}} \boldsymbol{q}^*_{\circ_7/\mathrm{j}} \boldsymbol{W}^{\mathrm{j}}_{\mathrm{act,j}}(O_{\mathrm{j}}) \boldsymbol{q}_{\circ_7/\mathrm{j}} - \sum_{j \in \{7\}} \boldsymbol{q}_{\mathrm{j}/\circ_7} \boldsymbol{W}^{\mathrm{j}}_{\mathrm{act,j}}(O_{\mathrm{j}}) \boldsymbol{q}^*_{\mathrm{j}/\circ_7} \\
(\boldsymbol{\mathcal{B}}_1)_8 &= -\boldsymbol{\omega}^{\circ_8}_{\circ_8/\mathrm{I}} \times (M_{\circ_8} \star (\boldsymbol{\omega}^{\circ_8}_{\circ_8/\mathrm{I}})^{\mathsf{S}}) + \boldsymbol{W}^{\circ_8}_{\circ_8}(O_{\circ_8}) \\
&\qquad + \sum_{j \in \{7\}} \boldsymbol{q}^*_{\circ_8/\mathrm{j}} \boldsymbol{W}^{\mathrm{j}}_{\mathrm{act,j}}(O_{\mathrm{j}}) \boldsymbol{q}_{\circ_8/\mathrm{j}} - \sum_{j \in \{8\}} \boldsymbol{q}_{\mathrm{j}/\circ_8} \boldsymbol{W}^{\mathrm{j}}_{\mathrm{act,j}}(O_{\mathrm{j}}) \boldsymbol{q}^*_{\mathrm{j}/\circ_8} \\
(\boldsymbol{\mathcal{B}}_1)_9 &= -\boldsymbol{\omega}^{\circ_9}_{\circ_9/\mathrm{I}} \times (M_{\circ_9} \star (\boldsymbol{\omega}^{\circ_9}_{\circ_9/\mathrm{I}})^{\mathsf{S}}) + \boldsymbol{W}^{\circ_9}_{\circ_9}(O_{\circ_9}) \\
&\qquad + \sum_{j \in \{8\}} \boldsymbol{q}^*_{\circ_9/\mathrm{j}} \boldsymbol{W}^{\mathrm{j}}_{\mathrm{act,j}}(O_{\mathrm{j}}) \boldsymbol{q}_{\circ_9/\mathrm{j}} - \sum_{j \in \{9\}} \boldsymbol{q}_{\mathrm{j}/\circ_9} \boldsymbol{W}^{\mathrm{j}}_{\mathrm{act,j}}(O_{\mathrm{j}}) \boldsymbol{q}^*_{\mathrm{j}/\circ_9} \\
(\boldsymbol{\mathcal{B}}_1)_{10} &= -\boldsymbol{\omega}^{\circ_{10}}_{\circ_{10}/\mathrm{I}} \times (M_{\circ_{10}} \star (\boldsymbol{\omega}^{\circ_{10}}_{\circ_{10}/\mathrm{I}})^{\mathsf{S}}) + \boldsymbol{W}^{\circ_{10}}_{\circ_{10}}(O_{\circ_{10}}) \\
&\qquad + \sum_{j \in \{9\}} \boldsymbol{q}^*_{\circ_{10}/\mathrm{j}} \boldsymbol{W}^{\mathrm{j}}_{\mathrm{act,j}}(O_{\mathrm{j}}) \boldsymbol{q}_{\circ_{10}/\mathrm{j}} - \sum_{j \in \{10\}} \boldsymbol{q}_{\mathrm{j}/\circ_{10}} \boldsymbol{W}^{\mathrm{j}}_{\mathrm{act,j}}(O_{\mathrm{j}}) \boldsymbol{q}^*_{\mathrm{j}/\circ_{10}} \\
(\boldsymbol{\mathcal{B}}_1)_{11} &= -\boldsymbol{\omega}^{\circ_{11}}_{\circ_{11}/\mathrm{I}} \times (M_{\circ_{11}} \star (\boldsymbol{\omega}^{\circ_{11}}_{\circ_{11}/\mathrm{I}})^{\mathsf{S}}) + \boldsymbol{W}^{\circ_{11}}_{\circ_{11}}(O_{\circ_{11}}) + \boldsymbol{q}_{\mathrm{G}_2/\circ_{11}} \boldsymbol{W}^{\mathrm{G}_2}_{\mathrm{ext,2}}(O_{\mathrm{G}_2}) \boldsymbol{q}^*_{\mathrm{G}_2/\circ_{11}} \\
&\qquad + \sum_{j \in \{10\}} \boldsymbol{q}^*_{\circ_{11}/\mathrm{j}} \boldsymbol{W}^{\mathrm{j}}_{\mathrm{act,j}}(O_{\mathrm{j}}) \boldsymbol{q}_{\circ_{11}/\mathrm{j}}
\end{aligned}
\tag{7.13}
$$

7.5.5 Vector $\boldsymbol{\mathcal{B}_2}$

The vector $\boldsymbol{\mathcal{B}_2}$ can be associated to the right-hand side of the constraint equation that arises at each joint. The general form of the $(\boldsymbol{\mathcal{B}}_2)_i$ term is given by

$$(\boldsymbol{\mathcal{B}}_2)_i = \Lambda_i \boldsymbol{q}^*_{\mathrm{i}/\mathfrak{o}_\mathrm{k}} (\boldsymbol{\omega}^{\mathfrak{o}_\mathrm{k}}_{\mathfrak{o}_\mathrm{k}/\mathrm{I}} \times \boldsymbol{\omega}^{\mathfrak{o}_\mathrm{k}}_{\mathrm{i}/\mathfrak{o}_\mathrm{k}}) \boldsymbol{q}_{\mathrm{i}/\mathfrak{o}_\mathrm{k}} = \Lambda_i \boldsymbol{q}^*_{\mathrm{i}/\mathfrak{o}_\mathrm{k}} \boldsymbol{\omega}^{\mathfrak{o}_\mathrm{k}}_{\mathfrak{o}_\mathrm{k}/\mathrm{I}} \boldsymbol{q}_{\mathrm{i}/\mathfrak{o}_\mathrm{k}} \times \boldsymbol{\omega}^{\mathrm{i}}_{\mathrm{i}/\mathfrak{o}_\mathrm{k}}, \quad k = N(C(i,:)). \tag{7.14}$$

There is one sub-vector $(\boldsymbol{\mathcal{B}}_2)_i$ associated to each joint. These are given as follows.

$$\begin{aligned}
(\boldsymbol{\mathcal{B}}_2)_1 &= \Lambda_1 \boldsymbol{q}^*_{1/\mathfrak{o}_1} (\boldsymbol{\omega}^{\mathfrak{o}_1}_{\mathfrak{o}_1/\mathrm{I}} \times \boldsymbol{\omega}^{\mathfrak{o}_1}_{1/\mathfrak{o}_1}) \boldsymbol{q}_{1/\mathfrak{o}_1} = \Lambda_1 \boldsymbol{q}^*_{1/\mathfrak{o}_1} \boldsymbol{\omega}^{\mathfrak{o}_1}_{\mathfrak{o}_1/\mathrm{I}} \boldsymbol{q}_{1/\mathfrak{o}_1} \times \boldsymbol{\omega}^{1}_{1/\mathfrak{o}_1} \\
(\boldsymbol{\mathcal{B}}_2)_2 &= \Lambda_2 \boldsymbol{q}^*_{2/\mathfrak{o}_2} (\boldsymbol{\omega}^{\mathfrak{o}_2}_{\mathfrak{o}_2/\mathrm{I}} \times \boldsymbol{\omega}^{\mathfrak{o}_2}_{2/\mathfrak{o}_2}) \boldsymbol{q}_{2/\mathfrak{o}_2} = \Lambda_2 \boldsymbol{q}^*_{2/\mathfrak{o}_2} \boldsymbol{\omega}^{\mathfrak{o}_2}_{\mathfrak{o}_2/\mathrm{I}} \boldsymbol{q}_{2/\mathfrak{o}_2} \times \boldsymbol{\omega}^{2}_{2/\mathfrak{o}_2} \\
(\boldsymbol{\mathcal{B}}_2)_3 &= \Lambda_3 \boldsymbol{q}^*_{3/\mathfrak{o}_3} (\boldsymbol{\omega}^{\mathfrak{o}_3}_{\mathfrak{o}_3/\mathrm{I}} \times \boldsymbol{\omega}^{\mathfrak{o}_3}_{3/\mathfrak{o}_3}) \boldsymbol{q}_{3/\mathfrak{o}_3} = \Lambda_3 \boldsymbol{q}^*_{3/\mathfrak{o}_3} \boldsymbol{\omega}^{\mathfrak{o}_3}_{\mathfrak{o}_3/\mathrm{I}} \boldsymbol{q}_{3/\mathfrak{o}_3} \times \boldsymbol{\omega}^{3}_{3/\mathfrak{o}_3} \\
(\boldsymbol{\mathcal{B}}_2)_4 &= \Lambda_4 \boldsymbol{q}^*_{4/\mathfrak{o}_4} (\boldsymbol{\omega}^{\mathfrak{o}_4}_{\mathfrak{o}_4/\mathrm{I}} \times \boldsymbol{\omega}^{\mathfrak{o}_4}_{4/\mathfrak{o}_4}) \boldsymbol{q}_{4/\mathfrak{o}_4} = \Lambda_4 \boldsymbol{q}^*_{4/\mathfrak{o}_4} \boldsymbol{\omega}^{\mathfrak{o}_4}_{\mathfrak{o}_4/\mathrm{I}} \boldsymbol{q}_{4/\mathfrak{o}_4} \times \boldsymbol{\omega}^{4}_{4/\mathfrak{o}_4} \\
(\boldsymbol{\mathcal{B}}_2)_5 &= \Lambda_5 \boldsymbol{q}^*_{5/\mathfrak{o}_5} (\boldsymbol{\omega}^{\mathfrak{o}_5}_{\mathfrak{o}_5/\mathrm{I}} \times \boldsymbol{\omega}^{\mathfrak{o}_5}_{5/\mathfrak{o}_5}) \boldsymbol{q}_{5/\mathfrak{o}_5} = \Lambda_5 \boldsymbol{q}^*_{5/\mathfrak{o}_5} \boldsymbol{\omega}^{\mathfrak{o}_5}_{\mathfrak{o}_5/\mathrm{I}} \boldsymbol{q}_{5/\mathfrak{o}_5} \times \boldsymbol{\omega}^{5}_{5/\mathfrak{o}_5} \\
(\boldsymbol{\mathcal{B}}_2)_6 &= \Lambda_6 \boldsymbol{q}^*_{6/\mathfrak{o}_1} (\boldsymbol{\omega}^{\mathfrak{o}_1}_{\mathfrak{o}_1/\mathrm{I}} \times \boldsymbol{\omega}^{\mathfrak{o}_1}_{6/\mathfrak{o}_1}) \boldsymbol{q}_{6/\mathfrak{o}_1} = \Lambda_6 \boldsymbol{q}^*_{6/\mathfrak{o}_1} \boldsymbol{\omega}^{\mathfrak{o}_1}_{\mathfrak{o}_1/\mathrm{I}} \boldsymbol{q}_{6/\mathfrak{o}_1} \times \boldsymbol{\omega}^{6}_{6/\mathfrak{o}_1} \\
(\boldsymbol{\mathcal{B}}_2)_7 &= \Lambda_7 \boldsymbol{q}^*_{7/\mathfrak{o}_7} (\boldsymbol{\omega}^{\mathfrak{o}_7}_{\mathfrak{o}_7/\mathrm{I}} \times \boldsymbol{\omega}^{\mathfrak{o}_7}_{7/\mathfrak{o}_7}) \boldsymbol{q}_{7/\mathfrak{o}_7} = \Lambda_7 \boldsymbol{q}^*_{7/\mathfrak{o}_7} \boldsymbol{\omega}^{\mathfrak{o}_7}_{\mathfrak{o}_7/\mathrm{I}} \boldsymbol{q}_{7/\mathfrak{o}_7} \times \boldsymbol{\omega}^{7}_{7/\mathfrak{o}_7} \\
(\boldsymbol{\mathcal{B}}_2)_8 &= \Lambda_8 \boldsymbol{q}^*_{8/\mathfrak{o}_8} (\boldsymbol{\omega}^{\mathfrak{o}_8}_{\mathfrak{o}_8/\mathrm{I}} \times \boldsymbol{\omega}^{\mathfrak{o}_8}_{8/\mathfrak{o}_8}) \boldsymbol{q}_{8/\mathfrak{o}_8} = \Lambda_8 \boldsymbol{q}^*_{8/\mathfrak{o}_8} \boldsymbol{\omega}^{\mathfrak{o}_8}_{\mathfrak{o}_8/\mathrm{I}} \boldsymbol{q}_{8/\mathfrak{o}_8} \times \boldsymbol{\omega}^{8}_{8/\mathfrak{o}_8} \\
(\boldsymbol{\mathcal{B}}_2)_9 &= \Lambda_9 \boldsymbol{q}^*_{9/\mathfrak{o}_9} (\boldsymbol{\omega}^{\mathfrak{o}_9}_{\mathfrak{o}_9/\mathrm{I}} \times \boldsymbol{\omega}^{\mathfrak{o}_9}_{9/\mathfrak{o}_9}) \boldsymbol{q}_{9/\mathfrak{o}_9} = \Lambda_9 \boldsymbol{q}^*_{9/\mathfrak{o}_9} \boldsymbol{\omega}^{\mathfrak{o}_9}_{\mathfrak{o}_9/\mathrm{I}} \boldsymbol{q}_{9/\mathfrak{o}_9} \times \boldsymbol{\omega}^{9}_{9/\mathfrak{o}_9} \\
(\boldsymbol{\mathcal{B}}_2)_{10} &= \Lambda_{10} \boldsymbol{q}^*_{10/\mathfrak{o}_{10}} (\boldsymbol{\omega}^{\mathfrak{o}_{10}}_{\mathfrak{o}_{10}/\mathrm{I}} \times \boldsymbol{\omega}^{\mathfrak{o}_{10}}_{10/\mathfrak{o}_{10}}) \boldsymbol{q}_{10/\mathfrak{o}_{10}} = \Lambda_{10} \boldsymbol{q}^*_{10/\mathfrak{o}_{10}} \boldsymbol{\omega}^{\mathfrak{o}_{10}}_{\mathfrak{o}_{10}/\mathrm{I}} \boldsymbol{q}_{10/\mathfrak{o}_{10}} \times \boldsymbol{\omega}^{10}_{10/\mathfrak{o}_{10}}
\end{aligned} \tag{7.15}$$

7.6 Numerical Results

The equations were implemented in MATLAB and simulated using the Simulink environment. The relative and absolute tolerances for the ODE45 solver were set to 1e-13. The satellite and all bodies are initially at rest and during the 20 second simulation, each of the joints is independently actuated for a duration of 1 s. The j-th degree of freedom corre-

sponding to the motion of generalized coordinate Γ_j (j-th entry of Γ) is actuated as

$$\begin{aligned} n_j(t) &= 0.2\sin(t-(j+1)) \quad \text{N}, \qquad j+1 < t < j+2 \quad \text{if translational,} \\ n_j(t) &= 0.1\sin(t-(j+1)) \quad \text{Nm}, \qquad j+1 < t < j+2 \quad \text{if rotational.} \end{aligned} \tag{7.16}$$

Additionally, as is common in numerical schemes that use dual quaternions, the dual quaternion $\boldsymbol{q}_{\mathbf{e}_1/\mathrm{I}}$ is normalized after every integration timestep using the following scheme introduced in equation (2.30), and restated here as

$$\begin{aligned} \boldsymbol{q}_r &\coloneqq \frac{\boldsymbol{q}_r}{\|\boldsymbol{q}_r\|}, \\ \boldsymbol{q}_d &\coloneqq \left(I_{4\times 4} - \frac{\boldsymbol{q}_r \boldsymbol{q}_r^{\mathrm{T}}}{\|\boldsymbol{q}_r\|^2}\right) \boldsymbol{q}_d. \end{aligned} \tag{7.17}$$

This ensures that the resulting dual quaternion satisfies the unit dual quaternion constraints (real part has unit norm; and real and dual parts are orthogonal). Figures 7.4 and 7.5 show the evolution of the system center of mass, and the evolution of its components with respect to the initial center of mass location respectively. Figure 7.6 shows the linear momentum of the system and Figure 7.7 shows the angular momentum of the system. These are, respectively, the real and dual part of the dual momentum, which can be computed from equation (2.53). Additionally, we provide the kinetic energy of the system for completeness in Figure 7.8, which can be easily computed from equation (2.54). Finally, we provide the reaction wrenches in Figure 7.9. Contrary to methods based on minimal representations of the state such as Kane's method or the Lagrangian method, the proposed framework does not require the computation of a virtual displacement to compute reaction wrenches.

These results confirm that the system conserves linear and angular momentum when exposed to internal wrenches, regardless of the type of joint selected, which is a step towards verification of the validity of the equations of motion.

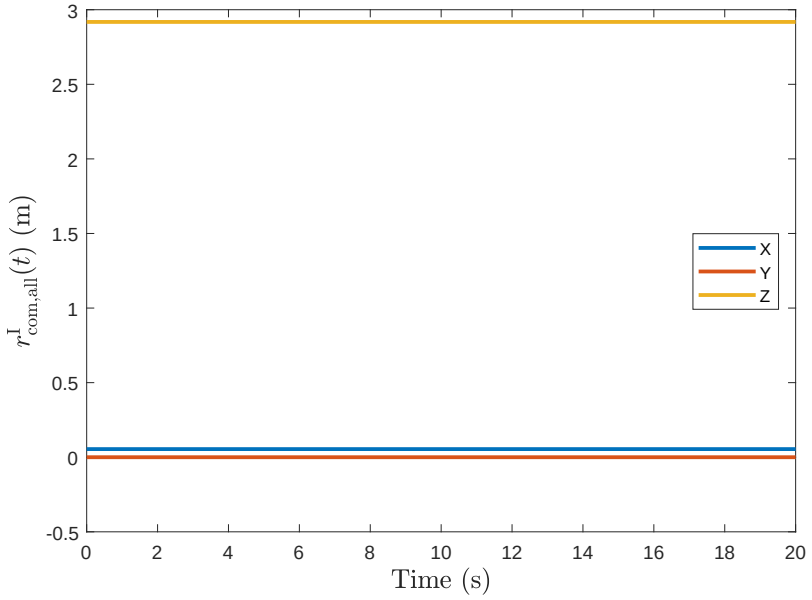

Figure 7.4: Center of mass position for two-arm satellite configuration.

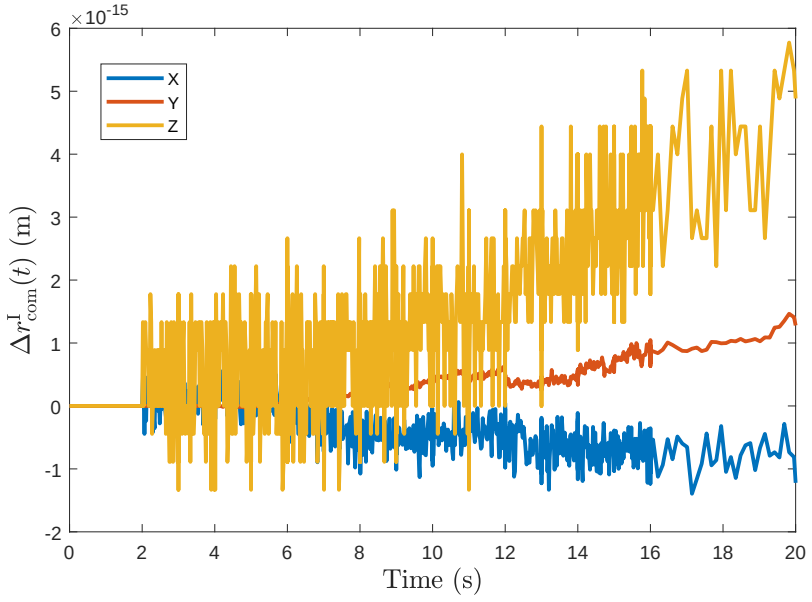

Figure 7.5: Center of mass position deviation with respect to initial position for two-arm satellite configuration.

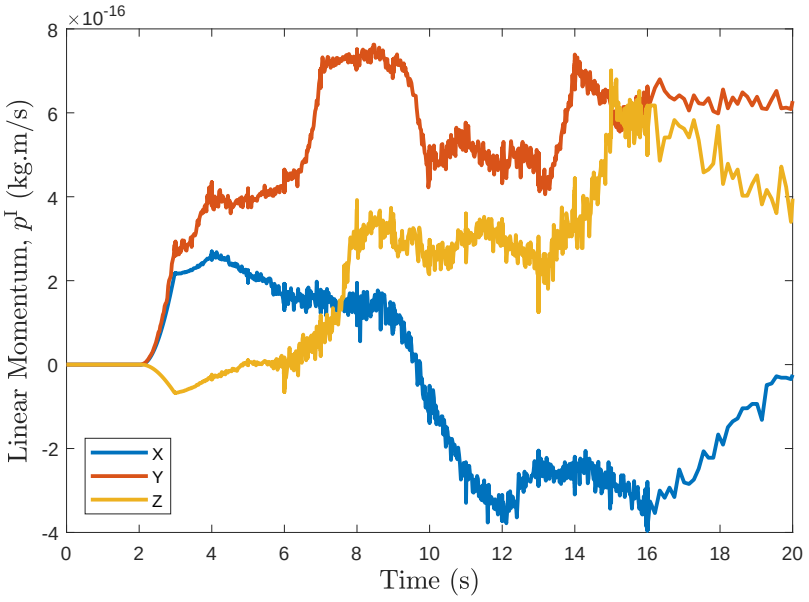

Figure 7.6: Linear momentum vector components for two-arm satellite configuration.

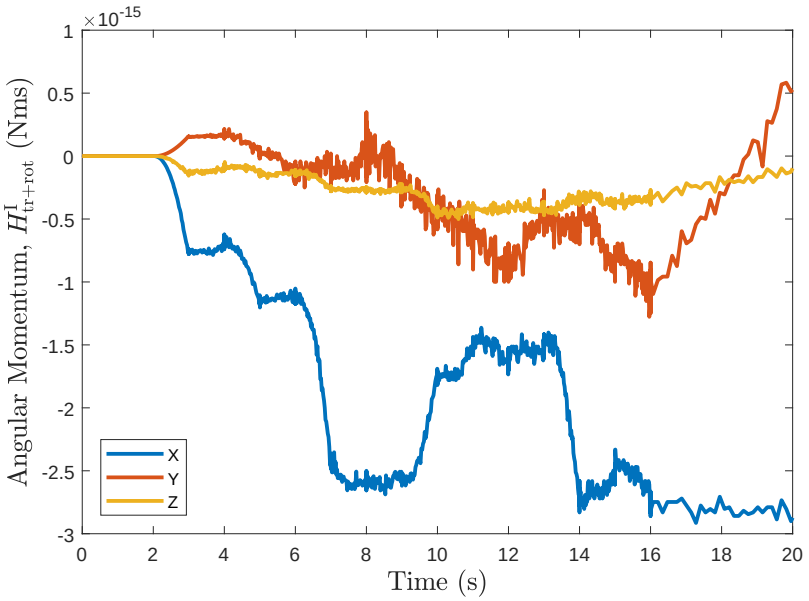

Figure 7.7: Angular momentum vector components for two-arm satellite configuration.

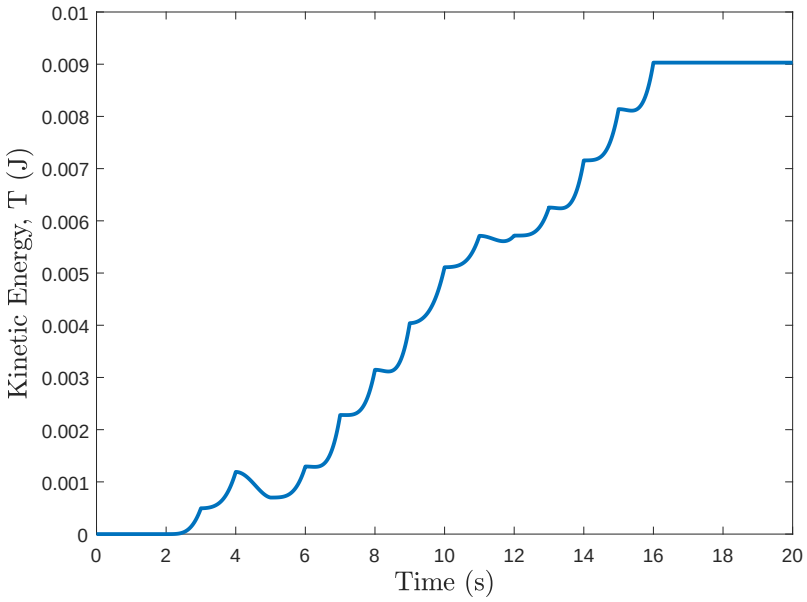

Figure 7.8: Kinetic energy for two-arms satellite configuration.

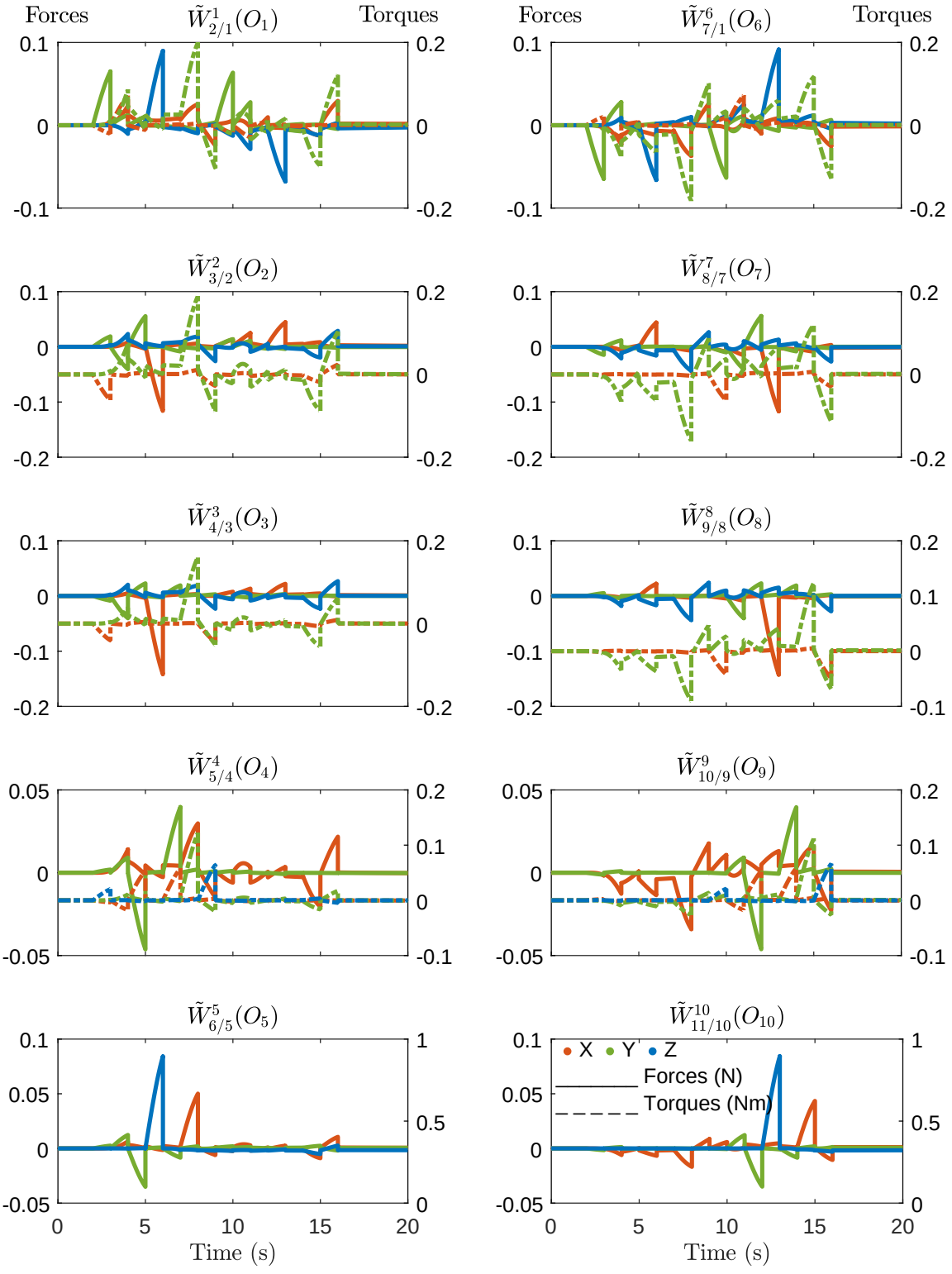

Figure 7.9: Reaction wrenches for a two-arm satellite configuration. Units: forces in N, torques in Nm.

CHAPTER 8
ROBOTIC END EFFECTOR CONTROL

In this chapter we will design a control strategy for use in robotic manipulation for space operations.

8.1 Differential Dynamic Programming

Differential dynamic programming (DDP) is a widely studied method developed for the control of dynamical systems. The application of DDP is based on the solution of the Hamilton-Jacobi-Bellman equation in the context of optimal control theory. Foundational work for DDP developed by Jacobson et al. in [147], followed by work by Yakowitz and Rutherford in [148], among others cited therein, laid the ground for the effective and efficient implementation of the algorithm to complicated, fully non-linear control problems. Yakowitz argues that DDP has the following benefits for unconstrained problems [148]:

- Overcomes the curse of dimensionality.
- Provides global convergence under "lenient" conditions.
- Quadratic convergence for well-behaved problems in which the Hessian is positive-definite on a neighborhood of the solution.

8.2 Derivation of Differential Dynamic Programming

The derivation presented herein is well known and closely follows the work in [148]. Given a continuous time system

$$\dot{x}(t) = f(x(t), u(t), t), \qquad x(0) = x_0, \tag{8.1}$$

where $f : \mathbb{R}^n \times \mathbb{R}^m \times \mathbb{R} \rightarrow \mathbb{R}^n$, we pose the optimal control problem which aims at minimizing the cost functional

$$J_c(x_0, U) = \ell_f(x(t_f), t_f) + \int_0^T \ell(x(t), u(t), t)\mathrm{d}t, \tag{8.2}$$

where $\ell(x(t), u(t), t)$ is the continuous-time running cost and $\ell_f(x(t_f), t_f)$ is the final cost. For such a system, we can compute the linearized continuous dynamics from a first order Taylor Series expansion about the nominal trajectory $(\bar{x}(t), \bar{u}(t), t)$ as

$$\frac{\mathrm{d}}{\mathrm{d}t}(\delta x(t)) = f_x(\bar{x}(t), \bar{u}(t), t)\delta x(t) + f_u(\bar{x}(t), \bar{u}(t), t)\delta u(t) \tag{8.3}$$

$$= \phi(\bar{x}(t), \bar{u}(t), t)\delta x(t) + \tilde{B}(\bar{x}(t), \bar{u}(t), t)\delta u(t). \tag{8.4}$$

Here, we have defined $\delta x(t) \triangleq x(t) - \bar{x}(t)$, $\delta u(t) \triangleq u(t) - \bar{u}(t)$, $\Delta t = t_{k+1} - t_k$, $f_x = \nabla_x f$ and $f_u = \nabla_u f$. Applying a first-order Newton discretization we get

$$\frac{\delta x(t_{k+1}) - \delta x(t_k)}{\Delta t} = \phi(\bar{x}(t_k), \bar{u}(t_k), t_k)\delta x(t_k) + \tilde{B}(\bar{x}(t_k), \bar{u}(t_k), t_k)\delta u(t_k). \tag{8.5}$$

Thus, our expression for $\delta x(t_{k+1})$ can be written as

$$\delta x(t_{k+1}) = \Phi(\bar{x}, \bar{u}, t_k)\delta x(t_k) + B(\bar{x}, \bar{u}, t_k)\delta u(t_k), \tag{8.6}$$

with

$$\Phi(\bar{x}, \bar{u}, t_k) = \mathbb{I}_n + \phi(\bar{x}, \bar{u}, t_k)\Delta t = \mathbb{I}_n + f_x(\bar{x}, \bar{u}, t_k)\Delta t \tag{8.7}$$

$$B(\bar{x}, \bar{u}, t_k) = \tilde{B}(\bar{x}, \bar{u}, t_k)\Delta t = f_u(\bar{x}, \bar{u}, t_k)\Delta t \tag{8.8}$$

$$\Delta t = t_{k+1} - t_k. \tag{8.9}$$

Given a sequence of control inputs $U = \{u(t_k)\}_{k=0}^{k=N-1}$, we can define the cost function

for this problem as

$$J(x_0, U) = \mathcal{L}_f(x(t_f), t_f) + \sum_{k=0}^{N-1} \mathcal{L}(x(t_k), u(t_k), t_k), \tag{8.10}$$

where the discrete-time running cost is denoted by $\mathcal{L}(x(t_k), u(t_k), t_k)$ and it is defined as

$$\mathcal{L}(x(t_k), u(t_k), t_k) \triangleq \ell(x(t_k), u(t_k), t_k)\Delta t, \tag{8.11}$$

and $\mathcal{L}_f(x(t_f), t_f)$ is the final cost.

The Bellman principle in discrete time is given as

$$V(x(t_k), t_k) = \min_{u(t_k)} Q(x(t_k), u(t_k), t_k), \tag{8.12}$$

where $Q(x(t_k), u(t_k), t_k)$ is the state-action value function, and it encompasses the running cost and the cost-to-go. We define Q as

$$Q(x(t_k), u(t_k), t_k) \triangleq \mathcal{L}(x(t_k), u(t_k), t_k) + V(x(t_{k+1}), t_{k+1}). \tag{8.13}$$

Finally, we will define the value function $V(x(t_k), t_k)$ to satisfy the final condition

$$V(x(t_f), t_f) \triangleq \mathcal{L}_f(x(t_f), t_f). \tag{8.14}$$

We want to relate the Q, $\mathcal{L}$, and V from equation (8.13) via the dynamics given in equation (8.6). Thus, we will expand each of the three using a second order Taylor series

expansion. Since Q and $\mathcal{L}$ are evaluated at t_k, their expansion is simply given by

$$Q(x(t_k), u(t_k), t_k) = Q(\bar{x}(t_k), \bar{u}(t_k), t_k) + Q_x \delta x(t_k) + Q_u \delta u(t_k) + \frac{1}{2} \begin{bmatrix} \delta x(t_k) \\ \delta u(t_k) \end{bmatrix}^T \begin{bmatrix} Q_{xx} & Q_{xu} \\ Q_{ux} & Q_{uu} \end{bmatrix} \begin{bmatrix} \delta x(t_k) \\ \delta u(t_k) \end{bmatrix}, \quad (8.15)$$

and

$$\mathcal{L}(x(t_k), u(t_k), t_k) = \mathcal{L}(\bar{x}(t_k), \bar{u}(t_k), t_k) + \mathcal{L}_x \delta x(t_k) + \mathcal{L}_u \delta u(t_k) + \frac{1}{2} \begin{bmatrix} \delta x(t_k) \\ \delta u(t_k) \end{bmatrix}^T \begin{bmatrix} \mathcal{L}_{xx} & \mathcal{L}_{xu} \\ \mathcal{L}_{ux} & \mathcal{L}_{uu} \end{bmatrix} \begin{bmatrix} \delta x(t_k) \\ \delta u(t_k) \end{bmatrix}. \quad (8.16)$$

In this expansion, all the partial derivatives of Q and $\mathcal{L}$ are evaluated at $\bar{x}(t_k)$, $\bar{u}(t_k)$, and time t_k.

On the other hand, $V(x(t_{k+1}), t_{k+1})$ is evaluated at the next time step. Its Taylor Series expansion is given as

$$V(x(t_{k+1}), t_{k+1}) = V(\bar{x}(t_{k+1}), t_{k+1}) + V_x(\bar{x}(t_{k+1}), t_{k+1}) \delta x(t_{k+1}) + \frac{1}{2} \delta x(t_{k+1})^T V_{xx}(\bar{x}(t_{k+1}), t_{k+1}) \delta x(t_{k+1}), \quad (8.17)$$

and substituting the dynamics given in equation (8.6) yields

$$V(x(t_{k+1}), t_{k+1}) = V(\bar{x}(t_{k+1}), t_{k+1}) + V_x(\bar{x}(t_{k+1}), t_{k+1})(\Phi \delta x(t_k) + B \delta u(t_k)) + \frac{1}{2} (\Phi \delta x(t_k) + B \delta u(t_k))^{\mathrm{T}} V_{xx}(\bar{x}(t_{k+1}), t_{k+1})(\Phi \delta x(t_k) + B \delta u(t_k)), \quad (8.18)$$

$$V(x(t_{k+1}),t_{k+1}) = V(\bar{x}(t_{k+1}),t_{k+1}) + V_x(\bar{x}(t_{k+1}),t_{k+1})\Phi\delta x(t_k) + V_x(\bar{x}(t_{k+1}),t_{k+1})B\delta u(t_k) + \frac{1}{2}\begin{bmatrix}\delta x(t_k)\\ \delta u(t_k)\end{bmatrix}^{\mathrm{T}}\begin{bmatrix}\Phi^{\mathrm{T}}V_{xx}(\bar{x}(t_{k+1}),t_{k+1})\Phi & \Phi^{\mathrm{T}}V_{xx}(\bar{x}(t_{k+1}),t_{k+1})B\\ B^{\mathrm{T}}V_{xx}(\bar{x}(t_{k+1}),t_{k+1})\Phi & B^{\mathrm{T}}V_{xx}(\bar{x}(t_{k+1}),t_{k+1})B\end{bmatrix}\begin{bmatrix}\delta x(t_k)\\ \delta u(t_k)\end{bmatrix}. \quad (8.19)$$

By comparison of equations (8.15), (8.16) and (8.19) through equation (8.13) we can obtain the following relationships for the terms that appear in the expansion of $Q(x(t_k),u(t_k),t_k)$:

$$Q(\bar{x}(t_k),\bar{u}(t_k),t_k) = \mathcal{L}(\bar{x}(t_k),\bar{u}(t_k),t_k) + V(\bar{x}(t_{k+1}),t_{k+1}), \quad (8.20)$$

$$Q_x(\bar{x}(t_k),\bar{u}(t_k),t_k) = \mathcal{L}_x(\bar{x}(t_k),\bar{u}(t_k),t_k) + V_x(\bar{x}(t_{k+1}),t_{k+1})\Phi, \quad (8.21)$$

$$Q_u(\bar{x}(t_k),\bar{u}(t_k),t_k) = \mathcal{L}_u(\bar{x}(t_k),\bar{u}(t_k),t_k) + V_x(\bar{x}(t_{k+1}),t_{k+1})B, \quad (8.22)$$

$$Q_{xx}(\bar{x}(t_k),\bar{u}(t_k),t_k) = \mathcal{L}_{xx}(\bar{x}(t_k),\bar{u}(t_k),t_k) + \Phi^{\mathrm{T}}V_{xx}(\bar{x}(t_{k+1}),t_{k+1})\Phi, \quad (8.23)$$

$$Q_{xu}(\bar{x}(t_k),\bar{u}(t_k),t_k) = \mathcal{L}_{xu}(\bar{x}(t_k),\bar{u}(t_k),t_k) + \Phi^{\mathrm{T}}V_{xx}(\bar{x}(t_{k+1}),t_{k+1})B, \quad (8.24)$$

$$Q_{ux}(\bar{x}(t_k),\bar{u}(t_k),t_k) = \mathcal{L}_{ux}(\bar{x}(t_k),\bar{u}(t_k),t_k) + B^{\mathrm{T}}V_{xx}(\bar{x}(t_{k+1}),t_{k+1})\Phi, \quad (8.25)$$

$$Q_{uu}(\bar{x}(t_k),\bar{u}(t_k),t_k) = \mathcal{L}_{uu}(\bar{x}(t_k),\bar{u}(t_k),t_k) + B^{\mathrm{T}}V_{xx}(\bar{x}(t_{k+1}),t_{k+1})B. \quad (8.26)$$

To determine the optimal control $u^*(t_k)$ we now minimize the functional $Q(x(t_k),u(t_k),t_k)$ with respect to $\delta u(t_k)$. Thus,

$$0 = \frac{\partial}{\partial\delta u(t_k)}Q(x(t_k),u(t_k),t_k),$$

which yields

$$0 = Q_u(\bar{x}(t_k),\bar{u}(t_k),t_k) + \tfrac{1}{2}\delta x(t_k)^{\mathrm{T}}Q_{ux}(\bar{x}(t_k),\bar{u}(t_k),t_k)^{\mathrm{T}} + \tfrac{1}{2}\delta x^{\mathrm{T}}(t_k)Q_{xu}(\bar{x}(t_k),\bar{u}(t_k),t_k) + \delta u^{\mathrm{T}}(t_k)Q_{uu}(\bar{x}(t_k),\bar{u}(t_k),t_k).$$

Now, assuming the positive definiteness of Q_{uu} so that

$$Q_{uu}(\bar{x}(t_k), \bar{u}(t_k), t_k) > 0, \tag{8.27}$$

and using the fact that

$$Q_{ux}(\bar{x}(t_k), \bar{u}(t_k), t_k) = Q_{xu}(\bar{x}(t_k), \bar{u}(t_k), t_k)^{\mathrm{T}}, \tag{8.28}$$

we obtain the following relationship for $\delta u^*(t_k)$:

$$\begin{aligned}\delta u^*(t_k) = &\overbrace{-Q_{uu}^{-1}(\bar{x}(t_k), \bar{u}(t_k), t_k) Q_{ux}(\bar{x}(t_k), \bar{u}(t_k), t_k)\delta x(t_k)}^{\text{feedback}} \\ &\underbrace{- Q_{uu}^{-1}(\bar{x}(t_k), \bar{u}(t_k), t_k) Q_u(\bar{x}(t_k), \bar{u}(t_k), t_k)^{\mathrm{T}}}_{\text{feedforward}}.\end{aligned} \tag{8.29}$$

In order to simplify the notation, we will remove the dependencies of Q and simply denote the optimal update of the controller as

$$\begin{aligned}\delta u^*(t_k) &= -Q_{uu}^{-1} Q_{ux} \delta x(t_k) - Q_{uu}^{-1} Q_u^{\mathrm{T}} \\ &= L\delta x(t_k) + l,\end{aligned} \tag{8.30}$$

where $L \triangleq -Q_{uu}^{-1} Q_{ux}$ is a time-dependent feedback matrix and $l \triangleq -Q_{uu}^{-1} Q_u^{\mathrm{T}}$ is a time-dependent feedforward term.

For the optimal control $u^*(t)$, the Bellman principle can now be written as

$$V(x(t_k), t_k) = Q(x(t_k), u^*(t_k), t_k).$$

Expanding both sides as a Taylor series we obtain the following relationships:

$$
\begin{aligned}
&V(\bar{x}(t_k),t_k) + V_x(\bar{x}(t_k),t_k)\delta x(t_k) + \tfrac{1}{2}\delta x(t_k)^{\mathrm{T}} V_{xx}(\bar{x}(t_k),t_k)\delta x(t_k) \\
&\quad = Q(\bar{x}(t_k),\bar{u}(t_k),t_k) + Q_x(\bar{x}(t_k),\bar{u}(t_k),t_k)\delta x(t_k) + Q_u(\bar{x}(t_k),\bar{u}(t_k),t_k)\delta u^*(t_k) \\
&\qquad + \tfrac{1}{2}\begin{bmatrix} \delta x(t_k) \\ \delta u^*(t_k) \end{bmatrix}^{\mathrm{T}} \begin{bmatrix} Q_{xx}(\bar{x}(t_k),\bar{u}(t_k),t_k) & Q_{xu}(\bar{x}(t_k),\bar{u}(t_k),t_k) \\ Q_{ux}(\bar{x}(t_k),\bar{u}(t_k),t_k) & Q_{uu}(\bar{x}(t_k),\bar{u}(t_k),t_k) \end{bmatrix} \begin{bmatrix} \delta x(t_k) \\ \delta u^*(t_k) \end{bmatrix}.
\end{aligned}
$$

Furthermore, if we substitute $\delta u^*(t_k)$ from equation (8.30) into the Taylor series expansion of $Q(x(t_k), u^*(t_k), t_k)$, we will obtain

$$
\begin{aligned}
&V + V_x\delta x(t_k) + \tfrac{1}{2}\delta x(t_k)^{\mathrm{T}} V_{xx}\delta x(t_k) \\
&\qquad = Q + Q_x\delta x(t_k) + Q_u[-Q_{uu}^{-1}Q_{ux}\delta x(t_k) - Q_{uu}^{-1}Q_u^{\mathrm{T}}] \\
&\qquad + \tfrac{1}{2}\delta x(t_k)^T Q_{xx}\delta x(t_k) \\
&\qquad + \tfrac{1}{2}\delta x(t_k)^T Q_{xu}[-Q_{uu}^{-1}Q_{ux}\delta x(t_k) - Q_{uu}^{-1}Q_u^T] \\
&\qquad + \tfrac{1}{2}[-Q_{uu}^{-1}Q_{ux}\delta x(t_k) - Q_{uu}^{-1}Q_u^T]^T Q_{ux}\delta x(t_k) \\
&\qquad + \tfrac{1}{2}[-Q_{uu}^{-1}Q_{ux}\delta x(t_k) - Q_{uu}^{-1}Q_u^T]^T Q_{uu}[-Q_{uu}^{-1}Q_{ux}\delta x(t_k) - Q_{uu}^{-1}Q_u^T].
\end{aligned}
$$

Comparing terms on both sides of the equation and using the symmetry of Q_{uu}^{-1} we get the following relationships

$$V = Q - \tfrac{1}{2}Q_u Q_{uu}^{-1} Q_u^T, \tag{8.31}$$

$$V_x = Q_x - Q_u Q_{uu}^{-1} Q_{ux}, \tag{8.32}$$

$$V_{xx} = Q_{xx} - Q_{xu} Q_{uu}^{-1} Q_{ux}, \tag{8.33}$$

where all V terms are evaluated at $(\bar{x}(t_k), t_k)$ and all Q terms are evaluated at $(\bar{x}(t_k), \bar{u}(t_k), t_k)$. We now have all the equations necessary for the implementation of DDP.

However, if we considered a second order Taylor series expansion of the dynamics

given by

$$f(x(t),u(t)) = f(\bar{x}(t),\bar{u}(t)) + f_x(\bar{x}(t),\bar{u}(t))\delta x(t) + f_u(\bar{x}(t),\bar{u}(t))\delta u(t) + \theta(\bar{x}(t),\bar{u}(t)), \quad (8.34)$$

where

$$\theta(\bar{x}(t),\bar{u}(t)) = \begin{bmatrix} \theta_1(\bar{x}(t),\bar{u}(t)) \\ \theta_2(\bar{x}(t),\bar{u}(t)) \\ \vdots \\ \theta_n(\bar{x}(t),\bar{u}(t)) \end{bmatrix}, \quad (8.35)$$

$$\theta_i(\bar{x}(t),\bar{u}(t)) = \frac{1}{2}\begin{bmatrix} \delta x(t) \\ \delta u(t) \end{bmatrix}^{\mathrm{T}} \begin{bmatrix} f_{xx,i}(\bar{x}(t),\bar{u}(t)) & f_{xu,i}(\bar{x}(t),\bar{u}(t)) \\ f_{ux,i}(\bar{x}(t),\bar{u}(t)) & f_{uu,i}(\bar{x}(t),\bar{u}(t)) \end{bmatrix} \begin{bmatrix} \delta x(t) \\ \delta u(t) \end{bmatrix}, \quad (8.36)$$

then equation (8.6) would become

$$\delta x(t_{k+1}) = \Phi(\bar{x}(t_k),\bar{u}(t_k),t_k)\delta x(t_k) + B(\bar{x}(t_k),\bar{u}(t_k),t_k)\delta u(t_k) + \Theta(\bar{x}(t_k),\bar{u}(t_k)), \quad (8.37)$$

where

$$\Theta(\bar{x}(t_k),\bar{u}(t_k)) = \theta(\bar{x}(t_k),\bar{u}(t_k))\mathrm{d}t. \quad (8.38)$$

Using this expansion of the dynamics in equation (8.17) and preserving up to the quadratic terms, equations (8.23), (8.25) and (8.26) would incorporate an additional term as

$$Q_{xx}(\bar{x}(t_k),\bar{u}(t_k),t_k) = \mathcal{L}_{xx}(\bar{x}(t_k),\bar{u}(t_k),t_k) + \Phi^{\mathrm{T}}V_{xx}(\bar{x}(t_{k+1}),t_{k+1})\Phi + \mathcal{Z}_1, \quad (8.39)$$

$$Q_{uu}(\bar{x}(t_k),\bar{u}(t_k),t_k) = \mathcal{L}_{uu}(\bar{x}(t_k),\bar{u}(t_k),t_k) + B^{\mathrm{T}}V_{xx}(\bar{x}(t_{k+1}),t_{k+1})B + \mathcal{Z}_2, \quad (8.40)$$

$$Q_{ux}(\bar{x}(t_k),\bar{u}(t_k),t_k) = \mathcal{L}_{ux}(\bar{x}(t_k),\bar{u}(t_k),t_k) + B^{\mathrm{T}}V_{xx}(\bar{x}(t_{k+1}),t_{k+1})\Phi + \mathcal{Z}_3. \quad (8.41)$$

Here,

$$\mathcal{Z}_1 = \sum_{j=1}^{n} \frac{\partial V}{\partial x_j}(\bar{x}(t_{k+1}), t_{k+1}) f_{xx,j}(\bar{x}(t_k), \bar{u}(t_k), t_k)\mathrm{d}t, \tag{8.42}$$

$$\mathcal{Z}_2 = \sum_{j=1}^{n} \frac{\partial V}{\partial x_j}(\bar{x}(t_{k+1}), t_{k+1}) f_{uu,j}(\bar{x}(t_k), \bar{u}(t_k), t_k)\mathrm{d}t, \tag{8.43}$$

$$\mathcal{Z}_3 = \sum_{j=1}^{n} \frac{\partial V}{\partial x_j}(\bar{x}(t_{k+1}), t_{k+1}) f_{ux,j}(\bar{x}(t_k), \bar{u}(t_k), t_k)\mathrm{d}t. \tag{8.44}$$

With the variation in the order of the dynamics, the basic DDP algorithm is described in algorithm 2.

Algorithm 2 Differential Dynamic Programming

Given: $x(0), V(x(t_f), t_f), N$
Initialize: $\{\bar{u}(t_k)\}_{k=0}^{k=N-1}$
While $J(x_0, U)$ not converged
Forward Pass: $k = 0$ *to* $N-1$
    $\{\bar{x}(t_k)\}_{k=0}^{k=N} \leftarrow \{x(t_k)\}_{k=0}^{k=N}$ from Eq. 8.1 using $\{\bar{u}(t_k)\}_{k=0}^{k=N-1}$
    Compute $\Phi, B, f_{xx,i}, f_{xu,i}, f_{ux,i}, f_{uu,i}$ at $(\bar{x}(t_k), \bar{u}(t_k), t_k)$
Backward Pass: $k = N-1$ *to* 1
    Find $Q(\bar{x}(t_k), t_k)$ using Eqs. [8.20-8.26] or Eqs. [8.39-8.41]
    Find $V(\bar{x}(t_k), t_k)$, $V_x(\bar{x}(t_k), t_k)$, $V_{xx}(\bar{x}(t_k), t_k)$ using Eqs. [8.31-8.33]
Control Update: $k = 0$ *to* $N-1$
    Propagate Eq. [8.6] or Eq. [8.37]
    Compute $\delta u(t_k)$ from equation (8.29)
    Set $\bar{u}(t_k) \leftarrow \bar{u}(t_k) + \delta u(t_k)$
End While

8.3 Control Update Step

The specific implementation used for control in this section is based on the work described by Tassa et al. [149]. One of the innovations in [149] is the ability to incorporate control limits (i.e., saturation limits) during planning, avoiding the negative consequences of simply clipping control inputs during implementation. Additionally, Tassa et al. make use of a backtracking search parameter, $\alpha \in \mathcal{A}_i \subset [0, 1]$, to perform a line search on the optimal update of the control input. That way, after the backward pass on a given iteration of DDP,

a sweep of control policies is parameterized as

$$\delta u^*(k;\alpha) = -Q_{uu}^{-1}Q_{ux}\delta x(k) - \alpha Q_{uu}^{-1}Q_u^{\mathrm{T}} = L\delta x(k) + \alpha l, \tag{8.45}$$

where L is again the time-dependent feedback gain matrix, and l is the time-dependent feedforward term. This control policy is evaluated forward in time for as many α values as the user selects. The control update is then selected as the one corresponding to the value α that yields the largest cost reduction.

8.4 End-Effector Kinematics

In order to aid the convergence of the algorithm, the pose of the end effector with respect to the inertial frame $\boldsymbol{q}_{\mathrm{G/I}}$ was added as a state to the formulation. This implies the need to derive the kinematics of the end effector. In dual quaternion algebra this is a simple derivation which we provide below.

Consider the pose of the end effector as the chain of relative pose transformations given by

$$\boldsymbol{q}_{\mathrm{G/I}} = \boldsymbol{q}_{\mathfrak{o}_0/\mathrm{I}}\boldsymbol{q}_{0/\mathfrak{o}_0}\boldsymbol{q}_{\mathfrak{o}_1/0}\boldsymbol{q}_{1/\mathfrak{o}_1}\boldsymbol{q}_{\mathfrak{o}_2/1}\boldsymbol{q}_{2/\mathfrak{o}_2}\boldsymbol{q}_{\mathfrak{o}_3/2}\boldsymbol{q}_{\mathrm{e}/\mathfrak{o}_3}\boldsymbol{q}_{\mathrm{G/e}}. \tag{8.46}$$

The dual quaternions $\boldsymbol{q}_{\mathfrak{o}_1/0}, \boldsymbol{q}_{\mathfrak{o}_2/1}, \boldsymbol{q}_{\mathfrak{o}_3/2}, \boldsymbol{q}_{\mathrm{G/e}}$ are constant, and their derivatives $\mathbf{0}$ because they represent pose transformations along the same rigid body. Therefore, using equation (2.37) we can easily take the derivative of $\boldsymbol{q}_{\mathrm{G/I}}$ as

$$\dot{\boldsymbol{q}}_{\mathrm{G/I}} = \dot{\boldsymbol{q}}_{\mathfrak{o}_0/\mathrm{I}}\boldsymbol{q}_{\mathrm{G}/\mathfrak{o}_0} + \boldsymbol{q}_{\mathfrak{o}_0/\mathrm{I}}\dot{\boldsymbol{q}}_{0/\mathfrak{o}_0}\boldsymbol{q}_{\mathrm{G}/0} + \boldsymbol{q}_{\mathfrak{o}_1/\mathrm{I}}\dot{\boldsymbol{q}}_{1/\mathfrak{o}_1}\,\boldsymbol{q}_{\mathrm{G}/1} + \boldsymbol{q}_{\mathfrak{o}_2/\mathrm{I}}\dot{\boldsymbol{q}}_{2/\mathfrak{o}_2}\boldsymbol{q}_{\mathrm{G}/2} + \boldsymbol{q}_{\mathfrak{o}_3/\mathrm{I}}\dot{\boldsymbol{q}}_{\mathrm{e}/\mathfrak{o}_3}\boldsymbol{q}_{\mathrm{G/e}} \tag{8.47}$$

$$\begin{aligned}\dot{\boldsymbol{q}}_{\mathrm{G/I}} = {} & \tfrac{1}{2}\boldsymbol{q}_{\mathfrak{o}_0/\mathrm{I}}\boldsymbol{\omega}^{\mathfrak{o}_0}_{\mathfrak{o}_0/\mathrm{I}}\boldsymbol{q}_{\mathrm{G}/\mathfrak{o}_0} + \tfrac{1}{2}\boldsymbol{q}_{\mathfrak{o}_0/\mathrm{I}}\boldsymbol{\omega}^{\mathfrak{o}_0}_{0/\mathfrak{o}_0}\boldsymbol{q}_{0/\mathfrak{o}_0}\boldsymbol{q}_{\mathrm{G}/0} + \tfrac{1}{2}\boldsymbol{q}_{\mathfrak{o}_1/\mathrm{I}}\boldsymbol{\omega}^{\mathfrak{o}_1}_{1/\mathfrak{o}_1}\boldsymbol{q}_{1/\mathfrak{o}_1}\boldsymbol{q}_{\mathrm{G}/1} \\ & + \tfrac{1}{2}\boldsymbol{q}_{\mathfrak{o}_2/\mathrm{I}}\boldsymbol{\omega}^{\mathfrak{o}_2}_{2/\mathfrak{o}_2}\boldsymbol{q}_{2/\mathfrak{o}_2}\boldsymbol{q}_{\mathrm{G}/2} + \tfrac{1}{2}\boldsymbol{q}_{\mathfrak{o}_3/\mathrm{I}}\boldsymbol{q}_{\mathrm{e}/\mathfrak{o}_3}\boldsymbol{\omega}^{\mathrm{e}}_{\mathrm{e}/\mathfrak{o}_3}\boldsymbol{q}_{\mathrm{G/e}}\end{aligned} \tag{8.48}$$

Finally, we simplify this expression to yield

$$\dot{\boldsymbol{q}}_{\text{G/I}} = \tfrac{1}{2}\boldsymbol{q}_{\mathfrak{o}_0/\text{I}}\boldsymbol{\omega}^{\mathfrak{o}_0}_{\mathfrak{o}_0/\text{I}}\boldsymbol{q}_{\text{G}/\mathfrak{o}_0} + \tfrac{1}{2}\boldsymbol{q}_{\mathfrak{o}_0/\text{I}}\boldsymbol{\omega}^{\mathfrak{o}_0}_{0/\mathfrak{o}_0}\boldsymbol{q}_{\text{G}/\mathfrak{o}_0} + \tfrac{1}{2}\boldsymbol{q}_{\mathfrak{o}_1/\text{I}}\boldsymbol{\omega}^{\mathfrak{o}_1}_{1/\mathfrak{o}_1}\boldsymbol{q}_{\text{G}/\mathfrak{o}_1} + \tfrac{1}{2}\boldsymbol{q}_{\mathfrak{o}_2/\text{I}}\boldsymbol{\omega}^{\mathfrak{o}_2}_{2/\mathfrak{o}_2}\boldsymbol{q}_{\text{G}/\mathfrak{o}_2} + \tfrac{1}{2}\boldsymbol{q}_{\text{e/I}}\boldsymbol{\omega}^{\text{e}}_{\text{e}/\mathfrak{o}_3}\boldsymbol{q}_{\text{G/e}}. \quad (8.49)$$

This differential equation yields the time evolution of the end-effector based on kinematics.

8.5 End-Effector Pose Stabilization Using DDP

We will take the definition of our state vector to be

$$\boldsymbol{x} = [\boldsymbol{q}^{\text{T}}_{\mathfrak{o}_0/\text{I}}, \theta_{1/0}, \theta_{2/1}, \theta_{3/2}, \psi_{\text{e}/\mathfrak{o}_3}, \theta_{\text{e}/\mathfrak{o}_3}, \phi_{\text{e}/\mathfrak{o}_3}, \boldsymbol{y}^{\text{T}}]^{\text{T}} \in \mathbb{R}^{46}, \quad (8.50)$$

where $\boldsymbol{y} = [\boldsymbol{\omega}^{\mathfrak{o}_0}_{\mathfrak{o}_0/\text{I}}{}^{\text{T}}, \boldsymbol{\omega}^{\mathfrak{o}_1}_{\mathfrak{o}_1/\text{I}}{}^{\text{T}}, \boldsymbol{\omega}^{\mathfrak{o}_2}_{\mathfrak{o}_2/\text{I}}{}^{\text{T}}, \boldsymbol{\omega}^{\mathfrak{o}_3}_{\mathfrak{o}_3/\text{I}}{}^{\text{T}}]^{\text{T}} \in \mathbb{R}^{32}$. The control inputs are taken to be

$$\boldsymbol{u} = [\tilde{\boldsymbol{W}}^{\mathfrak{o}_0}_{\mathfrak{o}_0}(O_{\mathfrak{o}_0})^{\text{T}}, (\bar{\tau}_{\text{act},1})_z, (\bar{\tau}_{\text{act},2})_z, (\bar{\tau}_{\text{act},3})_z, \dot{\psi}_{\text{e}/\mathfrak{o}_3}, \dot{\theta}_{\text{e}/\mathfrak{o}_3}, \dot{\phi}_{\text{e}/\mathfrak{o}_3}]^{\text{T}} \in \mathbb{R}^{12}, \quad (8.51)$$

allowing us to define the objective function for our spacecraft-mounted robotic manipulator application as

$$\begin{aligned} J(x_0, U) &= (\boldsymbol{q}_{\text{G/I}}(t_f) - \boldsymbol{q}_{\text{D/I}})^{\text{T}} W_{f,q} (\boldsymbol{q}_{\text{G/I}}(t_f) - \boldsymbol{q}_{\text{D/I}}) + \boldsymbol{\omega}^{\mathfrak{o}_0}_{\mathfrak{o}_0/\text{I}}(t_f)^{\text{T}} W_{f,\omega} \boldsymbol{\omega}^{\mathfrak{o}_0}_{\mathfrak{o}_0/\text{I}}(t_f) \quad (8.52) \\ &+ \sum_{k=0}^{N-1} (\boldsymbol{q}_{\text{G/I}}(t_k) - \boldsymbol{q}_{\text{D/I}})^{\text{T}} W_{k,q} (\boldsymbol{q}_{\text{G/I}}(t_k) - \boldsymbol{q}_{\text{D/I}}) + \boldsymbol{\omega}^{\mathfrak{o}_0}_{\mathfrak{o}_0/\text{I}}(t_k)^{\text{T}} W_{k,\omega} \boldsymbol{\omega}^{\mathfrak{o}_0}_{\mathfrak{o}_0/\text{I}}(t_k) + \boldsymbol{u}(t_k)^{\text{T}} R \boldsymbol{u}(t_k). \end{aligned}$$

The values of matrices $W_{f,q}$, $W_{f,\omega}$, $W_{k,q}$, $W_{k,\omega}$ and R are listed in Table 8.1. Finally, the target pose for the end effector, and the desired angular velocity of the base are given by

$$\boldsymbol{q}_{\text{D/I}} = \left(0.5, \begin{bmatrix} 0.50 & -0.50 & -0.50 \end{bmatrix}^{\text{T}}\right) + \epsilon \left(0.25, \begin{bmatrix} 2.25 & 0.25 & 2.25 \end{bmatrix}^{\text{T}}\right), \quad (8.53)$$

$$\boldsymbol{\omega}^{\text{D}}_{\text{D/I}} = \boldsymbol{0}. \quad (8.54)$$

The simulation was run for $T = 15$ s, $\Delta t = 0.015$ s, $N = 1000$. The reference aims

Table 8.1: Cost function parameters.

Matrix	Value	Variable Penalized
$W_{k,q}$	$15\mathbb{I}_8$	$\boldsymbol{q}_{\text{G/I}}(t_k)$
$W_{f,q}$	$150\mathbb{I}_8$	$\boldsymbol{q}_{\text{G/I}}(t_f)$
$W_{k,\omega}$	$\mathbb{I}_8$	$\boldsymbol{\omega}^{\mathfrak{s}_0}_{\mathfrak{s}_0/\text{I}}(t_k)$
$W_{f,\omega}$	$\mathbb{I}_8$	$\boldsymbol{\omega}^{\mathfrak{s}_0}_{\mathfrak{s}_0/\text{I}}(t_f)$
R	$\text{diag}(10\mathbb{I}_3, \mathbb{I}_3, 0.01\mathbb{I}_3, 0.1\mathbb{I}_3)$	$\boldsymbol{u}(t_k)$

to achieve pose stabilization of the end effector at a given desired pose, given that $\boldsymbol{q}_{\text{D/I}}$ is constant. Figure 8.1 shows a time sequence of the trajectory after convergence of the algorithm.

The error pose of the end effector frame is computed via dual quaternions as

$$\boldsymbol{q}_{\text{D/G}} = \boldsymbol{q}^*_{\text{G/I}} \boldsymbol{q}_{\text{D/I}}. \tag{8.55}$$

The error quaternion and position vector error, expressed in the end-effector frame G, is shown in Figure 8.2. Figure 8.3 shows a scalar measure of both, the angular and the linear errors. In the angular case, it shows the Euler angle of the error rotation. As a linear measure, it uses the norm of the error vector. Both of these quantities are directly derived from $\boldsymbol{q}_{\text{D/G}}$

Finally, we observe the control inputs for this optimal control problem. Figure 8.4 shows the actuation forces and torques applied on the base. One can notice that forces, usually generated by gases contained on-board the spacecraft, and a scarce resource in orbit, are penalized more than all other inputs. This can be appreciated by observation of the weighing matrices in Table 8.1. Thus, its utilization is kept low. The torque generated is also low for this maneuver, but since it can be generated by reaction wheels, CMGs, or VSCMGs, this component is penalized less aggressively. It is worth emphasizing that DDP allows for forces to be applied, effectively augmenting the reachable workspace of

the robotic arm. This can be juxtaposed to more conventional methods where the object of interest must already be in the reachable workspace in order for the algorithm to find a feasible maneuver, or other coordinate control methods that require a significant consumption of fuel to maintain constant attitude while the manipulator performs the maneuver. Finally, Figure 8.5 shows the torques applied at each of the joints, and the Euler angle rates for the end-effector motion. These are penalized less since these can be more easily generated in-orbit.

8.6 Objective Function Design for End-Effector Pose Tracking

The particular form of the objective function to be minimized for the tracking problem is given by

$$\begin{aligned} J(x_0, U; i) &= (\boldsymbol{q}_{\text{G/I}}(N) - \boldsymbol{q}_{\text{D/I}}(N))^{\text{T}} W_{f,q}(i)(\boldsymbol{q}_{\text{G/I}}(N) - \boldsymbol{q}_{\text{D/I}}(N)) + \boldsymbol{\omega}^{\mathcal{B}_0}_{\mathcal{B}_0/\text{I}}(N)^{\text{T}} W_{f,\omega}(i) \boldsymbol{\omega}^{\mathcal{B}_0}_{\mathcal{B}_0/\text{I}}(N) \\ &+ \sum_{k=0}^{N-1} (\boldsymbol{q}_{\text{G/I}}(k) - \boldsymbol{q}_{\text{D/I}}(k))^{\text{T}} W_{k,q}(i)(\boldsymbol{q}_{\text{G/I}}(k) - \boldsymbol{q}_{\text{D/I}}(k)) + \sum_{k=0}^{N-1} \boldsymbol{\omega}^{\mathcal{B}_0}_{\mathcal{B}_0/\text{I}}(k)^{\text{T}} W_{k,\omega}(i) \boldsymbol{\omega}^{\mathcal{B}_0}_{\mathcal{B}_0/\text{I}}(k) \\ &+ \sum_{k=0}^{N-1} \boldsymbol{u}(k)^{\text{T}} R(i) \boldsymbol{u}(k) + \sum_i \frac{K_i}{\exp((\theta_i - \bar{\theta}_i)^2 / \ell_{\theta_i}^2) + 1}, \end{aligned} \tag{8.56}$$

where $W_{f,q}(i),\ W_{f,\omega}(i) \in \mathbb{R}^8$ are positive-definite matrices that penalize the final end-effector pose error and the residual dual velocity of the satellite base at iteration i of the DDP algorithm respectively; $W_{k,q}(i),\ W_{k,\omega}(i) \in \mathbb{R}^8$ are positive-definite matrices that penalize the pose error of the end-effector and the residual dual velocity of the satellite base at timestep k of iteration i of the DDP algorithm, and $R(i) \in \mathbb{R}^{12}$ is a positive definite matrix that penalizes the control input at timestep k of iteration i. The last term in equation (8.56) penalizes the proximity of joint angle θ_i to $\bar{\theta}_i$ with bandwidth parameter ℓ_{θ_i} and weighing factor K_i. This term, in particular, can be used to circumvent singular configurations of the robotic manipulator, which arise regularly in this formulation since the algorithm aims to

minimize control effort, and often works at the boundary of the reachable workspace.

For our particular implementation of DDP, the matrices $W_{f,q}(i)$, $W_{f,\omega}(i)$, $W_{k,q}(i)$, $W_{k,\omega}(i)$, and $R(i)$, and the set $\mathcal{A}_i$ were designed to be dependent on the i-th iteration of the DDP framework. The rationale behind this decision lies in the fact that the system is highly non-linear, so for the initial iterations we would like to ensure $\boldsymbol{\omega}_{\mathfrak{s}_0/\mathcal{I}}^{\mathfrak{s}_0}$ remains close to $\mathbf{0}$, and the updates to the control remain relative small. For the latter iterations, the deviations in the state from the desired state are smaller, allowing us to increase the relative penalty of the end-effector pose error with respect to the control effort penalty. The exact values for each of the matrices is discussed in the next section, as is the set $\mathcal{A}_i$.

8.7 End-Effector Pose Tracking

In this section we discuss the details of the implementation of the DDP algorithm on the plant, and show the results of the simulation.

The timestep for the discretization of the problem was selected to be $\Delta t = 0.05$ s, with $t_f = 32$ s, yielding $N = 640$. The initial state of the system is such that the center of mass of the satellite is at the origin of the inertial frame, and its body frame aligned with the inertial frame. All bodies are initially stationary, and all generalized coordinates are set to zero, except $\theta_{2/1}(0) = 5^o$, $\theta_{3/2}(0) = -10^o$, and $\psi_{\mathfrak{e}/\mathfrak{s}_3}(0) = 5^o$. This implies that the end-effector lies at $r^{\text{I}}_{\text{G}/\mathcal{I}}(0) = (0, [6.727, 0, 5]^{\text{T}})$ m, with orientation $q_{\text{G}/\mathcal{I}} = (\cos(\pi/4), [\sin(\pi/4), 0, 0]^{\text{T}})$. The control sequence U for the initial forward propagation of the dynamics is sampled from the normal distribution $\boldsymbol{u}_k \sim \mathcal{N}(0_{12\times 1}, \text{diag}(1, 1, 1, 1, 1, 1, 1, 1, 1, 0.2^2, 0.2^2, 0.2^2))$.

The desired reference motion of the end-effector is composed of three different phases: a stabilization phase, a helicoid motion of radius ξ, which we parametrize using the exponential map, followed by another stabilization phase.

Phase 1: **(**$0 \text{ s} \leq t < 7 \text{ s}$**)** During this phase, the desired frame is fixed in inertial space and given by $\boldsymbol{q}_{\text{D}/\mathcal{I}}(t) = q_{\text{D}/\mathcal{I}}(t) + \epsilon\frac{1}{2} r^{\text{I}}_{\text{D}/\mathcal{I}}(t) q_{\text{D}/\mathcal{I}}(t)$, where $r^{\text{I}}_{\text{D}/\mathcal{I}}(t) = (0, \vec{r}^{\text{I}}_{\text{D}/\mathcal{I}}(t))$ and $q_{\text{D}/\mathcal{I}}(t)$ are

given by

$$(\bar{r}^{\mathrm{I}}_{\mathrm{D/I}}(t))^{\mathrm{T}} = [6.75, 0, 5] + [-0.5, \xi, 0]\ \mathrm{m} \tag{8.57}$$

$$q_{\mathrm{D/I}}(t) = (\cos(\pi/4), [\sin(\pi/4), 0, 0]^{\mathrm{T}}), \tag{8.58}$$

which represents a translation relative to the initial pose by $[-0.5, \xi, 0]^{\mathrm{T}}\ \mathrm{m}$.

Phase 2: ($7\ \mathrm{s} \leq t < 27\ \mathrm{s}$) During this phase, the desired reference frame performs a helicoid motion that we parametrize using the result of Lemma 5. The reference is parametrized by

$$\boldsymbol{q}_{\mathrm{D/I}}(t) = \boldsymbol{q}_{\mathrm{D/I}}(7)\boldsymbol{q}_{\mathrm{screw}}(t), \tag{8.59}$$

where

$$\boldsymbol{q}_{\mathrm{screw}}(t) = \exp(\tfrac{1}{2}\boldsymbol{\theta}(t)\boldsymbol{s}(t)). \tag{8.60}$$

The screw parameters $\boldsymbol{\theta}(t) = \theta(t) + \epsilon d(t)$ and $\boldsymbol{s}(t) = \ell + \epsilon m = \ell + \epsilon(\bar{r}^{I}_{\mathrm{P/\Gamma}} \times \ell)$ are fully described by

$$\begin{aligned} d(t) &= \Omega_{\mathrm{tr}}(t-7)\ \mathrm{m} \\ \theta(t) &= \Omega_{\mathrm{rot}}(t-7)\ \mathrm{rad} \\ \ell &= [1,\ 0,\ 0]^{\mathrm{T}} \\ \bar{r}^{\mathrm{I}}_{\mathrm{P/\Gamma}} &= [0,\ 0,\ \xi]^{\mathrm{T}}\ \mathrm{m}, \end{aligned} \tag{8.61}$$

where the translational speed is $\Omega_{\mathrm{tr}} = 0.20/20\ {}^{\mathrm{m}}/_{\mathrm{s}}$, the angular velocity of the screw motion is $\Omega_{\mathrm{rot}} = 2\pi/20\ {}^{\mathrm{rad}}/_{\mathrm{s}}$. The frame I' is aligned with the inertial frame, but its origin is located at $r^{\mathrm{I}}_{\Gamma/I} = [6.75, 0, 5] + [-0.5, \xi, 0]\ \mathrm{m}$.

Phase 3: ($27\ \mathrm{s} \leq t < 32\ \mathrm{s}$) During this phase, the desired reference frame remains stationary to allow for stabilization after the helicoid motion. The resulting reference frame is described by

$$\boldsymbol{q}_{\mathrm{D/I}}(t) = \boldsymbol{q}_{\mathrm{D/I}}(7)\boldsymbol{q}_{\mathrm{screw}}(27). \tag{8.62}$$

For the simulation, we selected the radius $\xi = 0.35\,\mathrm{m}$. For this example, soft-constraints for $\theta_{2/1}$ and $\theta_{3/2}$ were incorporated using the last term of equation (8.56). In both cases, $\bar{\theta} = 0^o$, $\ell_{\theta_i} = 1^o$, and $K_i = 0.1$. For this example, the parameter update α was polled from the set $\mathcal{A}_i = \{0.1\}$, i.e., $\alpha = 0.1$ always. The state penalty matrices were set to

$$\begin{aligned} W_{f,q}(i) &= \mathrm{diag}(\beta_{f,qr}(i)\mathbb{I}_4, \beta_{f,qd}(i)\mathbb{I}_4), \\ W_{f,\omega}(i) &= \beta_{f,\omega}(i)\mathbb{I}_8, \\ W_{k,q}(i) &= \mathrm{diag}(\beta_{k,qr}(i)\mathbb{I}_4, \beta_{k,qd}(i)\mathbb{I}_4), \\ W_{k,\omega}(i) &= \beta_{k,\omega}(i)\mathbb{I}_8, \end{aligned} \tag{8.63}$$

while the control effort penalty matrix was designed as

$$R(i) = \mathrm{diag}(\beta_{r,f}(i)\mathbb{I}_3, \beta_{r,\tau}(i)\mathbb{I}_3, \beta_{r,j}(i)\mathbb{I}_3, \beta_{r,e}(i)\mathbb{I}_3). \tag{8.64}$$

The parameters $\beta_{(\cdot,\cdot)}$ follow the iteration dependence depicted in Figure 8.6. After setting the maximum number of iterations for the DDP algorithm to $i_N = 150$, we selected $i_1 = 40$, $i_2 = 45$, $i_3 = 60$, and $i_4 = 65$, while the corresponding β value for each variable is given in Table 8.2.

The development of the control framework builds upon the iLQG/DDP implementation by Tassa et al. [150]. This implementation was modified by adding the time-dependent target state, providing analytical expressions for the partial derivatives of the cost function with respect to the state and the control, and implementing the iteration-dependence of $\mathcal{A}_i$ and $\beta_{(\cdot,\cdot)}$. Figure 8.7 shows snapshots from a time sequence of the trajectory after the convergence of the algorithm.

The error quaternion and position vector error expressed in the end-effector frame G, computed from equation (8.55), is shown in Figure 8.8 performing a successful tracking maneuver. Figure 8.9 shows a scalar measure of both the angular and the linear errors. In

Table 8.2: Parametrization parameters for iteration dependence.

Coefficient	Start Value (S)	Medium Value (M)	End Value (E)
$\beta_{f,qr}(i)$	168	240	648
$\beta_{f,qd}(i)$	84	120	324
$\beta_{f,\omega}(i)$	10	10	10
$\beta_{k,qr}(i)$	60	192	312
$\beta_{k,qd}(i)$	30	96	156
$\beta_{k,\omega}(i)$	2	2	2
$\beta_{r,f}(i)$	1.0	1.0	0.3000
$\beta_{r,\tau}(i)$	1.0	1.0	0.1250
$\beta_{r,j}(i)$	0.1	0.1	0.0025
$\beta_{r,e}(i)$	0.5	0.1	0.0010

the angular case, Figure 8.9 shows the Euler angle of the error rotation, while the norm of the error position vector is shown to quantify the translational error. The Euler angle and the error position vector are computed from $\boldsymbol{q}_{\text{D/G}}$ by

$$\begin{aligned} \theta_{\text{Euler}} &= 2\cos^{-1}\text{sc}\left((\boldsymbol{q}_{\text{D/G}})_r\right) = 2\cos^{-1}\text{sc}\left(q_{\text{D/G}}\right) \\ r^{\text{G}}_{\text{D/G}} &= 2(\boldsymbol{q}_{\text{D/G}})_d(\boldsymbol{q}^*_{\text{D/G}})_r = 2(\boldsymbol{q}_{\text{D/G}})_d q^*_{\text{D/G}}. \end{aligned} \tag{8.65}$$

Figure 8.10 shows the actuation forces and torques applied on the base of the satellite. The cost function has been chosen so that the forces, usually generated by gas jet actuators contained on-board the spacecraft, are kept low since thruster firing requires fuel, which is a scarce resource in orbit. The torque generated is also low for this maneuver, but since it can be generated by reaction wheels, CMG's, or VSCMG's, this component is penalized less aggressively in the cost term of the DDP formulation. Figure 8.11 shows the torques applied at each one of the three joints, and the Euler angle rates for the end-effector motion (assumed for simplicity to represent the end-effector actuation mechanism). These are penalized less since they can be easily generated on-board the satellite. Figure 8.12 provides an overlay of the actual trajectory of the end-effector over the desired trajectory.

Figure 8.13 shows the angular and linear velocities of the satellite base. It can be seen that while the end-effector is moving distances on the order of magnitude of 1 m, the DDP algorithm is able to maintain the satellite base relatively stationary. This is beneficial in terms of overall system stability, as well as fuel and energy expenditure. Finally, Figure 8.14 shows the joint angles for the motion. It also shows the soft keep-out constraint enforced on $\theta_{2/1}$ and $\theta_{3/2}$. It is important to highlight that even though the constraint is active, the algorithm finds a trajectory that traverses the constraint. This behavior is expected, and actually desired. The constraint exists for maneuvers that remain in this band for a significant period of time, such as in the case when the end-effector arrives at its desired pose in a fully extended configuration, which can lead to kinematic singularities.

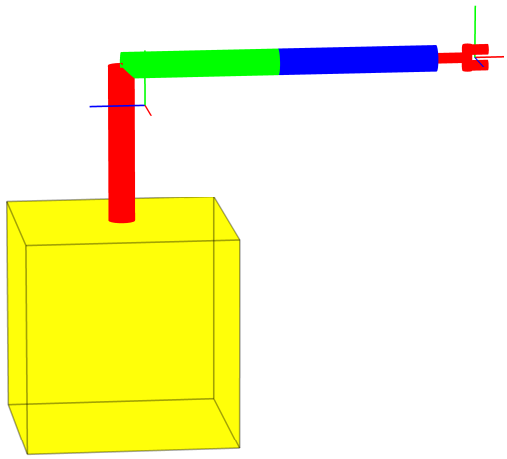

$t = 0.0$ s

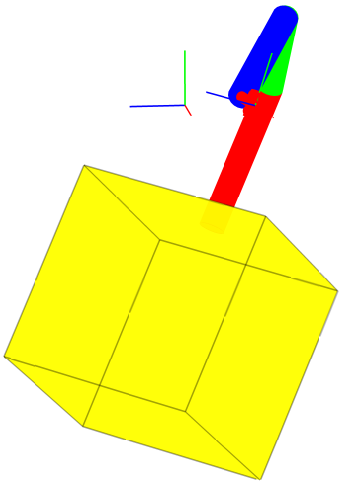

$t = 3.0$ s

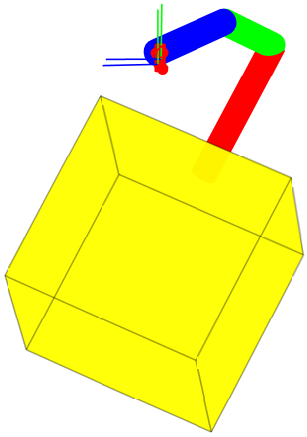

$t = 6.0$ s

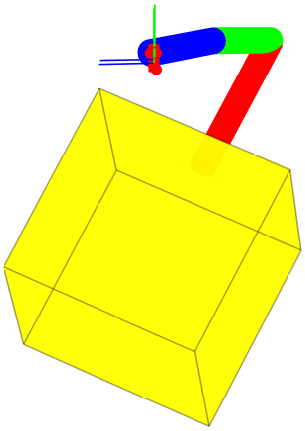

$t = 9.0$ s

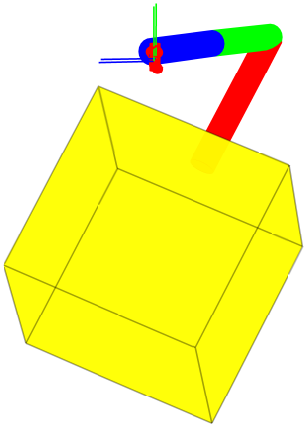

$t = 12.0$ s

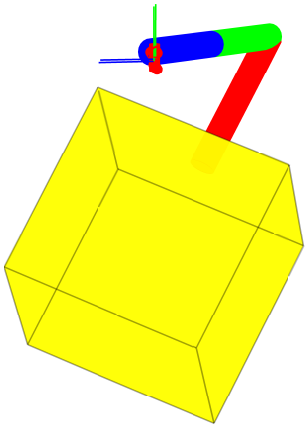

$t = 15.0$ s

Figure 8.1: Time sequence of end effector poses for stabilization maneuver.

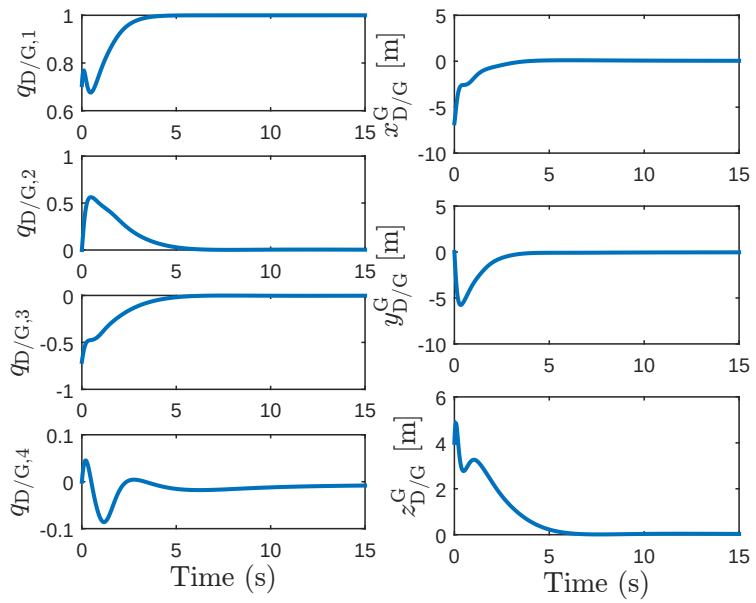

Figure 8.2: Pose stabilization maneuver: quaternion error and position error.

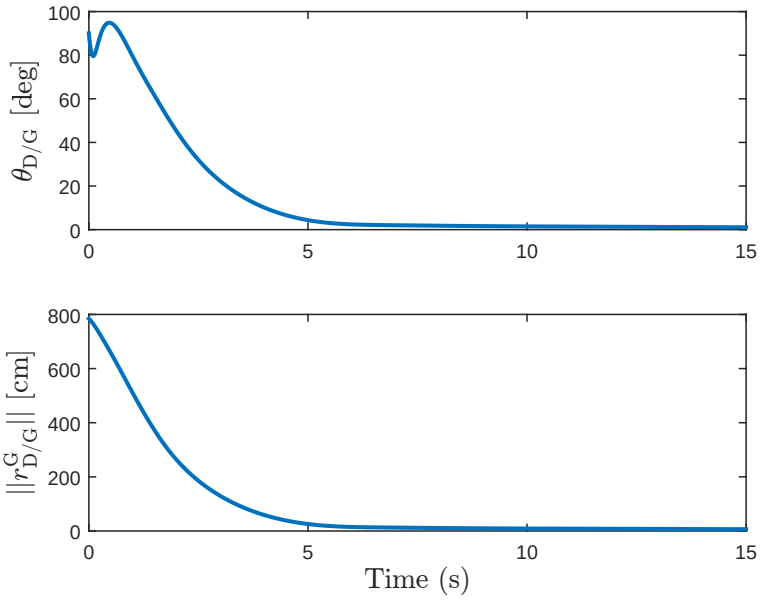

Figure 8.3: Pose stabilization maneuver: error Euler angle and error vector norm.

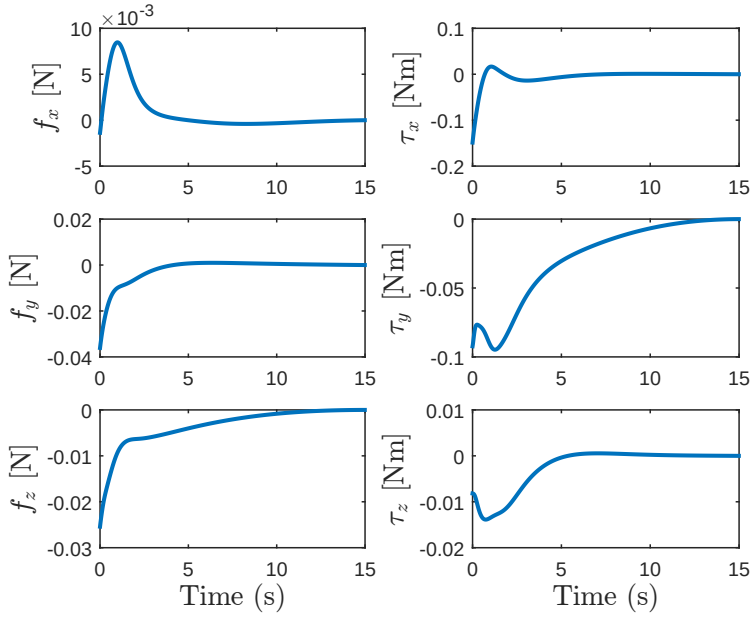

Figure 8.4: Control effort: forces and torques applied at the satellite base.

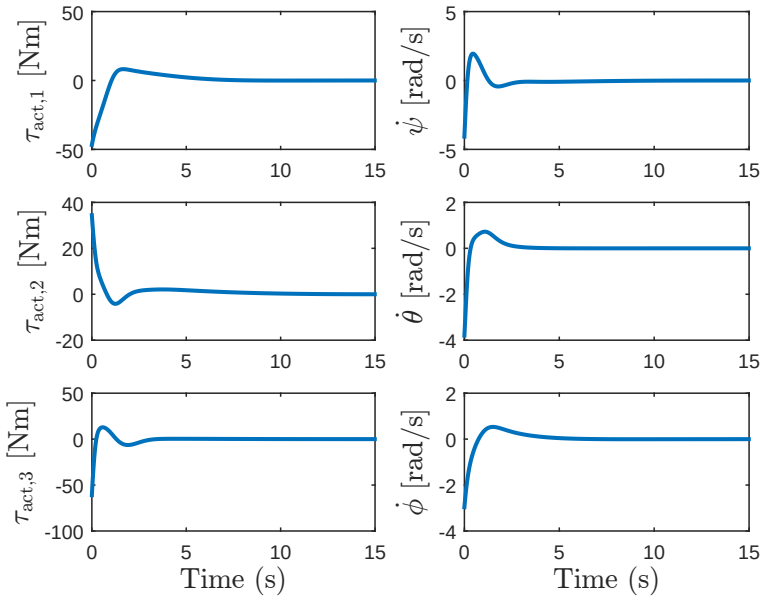

Figure 8.5: Control effort: joint torques and Euler rates.

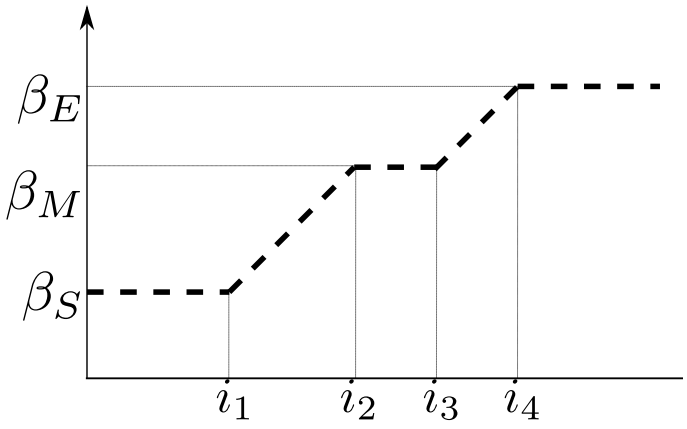

Figure 8.6: Iteration-dependent gain profile for penalty matrices.

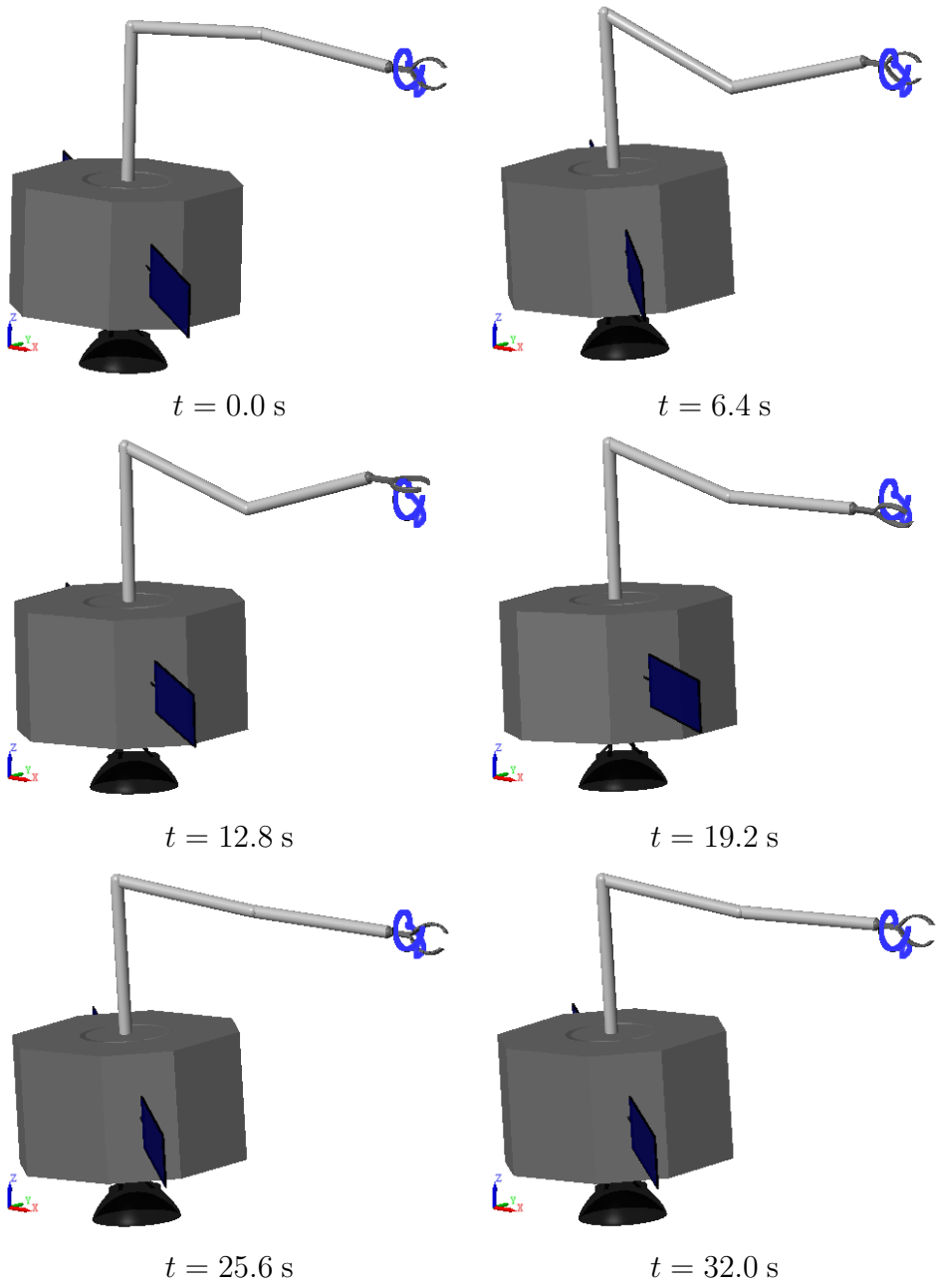

Figure 8.7: Time sequence of end effector poses for tracking maneuver.

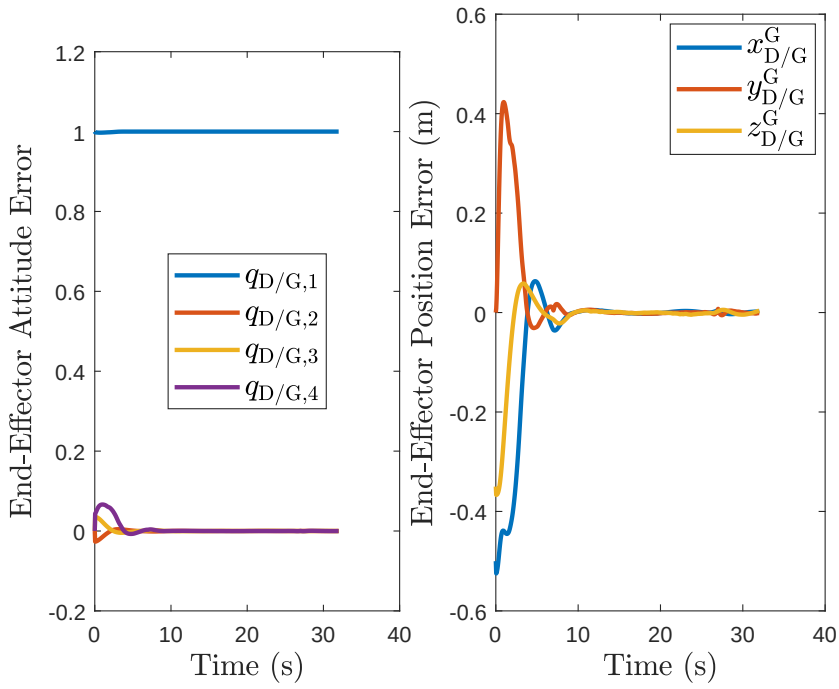

Figure 8.8: Pose tracking maneuver: quaternion error and position error.

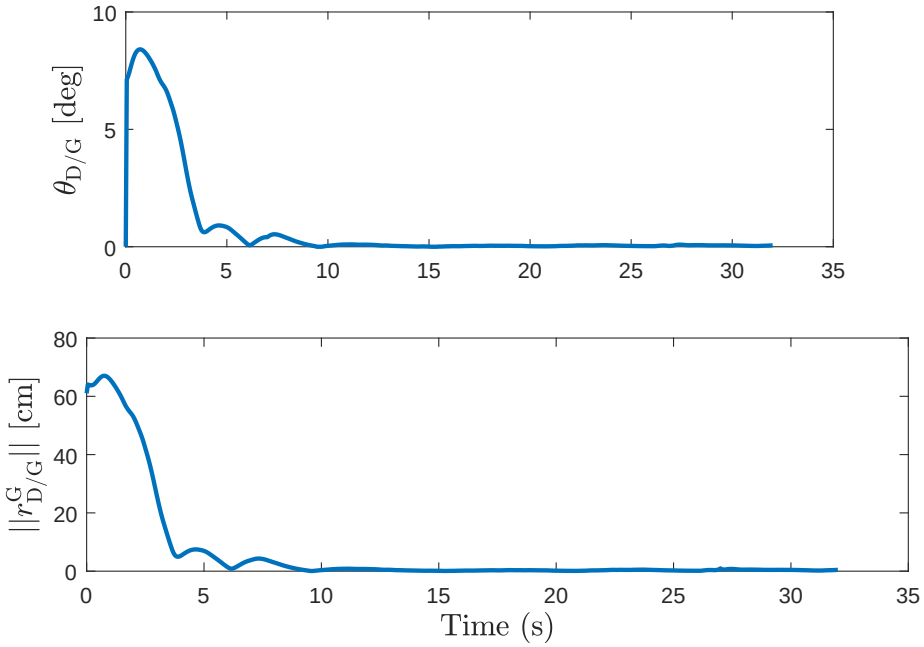

Figure 8.9: Pose tracking maneuver: error Euler angle and error vector norm.

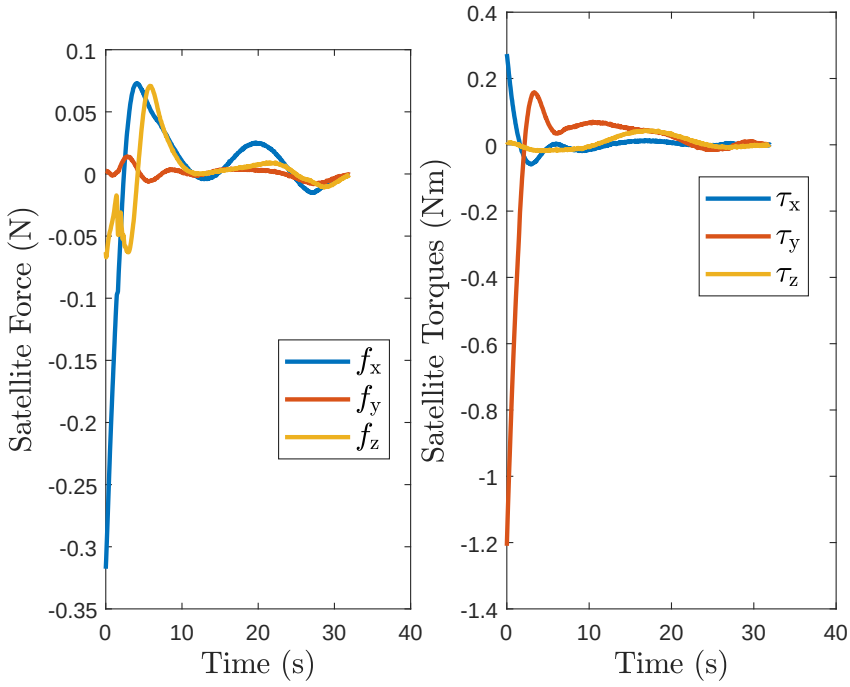

Figure 8.10: Control effort: forces and torques applied at the satellite base.

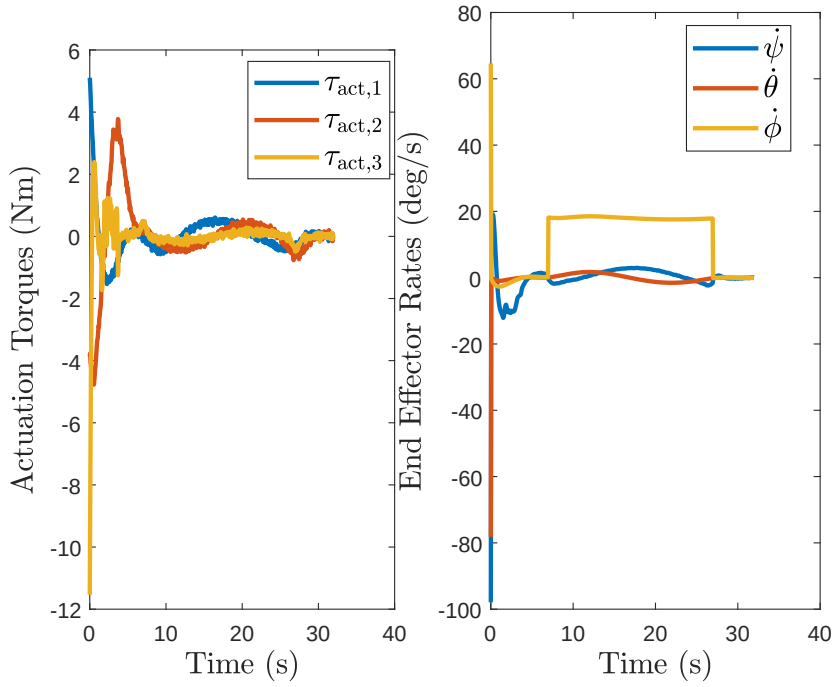

Figure 8.11: Control effort: joint torques and Euler rates.

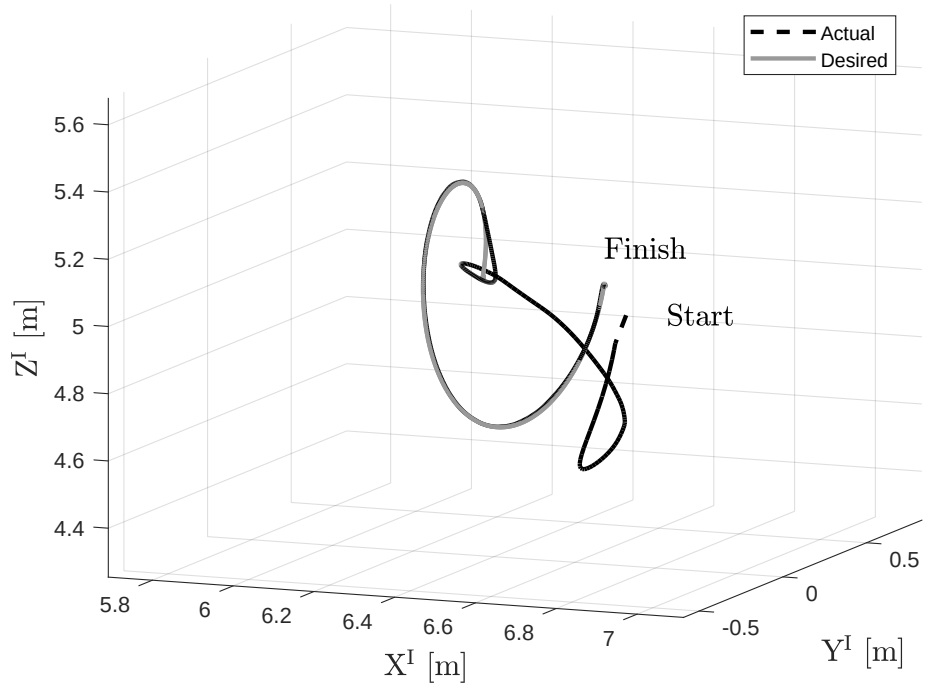

Figure 8.12: Desired and actual end-effector trajectories.

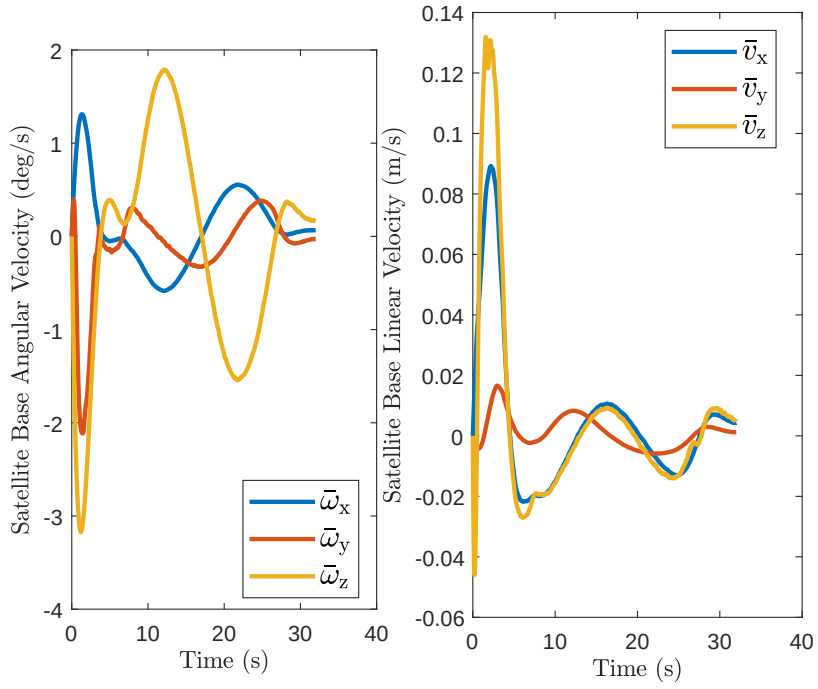

Figure 8.13: Angular and linear velocities of the satellite base in $\mathcal{O}_0$ coordinates.

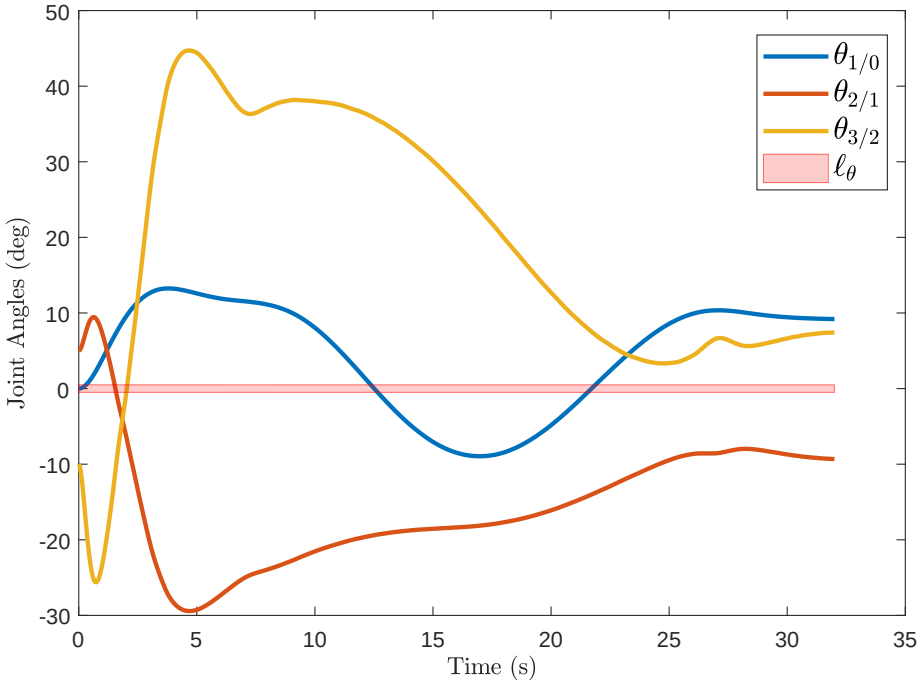

Figure 8.14: Joint angles with representative strip for soft keep-out constraint enforced for $\theta_{2/1}$ and $\theta_{3/2}$.

CHAPTER 9

ESTIMATION OF MASS PROPERTIES FOR SPACECRAFT-MOUNTED MANIPULATOR

In this chapter we explore the problem of estimating the inertia properties of each of the links of a spacecraft-mounted robotic manipulator. We will use the concurrent learning framework, which is also discussed in Chapter 4, as a method of incorporating data into the adaptive estimation of the dual inertia matrix of a satellite.

The following assumptions are made in this chapter:

1) The location of the center of mass for every rigid body is known.

2) All external and actuation wrenches are known, and the reaction wrenches can be calculated from the dynamical model.

3) All state variables are known, and the only unknowns are the dual inertia parameters to be estimated.

9.1 Incorporation into the Concurrent Learning Framework

We know from Chapter 7, equation (6.17) that

$$\begin{bmatrix} \boldsymbol{\mathcal{S}}_{11} & \boldsymbol{\mathcal{S}}_{12} \\ \boldsymbol{\mathcal{S}}_{21} & \boldsymbol{\mathcal{S}}_{22} \end{bmatrix} \begin{bmatrix} \dot{\boldsymbol{y}} \\ \boldsymbol{\mathcal{T}} \end{bmatrix} = \begin{bmatrix} \boldsymbol{\mathcal{B}}_1 \\ \boldsymbol{\mathcal{B}}_2 \end{bmatrix}. \tag{9.1}$$

We also know that the vector $\boldsymbol{\mathcal{B}}_1$ is given by sub-vectors of the form

$$\begin{aligned}(\boldsymbol{\mathcal{B}}_1)_i = -\boldsymbol{\omega}^{\mathfrak{o}_\mathrm{i}}_{\mathfrak{o}_\mathrm{i}/\mathrm{I}} \times (M_{\mathfrak{o}_\mathrm{i}} \star (\boldsymbol{\omega}^{\mathfrak{o}_\mathrm{i}}_{\mathfrak{o}_\mathrm{i}/\mathrm{I}})^{\mathsf{s}}) + \boldsymbol{W}^{\mathfrak{o}_\mathrm{i}}_{\mathfrak{o}_\mathrm{i}}(O_{\mathfrak{o}_\mathrm{i}}) + b_i \boldsymbol{q}_{\mathrm{G_i}/\mathfrak{o}_\mathrm{i}} \boldsymbol{W}^{\mathrm{G_i}}_{\mathrm{ext,i}}(O_{\mathrm{G_i}}) \boldsymbol{q}^*_{\mathrm{G_i}/\mathfrak{o}_\mathrm{i}} \\ + \sum_{j \in P(C(:,i))} \boldsymbol{q}^*_{\mathfrak{o}_\mathrm{i}/\mathrm{j}} \boldsymbol{W}^{\mathrm{j}}_{\mathrm{act,j}}(O_{\mathrm{j}}) \boldsymbol{q}_{\mathfrak{o}_\mathrm{i}/\mathrm{j}} - \sum_{j \in N(C(:,i))} \boldsymbol{q}_{\mathrm{j}/\mathfrak{o}_\mathrm{i}} \boldsymbol{W}^{\mathrm{j}}_{\mathrm{act,j}}(O_{\mathrm{j}}) \boldsymbol{q}^*_{\mathrm{j}/\mathfrak{o}_\mathrm{i}}.\end{aligned} \tag{9.2}$$

We can re-write the expression for $(\boldsymbol{\mathcal{B}}_1)_i$ as

$$(\boldsymbol{\mathcal{B}}_1)_i = -\boldsymbol{\omega}^{\mathfrak{e}_i}_{\mathfrak{e}_i/\mathcal{I}} \times (M_{\mathfrak{e}_i} \star (\boldsymbol{\omega}^{\mathfrak{e}_i}_{\mathfrak{e}_i/\mathcal{I}})^{\mathsf{s}}) + \boldsymbol{\mathcal{C}}_i, \tag{9.3}$$

where we have separated the expression into terms that contain the unknown dual inertia matrix $M_{\mathfrak{e}_i}$, and terms that do not. Therefore, the i-th Newton-Euler equation can be manipulated as

$$\begin{aligned}
&(\boldsymbol{\mathcal{S}}_{11})_{\{i,i\}} \star \dot{\boldsymbol{\omega}}^{\mathfrak{e}_i}_{\mathfrak{e}_i/\mathcal{I}} + (\boldsymbol{\mathcal{S}}_{12})_{\{i,:\}} \boldsymbol{\mathcal{T}} &&= (\boldsymbol{\mathcal{B}}_1)_i \\
\implies &\mathrm{H}\left(M_{\mathfrak{e}_i}\right) \star \dot{\boldsymbol{\omega}}^{\mathfrak{e}_i}_{\mathfrak{e}_i/\mathcal{I}} + (\boldsymbol{\mathcal{S}}_{12})_{\{i,:\}} \boldsymbol{\mathcal{T}} &&= -\boldsymbol{\omega}^{\mathfrak{e}_i}_{\mathfrak{e}_i/\mathcal{I}} \times (M_{\mathfrak{e}_i} \star (\boldsymbol{\omega}^{\mathfrak{e}_i}_{\mathfrak{e}_i/\mathcal{I}})^{\mathsf{s}}) + \boldsymbol{\mathcal{C}}_i \\
\implies &M_{\mathfrak{e}_i} \star (\dot{\boldsymbol{\omega}}^{\mathfrak{e}_i}_{\mathfrak{e}_i/\mathcal{I}})^{\mathsf{s}} + \boldsymbol{\omega}^{\mathfrak{e}_i}_{\mathfrak{e}_i/\mathcal{I}} \times (M_{\mathfrak{e}_i} \star (\boldsymbol{\omega}^{\mathfrak{e}_i}_{\mathfrak{e}_i/\mathcal{I}})^{\mathsf{s}}) &&= \boldsymbol{\mathcal{C}}_i - (\boldsymbol{\mathcal{S}}_{12})_{\{i,:\}} \boldsymbol{\mathcal{T}},
\end{aligned} \tag{9.4}$$

where we have used the fact that $\boldsymbol{\mathcal{S}}_{11}$ is a block-diagonal matrix. Now, using the $r(\cdot)$ function, defined in equation (4.2) as $r : \mathbb{H}^v_d \to \mathbb{R}^{8\times 7}$ that satisfies

$$M_{\mathfrak{e}_i} \star \boldsymbol{a} \triangleq r(\boldsymbol{a})\mathrm{v}(M_{\mathfrak{e}_i}) = \begin{bmatrix}
0 & 0 & 0 & 0 & 0 & 0 & 0 \\
0 & 0 & 0 & 0 & 0 & 0 & a_2 \\
0 & 0 & 0 & 0 & 0 & 0 & a_3 \\
0 & 0 & 0 & 0 & 0 & 0 & a_4 \\
0 & 0 & 0 & 0 & 0 & 0 & 0 \\
a_6 & a_7 & a_8 & 0 & 0 & 0 & 0 \\
0 & a_6 & 0 & a_7 & a_8 & 0 & 0 \\
0 & 0 & a_6 & 0 & a_7 & a_8 & 0
\end{bmatrix} \mathrm{v}(M_{\mathfrak{e}_i}), \tag{9.5}$$

we can express the i-th Newton-Euler equation as

$$\begin{aligned} M_{\mathfrak{o}_\mathfrak{i}} \star (\dot{\boldsymbol{\omega}}^{\mathfrak{o}_\mathfrak{i}}_{\mathfrak{o}_\mathfrak{i}/\mathcal{I}})^{\mathsf{s}} + \boldsymbol{\omega}^{\mathfrak{o}_\mathfrak{i}}_{\mathfrak{o}_\mathfrak{i}/\mathcal{I}} \times (M_{\mathfrak{o}_\mathfrak{i}} \star (\boldsymbol{\omega}^{\mathfrak{o}_\mathfrak{i}}_{\mathfrak{o}_\mathfrak{i}/\mathcal{I}})^{\mathsf{s}}) &= \boldsymbol{\mathcal{C}}_i - (\boldsymbol{\mathcal{S}}_{12})_{\{i,:\}}\boldsymbol{\mathcal{T}} \\ r((\dot{\boldsymbol{\omega}}^{\mathfrak{o}_\mathfrak{i}}_{\mathfrak{o}_\mathfrak{i}/\mathcal{I}})^{\mathsf{s}})\mathrm{v}(M_{\mathfrak{o}_\mathfrak{i}}) + [\boldsymbol{\omega}^{\mathfrak{o}_\mathfrak{i}}_{\mathfrak{o}_\mathfrak{i}/\mathcal{I}}]^{\times} r((\boldsymbol{\omega}^{\mathfrak{o}_\mathfrak{i}}_{\mathfrak{o}_\mathfrak{i}/\mathcal{I}})^{\mathsf{s}})\mathrm{v}(M_{\mathfrak{o}_\mathfrak{i}}) &= \boldsymbol{\mathcal{C}}_i - (\boldsymbol{\mathcal{S}}_{12})_{\{i,:\}}\boldsymbol{\mathcal{T}} \\ \hat{R}(\dot{\boldsymbol{\omega}}^{\mathfrak{o}_\mathfrak{i}}_{\mathfrak{o}_\mathfrak{i}/\mathcal{I}}, \boldsymbol{\omega}^{\mathfrak{o}_\mathfrak{i}}_{\mathfrak{o}_\mathfrak{i}/\mathcal{I}})\mathrm{v}(M_{\mathfrak{o}_\mathfrak{i}}) &= \boldsymbol{\mathcal{C}}_i - (\boldsymbol{\mathcal{S}}_{12})_{\{i,:\}}\boldsymbol{\mathcal{T}}. \end{aligned} \tag{9.6}$$

Here, we implicitly defined $\hat{R} : \mathbb{H}^v_d \times \mathbb{H}^v_d \to \mathbb{R}^{8\times 7}$ as

$$\hat{R}(\dot{\boldsymbol{\omega}}^{\mathfrak{o}_\mathfrak{i}}_{\mathfrak{o}_\mathfrak{i}/\mathcal{I}}, \boldsymbol{\omega}^{\mathfrak{o}_\mathfrak{i}}_{\mathfrak{o}_\mathfrak{i}/\mathcal{I}}) \triangleq r((\dot{\boldsymbol{\omega}}^{\mathfrak{o}_\mathfrak{i}}_{\mathfrak{o}_\mathfrak{i}/\mathcal{I}})^{\mathsf{s}}) + [\boldsymbol{\omega}^{\mathfrak{o}_\mathfrak{i}}_{\mathfrak{o}_\mathfrak{i}/\mathcal{I}}]^{\times} r((\boldsymbol{\omega}^{\mathfrak{o}_\mathfrak{i}}_{\mathfrak{o}_\mathfrak{i}/\mathcal{I}})^{\mathsf{s}}). \tag{9.7}$$

For the two-armed manipulator, there is a total of 11 bodies whose mass parameters need to be estimated. Therefore, we can stack these to yield the following equation

$$\boldsymbol{R}\boldsymbol{M} = \boldsymbol{F}, \tag{9.8}$$

where

$$\boldsymbol{R} = \text{blk-diag}(\hat{R}(\dot{\boldsymbol{\omega}}^{\mathfrak{o}_1}_{\mathfrak{o}_1/\mathcal{I}}, \boldsymbol{\omega}^{\mathfrak{o}_1}_{\mathfrak{o}_1/\mathcal{I}}), \ldots, \hat{R}(\dot{\boldsymbol{\omega}}^{\mathfrak{o}_\mathfrak{i}}_{\mathfrak{o}_\mathfrak{i}/\mathcal{I}}, \boldsymbol{\omega}^{\mathfrak{o}_\mathfrak{i}}_{\mathfrak{o}_\mathfrak{i}/\mathcal{I}}), \ldots, \hat{R}(\dot{\boldsymbol{\omega}}^{\mathfrak{o}_{11}}_{\mathfrak{o}_{11}/\mathcal{I}}, \boldsymbol{\omega}^{\mathfrak{o}_{11}}_{\mathfrak{o}_{11}/\mathcal{I}})), \tag{9.9}$$

$$\boldsymbol{M} = [\mathrm{v}(M_{\mathfrak{o}_1})^{\mathrm{T}}, \ldots, \mathrm{v}(M_{\mathfrak{o}_\mathfrak{i}})^{\mathrm{T}}, \ldots, \mathrm{v}(M_{\mathfrak{o}_{11}})^{\mathrm{T}}]^{\mathrm{T}}, \tag{9.10}$$

and

$$\boldsymbol{F} = \boldsymbol{\mathcal{C}} - \boldsymbol{\mathcal{S}}_{12}\boldsymbol{\mathcal{T}}. \tag{9.11}$$

Here it is worth emphasizing that at every timestep, $\boldsymbol{R}$ and $\boldsymbol{F}$ can be constructed from known quantities. We will store the data necessary to reconstruct $\boldsymbol{R}$ and $\boldsymbol{F}$ in the sets $\boldsymbol{\mathcal{X}}$ and $\boldsymbol{\mathcal{F}}$ correspondingly, which is analogous to the notation used in Chapter 4. The amount of data points to store is a user parameter and we will denote it as N_s. The selection of these points is discussed in a later section.

Remark 16. Equation (9.11) assumes perfect knowledge of all wrenches applied on all bodies. Without the true dual inertia matrices to evaluate a dynamics model, $\boldsymbol{\mathcal{T}}$ must be

obtained via measurement readings of forces and torques at the joints. Additionally, and as pointed out in Remark 8, the accuracy with which the wrenches are known is essential to the concurrent learning framework. Therefore, prior to using this approach, the system must be well characterized.

The variable to be estimated is $\boldsymbol{M} \in \mathbb{R}^{77}$, composed of seven independent mass parameters for each of the 11 bodies in the two-armed manipulator. We define $\widehat{\boldsymbol{M}}$ as the estimate of $\boldsymbol{M}$. Additionally, we define the estimation error $\Delta\boldsymbol{M} \in \mathbb{R}^{77}$ as

$$\Delta\boldsymbol{M} \triangleq \widehat{\boldsymbol{M}} - \boldsymbol{M}. \tag{9.12}$$

This allows us to define the quantity $\boldsymbol{\varepsilon}_k$ corresponding to data point k in sets $\boldsymbol{\mathcal{X}}$ and $\boldsymbol{\mathcal{F}}$ as

$$\boldsymbol{\varepsilon}_k \triangleq \boldsymbol{R}_k\widehat{\boldsymbol{M}} - \boldsymbol{F}_k. \tag{9.13}$$

Notice that using equation (9.8), $\boldsymbol{F}_k$ becomes $\boldsymbol{R}_k\boldsymbol{M}$ so that

$$\begin{aligned} \boldsymbol{\varepsilon}_k &= \boldsymbol{R}_k\widehat{\boldsymbol{M}} - \boldsymbol{R}_k\boldsymbol{M} \\ &= \boldsymbol{R}_k(\widehat{\boldsymbol{M}} - \boldsymbol{M}) \\ &= \boldsymbol{R}_k\Delta\boldsymbol{M}, \end{aligned} \tag{9.14}$$

which implies that $\boldsymbol{\varepsilon}_k$ is an error-like quantity for the estimation of $\boldsymbol{M}$.

9.2 Adaptive Estimation of Dual Inertia

The result described in this section provides assurances on the convergence of the mass parameters for a spacecraft-mounted manipulator subject to a given rank condition being satisfied. More specifically, the following theorem ensures that the estimates converge asymptotically to the true values.

Theorem 3. *Consider the dynamical system with kinematics given by equations* (7.7) *and* (7.8) *and dynamics described by equation* (9.1). $\widehat{\boldsymbol{M}}$ *is an estimate of* $\boldsymbol{M}$ *updated according to*

$$\frac{\mathrm{d}}{\mathrm{d}t}\widehat{\boldsymbol{M}} = -\sum_{k=1}^{N_s} \boldsymbol{R}_k^{\mathrm{T}} \boldsymbol{\varepsilon}_k, \tag{9.15}$$

where $\boldsymbol{\varepsilon}_k$ *is given by* (9.13)*, constructed from the data in the sets* $\boldsymbol{\mathcal{X}}$ *and* $\boldsymbol{\mathcal{F}}$*. Assume that*

$$\operatorname{rank} \sum_{k=1}^{N_s} \boldsymbol{R}_k^{\mathrm{T}} \boldsymbol{R}_k = 77. \tag{9.16}$$

Then, for all initial conditions, $\lim_{t\to\infty} \widehat{\boldsymbol{M}} \to \boldsymbol{M}$.

Proof. Note that $\Delta\boldsymbol{M} = 0_{77}$ is the equilibrium point of the update law in equation (9.15). Consider the Lyapunov function candidate

$$V(\Delta\boldsymbol{M}) = \tfrac{1}{2}\Delta\boldsymbol{M}^{\mathrm{T}}\Delta\boldsymbol{M}. \tag{9.17}$$

Note that V is a valid candidate Lyapunov since it satisfies $V(0_{77}) = 0$ and $V(\Delta\boldsymbol{M}) > 0 \quad \forall \Delta\boldsymbol{M} \in \mathbb{R}^{77}\backslash\{0_{77}\}$. The time derivative of V is equal to

$$\dot{V}(\Delta\boldsymbol{M}) = \Delta\boldsymbol{M}^{\mathrm{T}} \frac{\mathrm{d}}{\mathrm{d}t}\Delta\boldsymbol{M}. \tag{9.18}$$

Using the fact that the mass parameters of the two-armed manipulator are constant with respect to time, we know that $\frac{\mathrm{d}}{\mathrm{d}t}\Delta\boldsymbol{M} = \frac{\mathrm{d}}{\mathrm{d}t}(\widehat{\boldsymbol{M}} - \boldsymbol{M}) = \frac{\mathrm{d}}{\mathrm{d}t}\widehat{\boldsymbol{M}}$. Thus,

$$\dot{V}(\Delta\boldsymbol{M}) = \Delta\boldsymbol{M}^{\mathrm{T}} \frac{\mathrm{d}}{\mathrm{d}t}\widehat{\boldsymbol{M}}, \tag{9.19}$$

and evaluating the update law in equation (9.15), we get

$$\dot{V}(\Delta \boldsymbol{M}) = -\Delta \boldsymbol{M}^{\mathrm{T}} \sum_{k=1}^{N_s} \boldsymbol{R}_k^{\mathrm{T}} \boldsymbol{\varepsilon}_k. \tag{9.20}$$

Using the expression in equation (9.14), the Lyapunov derivative becomes

$$\dot{V}(\Delta \boldsymbol{M}) = -\Delta \boldsymbol{M}^{\mathrm{T}} \left(\sum_{k=1}^{N_s} \boldsymbol{R}_k^{\mathrm{T}} \boldsymbol{R}_k \right) \Delta \boldsymbol{M}. \tag{9.21}$$

Since $\sum_{k=1}^{N_s} \boldsymbol{R}_k^{\mathrm{T}} \boldsymbol{R}_k$ is symmetric, it is a positive semidefinite matrix, and by hypothesis $\operatorname{rank} \sum_{k=1}^{N_s} \boldsymbol{R}_k^{\mathrm{T}} \boldsymbol{R}_k = 77$. Therefore, we have that $\dot{V}(\Delta \boldsymbol{M}) < 0$, and by Lyapunov's first theorem we conclude that $\lim_{t\to\infty} \Delta \boldsymbol{M} \to 0_{77}$, which implies that $\lim_{t\to\infty} \widehat{\boldsymbol{M}} \to \boldsymbol{M}$, satisfying the estimation objective and concluding the proof. ■

9.3 Algorithm Description

In this section we discuss how the concurrent learning algorithm is implemented. In particular, two of the aspects that are worth emphasizing include:

1) How to populate the $\boldsymbol{\mathcal{X}}$ and $\boldsymbol{\mathcal{F}}$ storage sets.

2) How to compute equation (9.15) efficiently.

Assuming that an ODE4 integration scheme is used, the incorporation of new data should only happen every four evaluations of the dynamics. In SIMULINK, persistent variables were used to store data since this type of variable can be accessed in future function calls. Every time that a new data point is added to $\boldsymbol{\mathcal{X}}$, the corresponding timestep's information must be added to $\boldsymbol{\mathcal{F}}$. We define N_c as the amount of data points currently stored in $\boldsymbol{\mathcal{X}}$ and $\boldsymbol{\mathcal{F}}$. Additionally, denote as $\sigma(\boldsymbol{\mathcal{X}}, \boldsymbol{\mathcal{F}})$ the ordered set of singular values of $\sum_{k=1}^{N_s} \boldsymbol{R}_k^{\mathrm{T}} \boldsymbol{R}_k$ constructed from data contained in $\boldsymbol{\mathcal{X}}$ and $\boldsymbol{\mathcal{F}}$, and we use the permutation function $\pi(1, \ldots, N_s)$ to yield a random permutation of the indices 1 to N_s. Algorithm 3 outlines the procedure to populate the two sets.

Algorithm 3 Populating $\boldsymbol{\mathcal{X}}$ and $\boldsymbol{\mathcal{F}}$

Given: N_s, σ_{th}, and candidates X and F
  If $N_c < N_s$
    Accept $X \mapsto \boldsymbol{\mathcal{X}}$, $F \mapsto \boldsymbol{\mathcal{F}}$
  Else If $\min \sigma(\boldsymbol{\mathcal{X}}, \boldsymbol{\mathcal{F}}) < \sigma_{\text{th}}$
    For $i \in \pi(1, \ldots, N_s)$
      Construct sets $\boldsymbol{\mathcal{X}}_i, \boldsymbol{\mathcal{F}}_i$ by removing data point i from $\boldsymbol{\mathcal{X}}, \boldsymbol{\mathcal{F}}$.
      Append X to $\boldsymbol{\mathcal{X}}_i$ and F to $\boldsymbol{\mathcal{F}}_i$
      If $\sigma(\boldsymbol{\mathcal{X}}_i \cup X, \boldsymbol{\mathcal{F}}_i \cup F) \geq \sigma(\boldsymbol{\mathcal{X}}, \boldsymbol{\mathcal{F}})$
        $\boldsymbol{\mathcal{X}} \leftarrow \boldsymbol{\mathcal{X}}_i \cup X$ and $\boldsymbol{\mathcal{F}} \leftarrow \boldsymbol{\mathcal{F}}_i \cup F$
        Break
      End If
    End For
  End If

We now provide some remarks regarding Algorithm 3.

Remark 17. The conditional statement condition $\sigma(\boldsymbol{\mathcal{X}}_i \cup X, \boldsymbol{\mathcal{F}}_i \cup F) \geq \sigma(\boldsymbol{\mathcal{X}}, \boldsymbol{\mathcal{F}})$ is an element-wise comparison for each of the singular values of the two different sets, and for the statement to be true, the comparison must be satisfied for all entries. Notice as well that $\sigma(\boldsymbol{\mathcal{X}}, \boldsymbol{\mathcal{F}})$ can be stored from the previous timestep.

Remark 18. The computation of the matrix $\sum_{k=1}^{N_s} \boldsymbol{R}_k^{\mathrm{T}} \boldsymbol{R}_k$ every time that the sets $\boldsymbol{\mathcal{X}}$ and $\boldsymbol{\mathcal{F}}$ change can be computationally expensive. Thus, having a large N_s is not ideal. However, for large N_s and small T_{th}, the likelihood that $\sigma(\boldsymbol{\mathcal{X}}_i \cup X, \boldsymbol{\mathcal{F}}_i \cup F) \geq \sigma(\boldsymbol{\mathcal{X}}, \boldsymbol{\mathcal{F}})$ is increased since lower *quality* (i.e., as measured by their contribution to increasing the minimum singular value) X and F data points are accepted during the initial population phase.

Algorithm 4 describes an implementation of the concurrent learning framework used for the actual computation of the adaptive update of $\widehat{\boldsymbol{M}}$ as a function of the data contained in $\boldsymbol{\mathcal{X}}$ and $\boldsymbol{\mathcal{F}}$. The main characteristic of this implementation is the pre-computation of costly matrices once no new data is incorporated into the storage sets. We define T_{th} as a threshold amount of time during which we incorporate new data into our storage sets.

Algorithm 4 Adaptive Estimation Using Concurrent Learning

Given: t, $\widehat{\boldsymbol{M}}(0)$, T_{th}, N_s, $\boldsymbol{\mathcal{X}}$, $\boldsymbol{\mathcal{F}}$ and candidates X and F
If $t < T_{\text{th}}$
  Compute new $\boldsymbol{\mathcal{X}}$ and $\boldsymbol{\mathcal{F}}$ sets using Algorithm 3.
  For k = 1 to $\min(N_c, N_s)$
    $\text{RR} \coloneqq \text{RR} + \boldsymbol{R}_k^{\text{T}} \boldsymbol{R}_k$
    $\text{Rf} \coloneqq \text{Rf} + \boldsymbol{R}_k^{\text{T}} \boldsymbol{F}_k$
  End For
  $\text{RR}_{\text{STORED}} \leftarrow \text{RR}$
  $\text{Rf}_{\text{STORED}} \leftarrow \text{Rf}$
Else
  $\text{RR} \leftarrow \text{RR}_{\text{STORED}}$
  $\text{Rf} \leftarrow \text{Rf}_{\text{STORED}}$
End If
$\frac{\text{d}}{\text{d}t}\widehat{\boldsymbol{M}} = -(\text{RR}\widehat{\boldsymbol{M}} - \text{Rf})$

9.4 Aggressive Estimation

While the concurrent learning provides a simple data-driven method of estimating parameters that appear linearly in the equations of motion assuming that the rank condition in equation (9.16) is satisfied, the rate of convergence is highly dependent on the minimum singular value of the matrix $\sum_{k=1}^{N_s} \boldsymbol{R}_k^{\text{T}} \boldsymbol{R}_k$. Thus, for a small minimum singular value, the rate of convergence can be impractical. To increase the minimum singular value, the user can opt to increase the value of N_s, the amount of timesteps for which data is stored in matrices $\boldsymbol{\mathcal{X}}$ and $\boldsymbol{\mathcal{F}}$. However, this option is computationally costly, as pointed out in remark 18. Thus, in this section, we propose a modification of equation (9.15) that allows for aggressive convergence for low values of N_s, as long as the rank condition is satisfied.

The proposed approach hinges on the use of the singular value decomposition (SVD), which yields a decomposition of a matrix into the product of two unitary matrices and a diagonal matrix of appropriate sizes. The matrix whose singular values dictate convergence in this estimation problem is $\sum_{k=1}^{N_s} \boldsymbol{R}_k^{\text{T}} \boldsymbol{R}_k \in \mathbb{R}^{77\times 77}$. We define its SVD as

$$\sum_{k=1}^{N_s} \boldsymbol{R}_k^{\text{T}} \boldsymbol{R}_k = U \Sigma V^{\text{T}}, \tag{9.22}$$

where $U^{\mathrm{T}}U = UU^{\mathrm{T}} = \mathbb{I}_{77}$ and $V^{\mathrm{T}}V = VV^{\mathrm{T}} = \mathbb{I}_{77}$. For an extensive treatment of the SVD, the reader is referred to [151]. Since we assume that the condition given by equation (9.16) is satisfied, $\operatorname{rank}\Sigma = 77$, and every singular value $\sigma_i > 0$. Thus, we can introduce the gain matrix $K \in \mathbb{R}^{77\times 77}$ such that

$$\frac{\mathrm{d}}{\mathrm{d}t}\widehat{\boldsymbol{M}} = -K\sum_{k=1}^{N_s} \boldsymbol{R}_k^{\intercal}\boldsymbol{\varepsilon}_k, \tag{9.23}$$

where K is defined as

$$K \triangleq \begin{cases} \mathbb{I}_{77} & \text{if} \quad t < T_{\mathrm{th},2} \\ U\overline{\Sigma}U^{\mathrm{T}} & \text{if} \quad t \geq T_{\mathrm{th},2}. \end{cases} \tag{9.24}$$

Thus, for $t < T_{\mathrm{th},2}$, no modification of the adaptation law is in place. This allows for enough collection of data points so that the rank condition of equation (9.16) is satisfied. However, for $t \geq T_{\mathrm{th},2}$, we have that

$$\begin{aligned} &\frac{\mathrm{d}}{\mathrm{d}t}\widehat{\boldsymbol{M}} = -K\sum_{k=1}^{N_s} \boldsymbol{R}_k^{\intercal}\boldsymbol{\varepsilon}_k && t \geq T_{\mathrm{th},2} \\ \implies &\frac{\mathrm{d}}{\mathrm{d}t}\widehat{\boldsymbol{M}} = -\left(U\overline{\Sigma}U^{\mathrm{T}}\right)\left(\sum_{k=1}^{N_s} \boldsymbol{R}_k^{\intercal}\boldsymbol{R}_k\right)\Delta\boldsymbol{M} && t \geq T_{\mathrm{th},2} \\ \implies &\frac{\mathrm{d}}{\mathrm{d}t}\widehat{\boldsymbol{M}} = -\left(U\overline{\Sigma}U^{\mathrm{T}}\right)(U\Sigma V^{\mathrm{T}})\Delta\boldsymbol{M} && t \geq T_{\mathrm{th},2} \\ \implies &\frac{\mathrm{d}}{\mathrm{d}t}\widehat{\boldsymbol{M}} = -\left(U\overline{\Sigma}\Sigma V^{\mathrm{T}}\right)\Delta\boldsymbol{M} && t \geq T_{\mathrm{th},2}. \end{aligned} \tag{9.25}$$

This choice of gain K allows us to target specific singular values of $\sum_{k=1}^{N_s}\boldsymbol{R}_k^{\mathrm{T}}\boldsymbol{R}_k$. In particular, depending on the choice of $\overline{\Sigma}$, the aggressiveness of the convergence can be tuned. Representing the diagonal matrices Σ and $\overline{\Sigma}$ as

$$\begin{aligned} \Sigma &= \operatorname{diag}(\sigma_1, \ldots, \sigma_i, \ldots, \sigma_{77}) \\ \overline{\Sigma} &= \operatorname{diag}(\overline{\sigma}_1, \ldots, \overline{\sigma}_i, \ldots, \overline{\sigma}_{77}), \end{aligned} \tag{9.26}$$

we will select $\overline{\sigma}_i$ as

$$\overline{\sigma}_i = \begin{cases} \overline{\sigma}_i = 1 & \text{if} \quad \sigma_i > \sigma_{\text{th},2} \quad \text{or} \quad \sigma_i = 0, \\ \overline{\sigma}_i = \frac{\sigma_{\text{new}}}{\sigma_i} & \text{if} \quad \sigma_{\text{th},2} > \sigma_i > 0, \end{cases} \tag{9.27}$$

where the case $\sigma_i = 0$ accounts for circumstances when the matrix $\sum_{k=1}^{N_s} \boldsymbol{R}_k^{\mathrm{T}} \boldsymbol{R}_k$ is rank deficient, and the case $\sigma_i > \sigma_{\text{th},2}$ deems the current singular value sufficiently high.

9.5 Numerical Simulations

To evaluate the performance of the algorithm, a numerical simulation was run on MATLAB R2017a using ODE4 with a timestep equal to $\mathrm{d}t = 0.01$ s. The true mass properties of the satellite base are given as $m_{\mathcal{B}_1} = 50$ kg, $(\bar{I}_{\mathcal{B}_1})_{(1,1)} = (\bar{I}_{\mathcal{B}_1})_{(2,2)} = (\bar{I}_{\mathcal{B}_1})_{(3,3)} = 10 \text{ kg} \cdot \text{m}^2$, with all inertia cross terms equal to zero, and the mass properties of each link of the manipulator are set to $m_{\mathcal{B}_i} = 5$ kg, $(\bar{I}_{\mathcal{B}_i})_{(1,1)} = (\bar{I}_{\mathcal{B}_i})_{(2,2)} = (\bar{I}_{\mathcal{B}_i})_{(3,3)} = 1 \text{ kg} \cdot \text{m}^2$ for simplicity. We set the external wrenches applied at the center of mass of all bodies to zero, including control wrenches at the satellite base, and body wrenches, such as gravitational effects, and other perturbation wrenches. This assumption is acceptable in deep space, where the only significant perturbation is solar pressure, and its effect is negligible. For a simulation in which the spacecraft is orbiting an object, an accurate environmental model and its effects on the spacecraft is required. Additionally, it is assumed that the arms are not in contact with other bodies.

We apply a non-zero actuation wrench on each joint degree of freedom. The forcing function about each generalized coordinate is given as

$$n(t) = 0.5 \sin(t) \quad \text{N or Nm}, \qquad 2 \text{ s} \leq t \leq 3 \text{ s}. \tag{9.28}$$

Additionally, we set the concurrent learning parameters as follows: $T_{\text{th},2} = 4.9$ s, $T_{\text{th}} = 5.0$ s, $N_s = 10$, $\sigma_{\text{th}} = 0.001$, $\sigma_{\text{th},2} = 0.5$, and $\sigma_{\text{new}} = 100$. Finally, we set the final

simulation time to $T = 10.0$ s.

Figure 9.1 shows the singular values of the matrix $\sum_{k=1}^{N_s} \boldsymbol{R}_k^{\mathrm{T}} \boldsymbol{R}_k$. It is clear from this figure that the actuation of the joints is necessary to excite the singular values. In fact, knowledge of the singular values and the corresponding value of $U\Sigma_{(:,i)}$, where $\Sigma_{(:,i)}$ is the i-th column of Σ, can be used to determine how certain joint actuation maneuvers excite the different modes of the estimate vector. This has the potential of allowing the determination of effective actuation profiles that will aid in the estimation of the mass properties. However, it can also be appreciated that no new data points are taken into the matrices $\boldsymbol{\mathcal{X}}$ and $\boldsymbol{\mathcal{F}}$ after $t = 2.1$ s, represented by the constant singular values. Figure 9.2 shows the evolution of the estimates of the mass properties for the satellite base. Figures 9.3 and 9.4 show the evolution of the estimates of the mass properties for the links on the left (branch one), and right (branch 2) arms. In all three figures, the actuation of the joints jump-starts the estimation at $t = 2$ s and the application of gain K from equation (9.24) at $t = T_{\mathrm{th},2} = 4.9$ s leads to a jump in all estimates towards the true value. It is worth emphasizing at this point that it suffices to gather $10\ (= N_s)$ significantly exciting data points to accurately estimate 77 different mass-related properties.

Figures 9.1 to 9.4 were run for the remarkably low value of $N_s = 10$. To evaluate the significance of the parameter N_s in the current implementation, a series of simulations was run in which the parameter N_s was varied from $N_s = 10$ to $N_s = 300$ for a simulation with final time $T = 10$ s. Figure 9.5 shows the accuracy of the algorithm as a function of N_s, evaluated via the infinity norm of the error defined to act on the function $u(\cdot) : \mathbb{R} \to \mathbb{R}$ as $||u||_\infty = \sup_{9.7\ \mathrm{s} \leq t_k \leq 10\ \mathrm{s}} |u(t_k)|$. The results show that the convergence characteristics are not sensitive to changes in N_s. However, as it can be seen in Figure 9.6, the total run time is highly sensitive to the selection of N_s. This behavior is explained in Remark 18. To achieve asymptotic convergence up to machine precision, removing the gain K, increasing N_s, and setting a large final time T were all necessary.

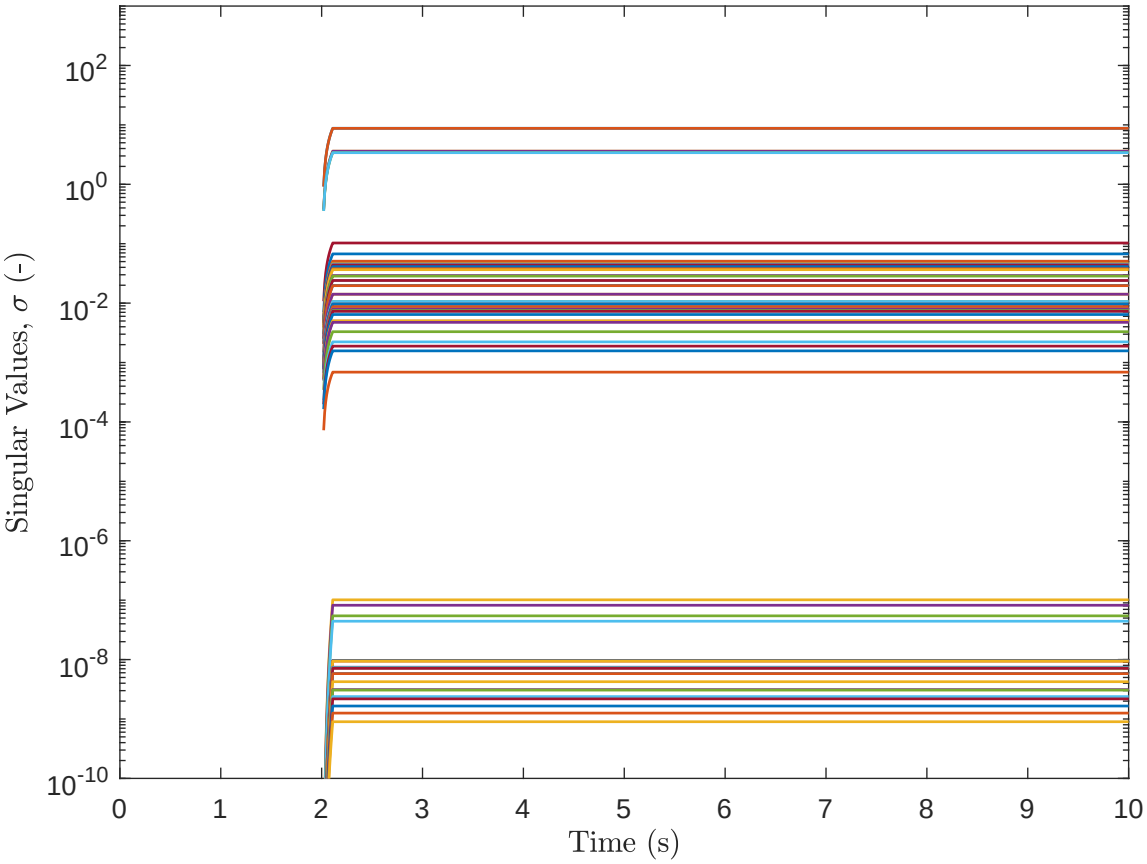

Figure 9.1: Evolution of the singular values of the matrix $\sum_{k=1}^{N_s} \boldsymbol{R}_k^{\mathrm{T}} \boldsymbol{R}_k$

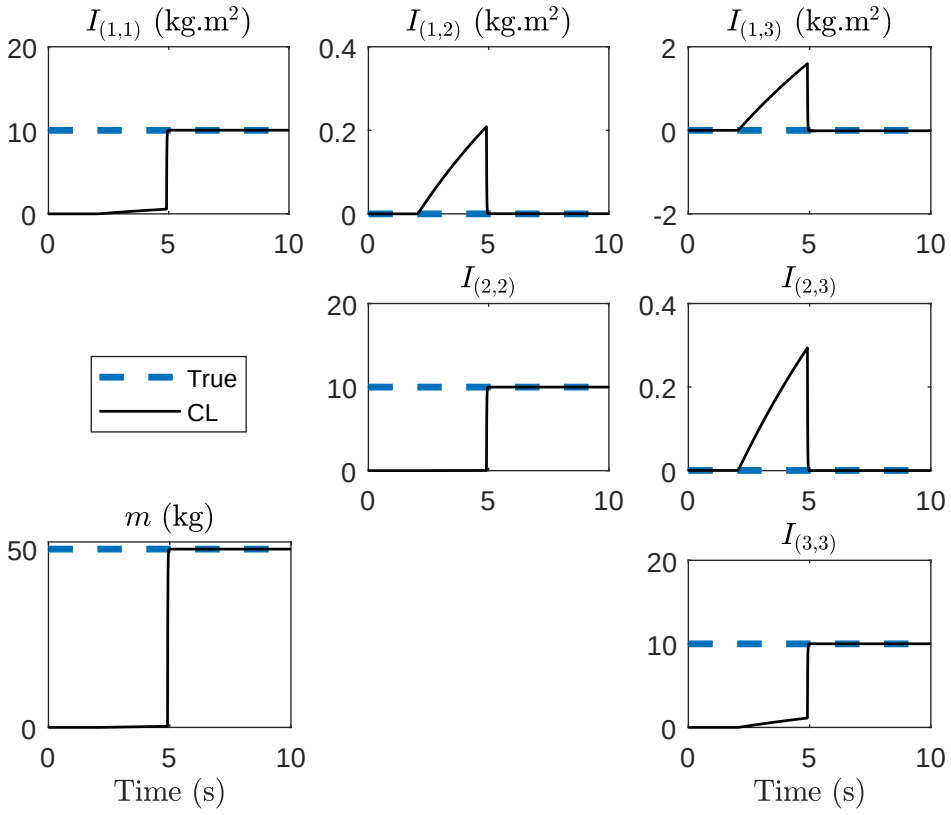

Figure 9.2: Evolution of mass parameters for the satellite base.

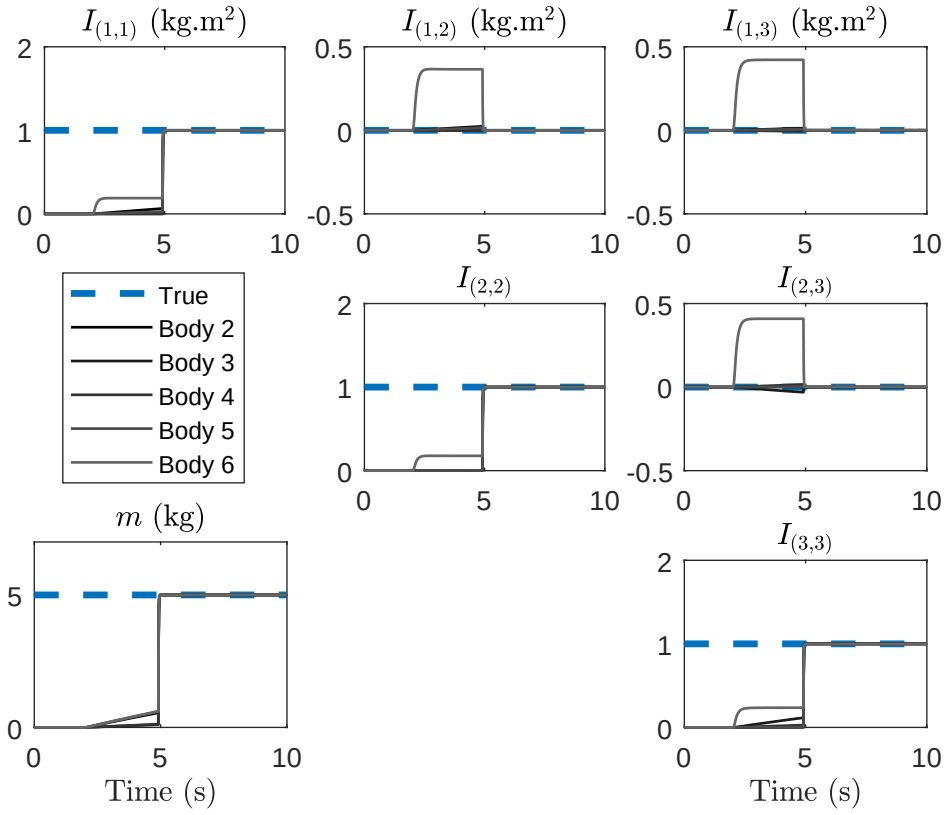

Figure 9.3: Evolution of mass parameters for links on the left branch.

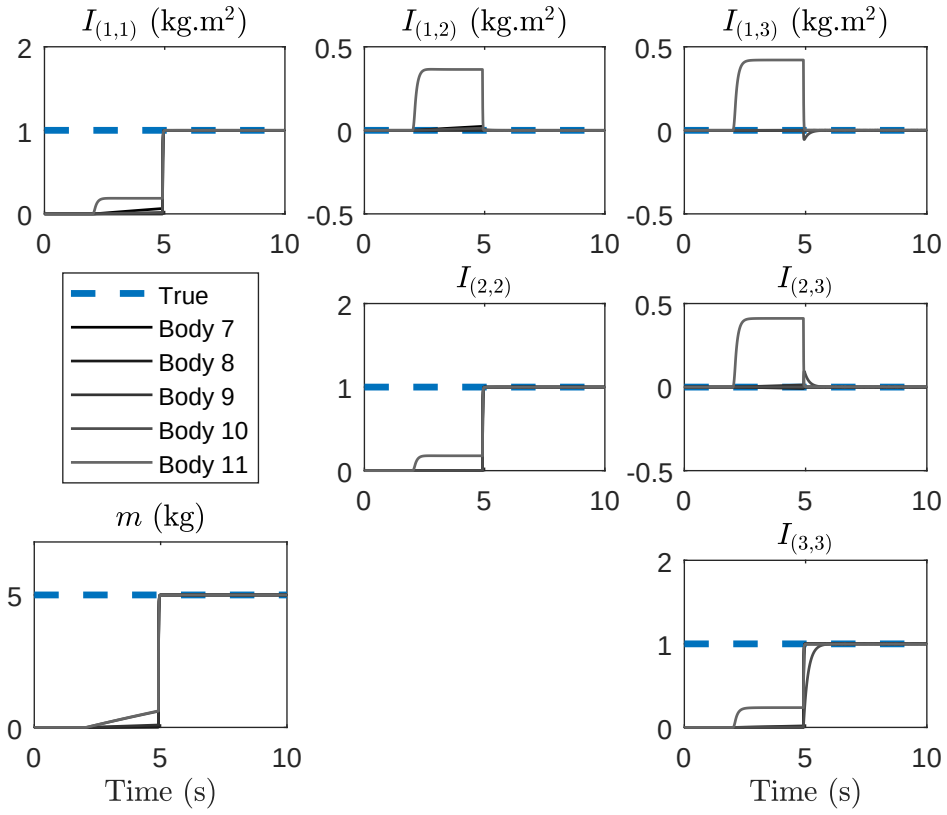

Figure 9.4: Evolution of mass parameters for links on the right branch.

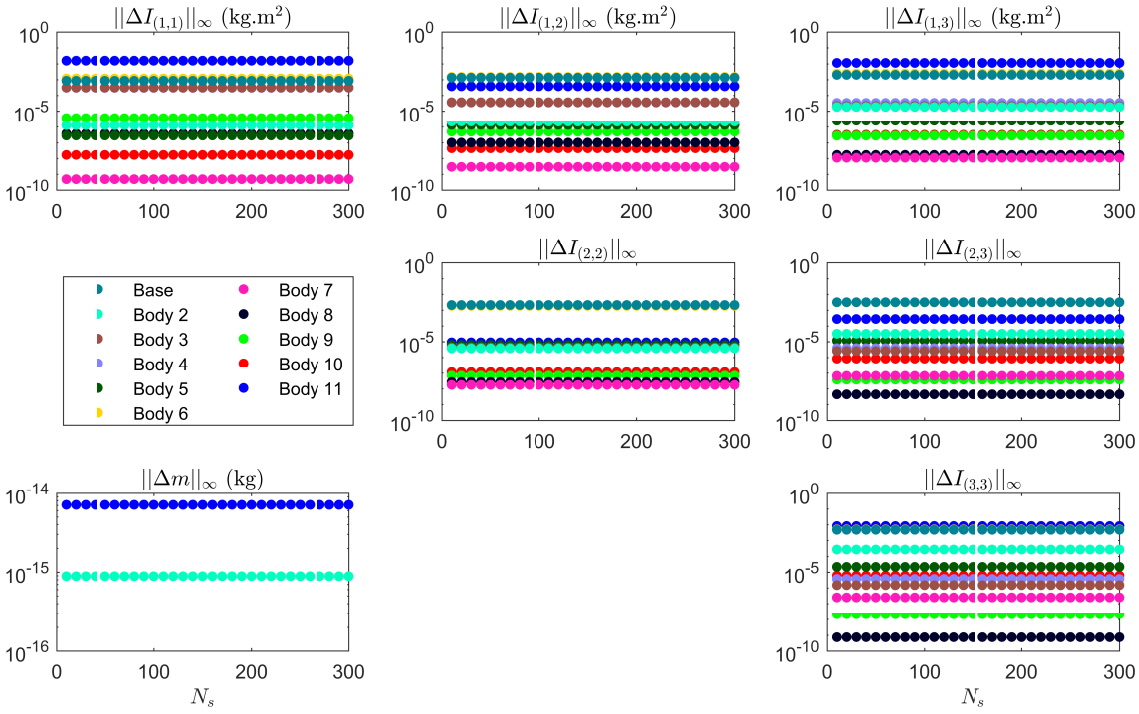

Figure 9.5: Comparison of convergence properties as a function of N_s.

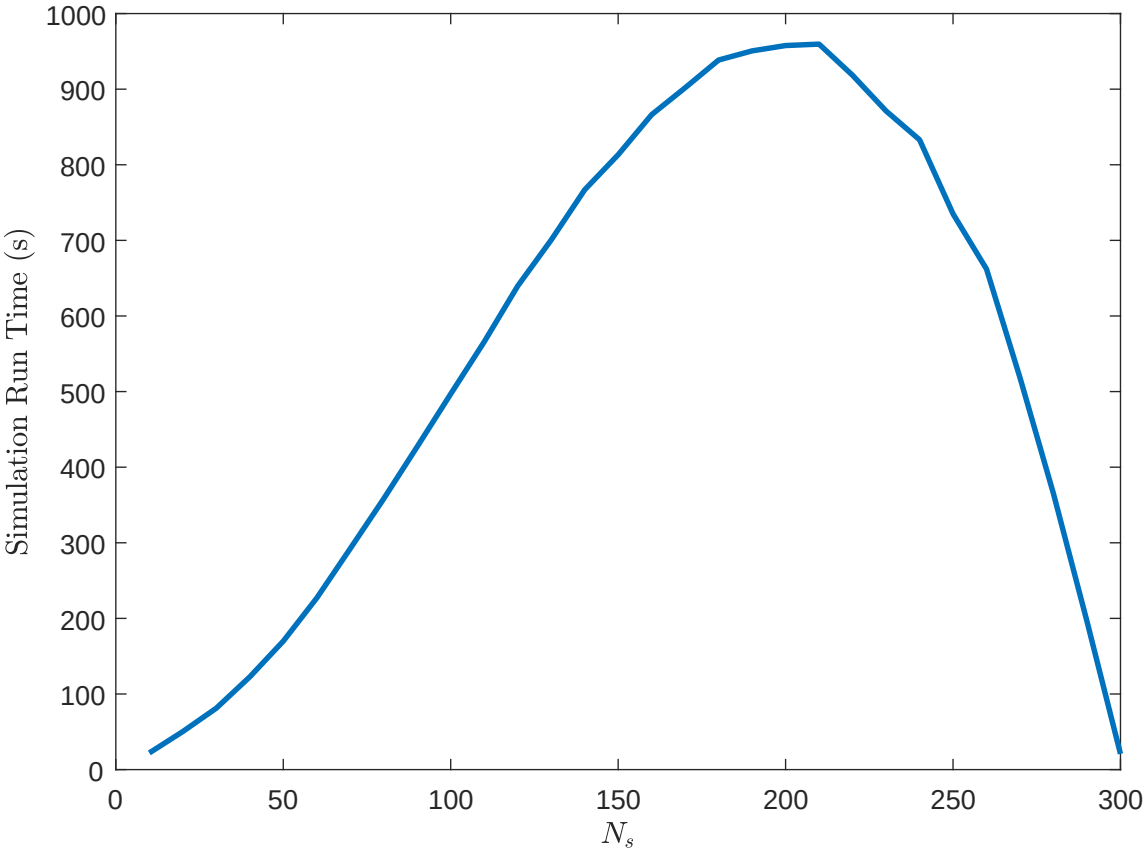

Figure 9.6: Total run time as a function of N_s for a 10 s simulation.

CHAPTER 10

CONCLUSIONS

The recent interest in the space servicing field to extend the lifetime of orbiting spacecraft has led to a flurry of academic, governmental, and private research into the topic, ranging from highly applied to deeply theoretical work. This dissertation has focused on the use of dual quaternions as a tool to model the different phases of a robotic servicing mission in space. In Chapter 1, we provided a thorough description of the existing literature. The areas of interest for this literature survey spanned the areas of 6-DOF control for orbiting spacecraft, and the modelling of robotic manipulators in space. In both cases, special emphasis was placed on the use of dual quaternions as the tool of choice for pose representations. We observed that besides formulations of dynamics that used the dual quaternion components as generalized coordinates, the use of dual quaternions in multibody dynamics was particularly scarce.

In Chapter 2 a formal introduction to dual quaternions and their relevance in the realm of mathematics was formulated, paying particular attention to their use as a tool to study rigid body mechanics. This implied the appropriate characterization of pose transformations and other important quantities such as velocities, accelerations, and wrenches. In Chapter 2 we also summarized some of the most important characteristics of dual quaternions in terms of rigid body motion in terms of the computation of important physical quantities, such as linear and angular momentum, as well kinetic energy. We also aimed at closing gaps that existing works did not address or captured incorrectly.

In Chapter 3 we provide common tools that exist in the literature regarding dual quaternions for many different applications, and steer them towards robotic manipulation in space. In particular, we compile results regarding the Plücker coordinates for dual lines, the product of exponentials, DH parameters, and convexity of common constraints. More

importantly, we provide elementary examples of how to use dual quaternions to derive kinematics for simple robotic chains in 2D.

The main technical contributions in this thesis, however, span four large fields of research: pose-control of a 6-DOF body, multibody dynamics, end-effector control in a multibody system, and estimation.

The first field of research explored in this dissertation is reference pose tracking for a satellite using adaptive control techniques. Chapter 4 builds upon an existing pose-tracking controller and incorporates the concurrent learning framework into the adaptation scheme. Two different controllers were introduced. The first one used the newly proposed continuous-time concurrent learning, which computes the regressor matrices as integrals. The second one used the more conventional formulation of concurrent learning, which introduces the data through a sum of regressor matrices built from stored data. In Chapter 4 we demonstrated that both controllers provides increased parameter convergence capabilities when compared to the baseline controller. In particular, an example is given with a reference that is (highly) not persistently exciting. In each case, the controllers are able to track the reference, but the introduction of concurrent learning enhances the estimation of parameters, even for cases when the reference might not be persistently exciting from the classical point of view. In Chapter 4 we also provide a direct link between the rank condition that arises in concurrent learning, and the persistency of excitation conditions. It was shown that these two concepts belong to the same family of positive-definiteness requirements, but that the concurrent learning will perform at least as well as the baseline controller that has no concurrent learning.

The next large area of focus for this dissertation was multibody dynamics Chapter 5. In Chapter 5 we chose a single-arm configuration with three revolute joints. The dynamics for this architecture were derived using the Newton-Euler approach using a formulation that treats the rotational equations separately from the translational equations, and a formulation that considers these in a coupled manner - the dual quaternion formulation. While the

dual quaternion formulation only provides similar numerical performance to the decoupled formulation, its simplicity of implementation was an important factor in deciding whether to pursue this direction of research and explore it further.

Thus, in Chapter 6 the equations were generalized to spacecraft that have a rooted-tree architecture. The dual nature of quaternions in dealing with translation and rotation in one single pose-transformation entity allowed minute changes in the equations to incorporate drastically different types of joints. In fact, five different types of joints were modeled: R, P, S, C and U. Additionally, another important advantage that this method possesses over other commonly used multibody dynamics frameworks is the fact that the analytical equations are straightforward to write, thus avoiding the need for iterative methods which are common in multibody dynamics. Even the most obvious downside to this method, the fact the number of equations grows faster than the number of degrees of freedom, has an upside: the method allows for simple calculation of the reaction wrenches at the joints, which are essential for sizing of the mechanical components during the design phases of a mission.

In Chapter 6 we also introduced the ability to lock - or prescribe - the motion of a degree of a given link. From the framework, the ability to compute the required actuation wrench by the joint to achieve the prescribed motion falls out naturally. In Chapter 7 the straightforward nature of the generalization of the multibody dynamics was put to use with a large, 11-body, two-arm spacecraft with three different types of joints: R, P, and S.

In Chapter 8 the problem of controlling the pose of the end-effector of a given manipulator is studied. The architecture of choice was the one developed in Chapter 5. In Chapter 8 both stabilization and tracking of the end-effector are addressed using the Differential Dynamic Programming framework. The framework is based on optimal control theory and allows penalizing states, which aids in achieving the desired motion, and control effort. The latter is of particular importance since control laws of spacecraft-mounted manipulators that allow actuation of the base tend to either require a fixed attitude or position

of the base, or tend to require strict zero initial linear and angular momentum conditions, which the proposed framework does not impose.

Finally, the developed dual quaternion framework is used to address the task of estimating the inertia properties of the links of a spacecraft manipulator in Chapter 9. In particular, the spacecraft model used was the one developed in Chapter 7, which consists of 11 rigid bodies and 77 parameters to be identified. In this case, the concurrent learning framework was used as an estimation tool. In particular, we observed that by multiplying the update law for the adaptive estimator by a particular gain, we could achieve "aggressive estimation" with as little as 10 stored data points, in only 10 seconds of simulation time.

10.1 Future Work

The scope of this dissertation was bounded by the following assumptions:

1) **Theoretical work**: even though this type of work ties in directly with experimental and applied work, the scope of this dissertation is of a theoretical nature, which aimed at exploring the use of dual quaternions as a tool to model all phases of a space servicing mission.

2) **Serial manipulators**: the work focused specifically on serial manipulators. This assumption allows for the existence of two or more arms, which in fact is explicitly addressed in Chapter 6. However, configuration topologies with loops were considered out of scope during this research.

3) **Rigid body assumption**: this work did not consider dynamics introduced by structural flexibility, restricting the domain of the work to rigid body dynamics and highly simplified joint models. Mechanical flexibility, particularly in space, can introduce instabilities. However, the emphasis of the work focused on the plausibility of the use of dual quaternions to model multibody systems.

Next, we propose and discuss relevant future directions of research that naturally arise from the work presented in this dissertation.

1) The work contained in this thesis is theoretical in nature. In cases where feedback was used as part of a control formulation, it was assumed that this full-state feedback was noise-free. Naturally, noise will impact performance. For example, measurement and actuation noise will affect the convergence characteristics of the estimation component of the control law presented in Chapter 4. An appropriate next step is to lift the noise-free assumption and evaluate the performance of each of the different control components proposed in this dissertation.

2) One of the main elements of this thesis is the derivation of the equations of motion for rigid multibody systems using dual quaternion algebra. This work was developed with the field of space-servicing in mind. In space, capturing flexible modes is of utmost importance, which the proposed theory neglects.

3) It is well known that Newton-Euler formulations of dynamics are not minimal to determine the time-evolution of the system, even though they can easily provide information such as reaction forces and torques. For mission design purposes, or to implement computationally costly algorithms, faster simulations might require a minimal representation of the dynamics such as those arrived at from Lagrangean mechanics, or equations arising from Kane's method. An interesting avenue of research would be to develop the equations of motion using Kane's approach within the dual algebra framework to avoid decoupling the rotational and translational dynamics. An appropriate reference to take as a starting point is [96], which uses Kane's method for the modeling of spacecraft-mounted robotic systems.

4) Current research in space servicing focuses on proposing different strategies for, and characterizing, the grappling stage. This dissertation excludes dealing with actual gripping of the end-effector to grab an orbiting satellite. In particular, different

impedance controllers exist to address the problem. It might be interesting to incorporate such a controller into a dual quaternion framework, which would be particularly well suited for screw-type motions. As far as the author is aware, this type of controller has not been addressed in dual quaternion algebra.

5) The topic of contact dynamics is a hard problem to address theoretically and to implement in software in a computationally efficient manner. In the spirit of this dissertation, studying ways to efficiently model contact between a spacecraft mounted robotic arm and external surfaces to test for collisions in dual quaternions might be of interest. However, reliable software packages that can model contact dynamics efficiently already exist, such as MuJoCo [152] or SD/FAST [111].

6) One of the main advantages of the DDP-based tracking controller presented in this dissertation is the ability to minimize, in an energy sense, the amount of control effort used. This includes the force applied on the base, which is directly related to the amount of fuel consumed. The ideal metric for fuel minimization is an $\mathcal{L}_1$ problem formulation. We believe it would be valuable to derive an analytical mixed $\mathcal{L}_1 - \mathcal{L}_2$ solution to implement the maneuvers proposed herein.

7) In the cost function used for DDP, a subtraction-based dual quaternion error was used. A better characterization of the error is one based on dual quaternion algebra. Exploring a cost function which is quadratic in $\boldsymbol{q}^*(\boldsymbol{q}^{\mathsf{s}} - \mathbf{1}^{\mathsf{s}})$, or some other form of dual quaternion error such as $\boldsymbol{q}^*_{\mathrm{D/I}}\boldsymbol{q}_{\mathrm{B/D}}$, might provide some numerical advantages that were not exploited in this work.

8) The literature in estimation involving robotic systems is vast. However, it would be valuable to append to the DQ-MEKF proposed in [130, 60, 50] the proposed dual quaternion dynamics model to improve the estimation performance of the end-effector state. This could be combined with vision-based methods that are currently in use to perform relative pose estimation during servicing of grappling.

9) The estimation approach used in Chapter 9 requires precise knowledge of all geometric properties of the satellite-mounted robotic arm. However, mechanical uncertainties will always exist or arise due to, for instance, thermal cycling. It might be an interesting research avenue to determine if the provided estimation framework has any sort of robustness properties with respect to these geometric issues.

10) The summation quantity used in concurrent learning $\sum_{i=1}^{N_s} R_k^{\mathrm{T}} R_k$ possesses information similar to what the Fisher Information matrix might contain in the case of a noisy system. Such a connection would be interesting to study.

11) The formulation of dynamics proposed in this dissertation was independently verified against a "decoupled" formulation. This only provides one sample point. It would be a great exercise to implement the one-arm configuration in different multi-body dynamics engines to paint a clearer picture of the performance of the proposed algorithm. Some of the metrics for the comparison could be: total run time, lines of code, and conservation of physical quantities, such as the center of mass location, angular momentum, and linear momentum, in the case when only internal torques and forces are applied.

12) Highly realistic environments exist that use photorealistic effects such as ray tracing for self-shadowing effects, etc. While Simulink's Simscape toolbox is fast and reliable, it is limited to the blocks provided by Mathworks for the mechanical components, joint motion, frame motion visualization, etc. Open-source software might provide an efficient, flexible visualization engine that allows high-quality video generation.

APPENDIX A
EXPANSION OF TRANSLATIONAL CONSTRAINT ENCODED IN DUAL QUATERNION FOR JOINT 0

The approach by which the kinematic joint constraint was derived in dual quaternion algebra is fundamentally different from the way the constraint was derived in the decoupled formulation. For the dual quaternion formulation, the kinematic constraint is determined by computing the distal body's acceleration as the combined effect of the proximal body's acceleration and the joint generalized acceleration. For the decoupled formulation, the constraint is derived by the physical premise that for a revolute joint, the linear accelerations of the two bodies connected to the joint must match exactly at the joint.

Since translational components are usually obscured in the dual part of a dual quaternion relationship, this appendix aims to provide an explicit expression for the translational information encoded by the kinematic acceleration relationship. It is worth emphasizing that this relationship is still to be premultiplied by $\boldsymbol{E}_{145}$ for a revolute joint, or Λ_i for the general joint when using the notation from the generalized framework for dynamics using dual quaternions, for incorporation into the framework as a constraint relationship.

A.1 Derivation

From the constraint equation derived in dual quaternions for joint 0, equation (5.94), we have that

$$\boldsymbol{q}_{\mathfrak{o}_1/0}\dot{\boldsymbol{\omega}}^{\mathfrak{o}_1}_{\mathfrak{o}_1/\mathrm{I}}\boldsymbol{q}^{*}_{\mathfrak{o}_1/0} = \dot{\boldsymbol{\omega}}^{0}_{0/\mathfrak{o}_0} + \boldsymbol{q}^{*}_{0/\mathfrak{o}_0}\left(\dot{\boldsymbol{\omega}}^{\mathfrak{o}_0}_{\mathfrak{o}_0/\mathrm{I}} + \boldsymbol{\omega}^{\mathfrak{o}_0}_{\mathfrak{o}_0/\mathrm{I}} \times \boldsymbol{\omega}^{\mathfrak{o}_0}_{0/\mathfrak{o}_0}\right)\boldsymbol{q}_{0/\mathfrak{o}_0}. \tag{A.1}$$

Expanding each of the dual elements in this equation yields

$$\begin{aligned}
&(q_{\mathfrak{s}_1/0} + \epsilon\tfrac{1}{2} r^0_{\mathfrak{s}_1/0} q_{\mathfrak{s}_1/0})(\dot{\omega}^{\mathfrak{s}_1}_{\mathfrak{s}_1/\mathrm{I}} + \epsilon \dot{v}^{\mathfrak{s}_1}_{\mathfrak{s}_1/\mathrm{I}})(q_{\mathfrak{s}_1/0} + \epsilon\tfrac{1}{2} r^0_{\mathfrak{s}_1/0} q_{\mathfrak{s}_1/0})^* = \dot{\omega}^0_{0/\mathfrak{s}_0} + \epsilon \dot{v}^0_{0/\mathfrak{s}_0} \\
&+(q_{0/\mathfrak{s}_0} + \epsilon\tfrac{1}{2} q_{0/\mathfrak{s}_0} r^0_{0/\mathfrak{s}_0})^* \left((\dot{\omega}^{\mathfrak{s}_0}_{\mathfrak{s}_0/\mathrm{I}} + \epsilon \dot{v}^{\mathfrak{s}_0}_{\mathfrak{s}_0/\mathrm{I}}) + (\omega^{\mathfrak{s}_0}_{\mathfrak{s}_0/\mathrm{I}} + \epsilon v^{\mathfrak{s}_0}_{\mathfrak{s}_0/\mathrm{I}}) \times (\omega^{\mathfrak{s}_0}_{0/\mathfrak{s}_0} + \epsilon(v^{\mathfrak{s}_0}_{0/\mathfrak{s}_0} + \omega^{\mathfrak{s}_0}_{0/\mathfrak{s}_0} \times r^{\mathfrak{s}_0}_{\mathfrak{s}_0/0})) \right) \\
&\quad (q_{0/\mathfrak{s}_0} + \epsilon\tfrac{1}{2} q_{0/\mathfrak{s}_0} r^0_{0/\mathfrak{s}_0}).
\end{aligned} \tag{A.2}$$

Applying the result of equation (2.42) to the left hand side yields

$$\begin{aligned}
&\dot{\omega}^0_{\mathfrak{s}_1/\mathrm{I}} + \epsilon(\dot{v}^0_{\mathfrak{s}_1/\mathrm{I}} + r^0_{\mathfrak{s}_1/0} \times \dot{\omega}^0_{\mathfrak{s}_1/\mathrm{I}}) = \dot{\omega}^0_{0/\mathfrak{s}_0} + \epsilon \dot{v}^0_{0/\mathfrak{s}_0} \\
&+(q_{0/\mathfrak{s}_0} + \epsilon\tfrac{1}{2} q_{0/\mathfrak{s}_0} r^0_{0/\mathfrak{s}_0})^* \left(\dot{\omega}^{\mathfrak{s}_0}_{\mathfrak{s}_0/\mathrm{I}} + \epsilon \dot{v}^{\mathfrak{s}_0}_{\mathfrak{s}_0/\mathrm{I}} \right) (q_{0/\mathfrak{s}_0} + \epsilon\tfrac{1}{2} q_{0/\mathfrak{s}_0} r^0_{0/\mathfrak{s}_0}) \\
&+(q_{0/\mathfrak{s}_0} + \epsilon\tfrac{1}{2} q_{0/\mathfrak{s}_0} r^0_{0/\mathfrak{s}_0})^* \left((\omega^{\mathfrak{s}_0}_{\mathfrak{s}_0/\mathrm{I}} + \epsilon v^{\mathfrak{s}_0}_{\mathfrak{s}_0/\mathrm{I}}) \times (\omega^{\mathfrak{s}_0}_{0/\mathfrak{s}_0} + \epsilon(v^{\mathfrak{s}_0}_{0/\mathfrak{s}_0} + \omega^{\mathfrak{s}_0}_{0/\mathfrak{s}_0} \times r^{\mathfrak{s}_0}_{\mathfrak{s}_0/0})) \right) (q_{0/\mathfrak{s}_0} + \epsilon\tfrac{1}{2} q_{0/\mathfrak{s}_0} r^0_{0/\mathfrak{s}_0}).
\end{aligned} \tag{A.3}$$

Applying the result of equation (2.41) to the third term of the right hand side and expanding the dual cross product that arises in the last term simplifies the equation to:

$$\begin{aligned}
&\dot{\omega}^0_{\mathfrak{s}_1/\mathrm{I}} + \epsilon(\dot{v}^0_{\mathfrak{s}_1/\mathrm{I}} + r^0_{\mathfrak{s}_1/0} \times \dot{\omega}^0_{\mathfrak{s}_1/\mathrm{I}}) = \dot{\omega}^0_{0/\mathfrak{s}_0} + \epsilon \dot{v}^0_{0/\mathfrak{s}_0} + \dot{\omega}^0_{\mathfrak{s}_0/\mathrm{I}} + \epsilon(\dot{v}^0_{\mathfrak{s}_0/\mathrm{I}} + r^0_{\mathfrak{s}_0/0} \times \dot{\omega}^0_{\mathfrak{s}_0/\mathrm{I}}) \\
&+(q_{0/\mathfrak{s}_0} + \epsilon\tfrac{1}{2} q_{0/\mathfrak{s}_0} r^0_{0/\mathfrak{s}_0})^* \left(\omega^{\mathfrak{s}_0}_{\mathfrak{s}_0/\mathrm{I}} \times \omega^{\mathfrak{s}_0}_{0/\mathfrak{s}_0} + \epsilon(v^{\mathfrak{s}_0}_{\mathfrak{s}_0/\mathrm{I}} \times \omega^{\mathfrak{s}_0}_{0/\mathfrak{s}_0} + \omega^{\mathfrak{s}_0}_{\mathfrak{s}_0/\mathrm{I}} \times (v^{\mathfrak{s}_0}_{0/\mathfrak{s}_0} + \omega^{\mathfrak{s}_0}_{0/\mathfrak{s}_0} \times r^{\mathfrak{s}_0}_{\mathfrak{s}_0/0})) \right) \\
&\quad (q_{0/\mathfrak{s}_0} + \epsilon\tfrac{1}{2} q_{0/\mathfrak{s}_0} r^0_{0/\mathfrak{s}_0}).
\end{aligned} \tag{A.4}$$

Now, for the sake of simplicity in our next step, we multiply out the cross product inside the dual part of the last term:

$$\begin{aligned}
&\dot{\omega}^0_{\mathfrak{s}_1/\mathrm{I}} + \epsilon(\dot{v}^0_{\mathfrak{s}_1/\mathrm{I}} + r^0_{\mathfrak{s}_1/0} \times \dot{\omega}^0_{\mathfrak{s}_1/\mathrm{I}}) = \dot{\omega}^0_{0/\mathfrak{s}_0} + \epsilon \dot{v}^0_{0/\mathfrak{s}_0} + \dot{\omega}^0_{\mathfrak{s}_0/\mathrm{I}} + \epsilon(\dot{v}^0_{\mathfrak{s}_0/\mathrm{I}} + r^0_{\mathfrak{s}_0/0} \times \dot{\omega}^0_{\mathfrak{s}_0/\mathrm{I}}) \\
&+(q_{0/\mathfrak{s}_0} + \epsilon\tfrac{1}{2} q_{0/\mathfrak{s}_0} r^0_{0/\mathfrak{s}_0})^* \left(\omega^{\mathfrak{s}_0}_{\mathfrak{s}_0/\mathrm{I}} \times \omega^{\mathfrak{s}_0}_{0/\mathfrak{s}_0} + \epsilon(v^{\mathfrak{s}_0}_{\mathfrak{s}_0/\mathrm{I}} \times \omega^{\mathfrak{s}_0}_{0/\mathfrak{s}_0} + \omega^{\mathfrak{s}_0}_{\mathfrak{s}_0/\mathrm{I}} \times v^{\mathfrak{s}_0}_{0/\mathfrak{s}_0} + \omega^{\mathfrak{s}_0}_{\mathfrak{s}_0/\mathrm{I}} \times (\omega^{\mathfrak{s}_0}_{0/\mathfrak{s}_0} \times r^{\mathfrak{s}_0}_{\mathfrak{s}_0/0})) \right) \\
&\quad (q_{0/\mathfrak{s}_0} + \epsilon\tfrac{1}{2} q_{0/\mathfrak{s}_0} r^0_{0/\mathfrak{s}_0}).
\end{aligned} \tag{A.5}$$

Finally, we apply equation (2.41) to the last term, yielding our final expression:

$$\dot{\omega}^0_{\mathfrak{s}_1/\mathrm{I}} + \epsilon(\dot{v}^0_{\mathfrak{s}_1/\mathrm{I}} + r^0_{\mathfrak{s}_1/0} \times \dot{\omega}^0_{\mathfrak{s}_1/\mathrm{I}}) = \dot{\omega}^0_{0/\mathfrak{s}_0} + \epsilon\dot{v}^0_{0/\mathfrak{s}_0} + \dot{\omega}^0_{\mathfrak{s}_0/\mathrm{I}} + \epsilon(\dot{v}^0_{\mathfrak{s}_0/\mathrm{I}} + r^0_{\mathfrak{s}_0/0} \times \dot{\omega}^0_{\mathfrak{s}_0/\mathrm{I}})$$
$$+\omega^0_{\mathfrak{s}_0/\mathrm{I}} \times \omega^0_{0/\mathfrak{s}_0} + \epsilon(v^0_{\mathfrak{s}_0/\mathrm{I}} \times \omega^0_{0/\mathfrak{s}_0} + \omega^0_{\mathfrak{s}_0/\mathrm{I}} \times v^0_{0/\mathfrak{s}_0} + \omega^0_{\mathfrak{s}_0/\mathrm{I}} \times (\omega^0_{0/\mathfrak{s}_0} \times r^0_{\mathfrak{s}_0/0}) + r^0_{\mathfrak{s}_0/0} \times (\omega^0_{\mathfrak{s}_0/\mathrm{I}} \times \omega^0_{0/\mathfrak{s}_0})) \tag{A.6}$$

We can now extract the rotational and translational components. The real part, which represent the rotational component, yields

$$\dot{\omega}^0_{\mathfrak{s}_1/\mathrm{I}} = \dot{\omega}^0_{0/\mathfrak{s}_0} + \dot{\omega}^0_{\mathfrak{s}_0/\mathrm{I}} + \omega^0_{\mathfrak{s}_0/\mathrm{I}} \times \omega^0_{0/\mathfrak{s}_0}, \tag{A.7}$$

while the dual part, which contains the translational component of the constraint equation, yields

$$\dot{v}^0_{\mathfrak{s}_1/\mathrm{I}} + r^0_{\mathfrak{s}_1/0} \times \dot{\omega}^0_{\mathfrak{s}_1/\mathrm{I}} = \dot{v}^0_{0/\mathfrak{s}_0} + \dot{v}^0_{\mathfrak{s}_0/\mathrm{I}} + r^0_{\mathfrak{s}_0/0} \times \dot{\omega}^0_{\mathfrak{s}_0/\mathrm{I}}$$
$$+v^0_{\mathfrak{s}_0/\mathrm{I}} \times \omega^0_{0/\mathfrak{s}_0} + \omega^0_{\mathfrak{s}_0/\mathrm{I}} \times v^0_{0/\mathfrak{s}_0} + \omega^0_{\mathfrak{s}_0/\mathrm{I}} \times (\omega^0_{0/\mathfrak{s}_0} \times r^0_{\mathfrak{s}_0/0}) + r^0_{\mathfrak{s}_0/0} \times (\omega^0_{\mathfrak{s}_0/\mathrm{I}} \times \omega^0_{0/\mathfrak{s}_0}). \tag{A.8}$$

REFERENCES

[1] D. L. Akin. (Jan. 2014). Innovative robotic systems for in-space operations. Future In-Space Operations (FISO) Colloquium, Space Systems Laboratory, University of Maryland.

[2] B. B. Reed. (Aug. 2011). Robotic refueling mission overview. Future In-Space Operations (FISO) Colloquium, NASA Goddard Space Flight Center.

[3] A. Ellery, C. Welch, and A. Curley, "A proposed public-private partnership for the funding of robotic in-orbit servicers," in *Space 2002 and Robotics 2002*, Albuquerque, New Mexico, United States, 2002.

[4] Y. Xu and H.-Y. Shum, "Dynamic control of a space robot system with no thrust jets controlled base," Robotics Institute, Pittsburgh, PA, Tech. Rep. CMU-RI-TR-91-33, 1991.

[5] "On-orbit satellite servicing study, project report," National Aeronautics and Space Administration, Goddard Space Flight Center, Tech. Rep., 2010.

[6] D. Akin, M. L. Misky, E. Thiel, and C. Kurtzman, "Space applications of automation, robotics and machine intelligence systems (ARAMIS), phase 2. volume 1: Telepresence technology base development," Massachusetts Institute of Technology, Cambridge, Massachusetts, United States, Tech. Rep. 19840002515, 1983, NASA Contract.

[7] M. Oda, "Space robot experiments on NASDA's ETS-VII satellite - preliminary overview of the experiment results," in *Proceedings 1999 IEEE International Conference on Robotics and Automation*, vol. 2, Detroit, Michigan, United States, May 1999, 1390–1395 vol.2.

[8] M. Oda, "ETS-VII: Achievements, troubles and future," in *Proceedings of the 6th International Symposium on Artificial Intelligence and Robotics & Automation in Space (i-SAIRAS)*, Canadian Space Agency, St.-Hubert, Quebec, Canada, Jun. 2001.

[9] A. Ogilvie, J. Allport, M. Hannah, and J. Lymer, "Autonomous satellite servicing using the orbital express demonstration manipulator system," in *Proceedings of the Ninth International Symposium on Artificial Intelligence Robotics and Automation in Space, iSAIRAS*, Los Angeles, U.S.A., 2008.

[10] K. Yoshida, "Achievements in space robotics," *IEEE Robotics & Automation Magazine*, vol. 16, no. 4, pp. 20–28, 2009.

[11] C. G. Henshaw. (Jul. 2009). NRL robotics overview. Future In-Space Operations (FISO) Colloquium, Naval Research Laboratory.

[12] G. Roesler. (Jun. 2016). Robotic servicing of geosynchronous satellites (RSGS) program overview. Future In-Space Operations (FISO) Colloquium, DARPA.

[13] B. B. Reed. (Jan. 2017). NASA satellite servicing evolution. Future In-Space Operations (FISO) Colloquium, NASA Goddard Space Flight Center.

[14] B. B. Reed, R. C. Smith, B. J. Naasz, J. F. Pellegrino, and C. E. Bacon, "The Restore-L servicing mission," in *AIAA SPACE Forum*, Long Beach, California, 2016.

[15] D. Dimitrov, "Dynamics and control of space manipulators during a satellite capturing operation," PhD thesis, Tohoku University, Feb. 2005.

[16] S. Xu, H. Wang, D. Zhang, and B. Yang, "Extended jacobian based adaptive zero reaction motion control for free-floating space manipulators," in *Proceedings of the 33rd Chinese Control Conference*, Nanjing, China, 2014.

[17] V. Dubanchet, D. Saussié, D. Alazard, C. Bérard, and C. L. Peuvédic, "Modeling and control of a space robot for active debris removal," *CEAS Space Journal*, vol. 7, no. 2, pp. 203–218, 2015.

[18] J. R. Brophy, L. Friedman, and F. Culick. (May 2012). Asteroid retrieval mission feasibility study. Future In-Space Operations (FISO) Colloquium, Jet Propulsion Laboratory, The Planetary Society, and California Institute of Technology.

[19] N. Strange, D. Landau, T. McElrath, G. Lantoine, T. Lam, M. McGuire, L. Burke, M. Martini, and J. Dankanich, "Overview of mission design for NASA asteroid redirect robotic mission concept," in *33rd International Electric Propulsion Conference*, Washington, D.C., 2013.

[20] R. W. Longman, R. E. Lindbergt, and M. F. Zedd, "Satellite-mounted robot manipulators - new kinematics and reaction moment compensation," *The International Journal of Robotics Research*, vol. 6, no. 3, pp. 87–103, 1987.

[21] Z. Vafa and S. Dubowsky, "On the dynamics of manipulators in space using the virtual manipulator approach," in *Proceedings 1987 IEEE International Conference on Robotics and Automation*, 1987.

[22] Y. Masutani, F. Miyazaki, and S. Arimoto, "Modeling and sensory feedback control for space manipulators," in *Proceedings of the NASA Conference on Space Telerobotics*, 1989, pp. 287 –296.

[23] J. R. Dooley and J. M. McCarthy, "On the geometric analysis of optimum trajectories for cooperating robots using dual quaternion coordinates," in *Proceedings 1993 IEEE International Conference on Robotics and Automation*, vol. 1, Atlanta, Georgia, 1993, pp. 1031–1036.

[24] K. Daniilidis, "Hand-eye calibration using dual quaternions," *The International Journal of Robotics Research*, vol. 18, no. 3, pp. 286–298, 1999.

[25] A. Perez, "Dual quaternion synthesis of constrained robotic systems," PhD thesis, Department of Mechanical and Aerospace Engineering, University of California, Irvine, 2003.

[26] A. Perez and J. McCarthy, "Dual quaternion synthesis of constrained robotic systems," *Journal of Mechanical Design*, vol. 126, no. 3, pp. 425–435, 2004.

[27] Y. Aydin and S. Kucuk, "Quaternion based inverse kinematics for industrial robot manipulators with Euler wrist," in *2006 IEEE International Conference on Mechatronics*, Budapest, Hungary, 2006, pp. 581 –586.

[28] D. Gan, Q. Liao, S. Wei, J. Dai, and S. Qiao, "Dual quaternion-based inverse kinematics of the general spatial 7R mechanism," *Proceedings of the Institution of Mechanical Engineers, Part C: Journal of Mechanical Engineering Science*, vol. 222, no. 8, pp. 1593–1598, 2008.

[29] X. Wang, D. Han, C. Yu, and Z. Zheng, "The geometric structure of unit dual quaternion with application in kinematic control," *Journal of Mathematical Analysis and Applications*, vol. 389, no. 2, pp. 1352–1364, 2012.

[30] G. Leclercq, P. Lefèvre, and G. Blohm, "3-D kinematics using dual quaternions: Theory and applications in neuroscience," *Frontiers in Behavioral Neuroscience*, vol. 7, no. 7, pp. 1–7, 2013.

[31] L. A. Radavelli, E. R. De Pieri, D. Martins, and R. Simoni, "Points, lines, screws and planes in dual quaternions kinematics," in *Advances in Robot Kinematics*, J. Lenarcic and O. Khatib, Eds., Springer, 2014, pp. 285–293.

[32] M. D.P. A. Fonseca and B. V. Adorno, "Whole-body modeling and hierarchical control of a humanoid robot based on dual quaternion algebra," in *2016 XIII Latin American Robotics Symposium and IV Brazilian Robotics Symposium (LARS/SBR)*, 2016, pp. 103–108.

[33] M. Ulrich and C. Steger, "Hand-eye calibration of SCARA robots using dual quaternions," *Pattern Recognition and Image Analysis*, vol. 26, no. 1, pp. 231–239, 2016.

[34] J. Cheng, J. Kim, Z. Jiang, and W. Che, "Dual quaternion-based graphical SLAM," *Robotics and Autonomous Systems*, vol. 77, no. C, pp. 15–24, 2016.

[35] F. E. Udwadia and A. D. Schutte, "An alternative derivation of the quaternion equations of motion for rigid-body rotational dynamics," *Journal of Applied Mechanics*, vol. 77, no. 4, pp. 044 505–1 –044505–4, 2010.

[36] F. E. Udwadia and R. E. Kalaba, "A new perspective on constrained motion," *Proceedings: Mathematical and Physical Sciences*, vol. 439, no. 1906, pp. 407–410, 1992.

[37] J. Dooley and J. McCarthy, "Spatial rigid body dynamics using dual quaternion components," in *Proceedings 1991 IEEE International Conference on Robotics and Automation*, Sacramento, California, 1991, pp. 90–95.

[38] V. Brodsky and M. Shoham, "Dual numbers representation of rigid body dynamics," *Mechanism and Machine Theory*, vol. 34, no. 5, pp. 693–718, 1999, Erratum for this paper has been published.

[39] J. Wang and Z. Sun, "6–DOF robust adaptive terminal sliding mode control for spacecraft formation flying," *Acta Astronautica*, vol. 73, pp. 76 –87, 2012.

[40] J.-Y. Wang, H.-Z. Liang, Z.-W. Sun, S.-N. Wu, and S.-J. Zhang, "Relative motion coupled control based on dual quaternion," *Aerospace Science and Technology*, vol. 25, no. 1, pp. 102 –113, 2013.

[41] Y. Wu, X. Hu, D. Hu, T. Li, and J. Lian, "Strapdown inertial navigation system algorithms based on dual quaternions," *IEEE Transactions on Aerospace and Electronic Systems*, vol. 41, no. 1, pp. 110–132, 2005.

[42] D. Han, Q. Wei, and Z. Li, "A dual-quaternion method for control of spatial rigid body," in *2008 IEEE International Conference on Networking, Sensing and Control*, Sanya, China, 2008, pp. 1 –6.

[43] X. Wang and C. Yu, "Unit-dual-quaternion-based PID control scheme for rigid-body transformation," in *Proceedings of the 18th IFAC World Congress*, Milan, Italy, 2011.

[44] J. Wang, H. Liang, Z. Sun, S. Zhang, and M. Liu, "Finite-time control for spacecraft formation with dual-number-based description," *Journal of Guidance, Control, and Dynamics*, vol. 35, no. 3, pp. 950–962, May 2012.

[45] N. Filipe and P. Tsiotras, "Rigid body motion tracking without linear and angular velocity feedback using dual quaternions," in *European Control Conference*, Zürich, Switzerland, 2013, pp. 329–334.

[46] ——, "Adaptive model-independent tracking of rigid body position and attitude motion with mass and inertia matrix identification using dual quaternions," in *AIAA Guidance, Navigation, and Control Conference*, ser. AIAA 2013-5173, Boston, MA, 2013.

[47] ——, "Adaptive position and attitude-tracking controller for satellite proximity operations using dual quaternions," *Journal of Guidance, Control, and Dynamics*, vol. 38, pp. 566–577, 2014.

[48] N. Filipe, A. Valverde, and P. Tsiotras, "Pose tracking without linear and angular-velocity feedback using dual quaternions," *IEEE Transactions on Aerospace and Electronic Systems*, vol. 52, no. 1, pp. 411–422, 2016.

[49] D. Seo, "Fast adaptive pose tracking control for satellites via dual quaternion upon non-certainty equivalence principle," *Acta Astronautica*, vol. 115, pp. 32–39, 2015.

[50] N. Filipe, "Nonlinear pose control and estimation for space proximity operations: An approach based on dual quaternions," PhD thesis, Georgia Institute of Technology, 2014.

[51] U. Lee and M. Mesbahi, "Dual quaternions, rigid body mechanics, and powered-descent guidance," in *51st IEEE Conference on Decision and Control*, Maui, Hawaii, 2012, pp. 3386–3391.

[52] U. Lee and M. Mesbahi, "Dual quaternion based spacecraft rendezvous with rotational and translational field of view constraints," in *AIAA/AAS Astrodynamics Specialist Conference*, San Diego, CA, 2014.

[53] ——, "Optimal power descent guidance with 6-DoF line of sight constraints via unit dual quaternions," in *AIAA Guidance, Navigation, and Control Conference*, 2015.

[54] Y. Wang, F. Yu, and C. Yu, "Distributed translation and attitude synchronization for multiple rigid bodies using dual quaternions," in *Proceedings of the 2016 American Control Conference*, 2016.

[55] Y. Wang and C. Yu, "Distributed attitude and translation consensus for networked rigid bodies based on unit dual quaternion," *International Journal of Robust and Nonlinear Control*, 2017.

[56] Y. Wang and C. B. Yu, "Translation and attitude synchronization for multiple rigid bodies using dual quaternions," *Journal of the Franklin Institute*, vol. 354, no. 8, pp. 3594–3616, Mar. 2017.

[57] E. Bayro-Corrochano and Y. Zhang, "The motor extended Kalman filter: A geometric approach for rigid motion estimation," *Journal of Mathematical Imaging and Vision*, vol. 13, no. 3, pp. 205–228, 2000.

[58] Y. Zu, U. Lee, and R. Dai, "Distributed motion estimation of space objects using dual quaternions," in *AIAA/AAS Astrodynamics Specialist Conference*, San Diego, California, 2014.

[59] Y. Zu, C. Sun, and R. Dai, "Distributed estimation for spatial rigid motion based on dual quaternions," in *53rd IEEE Conference on Decision and Control*, Los Angeles, California, 2014.

[60] N. Filipe, M. Kontitsis, and P. Tsiotras, "Extended Kalman filter for spacecraft pose estimation using dual quaternions," *Journal of Guidance, Control, and Dynamics*, vol. 38, no. 9, pp. 1625 –1641, 2015.

[61] X. Hou, C. Ma, Z. Wang, and J. Yuan, "Adaptive pose and inertial parameters estimation of free-floating tumbling space objects using dual vector quaternions," *Advances in Mechanical Engineering*, vol. 9, no. 10, pp. 1–17, 2017.

[62] J. Yuan, X. Hou, C. Sun, and Y. Cheng, "Fault-tolerant pose and inertial parameters estimation of an uncooperative spacecraft based on dual vector quaternions," *Proceedings of the Institution of Mechanical Engineers, Part G: Journal of Aerospace Engineering*, pp. 1–20, 2018.

[63] H. T. Kussaba, L. F. Figueredo, J. Y. Ishihara, and B. V. Adorno, "Hybrid kinematic control for rigid body pose stabilization using dual quaternions," *Journal of the Franklin Institute*, vol. 354, no. 7, pp. 2769 –2787, 2017.

[64] B. P. Malladi, E. A. Butcher, and R. G. Sanfelice, "Robust hybrid global asymptotic stabilization of rigid body dynamics using dual quaternions," in *AIAA Guidance, Navigation, and Control Conference, AIAA SciTech Forum*, 2018.

[65] N. Filipe and P. Tsiotras, "Simultaneous position and attitude control without linear and angular velocity feedback using dual quaternions," in *Proceedings of the 2013 American Control Conference*, Washington, DC, 2013, pp. 4815–4820.

[66] W. W. Hooker, "A set of r dynamical attitude equations for an arbitrary n-Body satellite having r rotational degrees of freedom," *AIAA Journal*, vol. 8, no. 7, pp. 1205–1207, 1970.

[67] Z. Vafa and S. Dubowsky, "The kinematics and dynamics of space manipulators: The virtual manipulator approach," *The International Journal of Robotics Research*, vol. 9, no. 4, pp. 3–21, 1990.

[68] Z. Vafa and S. Dubowsky, "On the dynamics of space manipulators using the virtual manipulator, with applications to path planning," *Journal of Astronautical Sciences*, vol. 38, no. 4, pp. 441–472, 1990.

[69] Z. Vafa and S. Dubowsky, "On the dynamics of space manipulators using the virtual manipulator, with applications to path planning," in *Space Robotics: Dynamics and Control*, X. Yangsheng and T. Kanade, Eds., Springer, 1993, pp. 45 –76.

[70] R. Longman, "The kinetics and workspace of a robot mounted on a satellite that is free to rotate and translate," in *AIAA Guidance, Navigation and Control Conference*, Minneapolis, MN, 1988.

[71] Y. Umetani and K. Yoshida, "Resolved motion rate control of space manipulators with generalized jacobian matrix," *IEEE Transactions on Robotics and Automation*, vol. 5, no. 3, pp. 303–314, 1989.

[72] Y. Masutani, F. Miyazaki, and S. Arimoto, "Sensory feedback control for space manipulators," in *Proceedings 1989 IEEE International Conference on Robotics and Automation*, 1989.

[73] S. Dubowsky, E. E. Vance, and M. A. Torres, "The control of space manipulators subject to spacecraft attitude control saturation limits," in *Proceedings of the NASA Conference on Space Telerobotics*, vol. 4, Jan. 1989, pp. 409 –418.

[74] S. Dubowsky and M. A. Torres, "Path planning for space manipulators to minimize spacecraft attitude disturbances," in *Proceedings 1991 IEEE International Conference on Robotics and Automation*, Sacramento, California, United States, 1991.

[75] Y. Nakamura and R. Mukherjee, "Nonholonomic path planning of space robots," in *Proceedings 1989 IEEE International Conference on Robotics and Automation*, 1989.

[76] ——, "Nonholonomic path planning of space robots via a bidirectional approach," *IEEE Transactions on Robotics and Automation*, vol. 7, no. 4, pp. 500–514, 1991.

[77] H. West, E. Papadopoulos, S. Dubowsky, and H. Cheah, "A method for estimating the mass properties of a manipulator by measuring the reaction moments at its base," in *Proceedings 1989 IEEE International Conference on Robotics and Automation*, vol. 3, 1989, pp. 1510–1516.

[78] E. Papadopoulos and S. Dubowsky, "On the nature of control algorithms for space manipulators," in *Proceedings 1990 IEEE International Conference on Robotics and Automation*, vol. 2, Cincinnati, Ohio, USA, 1990, pp. 1101–1108.

[79] E. Papadopoulos and S. Dubowsky, "On the nature of control algorithms for free-floating space manipulators," *IEEE Transactions on Robotics and Automation*, vol. 7, no. 6, pp. 750 –758, 1991.

[80] E. Papadopoulos and S. Dubowsky, "Coordinated manipulator/spacecraft motion control for space robotic systems," in *Proceedings 1991 IEEE International Conference on Robotics and Automation*, Sacramento, California, United States, 1991, pp. 1696–1701.

[81] ——, "Dynamic singularities in free-floating space manipulators," *Journal of Dynamic Systems, Measurement, and Control*, vol. 115, no. 1, pp. 44–52, Mar. 1993.

[82] E. Papadopoulos, "On the dynamics and control of space manipulators," PhD thesis, Massachusetts Institute of Technology, 1991.

[83] J. R. Spofford and D. L. Akin, "Redundancy control of a free-flying telerobot," *Journal of Guidance, Control, and Dynamics*, vol. 13, no. 3, pp. 515–523, 1990.

[84] F. Caccavale and B. Siciliano, "Quaternion-based kinematic control of redundant spacecraft/manipulator systems," in *Proceedings 2001 IEEE International Conference on Robotics and Automation*, Seoul, Korea, 2001.

[85] K. Nanos and E. Papadopoulos, "On the use of free-floating space robots in the presence of angular momentum," *Intelligent Service Robotics*, vol. 4, no. 1, pp. 3–15, 2011.

[86] ——, "On the dynamics and control of free-floating space manipulator systems in the presence of angular momentum," *Frontiers in Robotics and AI*, vol. 4, 2017.

[87] ——, "On cartesian motions with singularities avoidance for free-floating space robots," in *Proceedings of the IEEE International Conference on Robotics and Automation*, May 2012, pp. 5398–5403.

[88] ——, "Avoiding dynamic singularities in cartesian motions of free-floating manipulators," *IEEE Transactions on Aerospace and Electronic Systems*, vol. 51, no. 3, pp. 2305–2318, Jul. 2015.

[89] Y. Xu, H.-Y. Shum, J.-J. Lee, and T. Kanade, "Adaptive control of space robot system with an attitude controlled base," Carnegie Mellon University, Pittsburgh, Pennsylvania, United States, research rep. CMU-RI-TR-91-14, Aug. 1991.

[90] Y. Xu, H.-Y. Shum, T. Kanade, and J.-J. Lee, "Parameterization and adaptive control of space robot systems," *IEEE Transactions on Aerospace and Electronic Systems*, vol. 30, no. 2, pp. 435–451, 1994.

[91] M. Walker and L.-B. Weel, "An adaptive control strategy for space based robot manipulators," in *Proceedings of the IEEE International Conference on Robotics and Automation*, Sacramento, California, United States, 1991.

[92] K. Yoshida, D. Dimitrov, and H. Nakanishi, "On the capture of tumbling satellite by a space robot," in *Proceedings of the 2006 IEEE/RSJ International Conference on Intelligent Robots and Systems*, Beijing, China, 2006.

[93] P.-C. Cong, Y. F. Lan, and Y. F. Zhang, "Adaptive control of dual-arm space manipulator capturing object," *Proceedings of the Institution of Mechanical Engineers, Part G: Journal of Aerospace Engineering*, vol. 227, no. 6, pp. 992–999, 2013.

[94] E. Stoneking, "Newton-Euler dynamic equations of motion for a multi-body spacecraft," in *AIAA Guidance, Navigation and Control Conference and Exhibit*, 2007.

[95] B. Bishop, R. Gargano, A. Sears, and M. Karpenko, "Rapid maneuvering of multibody dynamic systems with motion compensation," in *AIAA/AAS Astrodynamics Specialist Conference*, 2014, pp. 1–20.

[96] E. Stoneking, "Implementation of Kane's method for a spacecraft composed of multiple rigid bodies," in *AIAA Guidance, Navigation, and Control (GNC) Conference*, Boston, MA, U.S.A., 2013.

[97] C. R. Carignan and D. L. Akin, "The Reaction Stabilization of On-Orbit Robots," *IEEE Control Systems Magazine*, vol. 20, no. 6, pp. 19–33, Dec. 2000.

[98] A. Jain, "Unified formulation of dynamics for serial rigid multibody systems," *Journal of Guidance, Control, and Dynamics*, vol. 14, no. 3, pp. 531–542, May 1991.

[99] G. Rodriguez, A. Jain, and K. Kreutz-Delgado, "A spatial operator algebra for manipulator modeling and control," *The International Journal of Robotics Research*, vol. 10, no. 4, pp. 371–381, 1991.

[100] G. Rodriguez, A. Jain, and K. Kreutz-Delgado, "Spatial operator algebra for multibody system dynamics," *Journal of the Astronautical Sciences*, vol. 40, no. 1, pp. 27–50, 1992.

[101] R. Featherstone and D. Orin, "Robot dynamics: Equations and algorithms," in *Proceedings 2000 IEEE International Conference on Robotics and Automation*, vol. 1, San Francisco, California, USA, 2000, pp. 826–834.

[102] R. Featherstone, *Rigid Body Dynamics Algorithms*. Springer-Verlag, Jan. 11, 2008, 228 pp., ISBN: 0387743146.

[103] A. Mohan and S. K. Saha, "A recursive, numerically stable, and efficient simulation algorithm for serial robots," *Multibody System Dynamics*, vol. 17, no. 4, pp. 291–319, 2007.

[104] S. Dubowsky and E. Papadopoulos, "The kinematics, dynamics, and control of free-flying and free-floating space robotic systems," *IEEE Transactions on Robotics and Automation*, vol. 9, no. 5, pp. 531–543, 1993.

[105] A. Ellery, "An engineering approach to the dynamic control of space robotic on-orbit servicers," *Proceedings of the Institution of Mechanical Engineers, Part G: Journal of Aerospace Engineering*, vol. 218, no. 2, pp. 79–98, 2004.

[106] S. A. A. Moosavian and E. Papadopoulos, "Free-flying robots in space: An overview of dynamics modeling, planning and control," *Robotica*, vol. 25, no. 5, 2007.

[107] ——, "Explicit dynamics of space free-flyers with multiple manipulators via spacemaple," *Advanced Robotics*, vol. 18, no. 2, pp. 223–244, 2004.

[108] J. Virgili-Llop *et al.*, *SPART: Spacecraft robotics toolkit*, https://github.com/NPS-SRL/SPART, 2017.

[109] K. Liu *et al.*, *DART: Dynamic animation and robotic toolkit*, Online: https://github.com/dartsim/dart, 2012.

[110] J. Lee, *Awesome robotics libraries*, https://github.com/jslee02/awesome-robotics-libraries/#dynamics-simulation.

[111] M. Sherman and D. Rosenthal, *SD/FAST*, www.sdfast.com, Jan. 2001.

[112] U. Lee and M. Mesbahi, "Constrained autonomous precision landing via dual quaternions and model predictive control," *Journal of Guidance, Control, and Dynamics*, vol. 40, no. 2, pp. 292–308, 2017.

[113] G. V. Chowdhary and E. N. Johnson, "Theory and flight-test validation of a concurrent-learning adaptive controller," *Journal of Guidance, Control, and Dynamics*, vol. 34, no. 2, pp. 592–607, Mar. 2011.

[114] D. Klawitter, *Clifford Algebras*. Springer Nature, 2015, ISBN: 978-3-658-07617-7.

[115] W. K. Clifford, "Preliminary sketch of bi-quaternions," *Proceedings of the London Mathematical Society*, vol. 4, no. 1, pp. 381–395, Nov. 1873.

[116] J. Rooney, "William Kingdon Clifford (1845 - 1879)," in *Distinguished Figures in Mechanism and Machine Science*, M. Ceccarelli, Ed., Springer Netherlands, 2007, pp. 79 –116.

[117] J. Rooney, "On the three types of complex number and planar transformations," *Environment and Planning B: Planning and Design*, vol. 5, no. 1, pp. 89–99, Nov. 1978.

[118] R. M. Murray, Z. Li, and S. S. Sastry, *A Mathematical Introduction to Robotic Manipulation*. CRC Press, 1994.

[119] E. Özgür and Y. Mezouar, "Kinematic modeling and control of a robot arm using unit dual quaternions," *Robotics and Autonomous Systems*, vol. 77, pp. 66 –73, 2016.

[120] E. Pennestrì and R. Stefanelli, "Linear algebra and numerical algorithms using dual numbers," *Multibody System Dynamics*, vol. 18, no. 3, pp. 323–344, 2007.

[121] R. N. Jazar, *Theory of Applied Robotics: Kinematics, Dynamics, and Control*. Springer Science & Business Media, 2010.

[122] D. Seo and M. R. Akella, "Separation property for the rigid-body attitude tracking control problem," *Journal of Guidance, Control, and Dynamics*, vol. 30, no. 6, pp. 1569–1576, 2007.

[123] J. Ahmed, V. T. Coppola, and D. S. Bernstein, "Adaptive asymptotic tracking of spacecraft attitude motion with inertia matrix identification," *Journal of Guidance, Control, and Dynamics*, vol. 21, no. 5, pp. 684–691, 1998.

[124] J. T.-Y. Wen and K. Kreutz-Delgado, "The attitude control problem," *IEEE Transactions on Automatic Control*, vol. 36, no. 10, pp. 1148–1162, 1991.

[125] N. A. Chaturvedi, A. K. Sanyal, and N. H. McClamroch, "Rigid-body attitude control using rotation matrices for continuous singularity-free control laws," *IEEE Control Systems Magazine*, pp. 30–51, 2011.

[126] F. L. Markley and J. L. Crassidis, *Fundamentals of Spacecraft Attitude Determination and Control*. Springer, 2014, vol. 33.

[127] D. Lee, J. E. Cochran Jr., and T. S. No, "Robust position and attitude control for spacecraft formation flying," *Journal of Aerospace Engineering*, vol. 25, no. 3, pp. 436–447, 2012.

[128] S. E. Lennox, "Coupled attitude and orbital control system using spacecraft simulators," Master's thesis, Virginia Polytechnic Institute and State University, Blacksburg, Virginia, 2004.

[129] G. Bourmaud, R. Mégret, M. Arnaudon, and A. Giremus, "Continuous-discrete extended kalman filter on matrix lie groups using concentrated gaussian distributions," *Journal of Mathematical Imaging and Vision*, vol. 51, no. 1, pp. 209–228, 2015.

[130] N. Filipe, M. Kontitsis, and P. Tsiotras, "An extended Kalman filter for spacecraft pose estimation using dual quaternions," in *Proceedings of the 2015 American Control Conference*, Chicago, Illinois, 2015.

[131] Y. Deng, Z. Wang, and L. Liu, "Unscented Kalman filter for spacecraft pose estimation using twistors," *Journal of Guidance, Control, and Dynamics*, vol. 39, no. 8, pp. 1844–1856, Jun. 2014.

[132] D. Lee and G. Vukovich, "Robust adaptive terminal sliding mode control on se(3) for autonomous spacecraft rendezvous and docking," *Nonlinear Dynamics*, vol. 83, no. 4, pp. 2263–2279, 2016.

[133] B.-E. Jun, D. S. Bernstein, and N. H. McClamroch, "Identification of the inertia matrix of a rotating body based on errors-in-variables models," *International Journal of Adaptive Control and Signal Processing*, vol. 24, no. 3, pp. 203–210, 2010.

[134] J. A. Keim, A. Behçet Açikmeşe, and J. F. Shields, "Spacecraft inertia estimation via constrained least squares," in *2006 IEEE Aerospace Conference*, Big Sky, Montana, 2006.

[135] U. Lee, D. Besson, and M. Mesbahi, "Fast inertia property estimation via convex optimization for the asteroid redirect mission," in *53rd IEEE Conference on Decision and Control*, 2014, pp. 3364–3369.

[136] Z. R. Manchester and M. A. Peck, "Recursive inertia estimation with semidefinite programming," in *AIAA Guidance, Navigation, and Control Conference, AIAA SciTech Forum*, Grapevine, Texas, 2017.

[137] P. Singla, K. Subbarao, and J. L. Junkins, "Adaptive output feedback control for spacecraft rendezvous and docking under measurement uncertainty," *Journal of Guidance, Control, and Dynamics*, vol. 29, no. 4, pp. 892–902, 2006.

[138] L. Sun, "Passivity-based adaptive finite-time trajectory tracking control for spacecraft proximity operations," *Journal of Spacecraft and Rockets*, vol. 53, no. 1, pp. 46–56, 2016.

[139] G. Chowdhary and E. Johnson, "Theory and flight test validation of long term learning adaptive flight controller," in *AIAA Guidance, Navigation, and Control*, Honolulu, Hawaii, United States, 2008.

[140] G. V. Chowdhary, "Concurrent learning for convergence in adaptive control without persistency of excitation," PhD thesis, Georgia Institute of Technology, 2010.

[141] N. Filipe and P. Tsiotras, "Adaptive position and attitude tracking controller for satellite proximity operations using dual quaternions," in *AAS/AIAA Astrodynamics Specialist Conference*, ser. AAS 13-858, Hilton Head, South Carolina, 2013, pp. 2313–2332.

[142] P. Müller, "Descriptor systems: Pros and cons of system modelling by differential-algebraic equations," *Mathematics and Computers in Simulation*, vol. 53, no. 4–6, pp. 273 –279, 2000.

[143] J. Lee, C. K. Liu, F. C. Park, and S. S. Srinivasa, "A linear-time variational integrator for multibody systems," *arXiv*, 2018. arXiv: 1609.02898v2.

[144] E. Barth and B. Leimkuhler, "Symplectic methods for conservative multibody systems," *Fields Institute Communications*, vol. 10, pp. 25–43, 1993.

[145] J. Xu and K. H. Halse, "Dual quaternion variational integrator for rigid body dynamic simulation," *arXiv*, 2016. arXiv: 1611.00616v2.

[146] Z. R. Manchester and M. A. Peck, "Quaternion variational integrators for spacecraft dynamics," *Journal of Guidance, Control, and Dynamics*, vol. 39, no. 1, pp. 69–76, 2016.

[147] D. H. Jacobson and D. Q. Mayne, *Differential Dynamic Programming*, ser. Modern Analytic and Computational Methods in Science and Mathematics. American Elsevier Publishing Company, 1970.

[148] S. Yakowitz and B. Rutherford, "Computational aspects of discrete-time optimal control," *Applied Mathematics and Computation*, vol. 15, no. 1, pp. 29 –45, 1984.

[149] Y. Tassa, N. Mansard, and E. Todorov, "Control-limited differential dynamic programming," in *Proceedings of the IEEE International Conference on Robotics and Automation*, Hong Kong, China, 2014.

[150] Y. Tassa, *iLQG/DDP Trajectory Optimization*, www.mathworks.com/matlabcentral/fileexchange/52069-ilqg-ddp-trajectory-optimization, Jul. 2015.

[151] D. S. Bernstein, *Matrix Mathematics: Theory, Facts, and Formulas, Second Edition*. Princeton University Press, 2009, ISBN: 9780691140391.

[152] E. Todorov, T. Erez, and Y. Tassa, "MuJoCo: A physics engine for model-based control," in *Proceedings of the 2012 IEEE/RSJ International Conference on Intelligent Robots and Systems*, Vilamoura, Algarve, Portugal, 2012.

VITA

Alfredo Valverde was born and raised in San José, Costa Rica. He is a Ph.D. candidate in the School of Aerospace Engineering at the Georgia Institute of Technology (Georgia Tech) and deputy project manager for the Irazú CubeSat mission, developed in Costa Rica, and launched in April of 2018. His current research lies in the field of dynamic modeling of robotic arms on spacecraft, nonlinear control, and estimation. He received his B.Sc. degree in aerospace engineering (2013) from Georgia Tech with highest honors, while holding research and teaching assistant positions in the aerospace engineering and computer science departments. He also received his M.Sc. degree in aerospace engineering (2014), with a specialization in the field of combustion and experimental research at the Aerospace Combustion Laboratory at Georgia Tech. He has held internship positions at the Guidance and Control section at JPL (2015 - 2017) and at the Département Aérodynamique, Energétique et Propulsion at ISAE-SUPAERO (2012), and is actively involved in outreach programs for the enhancement of STEM education.